1977

A Solution To The Time Dependent Schroedinger Equation With A Periodic Hamiltonian

Jerome Valentine Moloney

NOTICE

The quality of this microfiche is heavily dependent upon the quality of the original thesis submitted for microfilming. Every effort has been made to ensure the highest quality of reproduction possible.

If pages are missing, contact the university which granted the degree.

Some pages may have indistinct print especially if the original pages were typed with a poor typewriter ribbon or if the university sent us a poor photocopy.

Previously copyrighted materials (journal articles, published tests, etc.) are not filmed.

Reproduction in full or in part of this film is governed by the Canadian Copyright Act, R.S.C. 1970, c. C-30. Please read the authorization forms which accompany this thesis.

THIS DISSERTATION HAS BEEN MICROFILMED EXACTLY AS RECEIVED

AVIS

La qualité de cette microfiche dépend grandement de la qualité de la thèse soumise au microfilmage. Nous avons tout fait pour assurer une qualité supérieure de reproduction.

S'il manque des pages, veuillez communiquer avec l'université qui a conféré le grade.

La qualité d'impression de certaines pages peut laisser à désirer, surtout si les pages originales ont été dactylographiées à l'aide d'un ruban usé ou si l'université nous a fait parvenir une photocopie de mauvaise qualité.

Les documents qui font déjà l'objet d'un droit d'auteur (articles de revue, examens publiés, etc.) ne sont pas microfilmés.

La reproduction, même partielle, de ce microfilm est soumise à la Loi canadienne sur le droit d'auteur, SRC 1970, c. C-30. Veuillez prendre connaissance des formules d'autorisation qui accompagnent cette thèse.

LA THÈSE A ÉTÉ MICROFILMÉE TELLE QUE NOUS L'AVONS REÇUE

A SOLUTION TO THE TIME DEPENDENT SCHROEDINGER EQUATION WITH A PERIODIC HAMILTONIAN

by

Jerome V. Moloney
Department of Chemistry

Submitted in partial fulfillment
of the requirements for the degree of
Doctor of Philosophy

Faculty of Graduate Studies
The University of Western Ontario
London, Canada
December 1976

ABSTRACT

The time dependent Schroedinger equation describing the interaction of an N-level atomic or molecular quantum system with a classical oscillating field of arbitrary amplitude, frequency and phase, is solved exactly within the dipole approximation. The formal method of solution exploits fully the time periodicity of the total Hamiltonian, and although the method is developed with the oscillating field problem in mind, the formal results are equally applicable to any general periodic Hamiltonian. A matrix projection technique allows the general solution matrix to be constructed without specification of any initial conditions, the solution for a specified set of initial conditions being generated from this by a simple matrix multiplication. Finally, the general solution matrix can be transformed to Floquet form by a straightforward matrix diagonalization and the solution in the Floquet representation allows for the accurate evaluation of phase and/or time averaged properties of the N-level quantum system plus external field(s).

The method of solution is illustrated by evaluating induced transition probabilities and their phase and/or time averages for a two level system and a number of model multilevel systems. In these calculations, the importance of the phase δ of the applied sinusoidal field at strong couplings is readily apparent. A direct coincidence between the characteristic exponents of the Floquet solution and the energies derived from a fully quantized treatment is explicitly demonstrated for a two level system and the usefulness of the characteristic exponents, in general, for mapping out complicated spectra and evaluating resonance frequency shifts is also demonstrated. Static Stark and Zeeman fields which can both mix and tune the levels have also been included in this study and require no modification of the formalism. Degeneracies within multilevel systems pose no particular problem and the effects of nonresonant interactions with neighbouring states on the resonance frequency shifts have been quantitatively investigated. The present formalism also leads to a clarification of some apparent discrepancies between results in the

literature.

Finally, exact rotating field solutions for three level quantum systems resonantly coupled to two classical oscillating fields, are presented and represent an improvement on previously derived approximate rotating field results.

ACKNOWLEDGEMENTS

The author wishes to express his sincere gratitude to Professor W.J. Meath for his advice, patient guidance and continued encouragement during the course of this work.

He also wishes to express his deep appreciation to his colleauges for their useful discussions and assistance in general. In particular thanks are due to Dr. M.K. Ali and Dr. G.D. Zeiss for their advice and assistance on computations.

Finally the author wishes to thank Els for her understanding and patience.

TABLE OF CONTENTS

LIST OF FIGURES

LIST OF TABLES

CHAPTER 1

INTRODUCTION

The purpose of this work is to derive an exact reasonably economic solution for the time dependent Schroedinger wave equation that is capable of describing, within a well defined multipolar approximation, the behaviour of an N-level atomic or molecular system interacting with an arbitrarily strong sinusoidal time dependent field. Recent advances in laser technology have provided widely tunable intense monochromatic radiation sources [1,2,3], now available over a wide range of frequencies, which are capable of being used to elucidate fully the level structures of complex atomic or molecular systems. Such radiation sources have been available in the radiofrequency and microwave regions for many years [4,5,6,7,8] and have provided accurate measurements of the important constants in hyperfine and fine structure level configurations. Radiofrequency sources, in particular, have been used extensively to study the many nonlinear interactions occurring in hyperfine configurations [4,5,6,7] and such interactions are becoming increasingly important in microwave and optical spectroscopy [8,9,10,11] where they can provide accurate measurements of transition dipole moments, level separations, resonance frequency shifts and resonance widths at "half maximum".

Nonlinear interactions become increasingly important when the energy provided by the sinusoidal applied field becomes comparable to, or greater than, the energy difference between the pair of states involved in a particular transition. The developement of a satisfactory theoretical analysis of the linear and nonlinear interactions occurring in this energy regime, particularly when more than two levels are involved, remains an important problem [11,12,13].

Strong interactions in a two level system have been discussed extensively, particularly in recent years, by many authors [13,14,15,16,17,18]. The most elegant original treatment of these interactions has been given by Autler and Townes [14] and Shirley [13], who also discuss the limitations of their solutions to the problem when the interactions become very strong. The theory of linear differential equations with periodic coefficients has been used by these authors to express the solution of the time dependent Schroedinger equation, for a two level system interacting with an applied sinusoidal field, in Floquet form [19]. This form of the solution, when fully exploited, allows for an efficient computation of the induced absorption spectrum for this system, see Chapters 4 and 5, and involves the characteristic exponents which coincide precisely with the energies of the atom-radiation field, see Chapter 4. Shirley, in particular, has shown how plots of these characteristic exponents can be used to predict resonance peak positions and widths at "half maximum" for the two level Zeeman tuning experiment. To date discussions of the usefulness of the characteristic exponents has been essentially limited to Zeeman tuning of two levels where the frequency of the applied field is held fixed. Autler and Townes [14] have discussed the frequency dependence of these two level characteristic exponents, but their final results are complicated and not in a form particularly suited to the analysis of resonance frequency shifts and widths. The only discussion of the behaviour of the characteristic exponents for an N-level nondegenerate system appears to be that of Besset, Horowitz, Messiah and Winter [20], who work within the rotating field approximation. One of the major concerns of this thesis will be to examine the detailed behaviour of the characteristic exponents for arbitrarily strong couplings between a sinusoidal applied field and a N-level system of arbitrary level configuration. The usefulness of plots of the characteristic exponents for mapping out complicated spectra will be demonstrated explicitly for a variety of two and three level systems. Some confusion which has arisen in the literature recently regarding such plots will be cleared up [21].

The present work fully exploits the known form of the total wave function $\Psi(r,t)$, which describes the interaction of a sinusoidal time dependent field of arbitrary amplitude $\mathcal{E}$, frequency ν and phase δ, with a N-level system of arbitrary level configuration. A systematic means of constructing $\Psi(r,t)$, to any degree of accuracy, which is valid over arbitrarily long times, will be explicitly developed in what follows. A form of $\Psi(r,t)$, more suitable to the evaluation of the time and/or phase average properties of the system, can be ascertained from the Floquet theory [22] and these important average physical properties can be extracted in a straightforward manner. The important need for averaging these properties over the phase of the applied sinusoidal field, which has not received due consideration by many authors recently [16,18,21,23,24], will also be explicitly demonstrated. Finally, in order to illustrate the general applicability of the formal method of solution, induced transition probabilities and their various averages over phase and time will be calculated explicitly for various two level and a number of multilevel systems interacting with a single applied sinusoidal field.

The general time dependent Schroedinger equation, and some of the conventional methods developed to solve it approximately, are briefly reviewed in Chapter 2. The problem is reformulated as an infinite set of coupled differential equations for the complex amplitudes of the individual stationary states within the N-level system by employing the Dirac expansion of the total wavefunction [25,26], see Sections 2.1-2.2, and finally in Sections 2.3 and 2.4 the two most commonly employed approximate methods of solving these differential equations are briefly reviewed. In Section 2.3 time dependent perturbation theory and the many problems encountered in its application to problems involving relatively strong oscillating field amplitudes or reasonably large times are briefly outlined. The rotating field approximation, which is essentially a resonance approximation, is discussed in Section 2.4. The formulae derived within these approximations are very useful both as an interpretive guide and in providing conceptual insight into the nature of the exact solutions for problems where such approximations fail.

An exact method of solution* for the coupled differential equations describing the interaction of a general N-level system with a sinusoidal field of arbitrary amplitude, frequency and phase, is developed formally in Chapter 3. The general problem formulated in matrix notation for complete generality in Section 3.1, leads naturally to a representation of the final physical properties of the N-level system in terms of the density matrix. An accurate matching power series method [27,28] of solution for the coupled differential equations, as a function of time for fixed δ, $\mathcal{E}$ and ν is presented in Section 3.2 and the time periodicity of the coefficients in these differential equations, coupled with a straightforward matrix projection technique, leads to a highly accurate and efficient iterative method [28] of solution valid for arbitrarily long time, see Sections 3.3 and 3.4. For complete generality, the iterative solution is transformed to Floquet form in Section 3.5 which allows for the straightforward evaluation of the phase and time averaged properties of the general N-level system, see Section 3.6. Finally, in Section 3.7, specific formulae are presented for both the phase and phase/time averaged induced transition probabilities for the interaction of a sinusoidal field with a general N-level system. Chapters 4 and 5 are directly concerned with the specific applications of the general formalism, presented in Chapter 3, to the evaluation of the induced transition probabilities for a variety of level configurations interacting strongly with a sinusoidal field.

Chapter 4 is concerned specifically with the important [13,14,15,16,17,18] two level system. The exact method of solution for this system, within the context of the formal methods of Sections 3.1-3.4, is briefly reviewed in Section 4.1. The induced transition probabilities and their various time and phase averages are discussed

---

* In this work dipole (electric and magnetic) interactions are considered specifically, although higher multipole interactions could be included without a drastic modification of the general formalism.

in Section 4.2. The power of the iterative solution developed in Sections 3.3 and 3.4 is illustrated, using the two level system as a model, in Section 4.2.1 where the phase dependent induced transition probability is computed accurately over large times [28]. The various nonlinear induced transitions arising from the strong coupling of a two level degenerate or nondegenerate system to the oscillating field are discussed in the context of the induced phase and phase/time averaged transition probabilities [22] both as a function of the frequency ω of the applied field, see Section 4.2.2, and as a function of static Stark (or magnetic) fields which can both mix and tune the levels, see Sections 4.2.3 and 4.3. The detailed behaviour of the characteristic exponents derived from the Floquet solution discussed in Section 3.5, which provides a quantitative measure of both resonance frequency shifts and widths at half-maximum, is discussed in Section 4.4.

The strong interaction between a sinusoidal field and a number of multilevel systems is treated in Chapter 5. Transitions in a three level system from a nondegenerate ground state to an excited degenerate pair of states, of mutually opposite parities, is discussed in Section 5.1 in the context of the phase and phase/time averaged transition probabilities. Explicit results for these transition probabilities as a function of frequency and field strength are presented in Section 5.1.1 while the effect of mixing and splitting of the excited degenerate pair of states by a static Stark field is considered in Section 5.1.2. The effect of a similar static Stark field on the frequency spectrum of a three level system containing an excited nondegenerate state lying close to another excited state of opposite parity is discussed in Section 5.2. The three level nondegenerate configuration recently analysed by Vasilenko, Chebotaev and Shishaev [29], using second order perturbation theory, and suggested by these authors as a model for Doppler free two photon optical spectroscopy with low intensity lasers, is analysed in Section 5.3 for strong applied field strengths. This level configuration is such that strong overlap can occur between neighbouring single photon and two photon resonance profiles for large field intensities and the

importance of such interference effects is specifically studied in this section. The power of the characteristic exponent plots for mapping out complicated spectra is explicitly displayed for these level configurations . Finally, the importance of neighbouring states on the frequency shifts of a two photon resonance profile is quantitatively investigated for two multilevel configurations in Section 5.4.

Appendix A briefly summarizes the various numerical methods employed in the main text and contains a discussion of their accuracy. In Section A.1 the accuracy and convergence of the matching power series method for the solution of the time dependent Schroedinger equation is briefly discussed while Section A.2 explicitly demonstrates a symmetry relation which is employed in expediting the matching power series solution. Section A.3 summarizes the numerical quadratures employed to evaluate the integrals which provide both the phase and time averages of the induced transition probabilities. This section also contains a brief discussion of the use of the fourth order Runge Kutta [30] method employed to numerically integrate the time dependent Schroedinger equation and hence provide a numerical check on both the matching power series and the iterative methods discussed in Chapter 3. A recent erroneous calculation [31] of induced transition probabilities in a three level system with two applied fields is contrasted with an exact evaluation of these quantities by using the Runge Kutta method to integrate the time dependent Schroedinger equation.

The rotating field approximation, discussed explicitly in Chapter 2 for a two level system, is extended in Appendix B to the study of some three level systems interacting resonantly with two oscillating fields by using a Laplace transform technique discussed by Freed [32]. Exact expressions, within this approximation, for transition rates and absorbed and emitted power are derived for specific level configurations and represent an improvement on previously derived approximate expressions [33,34] which are valid as long as one of the applied fields is very weak. In particular, these exact expressions

can be used to study both the time evolution of frequency spectra and the behaviour of such spectra when both fields are comparable in magnitude.

Atomic units will be used throughout this thesis [35] and the relevant units and their appropriate conversion factors are listed below.

	Atomic Unit	Value in S.I. units
Mass	m_e	9.1095×10^{-31} kg
Charge	e	1.6022×10^{-19} C
Angular Momentum	$\hbar$	1.0546×10^{-34} J sec
Length	$a_o(\hbar^2 m_e^{-1} e^{-2})$	5.2918×10^{-11} m
Time	$\hbar^{-1} a_o^2 m_e (\hbar(\text{hartree})^{-1})$	2.4189×10^{-17} sec
Energy	$\hbar^2 a_o^{-2} m_e^{-1}$(hartree)	4.3598×10^{-18} J
μ_B (Bohr Magneton)*	$e\hbar/2m_e$	9.2740×10^{-24} J T^{-1}
μ (Electric Dipole Moment)	ea_o	8.4784×10^{-30} C m
B (Magnetic Induction)	$\hbar e^{-1} a_o^{-2}$	2.3505×10^{5} T
$\mathcal{E}$ (Electric Field Amplitude)	ea_o^{-2}	5.1423×10^{11} V m^{-1}
Frequency	$m_e e^4 \hbar^{-3}((\text{hartree})/\hbar)$	4.1341×10^{-16} sec^{-1}

* 1 tesla (T) = 10^4 gauss.

Note: The variable $\mathbf{r}$ occurring throughout this thesis can refer to one or more spatial co-ordinates.

CHAPTER 2

GENERAL REVIEW OF THE THEORY

2.1 TIME DEPENDENT SCHROEDINGER EQUATION

The effects of the interactions, $V(r,t)$ between any atomic or molecular system and an external perturbation, are described by the time dependent Schroedinger equation[26,36].

$$H(r,t)\,\Psi(r,t) = i\,\partial/\partial t\,\Psi(r,t) \qquad 2.1.1$$

where the total Hamiltonian $H(r,t)$ is composed of two parts

$$H(r,t) = H_o(r) + V(r,t) \qquad 2.1.2$$

and $\Psi(r,t)$ is the exact time dependent wavefunction for the problem defined by $H(r,t)$. In the absence of the time dependent perturbation $V(r,t)$ the partial differential equation 2.1.1, under the action of the stationary Hamiltonian $H_o(r)$, is separable and yields the more familiar time independent Schroedinger equation

$$H_o(r)\,\phi(r) = E\,\phi(r) \qquad 2.1.3$$

where $\phi(r)$, the stationary state solution and E its eigenenergy are obtained by solving the time independent wave equation 2.1.3. In what follows the solution to the stationary state problem, described by equation 2.1.3, is assumed to be known and the problem at hand will be to solve the more general partial differential equation given by equations 2.1.1 and 2.1.2. In particular, the system described by equation 2.1.3 will have a complete spectrum of solutions with each state of the system satisfying

$$H_o(r)\,\phi_j(r) = E_j\,\phi_j(r) \qquad 2.1.4$$

where the wavefunctions $\phi_j(r)$ describe a complete set of orthonormal basis functions with E_j their corresponding energy eigenvalues. The general solution to the unperturbed problem defined by

$$i\frac{\partial}{\partial t}\psi(r,t) = H_0(r)\,\psi(r,t) \qquad 2.1.5$$

can be written as an expansion in terms of this complete set of unperturbed eigenfunctions $\phi_j(r)$ and their corresponding eigenvalues E_j as follows

$$\psi(r,t) = \sum_k b_k\,\phi_k(r)\exp[-iE_k t] \qquad 2.1.6$$

where the constants b_k are independent of time and of the spatial co-ordinates r. The subscripts "k" contain the complete set of quantum numbers necessary to describe a particular stationary state $\phi_k(r)$; for example, in an atomic system "k" might represent a fine structure or hyperfine component of that system whereas in a molecular system it might represent an electronic-vibrational or an electronic-vibrational-rotational state.

2.2 DIRAC VARIATION OF CONSTANTS METHOD FOR THE SOLUTION OF THE TIME DEPENDENT SCHROEDINGER EQUATION.

Historically, the first method developed to solve equation 2.1.1 was introduced by Dirac [25,26] and was based on the "Variation of Constants" method used in the theory of differential equations. Dirac proposed that the more general problem described by equations 2.1.1 and 2.1.2 be solved by adopting the following expansion* of the wavefunction $\Psi(r,t)$, which is a generalization of equation 2.1.6,

---

* This expansion of $\Psi(r,t)$ is in the interaction representation [26,37] and will be employed throughout this chapter. For the exact solution to be derived in Chapter 3, the Schroedinger representation will prove more convenient with the state amplitudes $a_j(t)$ in this representation related to the interaction representation state amplitudes $b_j(t)$ as follows $a_j(t) = b_j(t)\exp[-iE_j t]$.

$$\Psi(r,t) = \sum_k b_k(t)\, \phi_k(r) \exp[-i E_k t] \qquad 2.2.1$$

where now the coefficients $b_k(t)$ are explicit functions of time but still constant with respect to spatial co-ordinates. The expansion given by equation 2.2.1 is formally exact as the eigenfunctions $\phi_k(r)$ span the complete Hilbert space of the problem and the coefficients $b_k(t)$ can be associated with the fluctuations in time of the amplitudes of the individual stationary states $\phi_k(r)$ under the action of the time dependent perturbation $V(r,t)$. The following normalization condition is imposed on the total wavefunction

$$\langle \Psi(r,t) | \Psi(r,t) \rangle = \sum_k |b_k(t)|^2 = 1 \qquad 2.2.2$$

which, in turn, guarantees unitarity of the solution for all time.

Substitution of the expansion given by equation 2.2.1 into the time dependent Schroedinger equation given by equations 2.1.1 and 2.1.2, followed by some elementary manipulations, yields the following infinite set of linear first order coupled differential equations for the state amplitudes $b_j(t)$

$$i \partial/\partial t\, b_j(t) = \sum_{k=0}^{\infty} V_{jk}(t)\, b_k(t) \exp[i(E_j - E_k)t] \qquad 2.2.3$$

where

$$V_{jk}(t) = \langle \phi_j(r) | V(r,t) | \phi_k(r) \rangle = \int \phi_j^*(r)\, V(r,t)\, \phi_k(r)\, d\tau \qquad 2.2.4$$

Equation 2.2.3 is normally solved subject to the condition that the system is in some pure state $\phi_k(r)$ at the instant the perturbation given by $V(r,t)$ is switched on, that is

$$b_k(0) = \delta_{jk} \qquad 2.2.5$$

where δ_{jk} denotes the Kronecker delta symbol. As the absolute value squared of the state amplitude $b_k(t)$, that is $|b_k(t)|^2$, is a measure of the population of that state at time t subject to the imposed initial conditions given by equation 2.2.5, we define the induced transition probability $P_{kk}(t)$ as follows

$$P_{kk}(t) = |b_k(t)|^2 \qquad 2.2.6$$

and equation 2.2.2 ensures that the total transition probability $P = \sum_k P_{kk}(t) = 1$, is conserved. For the problems considered in this thesis, it will be assumed that the dominant interaction of the

external perturbation $V(r,t)$ with the atomic or molecular system occurs only through a finite number of states so that the infinite sum occurring in equation 2.2.3 can be truncated to relatively few terms. While the purpose of this work is to derive exact solutions to the differential equations, given by equation 2.2.3, for situations where the interactions of the perturbation $V(r,t)$ with the original unperturbed system (described by the Hamiltonian $H_o(r)$) are strong and hence lie outside the region of validity of conventional approximation techniques, such approximation methods will prove useful in interpreting the behaviour of these exact solutions. Before proceeding to discuss such approximation methods however, the precise form of the perturbation term $V(r,t)$ must be specified.

For most of the work that follows the perturbation term $V(r,t)$ will represent a classical monochromatic radiation field interacting with a quantized atomic or molecular system (specified by the Hamiltonian $H_o(r)$). Interactions with more than one field will be considered briefly at a later stage of this thesis, but the generalization of the perturbation term $V(r,t)$ to include this situation is trivial and its inclusion at this stage would serve no useful purpose. It will also be assumed that the coupling of the quantized system with the external field occurs through an electric dipole interaction.* Thus the time dependent perturbation $V(r,t)$ can now be written explicitly as

---

* Magnetic dipole and various higher multipole interactions (electric quadrupole, etc.) may be included in the analysis without affecting the formal developements that follow. In fact, magnetic dipole interactions will be explicitly considered in Chapter 4 where the magnetic dipole interaction term is $V(r,t) = -\underline{\mu}_N \cdot \underline{B} \cos(\omega t+\delta)$ where $\underline{\mu}_N = \gamma \underline{I}$ and $\underline{B}$ is the magnetic field strength.

$$V(r,t) = -\underline{\mu}\cdot\underline{\mathcal{E}}\cos(\nu t+\delta) \qquad 2.2.7$$

where $\underline{\mu}$ is the electric dipole moment operator for the system, $\underline{\mathcal{E}}$ is the electric field amplitude, ν its frequency and δ an arbitrary phase factor. The use of this semiclassical approach to study the interaction of radiation with matter is justified because most laboratory fields correspond to high photon occupation numbers N in the quantized field [38,39] and exhibit classical behaviour in agreement with the Correspondence Principle. A direct correspondence between the results of the semiclassical and fully quantized approaches will be demonstrated explicitly in Chapter 4.

The only drawback of the semiclassical approach is that the spontaneous decay of excited states, a purely quantum phenomenon, is not accounted for by using a classical field [38,40,41]. These spontaneous decay terms can be phenomenologically included in the semiclassical treatment by assuming the exponential decay law, derived quantum mechanically by Weisskopf and Wigner. This amounts to replacing the real stationary state eigenvalue E_j by the complex number $(E_j - i\gamma_j/2)$ to yield the following generalization of the time dependent wavefunction for the stationary state j,

$$\psi_j(r,t) = \phi_j(r)\exp[-i(E_j - i\gamma_j/2)t] \qquad 2.2.8$$

The real part $\gamma_j/2$ of the exponential is generally much smaller in magnitude than the imaginary part E_j and it is a measure of the radiative width of the state $\phi_j(r)$. Comparison of equation 2.2.8 with equations 2.1.6 and 2.2.1 shows that the state amplitude $b_j(t)$ in the absence of the external field decays as

$$b_j(t) = \exp[(-\gamma_j/2)t] \quad , \quad V(r,t) = 0 \qquad 2.2.9$$

Thus, the transition probability $P_{jj}(t)$ decays as

$$P_{jj}(t) = |b_j(t)|^2 = \exp[-\gamma_j t] \quad , \quad V(r,t) = 0 \qquad 2.2.10$$

which is the familiar exponential decay law in the absence of an applied field. The system of coupled differential equations, given by equation 2.2.3, can now be modified to include these radiative widths γ_j as follows

$$i\,\partial/\partial t\, b_j(t) + i(\gamma_j/2)\, b_j(t) = \sum_k V_{jk}(t)\, b_k(t) \exp[i(E_j - E_k)t] \qquad 2.2.11$$

This equation, as required, yields equation 2.2.9 when the perturbing field is absent, that is $V(r,t) = 0$. An undesirable feature of equation 2.2.11 is that the solution $\Psi(r,t)$ is no longer unitary and hence the normalization condition given by equation 2.2.2 no longer holds ,see equation 2.2.10. As equation 2.2.2 provides a useful check on the accuracy of the exact solution for $b_k(t)$ we will retain equation 2.2.3 as our fundamental system of differential equations and damping effects, see Section 2.4, when needed will be introduced by adopting a more general approach which in certain cases will "reduce" to the result obtained by using equation 2.2.11 ,see Chapter 3, Section 3.7.

2.3 TIME DEPENDENT PERTURBATION THEORY.

Approximate solutions to the time dependent Schroedinger equation, given by equation 2.1.1, valid when the perturbation term $V(r,t)$ and time are sufficiently small, will be reviewed in this section. While our interest lies specifically in solutions to equation 2.1.1 when the perturbation term $V(r,t)$ is large, the perturbation results derived herein, although invalid for this situation*, will prove extremely useful in predicting and interpreting the various results derived through the exact treatment. In the following analysis we will deal specifically with nondegenerate systems as degeneracies can lead to singular perturbation expansions and require special consideration ,see Bohm [36] and Chapters 4 and 5. On the other hand, such degeneracies require no special consideration in the exact solution of Chapter 3.

2.3.1 PERTURBATION RESULTS FOR ARBITRARY $V(r,t)$.

Equation 2.1.2 for the complete Hamiltonian $H(r,t)$ can be written as follows

$$H(r,t) = H_o(r) + \lambda V(r,t) \qquad 2.3.1$$

where λ is a dimensionless parameter which provides a measure of the order of the perturbation and will be set equal to unity in the final results. The total wavefunction $\Psi(r,t)$ can now be expanded in powers of the parameter [42]

$$\Psi(r,t) = \sum_{s=0}^{\infty} \lambda^s \Psi^{(s)}(r,t) \qquad 2.3.2$$

Substituting equations 2.3.1 and 2.3.2 into 2.1.1 and grouping in powers of λ leads to the following set of time dependent perturbation differential equations

$$(H_o(r) - i\partial/\partial t)\Psi^{(0)}(r,t) = 0$$

$$(H_o(r) - i\partial/\partial t)\Psi^{(1)}(r,t) + V(r,t)\Psi^{(0)}(r,t) = 0$$

$$\cdots\cdots\cdots\cdots\cdots\cdots\cdots\cdots$$

$$(H_o(r) - i\partial/\partial t)\Psi^{(s)}(r,t) + V(r,t)\Psi^{(s-1)}(r,t) = 0 \qquad 2.3.3$$

The first equation in this set corresponds to the stationary state problem whose general solution is already known, see equation 2.1.6. This stationary state solution $\Psi^{(0)}(r,t)$ can now be substituted into the second of equations 2.3.3 to yield an inhomogenous differential equation for the first order correction $\Psi^{(1)}(r,t)$. Higher order corrections to the zeroth order wavefunction can be obtained by substituting $\Psi^{(1)}(r,t)$ in the next equation in 2.3.3 and solving for $\Psi^{(2)}(r,t)$. The following normalization condition is imposed on the unperturbed solution

$$\langle \Psi^{(0)}(r,t) | \Psi^{(0)}(r,t) \rangle = 1 \qquad 2.3.4$$

and using equations 2.2.4 and 2.3.2 the following normalization condition follows, by requiring $\Psi(r,t)$ to be normalized, through any given order in λ [43];

$$\sum_{n=0}^{\infty} \langle \Psi^{(n)}(r,t) | \Psi^{(s-n)}(r,t) \rangle = 0 \qquad \delta > 0 \qquad 2.3.5$$

---

* In certain cases the perturbation expansions can be summed to all orders but for $V(r,t)$ reasonably large this summation cannot be carried out analytically and some form of numerical evaluation is required [15].

While different approximation techniques have been employed to solve equations 2.3.3 subject to the above normalization conditions [43,44], we choose to return to the Dirac expansion of the total wavefunction $\Psi(r,t)$, given by equation 2.2.1 and expand its S^{th} order contribution $\Psi^{(s)}(r,t)$ as

$$\Psi^{(s)}(r,t) = \sum_{n=0}^{\infty} b_n^{(s)}(t)\, \phi_n(r) \exp[-iE_n t] \qquad 2.3.6$$

Comparing equations 2.3.6 and 2.3.2 with equation 2.2.1 we obtain the following result (taking $\lambda = 1$)

$$b_j(t) = \sum_{s=0}^{\infty} b_j^{(s)}(t) \qquad 2.3.7$$

Substituting equation 2.3.6 into 2.3.3, followed by some elementary manipulations, yields the following coupled differential equations for the coefficients $b_n^{(s)}(t)$, s=1,2,.....;

$$\partial/\partial t\, b_n^{(s)}(t) = -i \sum_{m=0}^{\infty} \langle \phi_n(r)|V(r,t)|\phi_m(r)\rangle\, b_m^{(s-1)}(t) \exp[i(E_n - E_m)t] \qquad 2.3.8$$

To satisfy the initial conditions, given by equation 2.2.5, the following requirements are imposed

$$b_k^{(0)} = \delta_{lk}$$
$$b_k^{(s)} = 0 \qquad s \neq 0 \qquad 2.3.9$$

Equation 2.3.9, together with the normalization condition given by equation 2.3.5, specifies the boundary conditions and guarantees unitarity of the solution for $\Psi(r,t)$ to a given order in λ and for all times. Writing out equation 2.3.8 explicitly for s=1 and s=2, we obtain, using equation 2.3.9

$$\partial/\partial t\, b_n^{(1)}(t) = -i \langle \phi_n(r)|V(r,t)|\phi_l(r)\rangle \exp[i(E_n - E_l)t]$$

or

$$b_n^{(1)}(t) = -i \int_0^t \langle \phi_n(r)|V(r,t')|\phi_l(r)\rangle \exp[i(E_n - E_l)t']\,dt' \qquad 2.3.10$$

while for s=2

$$\partial/\partial t\, b_n^{(2)}(t) = -i \sum_{m=0}^{\infty} \langle \phi_n(r)|V(r,t)|\phi_m(r)\rangle\, b_m^{(1)}(t) \exp[i(E_n - E_m)t]$$

or

$$b_n^{(2)}(t) = -i \int_0^t \sum_{m=0}^{\infty} \langle \phi_n(r)|V(r,t')|\phi_m(r)\rangle\, b_m^{(1)}(t') \exp[i(E_n - E_m)t']\,dt' \qquad 2.3.11$$

Substituting for $b_m^{(1)}(t)$ from equation 2.3.10 yields

$$b_n^{(2)}(t) = -i\int_0^t \sum_{m=0}^{\infty} \langle \phi_n^{(r)}|V(r,t')|\phi_m^{(r)}\rangle \exp[i(E_n-E_m)t']$$

$$\times\left\{\int_0^{t'} \langle \phi_m^{(r)}|V(r,t'')|\phi_\ell^{(r)}\rangle \exp[i(E_m-E_\ell)t'']dt''\right\}dt' \qquad 2.3.12$$

Higher order terms for $b_n(t)$ may be readily obtained by further successive substitutions of these results into 2.3.8 for $S>2$. Explicit forms for $b_n^{(s)}(t)$ will be derived in the next subsection for the perturbation given by equation 2.2.7.

2.3.2 EXPLICIT PERTURBATION RESULTS FOR $V(r,t) = -\mu\cdot\underline{\mathcal{E}}\cos(\nu t+\delta)$.

In this subsection explicit results will be derived for the near resonant interaction of the oscillating field, $\mathcal{E}\cos(\nu t+\delta)$, with a general atomic or molecular system specified by the Hamiltonian $H_o(r)$ in equation 2.1.2. Writing the perturbation $V(r,t)$ in exponential form we get

$$V(r,t) = -\frac{\mu_z\mathcal{E}}{2}\left(\exp[i(\nu t+\delta)] + \exp[-i(\nu t+\delta)]\right) \qquad 2.3.13$$

where the oscillating field will be assumed to lie in the z-direction. Substituting equation 2.3.13 into 2.3.10 for $b_n^{(1)}(t)$ we obtain

$$b_n^{(1)}(t) = \frac{\mu_{n\ell}\mathcal{E}}{2}\left\{\left(\exp[i(\omega_{n\ell}+\nu)t]-1\right)\exp[i\delta]/(\omega_{n\ell}+\nu)\right.$$
$$\left.+\left(\exp[i(\omega_{n\ell}-\nu)t]-1\right)\exp[-i\delta]/(\omega_{n\ell}-\nu)\right\} \qquad 2.3.14$$

where

$$\omega_{n\ell} = E_n - E_\ell\ ,\quad \mu_{n\ell} = \langle \phi_n^{(r)}|\mu_z|\phi_\ell^{(r)}\rangle \qquad 2.3.15$$

In general we are concerned with the resonant or near resonant absorption, corresponding to the transition $\ell\to n$ with $\omega_{n\ell}>0$ (for emission $\omega_{n\ell}<0$) of a photon of frequency ν. In this case the exponential term $\exp[i(\omega_{n\ell}+\nu)t]$ ($\exp[i(\omega_{n\ell}-\nu)t]$ for emission) is rapidly oscillatory and negligible relative to the slowly varying term $\exp[i(\omega_{n\ell}-\nu)t]$ (or $\exp[i(\omega_{n\ell}+\nu)t]$ for emission)[26,36]. Thus for the absorption process the first order induced transition probability is approximately given by*

$$P_{nn}^{(1)}(t) = |b_n^{(1)}(t)|^2 = \mathcal{E}^2|\mu_{n\ell}|^2 \sin^2\tfrac{1}{2}(\omega_{n\ell}-\nu)t/\ (\omega_{n\ell}-\nu)^2 \qquad 2.3.16$$

For the induced emission process the term $(\omega_{n\ell}-\nu)$ in equation 2.3.16 is replaced by $(\omega_{n\ell}+\nu)$. For the case in which the frequency ν is

approximately equal to the level separation $\omega_{n\ell}$, that is $\omega_{n\ell} - \nu \simeq 0$, equation 2.3.16 reduces further to

$$P_{nn}^{(1)}(t) \simeq \mathcal{E}^2 |\mu_{n\ell}|^2 t^2/4 \qquad 2.3.17$$

Equation 2.3.17 and equation 2.3.16 provide striking examples of the secular divergences which arise in time dependent perturbation theory. For example $P_{nn}^{(1)}(t)$, given by equation 2.3.16, can exceed unity as a function of time if $\mathcal{E}$ is fairly large. Such secular divergences also arise in the case of a static perturbation switched on instantaneously at a given time [43]. It should be emphasised that these secular divergences arise even when all terms are retained in the expression for $b_n^{(1)}(t)$, see equation 2.3.14, and they cannot be removed by going to higher order [45,46]. The divergence arising from the small denominator terms, $(\omega_{n\ell} - \nu)$ when $\omega_{n\ell} \simeq \nu$, in equation 2.3.16 is unique to the oscillating field perturbation and such terms are called "quasi secular" [46]. These "quasi secular" divergences are generally treated by the phenomenological introduction of the radiative width of the excited state into the perturbation formula which can be achieved by modifying equation 2.3.6 as follows

$$\Psi^{(s)}(r,t) = \sum_{n=0}^{\infty} b_n^{(s)}(t)\, \phi_n(r) \exp\left[-i(E_n - i\gamma_n/2)t\right] \qquad 2.3.18$$

and rederiving the perturbation results. As our interest in these perturbation results lies solely in their interpretive value, the explicit introduction of the radiative widths fulfils no useful purpose at this stage and we neglect them in the remainder of this section. Relaxation effects which will be introduced in the next

---

* As we are retaining only resonant terms in these approximations and the analgous perturbation results that follow, the phase dependence δ cancels out in the final expressions and for this reason we will not carry it through in the following results for $b_n^{(s)}(t)$. This phase dependence however will become very important when the exact solution is obtained for large coupling energies $|\mu\mathcal{E}|$; see Chapter 4.

section in the context of the rotating field approximation, and in the exact solution in Chapter 3, will incorporate radiative damping as a special case.

The first order perturbation results derived above are adequate to describe many conventional spectroscopic problems as the field intensities employed in such measurements lie well within their range of validity. However to understand the many effects (and in particular nonlinear effects) which are now being observed with more intense monochromatic light sources, the above perturbation results must be carried to higher orders. For example the two photon transition which corresponds to the lowest order nonlinear effect was first predicted by Goppart Mayer in 1949 [47,48] and arises from second order terms in the perturbation expansion. Substituting equations 2.3.14 and 2.3.13 into equation 2.3.11 yields the following result for the second order contribution to $b_n(t)$

$$b_n^{(2)}(t) = i\xi^2 \sum_{m=1}^{\infty} \mu_{nm}\mu_{m\ell}\left\{\frac{\exp[i(\omega_{n\ell}+2\nu)t]-1}{(\omega_{n\ell}+2\nu)(\omega_{m\ell}+\nu)} + \frac{\exp[i(\omega_{n\ell}-2\nu)t]-1}{(\omega_{n\ell}-2\nu)(\omega_{m\ell}+\nu)}\right.$$

$$\left. + \frac{2\omega_{m\ell}(\exp[i\omega_{m\ell}t]-1)}{(\omega_{m\ell}^2-\nu^2)\omega_{n\ell}} - \frac{4i\omega_{m\ell}\sin\nu t}{\nu(\omega_{m\ell}^2-\nu^2)}\right\} \qquad 2.3.19$$

The leading two terms in equation 2.3.19 represent the resonant emission and absorption of two photons of frequency ν, via an intermediate virtual state with respect to the transition $\ell \to n$, when the oscillating field frequency lies near $\nu \approx \pm\omega_{n\ell}/2$ where $\omega_{n\ell} < 0$ for emission and $\omega_{n\ell} > 0$ for absorption respectively. At this frequency the remaining two terms make a negligible contribution to either the emission or absorption process as they are rapidly oscillatory. Thus the induced transition probability for two photon absorption from state ℓ to state n is approximately given by

$$P_{nn}^{(2)} = \frac{\xi^4 \sin^2\tfrac{1}{2}(\omega_{n\ell}-2\nu)t}{4(\omega_{n\ell}-2\nu)^2} \sum_{m,k} \frac{\mu_{nm}\mu_{m\ell}\mu_{k\ell}^*\mu_{nk}^*}{(\omega_{m\ell}-\nu)(\omega_{n\ell}-\nu)} \qquad 2.3.20$$

Using the fact that the dipole matrix element μ_{ij} is nonzero only if the states ϕ_i and ϕ_j are of opposite parity, we can predict from equation 2.3.20 that a two photon transition can only occur between two states ϕ_n and ϕ_ℓ of the same parity and requires at least one extra

state ($k=m$) of opposite parity. This extra state ϕ_k can occur at any position relative to ϕ_ℓ and ϕ_n except precisely at their midway separation* and inspection of the denominator in the summations in equation 2.3.20 suggests that the optimum two photon transition rate can be achieved by having the third state ϕ_k as near as possible to the midway separation. Equations 2.3.20 also shows the nonlinear dependence of the two photon transition probability on the field intensity $I(\alpha\mathcal{E}^2)$ [38,48] with $P^{(2)}_{nn}(t)$ being proportional to $I^2(\alpha\mathcal{E}^4)$.

Finally, a general expression [38] for the q-photon induced transition probability, $P^{(q)}_{nn}(t)$ from state ϕ_ℓ to state ϕ_n, can be written down by induction

$$P^{(q)}_{nn}(t) = \mathcal{E}^{2q}\sin^2\tfrac{1}{2}(\omega_{n\ell}-q\nu)t\,/\,2^{2q}(\omega_{n\ell}-q\nu)^2$$

$$\times\left\{\sum_{m,k,\ldots,i,j}\frac{\mu_{nm}\mu_{mk}\cdots\mu^*_{in}\mu^*_{\ell j}}{(\omega_{m\ell}-(q-1)\nu)(\omega_{k\ell}-(q-2)\nu)\cdots(\omega_{i\ell}-(q-2)\nu)(\omega_{j\ell}-(q-1)\nu)}\right\} \qquad 2.3.21$$

where the summation indices in 2.3.21 are restricted by the requirement that the factor multiplying ν in the denominator must be greater than zero. Inspection of this general expression shows that the induced transition probability for q-photon absorption $P^{(q)}_{nn}(t)$ is proportional to $I^q(\alpha\mathcal{E}^{2q})$. In addition, to observe such nonlinear transitions, the frequency ν must lie close to $\nu\sim\omega_{n\ell}/q$ and relatively intense fields are required for higher q values; $\mathcal{E}\ll 1$ in most cases and $\mathcal{E}=1$ correspond to a field amplitude of $\sim 10^9$ Volts/cm. The effect of a general level configuration on the induced transition probability $P^{(q)}_{nn}(t)$ is reflected in the summation in equation 2.3.21 where the magnitude of this multiplicative term contributes to the overall amplitude of oscillation of $P^{(q)}_{nn}(t)$; the importance of these configurations will be described in Chapter 5.

---

* If ϕ_k occurs at the midway separation between ϕ_ℓ and ϕ_n we would also observe two stepwise single photon transitions, each of which depends linearly on $\mathcal{E}^2$ and would therefore dominate the $\mathcal{E}^4$ dependence of the two photon transition.

Using the parity selection rules for the dipole matrix elements μ_{ij} we can predict the basic types of level configurations needed to observe these q-photon nonlinear transitions. For example, in a simple two level system with states of opposite parity, all odd photon (q=1,3,5,..) transitions between states ϕ_n and ϕ_ℓ can occur ,See equation 2.3.21. To observe even photon transitions (q=2,4,6,..) requires at least three states with the initial and final states ϕ_ℓ and ϕ_n of the same parity and the third state ϕ_k of opposite parity ($\mu_{nk}\neq 0$, $\mu_{\ell k}\neq 0$). A particularly interesting case is a three state system in which transitions are being observed between the ground state ϕ_ℓ and an excited degenerate pair ϕ_n and ϕ_k, see Chapter 5. In this system all odd photon transitions are allowed between states ϕ_ℓ and ϕ_k of opposite parity while all even photon transitions are allowed between states ϕ_ℓ and ϕ_n of the same parity (ϕ_k acts as the third state of opposite parity).

While equation 2.3.21 is particularly useful for predictive purposes its practical application is severely restricted to very limited ranges of field intensity I , due to the various approximations inherent in its derivation; for example the problem of secular divergence discussed earlier and the dropping of the so-called non resonant terms in deriving it. These non resonant terms make an important contribution to frequency shifts of the resonance profile ,see Section 2.4 and Chapter 5. In addition, various relaxation or power broadening effects have not been incorporated* into the above perturbation results so that the transition probability expressions derived above predict that each q-photon resonance will appear as an infinitely narrow line centered at $\omega_{n\ell}=q\nu$. For our purposes these expressions are adequate as we are only using them as a predictive tool.

---

* Power broadening will appear naturally in the Rabi lineshape formula to be derived in the next section. In Chapter 3 this broadening will be exactly accounted for and relaxation effects will also be explicitly included in the results.

2.3.3. REMOVAL OF SECULAR DIVERGENCES FROM THE PERTURBATION EXPANSIONS OF THE DIRAC "VARIATION OF CONSTANTS METHOD".

The secular divergences appearing in the perturbation expansion of Dirac's "Variation of Constants" method ,see equation 2.2.1, restricts the method to short times even for relatively weak perturbations . [43,45,46]. These secular terms arise from the expansion of an exponential term (phase) in the wavefunction in powers of t , which in turn leads to practical difficulties as the final perturbation results have terms proportional to various powers of t ,see equation 2.3.17 for example, leading to unbounded perturbation solutions as t increases. The source of these difficulties becomes clear if we write out the known form of the exact solution to the Schroedinger equation using the Floquet theory [19],

$$\Psi(r,t) \propto \underline{Z}(t) \exp[i \underline{Q} t] \qquad 2.3.22$$

where $\underline{Z}(t) = \underline{Z}(t+2\pi/\omega)$ is a periodic matrix and $\underline{Q}$ is a constant diagonal matrix, called the characteristic exponent matrix, see Chapter 3 for details. The constant matrix $\underline{Q}$ contains the original unperturbed energy levels for the problem and their respective mean level shifts induced by the oscillating field. In the limit that the oscillating field amplitude $\mathcal{E}$ goes to zero the matrix $\underline{Q} \rightarrow \underline{E}$ where $\underline{E}$ is a diagonal matrix containing the original unperturbed energies. Comparing equation 2.3.22 with equation 2.2.1 for the expansion of the total wavefunction we observe that the state amplitudes $b_j(t)$ in equation 2.2.1 should contain an exponential term containing the level shifts for finite $\mathcal{E}$ values. The expansion of $b_j(t)$ in the perturbation series of equation 2.3.7 leads to an expansion of this exponential term in powers of t .

A number of methods have been developed to treat these secular terms arising from the perturbation expansion of the Dirac method. One such method, called "multiple time scales" perturbation theory, seeks to remove these secular divergences through each order in the perturbation expansion [43,45,46]. The basic idea in this method is to replace the time variable t by a multicomponent variable

$(t_0, t_1, t_2, \ldots)$ where $t_k = \lambda^k t$ and λ has the same meaning as before. Now the s^m order contribution to the state amplitude, $b_j^{(s)}(t)$, transforms to $b_j^{(s,k)}$ where k refers to that part of the s^m order state amplitude that depends on the time scale t_k only. An appropriate set of perturbation equations valid for each time scale are available and provide convergent solutions, within each order of λ, from which secular terms have been systematically removed. Considerable algebra is involved in deriving the final solutions and for a detailed discussion see [45,46]. Wong, Garrison and Einwohner [46] recently employed this method to study the induced transition probability in multilevel systems for an oscillating field of fixed phase. The limitations and restrictions of the multiple time scales perturbation method are discussed by these authors who show explicitly that the approximate induced transition probability rapidly goes out of phase with the numerically calculated exact result for large coupling strength.

Another method developed by Karplus, Langhoff and Epstein [43] seeks to remove both secular and normalization terms completely from the total wavefunction $\Psi(r,t)$ before carrying out a perturbation expansion on the remaining part. A detailed review of this method and its comparision with other perturbative methods is given by these authors in [43].

The difficulties encountered in a perturbation expansion of the Dirac differential equations suggests that an alternative method which reflects more precisely the true nature of the solution $\Psi(r,t)$ would be more appropriate. For a periodic Hamiltonian, the form of the solution is given by equation 2.3.22 and this prompted Young, Deal and Kestner [49] and Sen Gupta [50] to propose a direct perturbation expansion of the Floquet solution. Both the periodic matrix $\underline{\underline{F}}(t)$ and the characteristic exponent matrix $\underline{\underline{\Omega}}$ in equation 2.3.22 are expanded in ascending powers of the perturbation parameter λ. While this approach completely avoids secular behaviour it involves an eigenvalue problem, which must be solved to each order in λ. In the next Chapter both $\underline{\underline{F}}(t)$ and $\underline{\underline{\Omega}}$ will be computed exactly to any degree of

accuracy without recourse to perturbation expansions with their inherent convergence problems as a function of field intensity.

2.4 ROTATING FIELD APPROXIMATION.

The need for accurate solutions, free of the secular divergences present in perturbation theory, which are valid for relative large coupling energies $|\mu\mathcal{E}|$ and over large times, prompted Rabi [51] in 1939 to adopt a different approach to solve the time dependent Schroedinger equation. Although Rabi's method of solution was originally developed to exactly solve the problem of a two level (Spin 1/2) system interacting with a rotating magnetic field of arbitrary amplitude, it was later applied as a zeroth order problem in a perturbation treatment of the oscillating field problem by Bloch and Siegert [52] and more recently generalized to the problem of the resonant interaction of multiple oscillating fields with multilevel systems [32]. A formal analysis of the rotating field approximation and its range of validity is given by Messiah [37]. As this approximation is confined to resonant interactions ($\nu \sim \omega$) the analysis of any system with more than two levels becomes highly specific to the actual level configuration and for this reason we will only review the two level rotating field approximation in this section. Specific approximations to the problem of two oscillating fields resonantly coupled to a three level system will be dealt with in Appendix B.

The time evolution of a two level system interacting resonantly with a sinusoidal field* is described in the interaction representation ,see equation 2.2.3, by the following two coupled differential equations

---

* The oscillating field can be visualized as being made up of two rotating fields with opposite senses of rotation, each having an amplitude half that of the oscillating field [53].

$$i\partial/\partial t\, b_1(t) = -\frac{\mu_{12}\mathcal{E}}{2}\left\{ \exp[-i(\omega_{21}-\nu)t] + \exp[-i(\omega_{21}+\nu)t] \right\} b_2(t)$$

$$i\partial/\partial t\, b_2(t) = -\frac{\mu_{21}\mathcal{E}}{2}\left\{ \exp[i(\omega_{21}+\nu)t] + \exp[i(\omega_{21}-\nu)t] \right\} b_1(t) \qquad 2.4.1$$

where* $\omega_{21} = E_2 - E_1 > 0$, and $b_j(t)$, j=1 and 2, are the amplitudes of the states $\phi_j(r)\exp[-iE_jt]$, j=1 and 2. If we consider, for example, the resonant absorption of a photon of frequency ν from the ground state $\phi_1(r)$ to an excited state $\phi_2(r)$ of opposite parity to $\phi_1(r)$ (that is $b_1(0) = 1$ at $t=0$), one of the exponential terms occurring in each of the above coupled differential equations will be slowly varying (since $\omega_{21}-\nu \simeq 0$) while the second exponential where $(\omega_{21}+\nu) \simeq 2\nu$ will be rapidly oscillatory. The slowly varying term $\exp[i(\omega_{21}-\nu)t]$ is the main contributor to the change in state amplitudes $b_j(t)$ while the term $\exp[i(\omega_{21}+\nu)t]$ is rapidly oscillatory and its contribution to $b_j(t)$ will average to zero.** Thus the "anti-resonant" term $\exp[i(\omega_{21}+\nu)t]$ is neglected relative to the resonant term and equation 2.4.1 reduces to

$$i\partial/\partial t\, b_1(t) = -\frac{\mu_{12}\mathcal{E}}{2}\exp[-i(\omega_{21}-\nu)t]\, b_2(t)$$

$$i\partial/\partial t\, b_2(t) = -\frac{\mu_{21}\mathcal{E}}{2}\exp[i(\omega_{21}-\nu)t]\, b_1(t) \qquad 2.4.2$$

It should be emphasised that in principle these equations are a good

---

* The phase dependence of the sinusoidal field is ignored as it cancels in the final physical result in the rotating field approximation.

** This statement is only strictly true as long the period of oscillation of the state amplitudes $b_j(t)$ is much greater than the period of oscillation of the coefficient $\exp[i(\omega_{21}+\nu)t]$. This is a particular example of the " Method of Averaging" ,referred to in the next chapter

approximation only when $\omega_{21}-\nu \sim 0$, that is on or near resonance. These equations can be easily transformed to two coupled differential equations with constant coefficients by a suitable transformation of the state amplitudes $b_j(t)$ and the resulting differential equations solved by standard Laplace transform techniques, See Appendix B and [54]. The final solutions for the state amplitudes $b_j(t)$ are

$$b_1(t) = \frac{\exp\left[-i(\omega_{21}-\nu)t/2\right]}{\sqrt{(\omega_{21}-\nu)^2+|\mu_{12}\mathcal{E}|^2}}\left\{\sqrt{(\omega_{21}-\nu)^2+|\mu_{12}\mathcal{E}|^2}\cos\tfrac{1}{2}\sqrt{(\omega_{21}-\nu)^2+|\mu_{12}\mathcal{E}|^2}\,t - i(\omega_{21}-\nu)\sin\tfrac{1}{2}\sqrt{(\omega_{21}-\nu)^2+|\mu_{12}\mathcal{E}|^2}\,t\right\}$$

$$b_2(t) = \frac{-i|\mu_{12}\mathcal{E}|\exp\left[i(\omega_{21}-\nu)t/2\right]}{\sqrt{(\omega_{21}-\nu)^2+|\mu_{12}\mathcal{E}|^2}}\sin\tfrac{1}{2}\sqrt{(\omega_{21}-\nu)^2+|\mu_{12}\mathcal{E}|^2}\,t \qquad 2.4.3$$

The corresponding induced transition probability $P_{22}^R(t)$ for the transition $1\to 2$ is given by

$$P_{22}^R(t) = \frac{|\mu_{12}\mathcal{E}|^2}{(\omega_{21}-\nu)^2+|\mu_{12}\mathcal{E}|^2}\sin^2\tfrac{1}{2}\sqrt{(\omega_{21}-\nu)^2+|\mu_{12}\mathcal{E}|^2}\,t \qquad 2.4.4$$

Equation 2.4.4 is the Rabi formula and from it we see that the induced transition probability $P_{22}^R(t)$ is bounded for arbitrarily long times. Equation 2.4.4 assumes a particularly simple form when the frequency of the applied sinusoidal field is exactly on resonance ($\nu=\omega_{21}$)

$$P_{22}^R(t) = \sin^2|\mu_{12}\mathcal{E}|t/2 \qquad 2.4.5$$

Therefore, according to the rotating field approximation, when the applied field is exactly on resonance, the transition probability oscillates between 0 and 1 with a period of $2\pi/|\mu_{12}\mathcal{E}|$ in t.

It is instructive to compare the Rabi formula (equation 2.4.4) with the simple first order perturbation result $P_{22}^{(1)}(t)$, given by equation 2.3.16. These equations differ in that the Rabi formula contains the additional term $|\mu_{12}\mathcal{E}|$ in the denominator and in the argument of the Sine. Thus while the perturbation result "blows up" on resonance ($\nu=\omega_{21}$) the Rabi formula remains bounded and the transition probability oscillates in time. In the limit that $|\mu_{12}\mathcal{E}| \ll (\omega_{21}-\nu)$ the Rabi formula reduces to the simple perturbation result indicating that the perturbation result is severely restricted to small coupling energies $|\mu_{12}\mathcal{E}|$ as well as small times.

The Rabi result for the time averaged induced transition probability $\bar{P}_{22}^{R}$ can be obtained directly from equation 2.4.4 if we replace the $\sin^2$ term by its long time average or steady state result of 1/2;

$$\bar{P}_{22}^{R} = \lim_{T\to\infty} \frac{1}{T}\int_{0}^{T} P_{22}^{R}(t)\,dt = \frac{|\mu_{12}\mathcal{E}|^2}{2[(\nu-\omega_{21})^2 + |\mu_{12}\mathcal{E}|^2]} \qquad 2.4.6$$

Thus, the Rabi formula predicts that the single photon resonance profile is a Lorentzian peaking at $\bar{P}_{22}^{R} = 0.5$ when $\nu = \omega_{21}$. The half-width at half maximum of this Lorentzian is given by $\Gamma = |\mu_{12}\mathcal{E}|$ and as $\bar{P}_{22}^{R} = \bar{P}_{11}^{R} = 0.5$ when $\nu = \omega_{21}$, both states are equally populated (saturated) so that no further absorption of energy can occur. For this reason the term $|\mu_{12}\mathcal{E}|$ in the denominator of equation 2.4.6 is called the "saturation broadening" parameter or power broadening parameter. Thus as the field intensity is increased the resonance profile broadens and ultimately disappears in the Rabi approximation.

The Rabi lineshape formula (equation 2.4.6) is valid on the assumption that relaxation effects, such as spontaneous decay and collision damping, can be neglected relative to the saturation broadening term $|\mu_{12}\mathcal{E}|$. Such is not the case however in many situations and these relaxation effects must be incorporated explicitly in the above results. One of the most satisfactory methods of including such damping effects, which will be adequate for the results derived here and later, is based on collision damping.* This simple collision model assumes that the molecules in a gas, when interacting with the external oscillating field, can undergo random collisions which interrupt the radiation process. The probability that a molecule has survived under this interaction with the field in the interval $(t-t_0)$, where t_0 is the initial instant at which the interaction began, is given by [9,34,55]

---

* A general theory of collision damping is available which takes into account the detailed form of the interaction potential $V(r)$ between individual atoms or molecules [41,55]. For our purposes a simple collision model based on hard collisions will suffice, see below.

$\frac{1}{\tau} \exp\left[-(t-t_0)/\tau\right] dt_0$

where τ is the mean collision time and t represents the time of measurement. As $\rho_{22}^{R}(t)$ describes the interaction of a single molecule with the external field, the transition probability for an ensemble of molecules in a gas is obtained by averaging this quantity over the elapsed times $(t-t_0)$ and is given by [9,34,55]

$$\bar{\rho}_{22}^{R,\tau} = \frac{1}{\tau} \int_{-\infty}^{t} \rho_{22}^{R_q}(t-t_0) \exp\left[-(t-t_0)/\tau\right] dt_0 \qquad 2.4.7$$

Substituting equation 2.4.4 for $\rho_{22}^{R}(t)$ into equation 2.4.8 and integrating we obtain

$$\bar{\rho}_{22}^{R,\tau} = \frac{|\mu_{12}\mathcal{E}|^2}{2\left[(\nu-\omega_{21})^2 + |\mu_{12}\mathcal{E}|^2 + \tau^{-2}\right]} \qquad 2.4.8$$

While the resonance profile still retains its Lorentzian lineshape, the half width is now given by $\Gamma = \left(|\mu_{12}\mathcal{E}|^2 + \tau^{-2}\right)^{1/2}$. As long as $\tau^{-1} \gg |\mu_{12}\mathcal{E}|$, which is the case for most conventional field amplitudes, we do not observe saturation effects, that is $\bar{\rho}_{22}^{R,\tau} \neq \bar{\rho}_{11}^{R,\tau}$. Increasing the oscillating field amplitude $\mathcal{E}$ causes the transition to gradually saturate ($\bar{\rho}_{22}^{R,\tau} = \bar{\rho}_{11}^{R,\tau} = 0.5$) and the system being irradiated no longer absorbs power from the external field. This situation is described as optical bleaching and has been observed experimentally with intense laser beams [38]. Breene [55] has discussed the equivalence of the constant τ^{-1} to the radiative width γ of the excited state ($\gamma = \gamma_j$; $j = 1, 2, \ldots$; γ is taken to be equal for all states) in the limit that the gas becomes very dilute. In fact the constant τ can also represent the mean transit time of a molecule through a finite laser beam width [9] or the mean transit time of molecules through a molecular beam C-field region [9]. In general, in equation 2.4.8, τ represents the mean interaction time for the induced radiative process to which the several mechanisms outlined above can contribute so that in effect $\tau^{-1} = \tau_{RAD}^{-1} + \tau_{COLL}^{-1} + \tau_{BEAM}^{-1} + \cdots$; usually $\tau_{COLL}^{-1}, \tau_{BEAM}^{-1} \gg \tau_{RAD}^{-1}$ [9].

The importance of the nonresonant terms ignored in deriving the Rabi formula (Compare equations 2.4.1 and 2.4.2) was initially recognised by Bloch and Siegert [52] who included their contribution

to first order in perturbation theory using the Rabi approximation as the zeroth order problem. While these terms do not appreciably effect the shape or width of the spectral profile ,see equation 2.4.6, over the range of coupling energies $|\mu_{12}\mathcal{E}|$ for which the Rabi formula is valid, see for example Chapter 4, they do cause an appreciable shift of this profile from the centre frequency ($\nu = \omega_{21}$) predicted by the lineshape formula given by equation 2.4.6. The first order contribution to this shift is called the "Bloch-Siegert" shift and is given by [52]

$$\nu_{RES} - \omega_{21} = \delta\omega_{21} = \frac{|\mu_{12}\mathcal{E}|^2}{4\omega_{21}} \qquad 2.4.9$$

which predicts that the resonance shift increases in direct proportion to the coupling energy squared. In recent years the need for much more accurate frequency shifts has prompted a number of authors to extend the perturbation expansion up to tenth order[13,17,18].

Since the counter rotating terms are omitted in the derivation of the Rabi approximation, this approximation unlike perturbation theory can only account for the single photon transition ($\nu \sim \omega_{21}$). To account for n-photon transitions in multilevel systems within a rotating field type approximation, resonant terms of the form $\exp[i(\omega_{ji} - n\nu)t]$ must be extracted from the differential equations in the interaction representation and the remaining oscillatory terms dropped. Shirley [56,57] describes an elegant method for achieving this extraction which he calls the " Phase Factoring " method and this method yields equivalent results to those obtained in earlier treatments due to Salwen [58] and Besset, Horowitz, Messiah and Winter [20]. The basic idea behind this approach is to extract the n-photon resonant term ($\omega_{ji} - n\nu$) by redefining the state amplitudes as $b_j(t) = C_j(t)\exp[i\alpha_j t]$ and choosing the phase factor α_j appropriately. The effect of nonresonant terms can be accounted for by perturbation corrections [56,57] and Shirley points out that this treatment is limited to situations in which resonance lines do not overlap and to relatively weak oscillating field strengths. It should also be pointed out that while nonresonant interactions contribute mainly to resonant frequency shifts, they can also cause large

distortions of the n-photon resonance profile from its Lorentzian shape predicted by the rotating field approximation, particularly when the coupling energy $|\mu\mathcal{E}|$ becomes comparable in magnitude with the energy level separation ω, see Chapter 4. For these values of $|\mu\mathcal{E}|$ the phase dependence of the induced transition probabilities, which is neglected in the rotating field approximation and perturbation theory, is important. In such situations the time dependent Schroedinger equation must be solved exactly and the next chapter is concerned with the developement of an exact computationally convenient solution to the more general problem of a multilevel system of arbitrary configuration interacting with a field of arbitrary amplitude $\mathcal{E}$, frequency ν and phase δ.

CHAPTER 3

GENERAL N-LEVEL SYSTEM INTERACTING WITH A SINUSOIDAL FIELD

In the discussions of the previous chapter the need for a computationally convenient solution to the problem of a multilevel system of arbitrary configuration interacting with a sinusonidal field of arbitrary amplitude ,frequency and phase became apparent. The fact that even the simple two-level system does not admit an exact solution in terms of tabulated functions [14] dictates the need for some form of numerical integration. In this chapter an exact computationally convenient solution to the general multi-level system is developed and the theory of linear differential equations with periodic coefficients [19,61,62] is exploited to recast the general solution in a form suitable for the evaluation of some physically interesting steady state properties of the system. In addition the formal method of solution developed herein is equally applicable to the study of both degenerate and non-degenerate systems .

3.1 MATRIX REPRESENTATION FOR THE SOLUTION OF THE TIME DEPENDENT SCHROEDINGER EQUATION.

Both for complete generality and convenience of presentation matrix notation will be adopted throughout, making detailed specification of the system unnecessary. The two-level and certain N-level systems will be dealt with in chapters 4 and 5. The total time dependent wavefunction $\Psi(r,t)$ in the Schroedinger representation can be written in matrix form as follows

$$\underline{\Psi}(r,t) = \underline{\underline{\Phi}}(r)\,\underline{Q}(t) \qquad 3.1.1$$

where

$$\underline{\underline{\Phi}}(r) = (\phi_1(r), \phi_2(r), \ldots \phi_N(r)) \quad , \quad \underline{\underline{a}}(t) = \begin{pmatrix} a_1(t) \\ a_2(t) \\ \vdots \\ a_N(t) \end{pmatrix} \qquad 3.1.2$$

and equation 2.2.2 becomes

$$\underline{\underline{a}}(t)\, \underline{\underline{a}}^{\dagger}(t) = 1 \qquad 3.1.3$$

which ensures normalisation of the wavefunction for all times. Following a similar developement to that in Section 2.2, Chapter 2, the time dependent coefficients $a_j(t)$, in the dipole approximation [26,38] , satisfy the coupled first order differential equations

$$i\,\partial/\partial t\, \underline{\underline{a}}(t) = \underline{\underline{E}}\, \underline{\underline{a}}(t) - \mathcal{E}\, \underline{\underline{\mu}} \cos(\nu t + \delta)\, \underline{\underline{a}}(t) \qquad 3.1.4$$

where

$$\underline{\underline{E}} = \begin{pmatrix} E_1 & 0 & 0 & 0 & \cdots & 0 \\ 0 & E_2 & 0 & 0 & \cdots & 0 \\ \vdots & & & & & \\ & & & & & E_N \end{pmatrix} \; ; \; \underline{\underline{\mu}} = \begin{pmatrix} \mu_{11} & \mu_{12} & \cdots & \mu_{1N} \\ \mu_{21} & \mu_{22} & \cdots & \mu_{2N} \\ \vdots & & & \\ \mu_{N1} & & \cdots & \mu_{NN} \end{pmatrix} \qquad 3.1.5$$

As discussed earlier $\phi_j(r)$ and E_j are the wavefunction and the energy of the j^{th} stationary state of the unperturbed system, $\mathcal{E}$ and ν are the strength and frequency of the applied sinusoidal field which we arbitrarily take to be directed along the z co-ordinate axis, δ is an arbitrary phase which will prove quite important for large coupling strength $|\mu\mathcal{E}|$, see Chapter 4 and 5 for details, and the μ_{ij} are transition dipole matrix elements coupling the i^{th} and j^{th} stationary states, $\mu_{ij} = \mu_{ji} = \langle \phi_i(r) | \mu_z | \phi_j(r) \rangle$. The dipole matrix $\underline{\underline{\mu}}$ will have a zero diagonal in general which considerably reduces the computational labour in solving equation 3.1.4.* It will become

---

* If an additional static field is introduced in the total Hamiltonian, the $\underline{\underline{E}}$ matrix will contain off-diagonal nonzero elements. In this situation the symmetry arguments used, later in this chapter and in Appendix A, to expedite computation over the period of the Hamiltonian $H(r,t)$ will not hold.

obvious that both degenerate and non-degenerate systems are totally equivalent when solved exactly so that a zero diagonal dipole matrix may be consistently used to expedite computation . This equivalence will be explicitly shown in Chapter 5 but for completeness the modifications that are necessary when $\underline{\mu}$ has a nonzero diagonal will also be discussed, see Appendix A2.

The problem at hand is to solve equation 3.1.4 for the time-dependent expansion coefficients $\underline{a}(t)$ subject to the initial conditions, see Chapter 2.

$$\underline{a}(0) = \underline{A} \qquad 3.1.6$$

where $\underline{A}$ is a column matrix of known constants , $a_j(0) = A_j$ with $j=1,2,\ldots,N$,satisfying $\underline{a}^\dagger(0)\underline{a}(0) = 1$.

Although the formal method of solution will be developed to solve equation 3.1.4 for the state amplitudes $a_j(t)$,the final physical properties extracted from these solutions are more conveniently discussed in terms of the density matrix.

The matrix representation of the coupled differential equations for the state amplitudes $a_j(t)$,given by equation 3.1.4 ,leads naturally to a representation of the final physical results in terms of the density matrix $\underline{\rho}(t)$. The density matrix $\underline{\rho}(t)$ is defined in terms of the state amplitudes $\underline{a}(t)$ as follows

$$\underline{\rho}(t) = \underline{a}(t)\underline{a}^\dagger(t) = \begin{pmatrix} |a_1(t)|^2 & a_1(t)a_2^*(t) & \cdots \\ a_2(t)a_1^*(t) & |a_2(t)|^2 & \cdots \\ \vdots & \vdots & \\ a_N(t)a_1^*(t) & \cdots & |a_N(t)|^2 \end{pmatrix} \qquad 3.1.7$$

and an individual matrix element is given by

$$\rho_{kj}(t) = a_k(t)\,a_j^*(t) \qquad 3.1.8$$

The differential equation satisfied by $\underline{\rho}(t)$ can be derived by first differentiating equation 3.1.7 to yield

$$i\partial/\partial t\,\underline{\rho}(t) = \underline{a}(t)\left(i\partial_{\partial t}\underline{a}^\dagger(t)\right) + \left(i\partial_{\partial t}\underline{a}(t)\right)\underline{a}^\dagger(t) \qquad 3.1.9$$

Next ,using equation 3.1.4 ,its adjoint and the fact that the matrices $\underline{E}$ and $\underline{\mu}$ are real leads to the familar differential equation satisfied

by $\underline{\rho}(t)$

$$i\,\partial/\partial t\,\underline{\rho}(t) = [\underline{E}, \underline{\rho}(t)] - \mathcal{E}\cos(\omega t+\delta)[\underline{\mu}, \underline{\rho}(t)] \qquad 3.1.10$$

where [A, B] is a commutator, for example

$$[\underline{A}, \underline{B}] = \underline{A}\underline{B} - \underline{B}\underline{A} \qquad 3.1.11$$

It is easy to show that the normalization condition, given by equation 3.1.3 now becomes

$$\mathrm{tr}\,\underline{\rho}(t) = \sum_{j=1}^{N} \rho_{jj}(t) = 1 \qquad 3.1.12$$

where tr refers to the trace of a matrix. Finally, the expectation value of any operator $\mathcal{L}(r,t)$ with respect to the total wavefunction $\Psi(r,t)$ is given by

$$\langle \Psi(\bar{r},t) | \mathcal{L}(r,t) | \Psi(r,t) \rangle = \sum_{k,j} a^{*}_{k}(t)\, a_{j}(t) \langle \phi_{k}(r) | \mathcal{L}(r,t) | \phi_{j}(r) \rangle$$

$$= \sum_{k,j} \rho_{jk}(t)\, \mathcal{L}_{kj}(r,t) = \mathrm{tr}\left[\underline{\rho}(t)\,\underline{\mathcal{L}}(r,t)\right] \qquad 3.1.13$$

where an element of the matrix $\underline{\mathcal{L}}(r,t)$ is given by

$$\mathcal{L}_{ij} = \langle \phi_{i}(r) | \mathcal{L}(r,t) | \phi_{j}(r) \rangle \qquad 3.1.14$$

Equation 3.1.13 will prove particularly useful in Section 4.6 where the physical properties of an N-level system interacting with a sinusoidal field will be discussed.

3.2 POWER SERIES SOLUTION

The power series solution is a familiar means of solving linear differential equations which do not admit analytic solutions [63]. Equations 3.1.4 should in principle provide no difficulty as the coefficients are devoid of singularities, so that the only foreseeable problem which may arise would be slow convergence of the power series expansions and this in fact is the major difficulty encountered in their solution. Equations 3.1.4 have many analogues occurring predominantly in classical mechanics and these have been subjected to extensive formal investigations by mathematicians over the years [19,61,62].

The major difficulty arising in the solution to equations 3.1.4 is the occurrence of two time scales in the problem, one the time scale over which the periodic coefficients in these differential equations oscillate and ,secondly , the time scale over which the functions $\underline{\underline{Q}}(t)$ change appreciably. The latter time scale is normally much longer than the former, particularly when the perturbations arising from the oscillatory coefficients are weak, and a number of approximation methods have been developed to deal with such situations [19,61,62,64]. These approximation methods all assume that the system is basically a linear system weakly perturbed by the oscillating field. Hence any change in the system occurring over the period of the perturbation [short time scale] can be averaged out reducing the problem to a single time scale. The classic example in the solution to the differential equations of the Dirac method is the "ROTATING FIELD APPROXIMATION".

For our purposes equation 3.1.4 needs to be solved for arbitrary coupling strength $|\mu\mathcal{E}|$, frequency ν and phase δ (or equivalently starting times t_0 [13]) of the applied field. Of particular interest is the region where $|\mu\mathcal{E}|$ is large as it is over this range that most nonlinear spectroscopic effects become important. Clearly for these values of $|\mu\mathcal{E}|$ the short time scale over which the perturbation varies becomes increasingly important. In the spirit of the above discussion we adopt the short time scale as the natural variable for the problem and set $\theta = \nu t + \delta$. With this definition equation 3.1.4 transforms to

$$i\nu \partial/\partial\theta \, \underline{\underline{Q}}(\theta) = \underline{\underline{E}} \, \underline{\underline{Q}}(\theta) - \mathcal{E} \cos\theta \, \underline{\underline{\mu}} \, \underline{\underline{Q}}(\theta) \qquad 3.2.1$$

and equation 3.1.6 to

$$\underline{\underline{Q}}(\delta) = \underline{\underline{A}} \qquad 3.2.2$$

The following section will be devoted to solving equation 3.2.1 subject to equation 3.2.2 by using a matching power series expansion technique.

3.2.1 EXPANSION AND MATCHING OF SOLUTIONS OVER INTERVAL LENGTHS OF π IN THE VARIABLE $\theta = \nu t + \delta$.

For the reasons discussed earlier a conventional power series expansion of $\underline{Q}(\theta)$ in powers of the variable θ would meet with severe convergence difficulties due to the oscillatory nature of the coefficients in equation 3.2.1. Inspection of equation 3.2.1 shows explicitly that the coefficients have a period in θ of 2π so that equation 3.2.1 has the same general form over adjoining 2π θ-intervals. This immediately suggests a direct expansion of $\underline{Q}(\theta)$ in powers of θ over a limited range of θ $(0 \leq \theta \leq 2\pi)$, followed by a re-expansion over the same range in subsequent 2π θ-intervals. Matching of the solution at adjoining interval boundaries yields the solution $\underline{Q}(\theta)$, at least in principle, for arbitrary values of the variable θ.

If equation 3.2.1 is decoupled and written as a set of N, N^{th}- order, differential equations for each of the N individual amplitudes $Q_j(\theta)$, it is found that the coefficients of the differential equations satisfied by these amplitudes have a period of π in the variable θ (an explicit example is given for a two-level system later). It is therefore computationaly convenient to set a π-interval as the upper limit on the range of the power series expansion*. Making the transformation

$$(\nu t + \delta) = \theta = \gamma + n\pi \,, \qquad n = 0, 1, 2, \ldots \qquad 3.2.3$$

equations 3.2.1 on the appropriate θ-interval transform to

---

* It will be seen later that for very strong coupling the solution will even slowly converge for this choice of expansion interval, so that a further reduction in interval size becomes necessary.

$$\frac{\partial}{\partial\gamma}\underline{Q}^{(n)}(\gamma) = \frac{1}{i\nu}\left\{\underline{\underline{E}}\,\underline{Q}^{(n)}(\gamma) + (-1)^{n+1}\varepsilon\cos\gamma\,\underline{\underline{M}}\,\underline{Q}^{(n)}(\gamma)\right\} \qquad 3.2.4$$

and equation 3.2.2 becomes

$$\underline{Q}^{(0)}(\delta) = \underline{A} \qquad 3.2.5$$

Coupled power series solutions to equation 3.2.4 are readily obtained and are given by

$$\underline{Q}^{(n)}(\gamma) = \sum_{\ell=0}^{\infty}\underline{C}_{\ell}^{(n)}\gamma^{\ell} \qquad 3.2.6$$

where

$$\underline{C}_{\ell+1}^{(n)} = \frac{1}{i\nu(\ell+1)}\left\{\underline{\underline{E}}\,\underline{C}_{\ell}^{(n)} + (-1)^{n+1}\varepsilon\sum_{m=0}^{\infty}\frac{(-1)^m}{(2m)!}\underline{\underline{M}}\,\underline{C}_{\ell-2m}^{(n)}\right\} \qquad 3.2.7$$

Here $\ell - 2m \geq 0$ and from equation 3.2.6 it follows that

$$\underline{Q}^{(n)}(0) = \underline{C}_{0}^{(n)} \qquad 3.2.8$$

From equations 3.2.3-3.2.8 the matching requirement follows

$$\underline{Q}^{(n)}(\pi) = \underline{Q}^{(n+1)}(\delta) \equiv \underline{C}_{0}^{(n+1)} \qquad 3.2.9$$

Equations 3.2.7 and 3.2.6 can be used to obtain $\underline{Q}(\theta)$ in a stepwise manner by adopting the following computational procedure:

(i). Use equation 3.2.5 to set the appropriate initial conditions on equation 3.2.4 for a particular choice of phase δ of the sinusoidal field.

(ii). Generate the expansion coefficients $\underline{C}_{\ell}^{(0)}$ valid for the θ-interval $[0,\pi]$ by using equation 3.2.7 with n=0.

(iii). Reset $\underline{Q}^{(0)}(\pi)$ to $\underline{C}_{0}^{(1)}$ and generate the expansion coefficients $\underline{C}_{\ell}^{(1)}$ for the interval $[\pi,2\pi]$ by using equation 3.2.7 with n=1.

(iv). Reset $\underline{Q}^{(1)}(\pi)$ to $\underline{C}_{0}^{(2)}$ and repeat step (ii) for the θ-interval $[2\pi,3\pi]$.

(v). Iterate over any number of required θ-intervals.

It should be pointed out at this stage that the above matching power series scheme need only be used at most over the first $[0,2\pi]$ interval. In Sections 3.3 and 3.4 a much more efficient iterative method will be employed to carry the solution to larger values of θ.

In the above definition of γ the actual variable of the problem is ωt, with the phase* δ serving only to reset the ωt origin to different points along the sine wave, see Figure 3.1. In actual practice the above computational procedure is adopted only for $\delta = 0$, the solution for arbitrary δ being readily generated from this by a simple transformation, see Sections 3.3 and 3.4.

3.2.2 EXPANSION SUB-INTERVALS OF γ. $[n\pi \leq \gamma \leq (n+1)\pi]$

As mentioned previously equation 3.2.6 may only slowly converge, particularly in the very strong coupling $|\mu\varepsilon|$ limit. In such cases the expansion interval length of π in the variable θ must be further reduced to ensure rapid convergence of the power series expansion. This reduction in expansion interval size further reduces the symmetry of the problem and this section outlines a general method of solution using an arbitrary sub-interval expansion length.

The oscillatory coefficients in equation 3.2.4 must be modified so that they reflect the behaviour of the differential equations over the expansion sub-interval of interest. To achieve this the term $(-1)^n \cos\gamma$ in equation 3.2.4 will be replaced by the more general term

$$\cos(\gamma+\alpha) = \cos\gamma\cos\alpha - \sin\gamma\sin\alpha \qquad 3.2.10$$

The role of the phase factor α is solely to generate the coefficients of equation 3.2.1 appropriate to the sub-interval of interest on the θ-interval $[n\pi, (n+1)\pi]$. Equation 3.2.4 over this interval becomes

$$\partial/\partial\gamma\, \underline{Q}^{(n)}(\gamma) = \frac{1}{i\nu}\left\{\underline{E}\,\underline{Q}^{(n)}(\gamma) - \varepsilon[\cos\gamma\cos\alpha - \sin\gamma\sin\alpha]\underline{M}\,\underline{Q}^{(n)}(\gamma)\right\} \qquad 3.2.11$$

and the following recurrence relations can be easily derived for the

---

* The phase δ is equivalent to the initial time t_o at which the system is instantaneously exposed to some point along the sinusoidal wave. For weak couplings this phase dependence is unimportant and is ignored in most treatments of the problem. However in the strong coupling region it becomes extremely important [22,28].

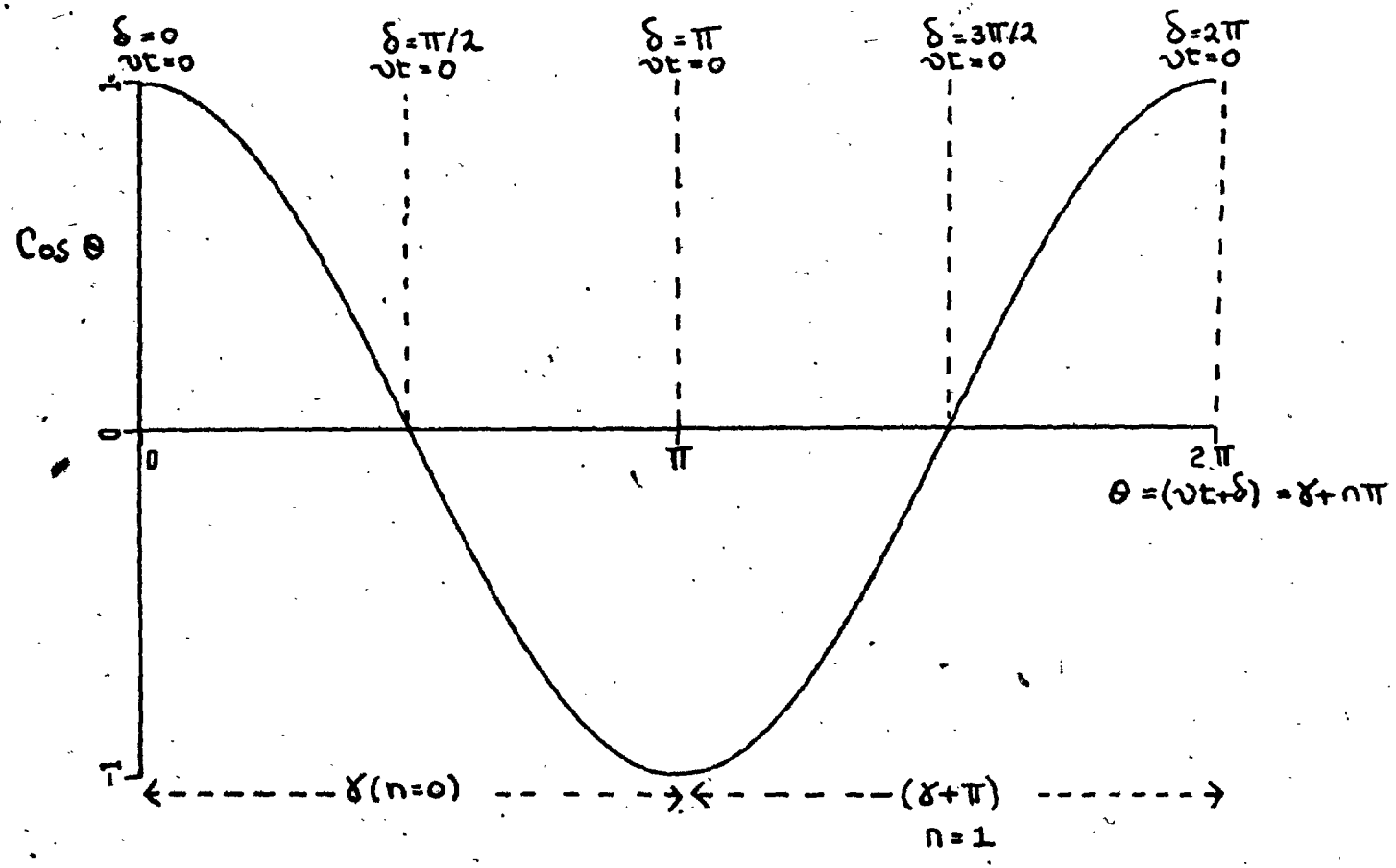

Figure 3.1. The behaviour of the oscillatory coefficient, Cos θ, in the differential equations, given by equation 3.2.1, over one period of θ. This figure shows explicitly how the time origin (νt=0) is located with respect to the θ(≡νt + δ) origin as a function of phase δ.

power series expansion coefficients $\underline{\underline{C}}_{\ell}^{(n)}$ [equation 3.2.6]

$$\underline{\underline{C}}_{\ell+1}^{(n)} = \frac{1}{(\ell+1)\omega}\left\{\underline{\underline{E}}\,\underline{\underline{C}}_{\ell}^{(n)} - \mathcal{E}\left[\cos\alpha \sum_{m=0}^{\infty}\frac{(-1)^m}{(2m)!}\underline{\underline{M}}^{2m}\,\underline{\underline{C}}_{\ell-2m}^{(n)} + \sin\alpha \sum_{m=0}^{\infty}\frac{(-1)^{2m+1}}{(2m+1)!}\underline{\underline{M}}^{2m+1}\,\underline{\underline{C}}_{\ell-2m-1}^{(n)}\right]\right\} \qquad 3.2.12$$

Equation 3.2.12 is a generalisation of the recurrence relation given by equation 3.2.7 for any arbitrary expansion sub-interval length on the $[n\pi,(n+1)\pi]$ θ-interval. In actual practice this recurrence relation will only be used at most on the first $[0,2\pi]$ θ-interval while the more efficient iterative method to be discussed in Sections 3.3 and 3.4 will be employed to carry the solution to larger values of θ. In order to illustrate the computational procedure over the $[0,\pi]$ interval Table I lists the coefficients in equation 3.2.11 appropriate to each sub-interval for both $\pi/2$ and $\pi/4$ expansion sub-intervals. Further details regarding the optimum choice of expansion sub-interval for a particular coupling strength $|\mu\mathcal{E}|$ will be given in Appendix A.1.

3.3 ITERATIVE SOLUTION OVER ADJOINING θ-INTERVALS OF LENGTH π.

While the above matching power series method is vastly superior to conventional numerical techniques [28,65] it still requires recomputation of (NxK) expansion coefficients $\underline{\underline{C}}_{\ell}^{(n)}$ for each θ-interval where K+1 corresponds to the number of terms retained in the power series expansion, given by equation 3.2.6, to ensure convergence of the solution to the desired accuracy;

$$\underline{\underline{Q}}^{(n)}(\gamma) = \sum_{\ell=0}^{K}\underline{\underline{C}}_{\ell}^{(n)}\gamma^{\ell}. \qquad 3.3.1$$

However according to the general theory of ordinary differential equations, the general solution to any N^{th}-order differential equation (or equivalent system of N first order differential equations) contains at most N arbitrary constants. In the power series expansion of each element $Q_j^{(n)}(\gamma)$ in equation 3.3.1, of the K+1 constants $C_{j,\ell}^{(n)}$ occurring in this expansion only $C_{j,0}^{(n)}$ is arbitrary with the K other constants $C_{j,\ell}$, $\ell=1,\ldots,K$, being directly dependent on it. This allows equation 3.3.1 to be regrouped into N parts that are proportional to the yet arbitrary constants $C_{j,0}$, $j=1,2,\ldots N$, for each

TABLE I, The oscillatory coefficients, $(\cos\gamma \cos\alpha - \sin\gamma \sin\alpha)$, of the differential equations given by equation 3.2.11 for (a) a $\pi/2$ expansion sub-interval and (b) a $\pi/4$ expansion sub-interval.

(a) $0 \leq \gamma \leq \pi/2$

$\alpha = 0$	$\cos\gamma$	$0 \leq \theta \leq \pi/2$
$\alpha = \pi/2$	$-\sin\gamma$	$\pi/2 \leq \theta \leq \pi$

(b) $0 \leq \gamma \leq \pi/4$

$\alpha = 0$	$\cos\gamma$	$0 \leq \theta \leq \pi/4$
$\alpha = \pi/4$	$[\cos\gamma - \sin\gamma]/\sqrt{2}$	$\pi/4 \leq \theta \leq \pi/2$
$\alpha = \pi/2$	$-\sin\gamma$	$\pi/2 \leq \theta \leq 3\pi/4$
$\alpha = 3\pi/4$	$[\cos\gamma + \sin\gamma]/\sqrt{2}$	$3\pi/4 \leq \theta \leq \pi$

θ π-interval. Writing out this result for the first θ-interval $[0,\pi]$ one obtains

$$\underline{a}^{(0)}(\gamma) = \underline{f}(\gamma)\,\underline{C}_0^{(0)} \qquad 3.3.2$$

and for the second θ-interval $[\pi,2\pi]$

$$\underline{a}^{(1)}(\gamma) = \underline{g}(\gamma)\,\underline{C}_0^{(1)} \qquad 3.3.3$$

where for the case in which the matrix $\underline{\mu}$ has zero diagonal elements the individual matrix elements of $\underline{f}(\gamma)$ and $\underline{g}(\gamma)$ are related as follows ,see Appendix A2,

$$f_{ij}(\gamma) = g_{ij}(\gamma) \quad , \mu_{ij} = 0$$

$$f_{ij}(\gamma) = -g_{ij}(\gamma) \quad , \mu_{ij} \neq 0 \qquad 3.3.4$$

In the case where $\underline{\mu}$ has nonzero diagonal elements such a simple relation does not exist between the elements of $\underline{f}(\gamma)$ and $\underline{g}(\gamma)$ and both matrices must be computed separately. The following generalization of 3.3.2 and 3.3.3 to any n^{th} π-interval of θ is obvious

$$\underline{a}^{(n)}(\gamma) = \underline{f}(\gamma)\,\underline{C}_0^{(n)} \qquad n \text{ even}$$

$$\underline{a}^{(n)}(\gamma) = \underline{g}(\gamma)\,\underline{C}_0^{(n)} \qquad n \text{ odd} \qquad 3.3.5$$

In general the matrix $\underline{f}(\gamma)$, and hence $\underline{g}(\gamma)$, which are independent of n and therefore have the same power series expansion in terms of γ on the appropriate adjoining θ π-intervals, are complicated functions of the parameters $|\mu\varepsilon|$, E_j and v. The elements of these matrices can be projected out of equation 3.2.6 by employing the following matrix technique.

It is clear from equations 3.2.6 and 3.2.7 for $n=0$ that the matrix $\underline{f}(\gamma)$ in equation 3.3.2 can be expanded as a power series in γ

$$\underline{f}(\gamma) = \sum_{\ell=0}^{\infty} \underline{a}_\ell\, \gamma^\ell \qquad 3.3.6$$

where, see equation 3.2.7, the recurrence relations for the expansion matrices are given by

$$\underline{a}_{\ell+1} = \frac{1}{i\omega(\ell+1)}\left\{ \underline{E}\,\underline{a}_\ell + (-1)\;\varepsilon \sum_{m=0}^{\infty} \frac{(-1)^m}{(2m)!}\,\underline{\mu}\,\underline{a}_{\ell-2m} \right\} \qquad 3.3.7$$

and

$$\underline{\underline{Q}}_\ell = \begin{pmatrix} q^\ell_{11} & q^\ell_{12} & \cdots & q^\ell_{1N} \\ q^\ell_{21} & q^\ell_{22} & & q^\ell_{2N} \\ q^\ell_{N1} & q^\ell_{N2} & \cdots & q^\ell_{NN} \end{pmatrix} \quad ; \quad \underline{\underline{Q}}_0 = \underline{\underline{I}} \qquad 3.3.8$$

where $\underline{\underline{I}}$ is the unit matrix. Each solution $a^{(n)}_j(\gamma)$ has N components which depend directly on the N arbitrary constants $C^{(n)}_{j,0}$, j=1,2,....,N and as there are N such solutions the matrix $\underline{\underline{Q}}_0$ projects out the N individual components of each solution. The matrix $\underline{\underline{f}}(\gamma)$ represents the (NxN) general solution matrix, see Section 3.4, on the θ interval $[0,\pi]$ and the matrix elements $q^\ell_{i,j}$ are the power series coefficients of $f_{i,j}(\gamma)$. These power series coefficients will be given explicitly in terms of the parameters $|\mu\varepsilon|$, E_j and ν up to $\ell=3$ in Chapter 4.

For the situation in which $\underline{\underline{\mu}}$ has zero diagonal elements the matrix $\underline{\underline{g}}(\gamma)$ is simply generated from $\underline{\underline{f}}(\gamma)$ by using equation 3.3.4 whereas when $\underline{\underline{\mu}}$ has non zero diagonal elements equation 3.3.7 with n=1 needs to be solved. The unitarity of the matrices $\underline{\underline{f}}(\gamma)$ and $\underline{\underline{g}}(\gamma)$ is easily shown from the normalization requirement for $\underline{\underline{Q}}(\gamma)$, see equation 3.1.3

$$\underline{\underline{Q}}^{(e)\dagger}(\gamma)\,\underline{\underline{Q}}^{(e)}(\gamma) = 1 = \underline{\underline{C}}^{(e)\dagger}_0\,\underline{\underline{f}}^{\dagger}(\gamma)\,\underline{\underline{f}}(\gamma)\,\underline{\underline{C}}^{(e)}_0$$

$$\underline{\underline{Q}}^{(i)\dagger}(\gamma)\,\underline{\underline{Q}}^{(i)}(\gamma) = 1 = \underline{\underline{C}}^{(i)\dagger}_0\,\underline{\underline{g}}^{\dagger}(\gamma)\,\underline{\underline{g}}(\gamma)\,\underline{\underline{C}}^{(i)}_0 \qquad 3.3.9$$

which requires that both $\underline{\underline{f}}^{\dagger}(\gamma)\underline{\underline{f}}(\gamma)=\underline{\underline{I}}$ and $\underline{\underline{g}}^{\dagger}(\gamma)\underline{\underline{g}}(\gamma)=\underline{\underline{I}}$. From equations 3.3.2 and 3.2.5 the following relation for the constant matrix $\underline{\underline{C}}^{(o)}_0$ follows

$$\underline{\underline{C}}^{(o)}_0 = \underline{\underline{f}}^{-1}(0)\,\underline{\underline{A}} \qquad 3.3.10$$

In other words the matrix $\underline{\underline{C}}^{(o)}_0$ depends on the phase δ of the applied sinusoidal field and this result shows explicitly that the solution need be determined only for a single phase, see later.

Once the matrices $\underline{\underline{f}}(\gamma)$ and $\underline{\underline{g}}(\gamma)$ have been determined on the $[0,2\pi]$ θ-interval from the above relations they can be used to generate $\underline{\underline{Q}}(\theta)$ iteratively over any number of θ 2π-intervals. The computational procedure follows

(1). Determine $\underline{C}_o^{(o)}$ from equation 3.3.10 for the appropriate choice of δ.

(2). Generate $\underline{Q}(\theta)$ on the $[0,\pi]$ interval by using this value of $\underline{C}_o^{(o)}$ and $\underline{f}(\gamma)$, determined from equations 3.3.7 and 3.3.6 with $n=0$, in equation 3.3.2 (or equation 3.3.5;n even).

(3). Set $\underline{C}_o^{(1)} = \underline{Q}(\pi)$ and generate $\underline{Q}(\theta)$ on the interval $[\pi, 2\pi]$ by using equation 3.3.5, if $\underline{\mu}$ has zero diagonal elements (or equation 3.3.7 and 3.3.6 with n=1 for $\underline{g}(\gamma)$ if $\underline{\mu}$ has nonzero diagonal elements)

(4). Iterate over any number of required θ-intervals using equation 3.3.5 for $n = 2,3,\ldots$ setting $\underline{C}_o^{(n)} = \underline{Q}(n\pi)$ at each interval boundary.

The iterative method presented in this section is obviously far superior to the matching power series method discussed earlier. It requires at most a power series expansion on the first two θ π-intervals, $[0,\pi]$,$[\pi,2\pi]$, and once $\underline{f}(\gamma)$ and $\underline{g}(\gamma)$ have been determined on these intervals respectively, the constants $C_{j,o}^{(n)}$, $j=1,\ldots N$, need only be determined on subsequent intervals whereas the original power series method would require recomputation of (NxK) constants $C_{j,\ell}^{(n)}$ $j=1,..N$; $\ell = 1,\ldots K$.. on each interval.*

In order to illustrate how the iterative scheme discussed above is implemented, equations 3.3.5 are written out explicitly for $0 \le \theta \le 4\pi$.

$$\underline{Q}^{(o)}(\gamma) = \underline{f}(\gamma)\,\underline{C}_o^{(o)} \qquad 0 \le \theta \le \pi \qquad 3.3.11(a)$$

$$\underline{Q}^{(1)}(\gamma) = \underline{g}(\gamma)\,\underline{C}_o^{(1)} = \underline{g}(\gamma)\,\underline{f}(\pi)\,\underline{C}_o^{(o)} \qquad \pi \le \theta \le 2\pi \qquad 3.3.11(b)$$

since $\underline{C}_o^{(1)} = \underline{Q}(\pi) = \underline{Q}^{(o)}(\pi)$

---

* In the power series expansion on the number of terms retained to ensure convergence is generally quite large, see Appendix A. Also $K \gg N$ so that the labour saved in using the above iterative scheme is considerable.

$$\underline{\underline{Q}}^{(2)}(\gamma) = \underline{\underline{f}}(\gamma)\,\underline{C}_o^{(2)} = \underline{\underline{f}}(\gamma)\,\underline{\underline{g}}(\pi)\,\underline{C}_o^{(1)} = \underline{\underline{f}}(\gamma)\,\underline{\underline{g}}(\pi)\,\underline{\underline{f}}(\pi)\,\underline{C}_o^{(0)}, \quad 2\pi \le \theta \le 3\pi \qquad 3.3.11(c)$$

$$\underline{\underline{Q}}^{(3)}(\gamma) = \underline{\underline{g}}(\gamma)\,\underline{C}_o^{(3)} = \underline{\underline{g}}(\gamma)\,\underline{\underline{f}}(\pi)\,\underline{C}_o^{(2)} = \underline{\underline{g}}(\gamma)\,\underline{\underline{f}}(\pi)\,\underline{\underline{g}}(\pi)\,\underline{\underline{f}}(\pi)\,\underline{C}_o^{(0)}, \quad 3\pi \le \theta \le 4\pi \qquad 3.3.11(d)$$

Closer inspection of equations 3.3.11 shows explicitly that the solution $\underline{\underline{Q}}(\theta)$ when $\theta = n(2\pi)$, $n = 1, 2 \ldots$, occurs as products of the pair $\underline{\underline{g}}\,\underline{\underline{f}}$. This is a reflection of the fact that, as mentioned previously, the actual period of the Hamiltonian and hence that of equation 3.2.1, is 2π and not π. The choice of a π-interval in θ was dictated by the fact that it provided an upper limit on the expansion interval for which rapidly convergent solutions could be obtained and even this choice of expansion interval proved inadequate in the strong coupling region [22,28]. Thus while it is possible to use the above iterative approach over adjoining π θ-intervals it proves even more efficient to interrupt the above iterative scheme at step (3) and adopt an interval length of 2π in θ for the iterative solution.

3.4 ITERATIVE SOLUTION OVER ADJOINING θ-INTERVALS OF LENGTH 2π.

As discussed at the end of the last section the period of the Hamiltonian is 2π in the variable θ and as is obvious from equations 3.2.1 and 3.2.4 the transformation from the variable θ in equation 3.2.1 to the variable γ spanning a π-interval in θ introduces a phase factor of $(-1)^n$ in equation 3.2.4. Once the solution $\underline{\underline{Q}}(\theta)$ has been determined over the $[\,0\,, 2\pi\,]$ θ-interval by adopting the procedures outlined in the previous sections, it becomes more convenient to use a 2π θ-interval for iteration as this choice removes the phase factor $(-1)^n$ from the problem. Making the transformation

$$(\nu t + \delta) = \theta = \beta + s(2\pi) \quad , \quad s = 0, 1, 2, \ldots \qquad 3.4.1$$

in equation 3.2.1, yields on the appropriate θ-interval

$$\partial/\partial\beta\, \underline{\underline{Q}}^{(s)}(\beta) = \frac{1}{i\nu}\left\{ \underline{\underline{E}}\, \underline{\underline{Q}}^{(s)}(\beta) - \varepsilon \cos\beta\, \underline{\underline{M}}\, \underline{\underline{Q}}^{(s)}(\beta) \right\}. \qquad 3.4.2$$

The solution for $\underline{Q}(\theta)$ on the first 2π-interval is now given by

$$\underline{Q}^{(0)}(\beta) = \underline{\underline{F}}(\beta)\,\underline{C}_0^{(0)} \qquad 3.4.3$$

From equations 3.3.11(a) and (b) the (NxN) matrix $\underline{\underline{F}}(\beta)$ is directly expressible in terms of the matrices $\underline{\underline{f}}$ and $\underline{\underline{g}}$ valid on adjoining π θ-intervals, that is.

$$\underline{\underline{F}}(\beta) = \underline{\underline{f}}(\beta) \qquad 0 \le \beta \le \pi$$

$$\underline{\underline{F}}(\beta) = \underline{\underline{g}}(\beta-\pi)\,\underline{\underline{f}}(\pi) \qquad \pi \le \beta \le 2\pi \qquad 3.4.4$$

An iterative scheme analgous to that outlined in the previous section, for iteration over adjoining θ-intervals, can be adopted using $\underline{\underline{F}}(\beta)$ over adjoining 2π θ-intervals but with the important exception that the phase factor $(-1)^n$ occurring in the earlier iterative scheme is completely removed. The generalisation of equation 3.4.3 to any s interval is analgous to that outlined for a π interval, see Section 3.3;

$$\underline{Q}^{(s)}(\beta) = \underline{\underline{F}}(\beta)\,\underline{C}_0^{(s)} \qquad 3.4.5$$

Using equations 3.4.3 and 3.4.5 ($s \geq 1$) iteratively, in an analgous manner to equation 3.3.5 in the previous section, it can be readily shown that

$$\underline{Q}^{(s)}(\beta) \equiv \underline{Q}(\beta+2s\pi) = \underline{\underline{F}}(\beta+2s\pi)\,\underline{C}_0^{(0)} \qquad 3.4.6$$

where

$$\underline{\underline{F}}(\beta+2s\pi) = \underline{\underline{F}}(\beta)\,\underline{\underline{F}}(2s\pi) \qquad 3.4.7$$

Also using equation 3.4.7 iteratively it follows that

$$\underline{\underline{F}}(2s\pi) = \left[\underline{\underline{F}}(2\pi)\right]^s \qquad 3.4.8$$

Finally it is easy to show from equations 3.4.4 and 3.3.6 that

$$\underline{\underline{F}}(0) = \underline{\underline{I}} \qquad 3.4.9$$

Combining the results of equations 3.4.5 - 3.4.7 enables us to write the general solution for $\underline{Q}(\theta)$ in equation 3.2.1 in the form

$$\underline{Q}(\theta) \equiv \underline{Q}(\beta+2s\pi) = \underline{\underline{F}}(\beta)\left[\underline{\underline{F}}(2\pi)\right]^s \underline{C}_0 \qquad 3.4.10$$

and in addition, from equation 3.4.3 and 3.2.5, we obtain

$$\underline{C}_o(\delta) = \underline{F}^{-1}(\delta)\,\underline{A} \qquad 3.4.11$$

The superscript on $\underline{C}_o$ has been dropped as it clearly becomes redundant in the above results. Equation 3.4.10 represents the exact formal solution to the problem of a sinusoidal field of arbitrary frequency ν, amplitude $\mathcal{E}$ and phase δ interacting with an N-level system of arbitrary configuration. In addition it shows explicitly that the solution for $\underline{a}(\theta)$ on the first $[0, 2\pi]$ θ-interval provides all the information necessary to generate the complete solution to equation 3.2.1, for arbitrary values of θ or t. This particular property of the solution will be shown to be especially suited for the computation of many steady state and damped average properties of multi-level systems interacting with a sinusoidal field.

The matrix* $\underline{F}(\beta)$ merits some further discussion as its determination is crucial to solving the problem, see equations 3.4.10 and 3.4.11. The properties of this matrix expressed by equations 3.4.7 - 3.4.9 are formally discussed by Erugin [62] and others [19,61].

Using equation 3.4.5 it is easy to show that the individual columns of the integral matrix $\underline{F}(\beta)$ also satisfy equation 3.4.2. As $\underline{F}(\beta)$ is unitary its columns are orthogonal and each represents a solution to equation 3.4.2. The matrix $\underline{C}_o(\delta)$ projects out the appropriate columns for the particular imposed initial conditions. As a specific example suppose that the N-level system initially in its ground state, that is $a_1(\omega)=1$, $a_j(\omega)=0$, $j>1$, interacts with a cosine wave ($\delta=0$), see equation 3.1.4. The initial condition matrix $\underline{C}_o(\omega)$ becomes

---

* Formally the matrix $\underline{F}(\beta)$ can be identified with the integral matrix solution to a general system of differential equations with periodic coefficients discussed by Erugin [62] and others [19,61]. $\underline{F}(\beta)$ is also called the monodromy matrix [61] or the principal matrix solution [19].

$$\underline{C}_0(\varphi) = \begin{pmatrix} 1 \\ 0 \\ 0 \\ \vdots \end{pmatrix} = \underline{A} \qquad 3.4.12$$

and the solution $\underline{Q}(\theta)$ on the $[0, 2\pi]$ interval becomes, see equation 3.4.3

$$\underline{Q}(\beta) = \begin{pmatrix} \mathbb{F}_{11}(\beta) \\ \mathbb{F}_{21}(\beta) \\ \mathbb{F}_{N1}(\beta) \end{pmatrix} ; \quad Q_k(\beta) = \mathbb{F}_{k1}(\beta) \qquad 0 \le \theta \le 2\pi . \quad 3.4.13$$

If, as in a number of experiments, the system is initially an admixture of states, then the matrix $\underline{C}_0$ represents the appropriate weighting of each column of $\underline{\mathbb{F}}(\varphi)$ in the solution $\underline{Q}(\theta)$.

Finally some remark should be made concerning the computational ease with which $\underline{\mathbb{F}}(\beta)$ can be generated. The ability of the matching power series method to represent the solution over arbitrary sub-intervals of π, see Section 3.2, ensures that the integral matrix $\underline{\mathbb{F}}(\beta)$ can be generated close to machine accuracy in most cases by an appropriate choice of the expansion sub-intervals length, see Appendix A. This feature is particularly important in the strong coupling region where other numerical methods tend to fail or to become impractical [13,14,65]. For large times t, or equivalently large θ in equation 3.4.10, the evaluation of $[\mathbb{F}(2\pi)]^S$ is facilitated by using the relation $(X)^{2n} = (X^n)^2$ iteratively.

3.5 ITERATIVE SOLUTION IN FLOQUET FORM.

The exact iterative solution, see equation 3.4.10, provides a powerful method for the investigation of the behaviour of the general solution $\underline{Q}(t)$ to the system of coupled differential equations; given by equation 3.1.4, for arbitrary coupling strengths $|\mu\ell|$, frequencies ν and phase δ of the applied sinusoidal field over arbitrary time intervals. The integral matrix $\underline{\mathbb{F}}(\varphi)$, which represents the general solution to equation 3.2.1, is not in a form particularly suited to the evaluation of steady state or average properties of the system. Since such a form is desirable for complete generality of the method, this section will be devoted to the transformation of $\underline{\mathbb{F}}(\theta)$ to a more

useful form for the the evaluation of these properties.

The general form of the solution to a system of linear differential equations with periodic coefficients has been known for some time. It was first derived by Floquet in 1880 and since then has been the object of extensive formal investigation by mathematicians over the years.

Floquet's theorem [19] asserts that the general solution to equation 3.2.1 can be written in the form

$$\underline{\underline{\Phi}}(\theta) = \underline{\underline{Z}}(\theta)\, \exp[i\,\underline{\underline{\Delta}}\,\theta] \qquad 3.5.1$$

where $\underline{\underline{Z}}(\theta)$ is a periodic (NxN) matrix,

$$\underline{\underline{Z}}(\theta+2\pi) = \underline{\underline{Z}}(\theta) \qquad 3.5.2$$

and $\underline{\underline{\Delta}}$ is a real (NxN) constant diagonal matrix, the elements of which are called the characteristic exponents. The characteristic exponents are real as the matrices $\underline{\underline{\Phi}}(\theta)$ and $\underline{\underline{Z}}(\theta)$ are unitary. The major concern of this section is to seek a transformation which places the integral matrix $\underline{\underline{F}}(\theta)$ in the form of equation 3.5.1. To achieve this transformation of the integral matrix we exploit further its properties outlined in equations 3.4.7 - 3.4.9 of the previous section. From equation 3.4.8

$$\underline{\underline{F}}(2n\pi) = \underline{\underline{F}}^{n}(2\pi) \qquad 3.5.3$$

However the integral matrix $\underline{\underline{F}}(2\pi)$ can be diagonalized

$$\underline{\underline{F}}(2\pi) = \underline{\underline{S}}\,\underline{\underline{\lambda}}\,\underline{\underline{S}}^{-1} \qquad 3.5.4$$

where $\underline{\underline{S}}$ is a constant (NxN) unitary matrix whose columns are the orthonormal eigenvectors $\underline{S}_j$ corresponding to the complex eigenvalues λ_j, $j=1,2,\ldots N$, of $\underline{\underline{F}}(2\pi)$. As $\underline{\underline{F}}(\theta)$ is unitary the complex eigenvalues λ_j satisfy the condition [63]

$$|\lambda_j| = 1 \qquad 3.5.5$$

and this property allows equation 3.5.4 to be written as

$$\underline{\underline{F}}(2\pi) = \underline{\underline{S}}\,\exp[i\,\underline{\underline{\Delta}}\,2\pi]\,\underline{\underline{S}}^{-1} \qquad 3.5.6$$

where the characteristic exponents Δ_j, $j=1,2,\ldots N$, are determined from the following relation

$$i\Delta_j = \frac{1}{2\pi} \ln \lambda_j \qquad 3.5.7$$

Substituting equation 3.5.6 in equation 3.5.3 yields the general solution to equation 3.2.1 at $\theta = 2n\pi$, that is

$$\underline{\underline{F}}(2n\pi) = \underline{\underline{S}} \exp[i \underline{\underline{\Delta}} 2n\pi] \underline{\underline{S}}^{-1} \qquad 3.5.8$$

Direct comparison of equations 3.5.8 and 3.5.1 for the matrix $\underline{\underline{\ell}}_d(\theta)$ yields the following result

$$\underline{\underline{\ell}}_d(2n\pi) = \underline{\underline{F}}(2n\pi)\underline{\underline{S}} = \underline{\underline{S}} \exp[i \underline{\underline{\Delta}} 2n\pi] \qquad 3.5.9$$

and this result in turn requires that

$$\underline{\underline{Z}}(2n\pi) = \underline{\underline{S}} \qquad 3.5.10$$

Equations 3.5.1 and 3.5.8 - 3.5.10 lead to definition of the the matrix $\underline{\underline{Z}}(\theta)$ in terms of the original integral matrix $\underline{\underline{F}}(\theta)$ for arbitrary θ,

$$\underline{\underline{Z}}(\theta) = \underline{\underline{F}}(\theta)\underline{\underline{S}} \exp[-i \underline{\underline{\Delta}} \theta] \qquad 3.5.11$$

and it is clear that equation 3.5.11 satisfies equation 3.5.1 with

$$\underline{\underline{\ell}}_d(\theta) = \underline{\underline{F}}(\theta)\underline{\underline{S}} \qquad 3.5.12$$

It is easy to show using equation 3.5.6 and equation 3.5.8 that $\underline{\underline{Z}}(\theta)$ satisfies the periodicity requirement, given by equation 3.5.2. Using equations 3.4.7 - 3.4.10 the exact solution $\underline{Q}(\theta)$ to equation 3.2.1 can be written completely in terms of the variable θ

$$\underline{Q}(\theta) = \underline{\underline{F}}(\theta)\underline{C}_o(\delta) \qquad 3.5.13$$

where for $\theta > 2\pi$, $\underline{\underline{F}}(\theta)$ is generated iteratively as in equation 3.4.10. Combining equations 3.5.11 and 3.5.13 the complete solution $\underline{Q}(\theta)$ can be written explicitly in Floquet form

$$\underline{Q}(\theta) = \underline{\underline{Z}}(\theta) \exp[i \underline{\underline{\Delta}} \theta] \underline{b}_o(\delta) \qquad 3.5.14$$

where

$$\underline{b}_o(\delta) = \underline{\underline{S}}^{-1} \underline{C}_o(\delta) \qquad 3.5.15$$

In the next section the exact solution $\underline{Q}(\theta)$ given by equation 3.5.14 will be shown to be particularly suited to the evaluation of steady state and average properties of the system.

An important relation between the characteristic exponents Δ_j and the original unperturbed energies E_j can be derived by using the following expression [19] for the determinant of $\underline{\underline{F}}(\theta)$

$$\det \underline{\underline{F}}(\theta) = \exp\left[-\frac{i}{\nu}\int_0^{\theta} \mathrm{tr}\left[\underline{\underline{H}}(\theta')\right] d\theta'\right] \qquad 3.5.16$$

where

$$\underline{\underline{H}}(\theta) = \underline{\underline{E}} - \underline{\underline{\mu}}\,\xi \cos\theta \;, \quad \mathrm{tr}\left[\underline{\underline{H}}(\theta)\right] = \mathrm{tr}\left[\underline{\underline{E}}\right] \qquad 3.5.17$$

However, from equations 3.5.4 and 3.5.6

$$\det \underline{\underline{F}}(2\pi) = \prod_{j=1}^{N} \lambda_j = \exp\left[2\pi i \sum_{j=1}^{N} \Delta_j\right] \qquad 3.5.18$$

Comparing equations 3.5.18 and 3.5.16, yields the required result, that is

$$-\nu \sum_{j=1}^{N} (\Delta_j + m) = \sum_{j=1}^{N} E_j \;, \qquad m = 0, \pm 1, \pm 2, \ldots \qquad 3.5.19$$

The condition, $\mathrm{mod}(\nu)$, in equation 3.5.19 follows since $\exp[i(\alpha+m)2\pi] = \exp[i 2\pi\alpha]$. The Δ_j's can be evaluated from the complex eigenvalues λ_j by using equation 3.5.7. Using the polar form for the complex number λ_j and equation 3.5.5 yields [66]

$$\Delta_j = \frac{1}{2\pi} \tan^{-1}\left[\mathrm{Im}\,\lambda_j / \mathrm{Re}\,\lambda_j\right] + n/2 \;, \quad n = 0, \pm 1, \pm 2, \ldots \qquad 3.5.20$$

Equations 3.5.19 and 3.5.20 show that the characteristic exponents Δ_j have infinitely many branches bounded by the branch lines $m/2$, $m = 0, \pm 1, \ldots$. For operational purposes we shall define [13] a full branch as being bounded by the branch lines $m \pm 1/2$, $m = 0, \pm 1 \ldots$; here a full branch includes a positive or negative rotation of λ_j through an angle of π radians in the upper or lower half of the complex plane, respectively. Equation 3.5.20 shows that there is a simple periodic relationship between the characteristic exponents in adjoining branches and that they are essentially arbitrary. It will be shown later that the physical properties computed with these Δ_j's do not depend on their arbitrariness, see also [13,14]. In the calculations reported in Chapters 4 and 5 the evaluation of the characteristic exponents Δ_j is carried out by using equation 3.5.20 and the values of Δ_j are confined to the branch bounded by the branch lines $\pm 1/2$ ($n = 0, \pm 1$, $m = 0$) In discussing the behaviour of the Δ_j's, as a function of frequency for example, their plots will appear discontinous at the

branch lines $\pm 1/2$. Continous plots can be obtained by using equation 3.5.19 with $m \neq 0$.

The formal scheme developed above for constructing the Floquet solution, equation 3.5.14, from the integral matrix $\underline{\underline{F}}(\theta)$, given by equation 3.4.4, can be briefly summarized in the following computational steps.

(1). Determine the integral matrix $\underline{\underline{F}}(\theta)$ over the interval $0 \leq \theta \leq 2\pi$ for the appropriate coupling strength $|\mu\varepsilon|$, frequency ν and phase δ of the applied sinusoidal field, utilizing the methods outlined in Sections 3.3-3.4.

(2). Diagonalize the unitary matrix $\underline{\underline{F}}(2\pi)$ to obtain the appropriate eigenvalues λ_j and eigenvectors $\underline{S}_j$ and use these to construct the periodic matrix $\underline{\underline{Z}}(\theta)$ and the characteristic exponents Δ_j according to equations 3.5.11 and 3.5.7 respectively.

(3). Construct the initial condition array $\underline{b}_0(\delta)$ from $\underline{C}_0(\delta)$ defined in equation 3.4.11.

(4). Use equations 3.5.14 - 3.5.15 to generate $\underline{Q}(\theta)$ for arbitrary θ .

One possible limitation on the accuracy of the Floquet solution, equation 3.5.14, relative to the iterative solution, equation 3.4.10, lies in the diagonalization of the integral matrix $\underline{\underline{F}}(2\pi)$. This does not pose a particular problem as very accurate diagonalization routines are available on standard program packages [67,68].* It should probably be re-emphasised at this point that while the Floquet form of the solution for $\underline{Q}(t)$ is particularly suited to the evaluation of average and steady state properties of the system [13,22], it provides no particular advantage over the iterative solution, equation 3.4.10, as far as the evaluation of the temporal behaviour of $\underline{Q}(t)$ is concerned.

3.6 EXPECTATION VALUES OF OPERATORS AND THEIR PHASE AND TIME AVERAGES

The physical properties of any quantum mechanical system are directly expressible in terms of the expectation values, of appropriate operators $\underline{\underline{\mathcal{L}}}$, with respect to the total wavefunction $\Psi(r,t)$. This section will be mainly concerned with outlining some interesting features of the evaluation of the phase and time averages of these expectation values when obtained through the Floquet formulism.

3.6.1 NEGLECTING RELAXATION EFFECTS

In this section average properties will be formally represented in terms of an expectation value of a general operator $\mathcal{L}(r,t)$ with respect to the total wavefunction $\Psi(r,t)$. Our sole interest in this thesis, however, will be to evaluate the various averages of the induced transition probability and explicit formulae for these quantities will be presented in Section 3.7.

In order to evaluate these expectation values and their phase and time averages conveniently, density matrix notation will be adopted [38,70], and see Section 3.1. The density matrix $\underline{\underline{\rho}}(t)$ in terms of equation 3.5.14 becomes

$$\underline{\underline{\rho}}(t) = \underline{\underline{Q}}(t)\,\underline{\underline{Q}}^{\dagger}(t) = \underline{\underline{Z}}(t)\,\underline{\underline{\beta}}(t,\delta)\,\underline{\underline{Z}}^{\dagger}(t) \qquad 3.6.1$$

where

$$\underline{\underline{\beta}}(t,\delta) = \exp\left[i\underline{\underline{\Delta}}(\omega t+\delta)\right]\underline{\underline{b}}_{0}(\delta)\,\underline{\underline{b}}_{0}^{\dagger}(\delta)\exp\left[-i\underline{\underline{\Delta}}(\omega t+\delta)\right] \qquad 3.6.2$$

and the expectation value in this formalism is written [38,70], see

---

* While diagonalization routines are available for complex matrices on most program packages, even more common are very accurate routines for the diagonalization of real matrices. As any general complex (NxN) array can be written as a real (2Nx2N) array the latter routines may prove more appropriate [69].

Section 3.1

$$\langle \Psi(r,t)| \underline{\ell}(r,t) |\Psi(r,t)\rangle = Tr\left[\underline{\rho}(t)\underline{\ell}(r,t)\right] \qquad 3.6.3$$

where the operator ℓ is represented on the right hand side by its appropriate matrix representation ,

$$\ell_{ij}(r,t) = \langle \phi_i(r)| \ell(r,t) |\phi_j(r)\rangle \qquad 3.6.4$$

and ℓ is assumed to have the following periodic property with respect to time

$$\ell(r,t) = \ell(r, t+2\pi/\upsilon) \qquad 3.6.5$$

which includes $\ell(r)$ =constant in time.

For a specified frequency υ and phase δ of the applied sinusoidal field, the expectation value of ℓ, defined by equation 3.6.3, could be directly computed with the result for $\underline{\rho}(t)$ given by equation 3.6.1. However, as mentioned at the end of Section 3.4, the Floquet form of the solution provides no particular advantage over the iterative form given by equation 3.4.10 and indeed equation 3.4.10 provides the more direct route to the evaluation of equation 3.6.3. Further details regarding the evaluation of equation 3.6.3 will be given in the next two chapters when specific level configurations will be dealt with.

It now remains to be shown why the Floquet solution, given by equations 3.5.14 and 3.6.1, is particularly advantageous when phase and time averages of equation 3.6.3 are to be computed. At this stage it is convenient to define the following phase, long-time and long-time/phase averages of equation 3.6.3,

$$\{\ell\}_\delta = \frac{1}{\pi}\int_0^\pi Tr\left[\underline{\rho}(t)\underline{\ell}(r,t)\right] d\delta \qquad 3.6.6$$

$$\{\ell\}_{\tau\to\infty} = \lim_{\tau\to\infty}\frac{1}{\tau}\int_0^\tau Tr\left[\underline{\rho}(t)\underline{\ell}(r,t)\right] dt \qquad 3.6.7$$

$$\{\ell\}_{\tau\to\infty,\delta} = \frac{1}{\pi}\int_0^\pi \{\ell\}_{\tau\to\infty} d\delta = \{\ell\}_{\delta,\tau\to\infty} = \lim_{\tau\to\infty}\frac{1}{\tau}\int_0^\tau \{\ell\}_\delta dt . \qquad 3.6.8$$

The phase averaged expectation value defined by equation 3.6.6 will first be considered in some detail. From equations 3.6.1 and 3.6.2 it is clear that the time-dependent expectation value is a function of the phase of the applied sinusoidal field. This phase dependence allows for the randomness of excited state formation

[2,13,22] with respect to the interaction of the original stationary state system with the applied time-dependent field. The physically meaningful temporal behaviour of the expectation value will be normally independent of δ and will correspond to the phase averaged result given by equation 3.6.6. For example, if the system being irradiated is in the gaseous state, then random collisions between atoms or molecules in the gas or collisions with the walls of the container can completely terminate the radiation process. In this case the phase δ would correspond to the instant (t_o) after such a collision at which time the system is again exposed to some point along the sinusoidal wave representing the applied radiation. Another possible source of this phase dependence in molecular beam or pulse experiments could correspond to the instant (t_o) at which the atom or molecule enters the radiation interaction region. To facilitate the evaluation of equation 3.6.6, it is more convenient to rewrite equation 3.6.1 for $\underline{\rho}(t)$, after some straightforward manipulations, in the following form

$$\underline{\rho}(t) = \sum_{K,L} \underline{Z}_K(\omega t+\delta)\, \underline{Z}_L^{\dagger}(\omega t+\delta)\, b_K(\delta)\, b_L(\delta) \exp\left[i(\Delta_K-\Delta_L)(\omega t+\delta)\right] \qquad 3.6.9$$

which, in turn, allows the phase averaged expectation value, given by equation 3.6.6, to be written as

$$\{\ell\}_\delta = \sum_{K,L} \exp\left[i(\Delta_K-\Delta_L)\omega t\right] \mathrm{Tr}\left[\underline{\Omega}_{K,L}(\omega t)\right] \qquad 3.6.10$$

where

$$\underline{\Omega}_{K,L}(\omega t) = \frac{1}{\pi}\int_0^{\pi}\left[\underline{Z}_K(\omega t+\delta)\, \underline{Z}_L^{\dagger}(\omega t+\delta)\, \underline{\ell}\, b_K(\delta)\, b_L(\delta) \exp\left[i(\Delta_K-\Delta_L)\delta\right]\right] d\delta \qquad 3.6.11$$

and, because of the periodicity of $\underline{Z}(t)$ and $\underline{\ell}(r,t)$, the following condition on $\underline{\Omega}_{K,L}(\omega t)$ holds

$$\underline{\Omega}_{K,L}(\omega t) = \underline{\Omega}_{K,L}(\omega t+2\pi). \qquad 3.6.12$$

Once the phase integral in equation 3.6.11 has been evaluated over the time interval, $0 \le t \le 2\pi/\omega$, the periodic property of the matrix $\Omega_{K,L}(\omega t)$ given by equation 3.6.12 allows $\{\ell\}_\delta$, equation 3.6.10, to be easily computed over arbitrary time intervals. Further details regarding the evaluation of the phase integral in equation 3.6.11 will be given later, see Appendix A.3.

Next we consider the long time average of equation 3.6.3, defined by equation 3.6.7, which corresponds to the steady state response of the system when perturbed by a sinusoidal field of well defined phase . For the same reasons as discussed in the preceding paragraph, the physical response of the system will normally correspond to the long time average of $\{\ell\}_\delta$. Substituting equation 3.6.9 into equation 3.6.7, gives

$$\{\ell\}_{\tau\to\infty} = \lim_{\tau\to\infty}\frac{1}{\tau}\Big\{\int_0^\tau \mathrm{tr}\Big[\sum_K \underline{\underline{Z}}_K(\omega t+\delta)\,\underline{\underline{Z}}_K^\dagger(\omega t+\delta)\,\underline{\underline{\ell}}(r,t)\Big]dt\,|b_K(\delta)|^2 +$$

$$\int_0^\tau \mathrm{tr}\Big[\sum_{K\neq L}\underline{\underline{Z}}_K(\omega t+\delta)\,\underline{\underline{Z}}_L^\dagger(\omega t+\delta)\,\underline{\underline{\ell}}(r,t)\exp\big[i(\Delta_K-\Delta_L)(\omega t+\delta)\big]\Big]dt\,b_K(\delta)b_L^*(\delta)\Big\} \qquad 3.6.13$$

The integrand in the second term of equation 3.6.13 is bounded and oscillates in sign so that its integral is zero. In addition, the periodicity of $\underline{\underline{Z}}(t)$ and $\underline{\underline{\ell}}(r,t)$ in the first integrand allows $\{\ell\}_{\tau\to\infty}$ to be written in the following convenient form.

$$\{\ell\}_{\tau\to\infty} = \Big\{\mathrm{tr}\Big[\sum_K \underline{\underline{Z}}_K(\omega t+\delta)\,\underline{\underline{Z}}_K^\dagger(\omega t+\delta)\,\underline{\underline{\ell}}(r,t)\Big]\Big\}_{\tau=2\pi/\omega}|b_K(\delta)|^2$$

$$= \omega/2\pi\int_0^{2\pi/\omega}\mathrm{tr}\Big[\sum_K \underline{\underline{Z}}_K(\omega t+\delta)\,\underline{\underline{Z}}_K^\dagger(\omega t+\delta)\,\underline{\underline{\ell}}(r,t)\Big]dt\,|b_K(\delta)|^2 \qquad 3.6.14$$

Equation 3.6.14 shows very clearly the power of the Floquet form of the solution for $\underline{\underline{\rho}}(t)$ with the steady state response of the system to a sinusoidal field of well defined phase δ, reducing to a simple time average of the expectation value over one period of the Hamiltonian $H(r,t)$. Further details regarding the evaluation of the time integral in equation 3.6.14 will be given in Appendix A.3.

Finally the phase averaged steady state response $\{\ell\}_{\tau\to\infty,\delta}$ or equivalently $\{\ell\}_{\delta,\tau\to\infty}$, can be written, with the aid of equation 3.6.14, and the definition of the matrix $\underline{\underline{\Omega}}_{K,L}(\omega t)$, given by equation 3.6.11, in the following convenient form.

$$\{\ell\}_{\tau\to\infty,\delta} = \Big\{\mathrm{tr}\Big[\sum_K \underline{\underline{\Omega}}_{K,K}(\omega t)\Big]\Big\}_{\tau=2\pi/\omega}$$

$$= \omega/2\pi\int_0^{2\pi/\omega}\mathrm{tr}\Big[\sum_K \underline{\underline{\Omega}}_{K,K}(\omega t)\Big]dt = \{\ell\}_{\delta,\tau\to\infty} \qquad 3.6.15$$

Equation 3.6.15 will normally correspond to the physical steady state response if the N-level system and the external sinusoidal field can

set up steady-state oscillations before important relaxation effects set in. Otherwise relaxation effects can be explicitly incorporated into the above results by replacing the infinite time average, defined in equations 3.6.7 and 3.6.8, by the appropriate damped averages $\{\mathcal{L}\}_\tau$ and $\{\mathcal{L}\}_{\tau,\delta}$, respectively.

The general form of equation 3.6.14, coupled with equations 3.6.13 and 3.6.7, suggests that the total wavefunction $\Psi(r,t)$ in equation 3.1.1 be rewritten in the following alternative form

$$\Psi(r,t) = \sum_K \psi_K(r,t)\, b_K(\delta) = \sum_K \chi_K(r,t)\, b_K(\delta) \exp[i\Delta_K(\omega t+\delta)] \qquad 3.6.16$$

where $\chi_K(r,t)$ is the periodic part of $\psi_K(r,t)$ defined by

$$\chi_K(r,t) = \underline{\underline{\Phi}}(r)\, \underline{Z}_K(\omega t+\delta) = \chi_K(r, t+2\pi/\omega) \qquad 3.6.17$$

Equations 3.6.16 and 3.6.17 provide an alternative representation of the total wavefunction $\Psi(r,t)$ and the steady state response of the system to the periodic perturbation, given by equation 3.6.14, in this new representation becomes

$$\{\mathcal{L}\}_{\tau\to\infty} = \sum_K \{\langle \chi_K(r,t)|\mathcal{L}(r,t)|\chi_K(r,t)\rangle\}_{2\pi/\omega} |b_K(\delta)|^2 \qquad 3.6.18$$

In addition if equation 3.6.16 is substituted into the time-dependent Schroedinger equation, equation 2.1.1 , the following eigenvalue equation can be derived [49] for the characteristic exponents

$$[H(r,t) + \omega\Delta_K - i\partial/\partial t]\, \chi_K(r,t) = 0 \qquad 3.6.19$$

It is easy to show using the unitarity of the matrix $\underline{Z}(t)$ that $\chi_K(r,t)$ form a set of orthonormal functions, that is

$$\langle \psi_K(r,t)|\psi_L(r,t)\rangle = \sum_{i,j} Z^*_{iK}(\omega t+\delta)\, Z_{jL}(\omega t+\delta)\, b^*_K(\delta)\, b_L(\delta) \exp[i(\Delta_L-\Delta_K)(\omega t+\delta)]$$

$$= 1 \quad K=L$$
$$= 0 \quad K\neq L \qquad 3.6.20$$

The functions $\psi_K(r,t)$ and their eigenvalues $(\omega\Delta_K)$ have been discussed formally by Young, Deal and Kestner [49], see Section 2.4, who derive perturbation expansions for both $\psi_K(r,t)$, which they term "quasi-periodic" states, and $(\omega\Delta_K)$, which are their corresponding "quasi-energies". The present formulation is equivalent to calculating $\psi_K(r,t)$ and $(\omega\Delta_K)$ exactly and thus would correspond to the perturbation results summed through all orders.

3.6.2 INCLUSION OF RELAXATION EFFECTS

The results derived in Section 3.6.1 were obtained on the assumption that relaxation effects in the N-level system were unimportant in determining the final physical response of this system to the applied sinusoidal perturbation. As discussed previously, this assumption is only valid as long as the coupled system of oscillating field and atom can set up steady state oscillations before relaxation effects set in. These relaxation effects, when important, can be included in the analysis by directly incorporating the phenomenological decay constants γ_j (representing the radiative widths of the stationary states $\phi_j(r)$) into the original set of coupled differential equations, see Chapter 2 . Alternatively, as in the case of collision damping, these relaxation effects can be accounted for by a statistical weighting of the physical property of interest over some mean interaction time τ, see Chapter 2. The latter approach provides a much more meaningful physical picture of the experimental situation as it can account for the many different damping effects operative in real gaseous systems, including the spontaneous decay terms γ_j of the former method in the limit that the gas is very dilute.* An undesirable feature of the former method is that the integral matrix $\underline{\underline{F}}$ in equation 3.4.10 is no longer unitary. Thus the following analysis of damping phenomena will be solely concerned with the statistical collision damping which has already been employed in Chapter 2 in modifying the Rabi lineshape.

The damped average of some physical property defined by the expectation value of the operator $\underline{\underline{\ell}}$ in equation 3.6.3 is written

$$\{\underline{\underline{\ell}}\}_\tau = \frac{1}{\tau}\int_{-\infty}^{t} \mathrm{tr}\left[\underline{\underline{\rho}}(t-t_1)\,\underline{\underline{\ell}}(r,t-t_1)\right]\exp\left[-(t-t_1)/\tau\right]dt_1 \qquad 3.6.21$$

which corresponds to a weighted average of the property of interest over the initial times t_1, see Chapter 2, where the constant τ refers to the mean interaction time of the system with the oscillating field. Equation 3.6.21 can be easily made consistent with the previous

---

* In the limit that the gaseous system is very dilute, the damping constant τ approaches the spontaneous decay lifetime of the state under investigation and if all of these lifetimes are assumed equal then $\tau = \gamma^{-1}$ where $\gamma = \gamma_1 = \gamma_2 = \cdots$ [9.55].

definitions of steady state averages (equations 3.6.6 -3.6.8) by the simple change of variable

$$t' = (t - t_1) \qquad 3.6.22$$

which transforms equation 3.6.21 to

$$\{\underline{\ell}\}_\tau = \frac{1}{\tau}\int_0^\infty tr\left[\underline{\rho}(t)\underline{\ell}(r,t)\right]\exp[-t/\tau]\,dt \qquad 3.6.23$$

Equation 3.6.23 is now in a convenient form for the evaluation of the damped average properties both for fields of well defined phase δ and for their phase averaged counterparts. For example, the damped analogue to equation 3.6.13 becomes

$$\{\underline{\ell}\}_\tau = \frac{1}{\tau}\int_0^\infty tr\left[\sum_{K,L}\underline{Z}_K(\omega t+\delta)\underline{Z}_L^\dagger(\omega t+\delta)\underline{\ell}(r,t)\right]\exp\left[i\Gamma_{KL}t\right]dt\,\exp\left[i(\Delta_K-\Delta_L)\delta\right]b_K(\delta)b_L^*(\delta) \qquad 3.6.24$$

where

$$\Gamma_{KL} = (\Delta_K - \Delta_L)\omega + i/\tau \qquad 3.6.25$$

Equation 3.6.24 can be further simplified by exploiting the periodic property of the matrix

$$\{\underline{\ell}\}_\tau = \frac{1}{\tau}\sum_{K,L}\Bigg[\int_0^{2\pi/\omega} tr\left[\underline{Z}_K(\omega t+\delta)\underline{Z}_L^\dagger(\omega t+\delta)\underline{\ell}(r,t)\right]\exp\left[i\Gamma_{KL}t\right]dt +$$

$$\int_{2\pi/\omega}^{4\pi/\omega} tr\left[\underline{Z}_K(\omega t+\delta)\underline{Z}_L^\dagger(\omega t+\delta)\underline{\ell}(r,t)\right]\exp\left[i\Gamma_{KL}t\right]dt + \cdots\Bigg]\exp\left[i(\Delta_K-\Delta_L)\delta\right]b_K(\delta)b_L^*(\delta)$$

$$= \frac{1}{\tau}\sum_{K,L}\exp\left[i(\Delta_K-\Delta_L)\delta\right]b_K(\delta)b_L^*(\delta)\int_0^{2\pi/\omega} tr\left[\underline{Z}_K(\omega t+\delta)\underline{Z}_L^\dagger(\omega t+\delta)\underline{\ell}(r,t)\right]\exp\left[i\Gamma_{KL}t\right]dt$$

$$\times\left[1 + \exp\left[i\Gamma_{KL}2\pi/\omega\right] + \exp\left[i\Gamma_{KL}4\pi/\omega\right] + \cdots\right]$$

$$= \sum_{K,L}\frac{\exp\left[i(\Delta_K-\Delta_L)\delta\right]b_K(\delta)b_L^*(\delta)}{\tau\left[1-\exp\left[i\Gamma_{KL}2\pi/\omega\right]\right]}\int_0^{2\pi/\omega} tr\left[\underline{Z}_K(\omega t+\delta)\underline{Z}_L^\dagger(\omega t+\delta)\underline{\ell}(r,t)\right]\exp\left[i\Gamma_{KL}t\right]dt \qquad 3.6.26$$

In the limit $\tau\to\infty$ equation 3.6.26 reduces to equation 3.6.14 as expected. Finally the damped counterpart to equation 3.6.15 for the phase averaged steady state response, is given by

$$\{\underline{\ell}\}_{\tau,\delta} = \sum_{K,L}\frac{1}{\tau\left(1-\exp\left[i\Gamma_{KL}2\pi/\omega\right]\right)}\int_0^{2\pi/\omega} tr\left[\underline{\Omega}_{KL}(\omega t)\right]\exp\left[i\Gamma_{KL}t\right]dt \qquad 3.6.27$$

where $\underline{\Omega}_{KL}(\omega t)$ is given by equation 3.6.11. The above results for the damped averages, given by equations 3.6.26 and 3.6.27, differ from

their steady state analogues in that the terms with $K \neq L$ have to be retained in their evaluation, as the integrands are no longer purely oscillatory due to the presence of the damping term $\exp[-t/\tau]$. However, as in the case of the steady state results, they still reduce to a simple integration over the period of the Hamiltonian $H(r,t)$. One would expect however that the contributions of these nondiagonal terms $(K \neq L)$ to the final result should become smaller if (1) for fixed coupled energy $|\mu\mathcal{E}|$ the relaxation time τ is increased or (2) for fixed τ the coupling energy $|\mu\mathcal{E}|$ is increased. These expectations are further substantiated in the following two chapters where explicit calculations will show that these non-diagonal $(K \neq L)$ terms make negligible contributions in many cases for finite values of τ, with the physical results in such cases being given by the simpler steady state response, see equations 3.6.13 and 3.6.15.

3.7 PHASE AND TIME AVERAGED INDUCED TRANSITION PROBABILITIES

The discussions and results of the previous section show explicitly the power of the Floquet solution in evaluating average properties of the N-level system. Explicit formulae will now be presented for the phase and phase/time averages of the induced transition probabilities.

The induced transition probability to any state f of the N-level system, subject to the appropriate initial conditions given by equation 3.1.6, is determined directly from the right hand side of equation 3.6.3, with the individual elements of the matrix $\underline{\mathcal{L}}$ defined by

$$\mathcal{L}_{ij} = \delta_{if}\delta_{jf} \qquad 3.7.1$$

This yields the well known result for the induced transition probability to state f

$$P_{ff}(t) = \rho_{ff} \equiv |Q_f(t)|^2 \qquad 3.7.2$$

With this definition of $\underline{\mathcal{L}}$ in equations 3.6.6 and 3.6.10, the phase averaged induced transition probability becomes

$$\bar{P}_{ff}(t) = \sum_{K,L} \exp\left[i(\Delta_K - \Delta_L)\nu t\right] \Omega^{ff}_{KL}(\nu t) \qquad 3.7.3$$

where $\Omega^{ff}_{KL}(\nu t)$ refers to the (f,f) element of the $(N\times N)$ periodic matrix $\underline{\Omega}_{KL}(\nu t)$ given by equation 3.6.11. Its explicit form is [22]

$$\Omega^{ff}_{KL}(\nu t) = \frac{1}{\pi}\int_0^{\pi}\left[Z_{fK}(\nu t+\delta) Z^{*}_{fL}(\nu t+\delta)\right] b_K(\delta) b^{*}_L(\delta) \exp\left[i(\Delta_K - \Delta_L)\delta\right] d\delta \qquad 3.7.4$$

The steady state induced transition probability follows immediately from equations 3.6.7 and 3.6.14;

$$\bar{P}_{ff}(\delta) = \nu/2\pi \int_0^{2\pi/\nu} \sum_K |Z_{fK}(\nu t)|^2 dt\, |b_K(\delta)|^2 \qquad 3.7.5$$

Finally the phase averaged steady state induced transition probability, $\bar{P}_{ff}$, can be derived directly from equation 3.6.15

$$\bar{P}_{ff} = \nu/2\pi \int_0^{2\pi/\nu} \sum_K \Omega^{ff}_{KK}(\nu t)\, dt \qquad 3.7.6$$

where the matrix element $\Omega^{ff}_{KK}(\nu t)$ is easily obtained from equation 3.7.4

$$\Omega^{ff}_{KK}(\nu t) = \frac{1}{\pi}\int_0^{\pi} |Z_{fK}(\nu t+\delta)|^2 |b_K(\delta)|^2 d\delta \qquad 3.7.7$$

In actual calculations a convenient numerical check is provided by the conservation of transition probability,

$$1 = \underline{\mathbf{P}} = \sum_f P_{ff}(t) = \sum_f \bar{P}_{ff}(\delta) = \sum_f \bar{P}_{ff}(t) = \sum_f \bar{P}_{ff} \qquad 3.7.8$$

which follows immediately from the fact that $H(r,t)$ is self adjoint. In actual practice a numerical check on the accuracy at each stage of the above averaging processes can be made by setting the matrix $\underline{\rho} = \underline{I}$ in the appropriate equations.

We conclude this section by presenting the damped analogues to equations 3.7.5 and 3.7.6. Substituting equation 3.7.1 into equation 3.6.26 yields the damped induced transition probability for a sinusoidal field of well defined phase δ,

$$\bar{P}^{\tau}_{ff}(\delta) = \sum_{K,L} \frac{\exp\left[i(\omega_K - \Delta_L)\delta\right] b_K(\delta) b^{*}_L(\delta)}{\tau\left[1 - \exp\left[i\Gamma_{KL}\, 2\pi/\nu\right]\right]} \int_0^{2\pi/\nu} Z_{fK}(\nu t+\delta) Z^{*}_{fL}(\nu t+\delta) \exp\left[i\Gamma_{KL} t\right] dt \qquad 3.7.9$$

where the relaxation constant τ has been discussed earlier [9,55]. Finally the damped phase averaged induced transition probability is obtained from equation 3.6.27

$$\bar{P}^{\tau}_{ff} = \sum_{K,L} \frac{1}{\tau\left[1 - \exp\left[-\Gamma_{KL}\frac{2\pi}{\upsilon}\right]\right]} \int_0^{2\pi/\upsilon} \Omega^{ff}_{KL}(\upsilon t) \exp\left[-\Gamma_{KL} t\right] dt \qquad 3.7.10$$

where $\Omega_{K,L}(\upsilon t)$ is defined by equation 3.6.11. Equation 3.7.10 will normally yield the physically observed spectrum when relaxation effects become important [9,39] and it will be compared directly to the simpler steady state result for specific level configurations in the next two chapters.

Finally, another source of line broadening, which will not be considered in this thesis, but which can be important at microwave through optical frequencies, arises from the Doppler effect. Molecular beams or oppositely directed laser beams can be used to eliminate Doppler broadening at these frequencies[9,83]. If Doppler broadening is to be included in the above results, the property of interest, say $\{f(\upsilon)\}$, needs to be integrated over an appropriate velocity distribution $W(v)$ whose explicit form depends on the experimental conditions[4,9]. Formally, this velocity integral may be written as follows

$$\int_{-\infty}^{\infty} W(v) \{f(\upsilon[1+v/c])\} dv$$

Unfortunately, none of the periodic properties exploited earlier in evaluating the collision damping integrals can be used to evaluate this velocity integral and a direct numerical integration would be required.

CHAPTER 4

THE TWO LEVEL SYSTEM.

The problem in which the infinite set of coupled first order differential equations, given by equation 3.1.4, is truncated to a set of two coupled first order differential equations will be considered in detail in this chapter. Historically the two level system has provided the basis for the study of both linear and non-linear transition processes [7,13,14,18], including the fundamental oscillations of the different modes within laser systems [1-3,39,71]. The validity of this two state approximation has been discussed qualitatively by different authors previously [13-15] and it is assumed to provide an adequate description of the transition process as long as the spectral profile arising from the transition of interest does not overlap appreciably with any other lineshapes arising from transitions to neighbouring states of the quantum system. A more quantitative test of this two state approximation will be presented in the next chapter when these neighbouring states will be explicitly included in the analysis. The formal results derived in the previous chapter will now be employed to extract explicit information regarding induced transitions in a two-level system.

4.1 THE SOLUTION OF THE TIME DEPENDENT WAVE EQUATION FOR THE TWO LEVEL PROBLEM.

At the risk of being somewhat repetitive, but in the hope that the formal developements of the previous chapter will be further clarified, some of the general results derived therein will be written out in detail for the two-level nondegenerate system. Equation 3.1.4

is now written explicitly as

$$i\frac{\partial}{\partial t}\begin{pmatrix} a_1(t) \\ a_2(t) \end{pmatrix} = \begin{pmatrix} E_1 & 0 \\ 0 & E_2 \end{pmatrix}\begin{pmatrix} a_1(t) \\ a_2(t) \end{pmatrix} - \mathcal{E}\cos(\nu t+\delta)\begin{pmatrix} 0 & \mu_{12} \\ \mu_{21} & 0 \end{pmatrix}\begin{pmatrix} a_1(t) \\ a_2(t) \end{pmatrix} \qquad 4.1.1$$

and the normalization condition (equation 3.1.3) becomes

$$\sum_{j=1}^{2} |a_j(t)|^2 = 1 \qquad 4.1.2$$

Equation 4.1.1, in spite of its rather simple appearance, has not been solved in general in terms of tabulated functions [14] and the reason for this becomes more apparent if 4.1.1 is decoupled and written as two independent second order differential equations for the individual state amplitudes $a_j(t)$, j=1,2, see also [14];

$$\frac{\partial^2}{\partial t^2}a_j(t) + [i(E_j+E_k) - \nu\tan(\nu t+\delta)]\frac{\partial}{\partial t}a_j(t) + [E_j(E_k - i\nu)\tan(\nu t+\delta) + |\mu\mathcal{E}|^2\cos^2(\nu t+\delta)]\,a_j(t) = 0 \qquad 4.1.3$$

where $j,k=1,2;\ j\neq k$, and $\mu = \mu_{12} = \mu_{21}$. The complexity of the coefficients in equation 4.1.3 shows why an analytic closed form solution has remained elusive for so long and closed form solutions have only been obtained in certain limiting cases which will be briefly summarized below.

In the special case that both states are degenerate, $E_0 = E_1 = E_2$, equation 4.1.1 can be solved exactly in closed form by taking the following linear combinations of the state amplitudes $a_\pm(t)$,

$$a_\pm(t) = (a_1(t) \pm a_2(t)) \qquad 4.1.4$$

In terms of these symmetric and anti-symmetric linear combinations equation 4.1.1 decouples to yield the following simple first order differential equations for $a_\pm(t)$

$$i\frac{\partial}{\partial t}a_\pm(t) = E_0\,a_\pm(t) \mp (\mu\mathcal{E})\cos(\nu t+\delta)\,a_\pm(t) \qquad 4.1.5$$

and the solutions to these equations can be written down by inspection

$$a_\pm(t) = \text{constant} \times \exp\left[-i\left(E_0 t \mp \frac{(\mu\mathcal{E})}{\nu}\sin(\nu t+\delta)\right)\right] \qquad 4.1.6$$

Finally, the general solution for the individual state amplitudes $a_j(t)$ can be written in the following compact matrix form

$$\begin{pmatrix} a_1(t) \\ a_2(t) \end{pmatrix} \propto \begin{bmatrix} \cos\left[\frac{|\mu\mathcal{E}|}{\upsilon}\sin(\upsilon t+\delta)\right] & i\sin\left[\frac{|\mu\mathcal{E}|}{\upsilon}\sin(\upsilon t+\delta)\right] \\ i\sin\left[\frac{|\mu\mathcal{E}|}{\upsilon}\sin(\upsilon t+\delta)\right] & \cos\left[\frac{|\mu\mathcal{E}|}{\upsilon}\sin(\upsilon t+\delta)\right] \end{bmatrix} \begin{pmatrix} a_1(0) \\ a_2(0) \end{pmatrix} \times \exp[-iE_0 t] \qquad 4.1.7$$

It is interesting to compare the general solution 4.1.7 for the two-level degenerate system with a recent solution by Rahman [16] to the two-level nondegenerate system obtained in the asymptotic limit $|\mu\mathcal{E}|/\omega \to \infty$. As expected, both solutions agree precisely, which is not surprising as the degenerate system corresponds exactly to this asymptotic limit. Indeed such asymptotic solutions were previously derived by Shirley [13] and a number of other authors [6.17,18]. In view of the above discussion the exact formal solution derived in the previous chapter can be used to obtain a quantitative check on the lower limit of $|\mu\mathcal{E}|/\omega$ for which the asymptotic solution remains valid. This point will be discussed further in Sections 4.2 and 4.3.

The remainder of this chapter will be devoted to the presentation of explicit results for the two level system, using the formal expressions derived for the more general N-level system in the previous chapter. In what follows a dimensionless parameter β which will provide a direct measure of the coupling strength will be used

$$\beta = |\mu\mathcal{E}|/\omega \qquad 4.1.8$$

and we define the following ranges of coupling strength in agreement with Autler and Townes [14],

$\beta \ll 1$	$\beta \lesssim 1$	$\beta \gtrsim 1$	4.1.9
weak	intermediate	strong	

In the results that follow the latter two ranges of β will be the main concern as the weak coupling region, $\beta \ll 1$, is more than adequately represented by both perturbation and rotating field approximations, see Chapter 2. The coupling strength ranges presented above are meant to be a very rough guide as there is no clear delineation between each range.

The exact iterative solution to equation 4.1.1, describing the interaction of a two-level nondegenerate system with an external sinusoidal field of well defined phase δ, can now be written directly from the formal solution given by equation 3.4.10 of the preceding chapter [22,28],

$$\underline{\underline{Q}}(\theta) = \underline{\underline{F}}(\theta)\left[\underline{\underline{F}}(2\pi)\right]^{S}\underline{\underline{C}}_0(\delta), \qquad 0 \le \theta \le 2\pi \qquad 4.1.10$$

and the initial condition array $\underline{\underline{C}}_0(\delta)$ is given by

$$\underline{\underline{C}}_0(\delta) = \underline{\underline{F}}^{-1}(\delta)\,\underline{\underline{A}} \qquad 4.1.11$$

where

$$\underline{\underline{F}}(\theta) = \begin{pmatrix} F_{11}(\theta) & F_{12}(\theta) \\ F_{21}(\theta) & F_{22}(\theta) \end{pmatrix}, \quad \underline{\underline{A}} = \begin{pmatrix} a_1(0) \\ a_2(0) \end{pmatrix}, \quad \underline{\underline{C}}_0(\delta) = \begin{pmatrix} C^{(0)}_{1,0}(\delta) \\ C_{2,0}(\delta) \end{pmatrix} \qquad 4.1.12$$

To clarify further the method of solution for this two-level nondegenerate system, equation 3.4.4 for $\underline{\underline{F}}(\theta)$ occurring in equation 4.1.10 is written out explicitly in terms of the individual matrix elements of $\underline{\underline{f}}(\theta)$,

$$F_{ij}(\theta) = f_{ij}(\theta) \qquad 0 \le \theta \le \pi$$

$$F_{ij}(\theta) = f_{ii}(\theta-\pi)f_{ij}(\pi) - f_{ik}(\theta-\pi)f_{kj}(\pi) \qquad \pi \le \theta \le 2\pi \qquad 4.1.13$$

where $i,j,k = 1,2;\ i \neq k$ and the definition of $\underline{\underline{Q}}(\theta)$, given by equation 3.3.4, is used to obtain this result. The leading four expansion matrices, $\underline{\underline{Q}}_\ell$, for $\underline{\underline{f}}(\theta)$ are now written out explicitly for the two-level nondegenerate system, see Equations 3.3.6-3.3.8;

$$\underline{\underline{Q}}_0 = \begin{pmatrix} 1 & 0 \\ 0 & 1 \end{pmatrix} \qquad \underline{\underline{Q}}_1 = \frac{1}{i\upsilon}\begin{pmatrix} E_1 & -\mu\ell \\ -\mu\ell & E_2 \end{pmatrix} \qquad \underline{\underline{Q}}_2 = \frac{1}{2!(i\upsilon)^2}\begin{pmatrix} E_1^2+(\mu\ell)^2 & -\mu\ell(E_1+E_2) \\ -\mu\ell(E_1+E_2) & E_2^2+(\mu\ell)^2 \end{pmatrix}$$

$$\underline{\underline{Q}}_3 = \frac{1}{3!(i\upsilon)^3}\begin{pmatrix} E_1^3+(\mu\ell)^2(2E_1+E_2) & -\mu\ell(E_1(E_1+E_2)+E_2^2+(\mu\ell)^2+\upsilon^2) \\ -\mu\ell(E_2(E_2+E_1)+E_1^2+(\mu\ell)^2+\upsilon^2) & E_2^2+(\mu\ell)^2(2E_2+E_1) \end{pmatrix} \qquad 4.1.14$$

The higher order terms in the expansion of $\underline{\underline{f}}(\theta)$ become increasingly complicated functions of the parameters E_j, $\mu\ell$ and υ showing the need for a recursive computational evaluation of these terms using equation 3.3.7. Further details regarding the convergence of these power series expansions and the optimum choice of expansion interval in θ are given in Appendix A.

The exact solution for $\underline{\underline{Q}}(t)$ has been generated for different phases δ and for a wide variety of frequencies υ and coupling energies $(\mu\ell)$ of the applied sinusoidal field. These solutions are employed in the following sections where specific properties of the two-level nondegenerate system are evaluated. In all cases rapidly convergent solutions were obtained to any required degree of accuracy. For

example, by using expansion intervals ranging from π to $\pi/10$ in θ, see Chapter 3, Section 3.2, results accurate to sixteen significant figures can be readily obtained for values of β spanning the intermediate to strong coupling regions [22,28]; these results require at most the retention of 30-50 terms in the corresponding power series expansions, see equations 3.2.6 and 3.3.1. Equation 4.1.1 was also numerically integrated over a finite range of t using a fourth order Runge-Kutta method to provide a further check on the solution for $\underline{a}(t)$; a number of values of the parameters occurring in equation 4.1.1 were considered. In all cases the numerical results agreed with the iterative solution to the number of figures to which the numerical method was reliable. Further details regarding the numerical solution are also given in Appendix A.

4.2 INDUCED TRANSITION PROBABILITIES FOR THE TWO-LEVEL SYSTEM IN A SINUSOIDAL ELECTRIC FIELD.

The formal results derived in Section 3.7 of the previous chapter will now be employed to extract the induced transition probability and its various averages for the two-level system. The density matrix for this two-level system, from which the various physical properties can be readily obtained, is given by

$$\underline{\rho}(t) = \begin{pmatrix} |a_1(t)|^2 & a_1(t)a_2^*(t) \\ a_1^*(t)a_2(t) & |a_2(t)|^2 \end{pmatrix} \qquad 4.2.1$$

Using the trace prescription given by equation 3.6.3 along with the definition of the matrix $\underline{\beta}$ given by equation 3.7.1, the induced transition probability for the two-level system becomes

$$P_{jj}(t) = |a_j(t)|^2 \qquad j = 1,2 \qquad 4.2.2$$

Equation 4.2.2 and its various averages, see Section 3.7, will be discussed in detail in the remainder of this section.

4.2.1 THE TEMPORAL BEHAVIOUR OF THE INDUCED TRANSITION PROBABILITY FOR A SINUSOIDAL FIELD OF WELL DEFINED PHASE

The induced temporal transition probability, for both the ground and excited state of the two-level system, has been evaluated for different phases δ and for a wide range of frequencies υ and coupling energies ($\mu\mathcal{E}$) of the applied sinusoidal field. Graphical results for $P_{11}(t)$ for three coupling strengths ranging from intermediate to very weak, are presented in Figure 4.1 (a), (b) and (c), for the system initially in the ground state, $|a_1(0)|^2 = 1$, subjected at t=o to a cosine wave ($\delta = 0$). The iterative method is vastly superior to the stepwise power series method outlined in Section 3.2, particularly when the solution is required over large values of θ or t. For example, to generate the results in Figure 4.1(c), using the stepwise power series approach, would require approximately a 50-term power series expansion and boundary matching in each of 10^8 θ-intervals of length π, a clearly prohibitive calculation, see equations 3.3.1 - 3.3.7. On the other hand the iterative solution given by equations 3.4.10 and 3.4.11 requires well under one minute on a CDC CYBER 73-14. Conventional numerical integration techniques being much less efficient than the stepwise power series method, see [22,65], become totally impractical when solutions over physically meaningful time scales are required.

A number of interesting features come to light on studying the graphical results in Figure 4.1. The very weak coupling result in Figure 4.1(c) exhibits the pure sinusoidal pattern predicted by the Rabi formula with the induced transition probabilities for frequencies equally distributed about the resonance frequency $\upsilon = \omega$, agreeing precisely with one another [65]. As the intermediate coupling region is approached ($\beta = 2 \times 10^{-2}$), Figure 4.1(b), the on-resonant results still agree quite closely with the Rabi result, but the off-resonant induced transition probabilities begin to deviate from one another until finally in Figure 4.1(a) they are out of phase with one another by $\sim \pi/2$. The undulations which first appear on the induced transition probability envelopes in Figure 4.1(b), and become much more pronounced in Figure 4.1(a), reflect the increasingly important

Figure 4.1. The induced transition probability; $P_{11}(t) = |a_1(t)|^2$, as a function of time over two "periods" of $P_{11}(t)$ for $\delta = 0$. (a) $\beta = 0.2$; (b) $\beta = 2.0 \times 10^{-2}$; (c) $\beta = 2.0 \times 10^{-8}$. Actual numerical values of the additional parameters needed to generate this figure are; $|a_1(0)|^2 = 1$, $\mu_{12} = 1.0$, $\omega = E_2 - E_1 = 1.0$, $E_1 = -2.0$, $E_1 = -1.0$. The results of this figure depend solely on the initial conditions and the value of β and not on the magnitudes of the individual parameters.

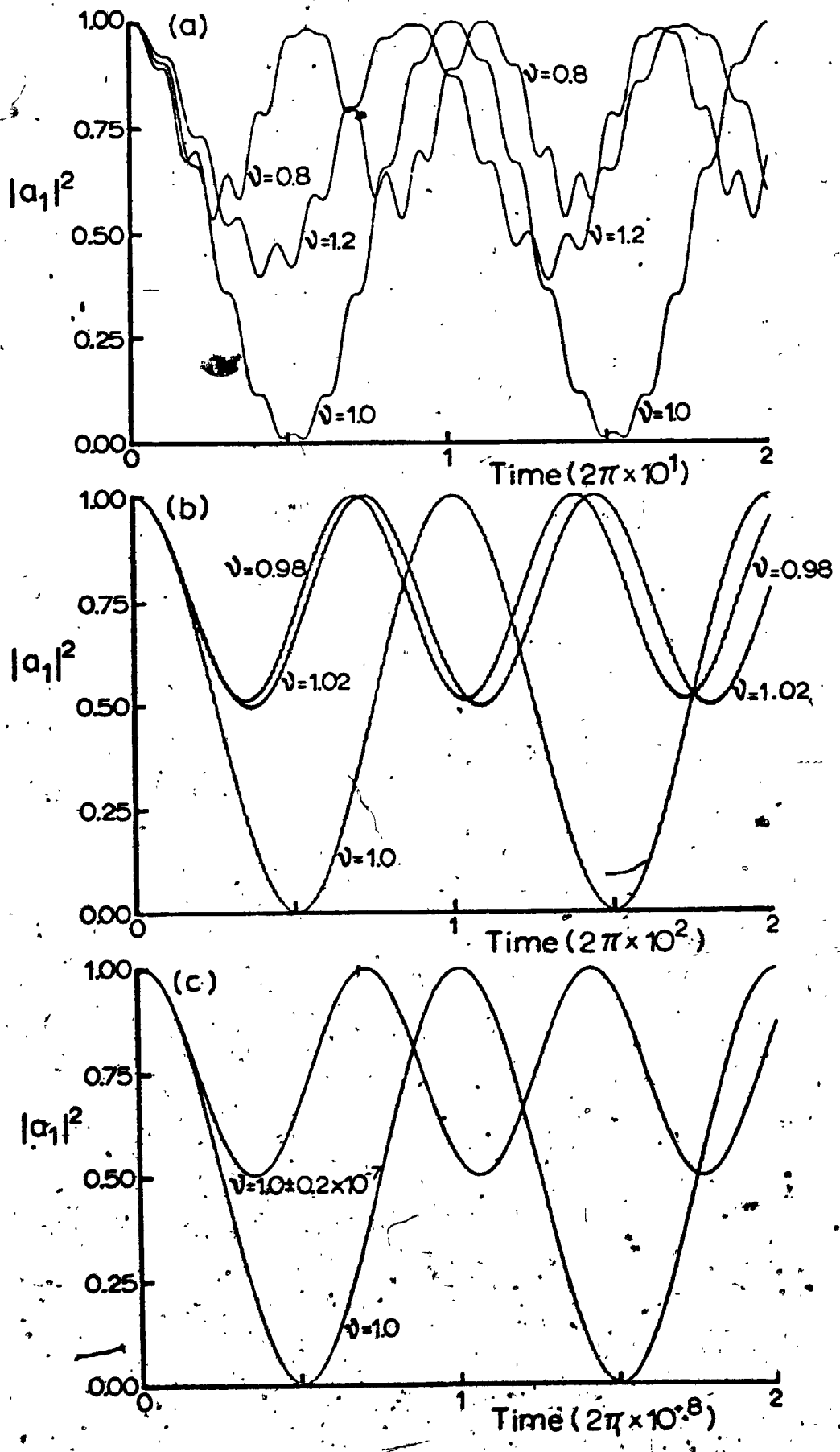
(a)
1.00
0.75
0.50
0.25
0.00
$|a_1|^2$
ν=0.8
ν=1.2
ν=1.0
ν=0.8
ν=1.2
ν=1.0
0
1
2
Time ($2\pi \times 10^1$)
(b)
ν=0.98
ν=1.02
ν=1.0
ν=0.98
ν=1.02
Time ($2\pi \times 10^2$)
(c)
ν=1.0±0.2×10⁻⁷
ν=1.0
Time ($2\pi \times 10^8$)

contribution of the anti-resonant terms ignored in the Rabi approximation [22,28,65]. The period of these undulations corresponds to $t=\frac{\pi}{\omega}$, which is also the period of the coefficients in the differential equation for $a_1(t)$ given by equation 4.1.3 [65]. Figures 4.1(a) and (b) illustrate very clearly the two time scales occurring in the solution of the differential equations with periodic coefficients described by equations 4.1.1 or 4.1.3 with the short time scale corresponding to $t=\frac{\pi}{\omega}$ and the long time scale corresponding closely to that predicted by the Rabi formula ($t \sim 2\pi/|\mu\mathcal{E}|$).

Recently, Salzman [65] numerically integrated equation 4.1.1 with $\beta=0.1$ for a number of phases δ of the sinusoidal field and concluded that the on-resonant Rabi formula closely represents the exact on-resonant solution averaged over the phase δ of the sinusoidal field. The dependence of the induced transition probability on the phase δ of the applied sinusoidal becomes increasingly important as β increases, see Section 4.2.2. These results are not surprising from a physical standpoint since if the transition probability changes appreciably over a single cycle of the applied field, the transition rate should be highly sensitive to the phase δ. For example the phases $\delta=0$ and $\delta=\pi/2$ in equation 4.1.1 would correspond to the "sudden switching on" and the "slow switching on" of the applied perturbation respectively. The physically observed induced transition probability will normally correspond to the phase averaged result and the next section will be devoted to this problem.

Autler and Townes [14] obtained an exact solution to equation 4.1.1 with $\delta=0$ by expanding the periodic part of the Floquet solution, see Section 3.5, Chapter 3, as a fourier series and evaluated the characteristic exponents and the fourier expansion coefficients as a function of ω and β. by solving an infinite set of homogenous equations by continued fraction techniques. These authors extract very useful analytic approximations for the induced transition probability when the coupling strength β is not too large. For intermediate coupling strengths the continued fraction expansions must be evaluated numerically and these numerical evaluations become slowly

convergent as β is increased. A detailed analysis of these continued fraction expansions and their limitations is given by Shirley [58] and he himself resorts to numerical integration of equation 4.1.1 when these expansions fail. Shirley's results will be discussed further in the context of the phase averaged steady state induced transition probabilities in Section 4.4.

Before concluding this discussion of temporal induced transition probabilities, reference should be made to an abortive attempt by Wallace [31] to evaluate these transition probabilities using a finite difference numerical integration scheme. The graphical results presented by this author, purporting to represent the induced transition probability in a two-level system and resonance Raman scattering in a three level system, lack any physical significance. The following analysis will show that this author adopts a differential equation previously proposed by Brooks and Scarfone [45] in their perturbation analysis of equation 2.2.3 and numerically integrates it in a coupling region where it is invalid. Brooks and Scarfone's equation (4), representing the matrix element of the perturbation, becomes in our notation

$$V_{ij}(t) = \left(\frac{\mu_{ij}\mathcal{E}}{2}\right) \exp[i\nu t] + \left(\frac{\mu_{ij}\mathcal{E}}{2}\right) \exp[-i\nu t] \qquad 4.2.3$$

These authors propose, for example, that if either an induced emission or an induced absorption process is being considered from a single stationary state of a system, subjected to the perturbation given by equation 4.2.3 at time t=o, that only one of the two terms appearing in equation 4.2.3 will be responsible for this induced emission/absorption process with the second term making a negligible contribution. In this approximation the exact differential equation 2.2.3 can be separated into two approximate differential equations describing separately the induced emission process

$$i\,\partial/\partial t\, a_2(t) = \frac{\mu_{21}\mathcal{E}}{2} \exp[i(E_2 - E_1 + \nu)t]\, a_1(t) \,, \quad E_2 - E_1 < 0 \qquad 4.2.4$$

and the induced absorption process

$$i\,\partial/\partial t\, a_1(t) = \frac{\mu_{12}\mathcal{E}}{2} \exp[i(E_1 - E_2 - \nu)t]\, a_2(t) \qquad 4.2.5$$

Clearly, equations 4.2.4 and 4.2.5 remain valid only as long as the process ignored in each of them makes a negligible contribution to the state amplitudes. In other words the population of the final state in either process must remain sufficiently small, so that reabsorption or reemission processes are unimportant. The results presented by Wallace clearly violate this above requirement, see Figure 4.2(a), and it is not surprising that his solution requires renormalization at each numerical grid step in order to remain bounded. Indeed, without this renormalization his solution becomes unbounded at the same rate as the perturbation solution, see Figure 4.2(a). The same conclusions can be drawn regarding the graphical results for resonance Raman scattering and this will be discussed further in Appendix A.3. The correct solution for the perturbation given by equation 4.2.3 with the same parameters as used in Figure 4.2(a) is presented in Figure 4.2.(b) for comparative purposes. It should be emphasised that this solution does not require renormalization in order to remain bounded as the hermiticity of equation 4.2.3 guarantees unitarity of the solution.

4.2.2 PHASE AND TIME AVERAGED INDUCED TRANSITION PROBABILITIES

The behaviour of the phase and or time averaged induced transition probabilities for both intermediate and strong coupling strengths β and over a wide frequency domain, encompassing both linear and non-linear transitions, will be studied in detail in this section. Before proceeding further however, a distinction should be made between two types of experiment which yield quite different results. In one experiment transitions between two states are monitored by sweeping the frequency ν of the applied radiation through the transition of interest while in the other the frequency ν is held fixed and the level separation ω is varied by applying a static electric or magnetic field perpendicular to the oscillatory field. The latter technique, for example, is the basis of Stark switching spectroscopy [9,11] and has also been extensively applied in radiofrequency spectroscopy [5,6,17,18]. In the former experiment the

Figure 4.2. The phase dependent induced transition probability, $P_{22}(t)$, as a function of time and for $\beta = 0.2$. (a) Wallace's [31] nonphysical result, (b) the correct result, both for $\delta = 0$. The perturbation theory result, (c), included in [31] is also shown for comparative purposes. Here $|a_1(0)|^2 = 1$, $\mu_{12} = 1.0$, $\omega = E_2 - E_1 = 1.0$, $E_1 = -2.0$ and $E_2 = -1.0$.

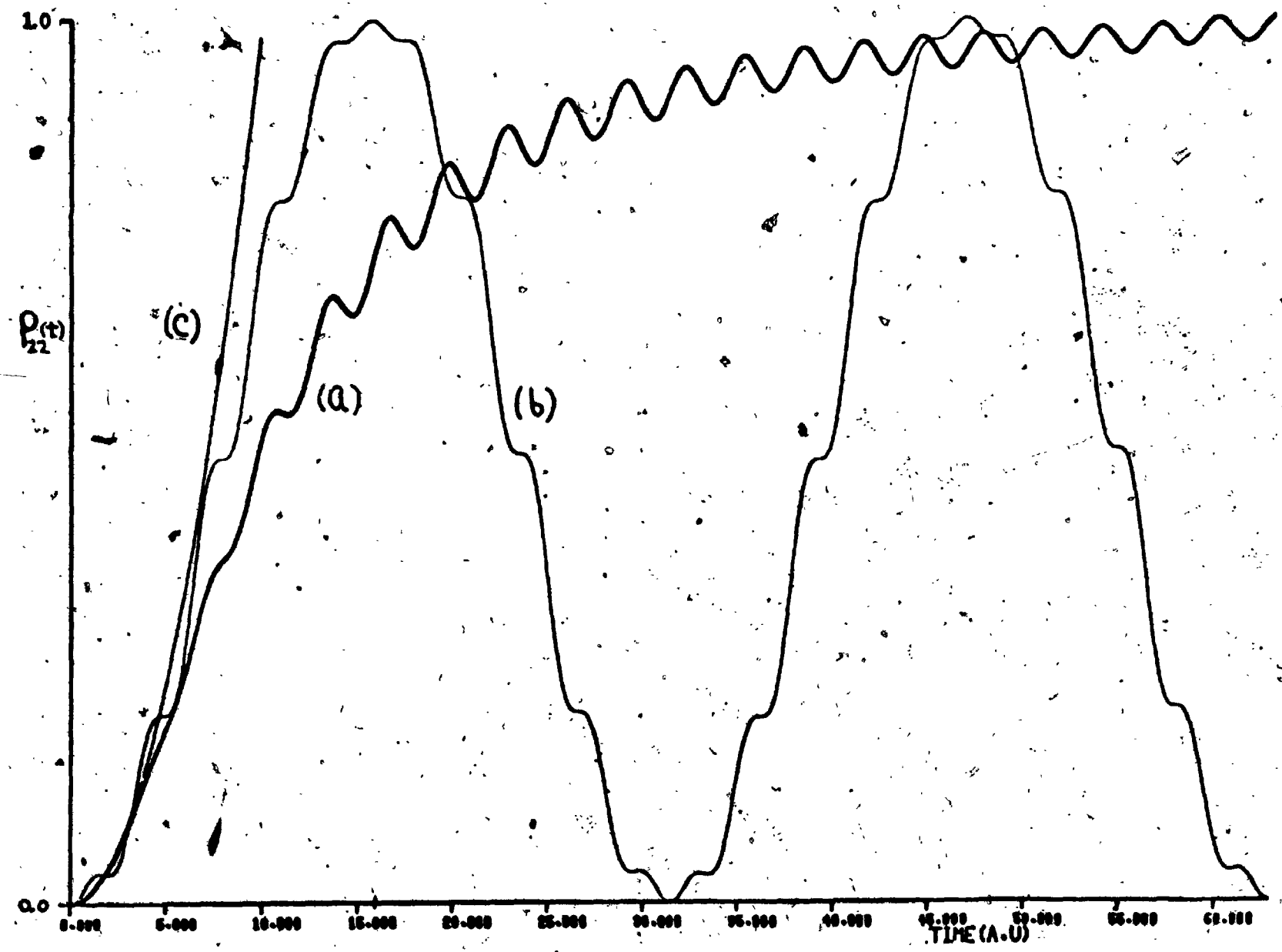
1.0
0.0
$\rho_{22}(t)$
(c)
(a)
(b)
0.000
5.000
10.000
15.000
20.000
25.000
30.000
35.000
40.000
45.000
50.000
55.000
60.000
TIME (A.U)

2 3

OF/DE

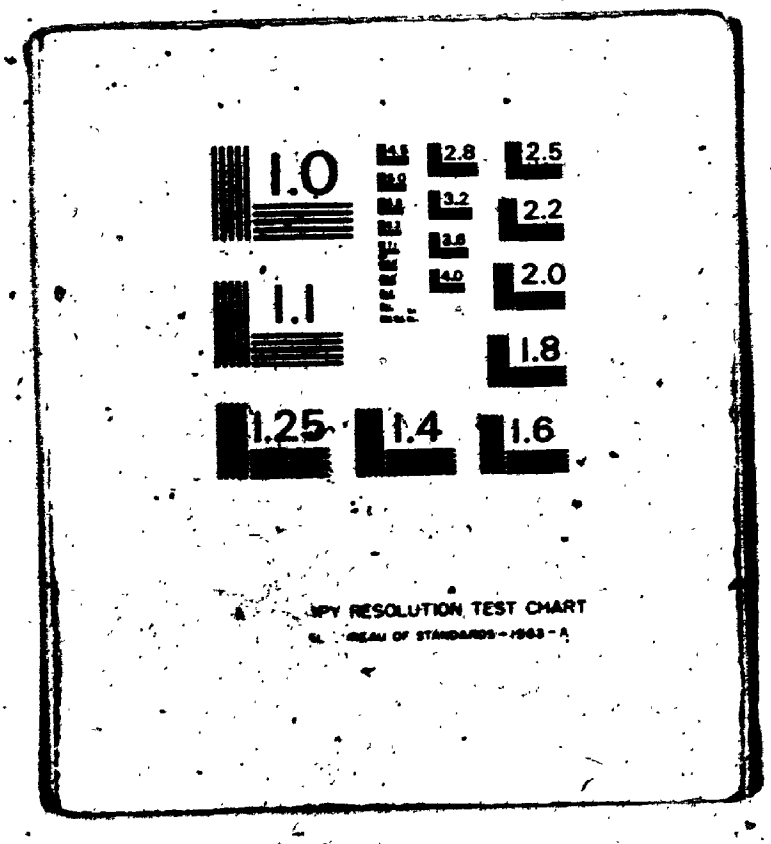
1.0
1.1
1.25
1.4
1.6
2.8
3.2
3.6
4.0
2.5
2.2
2.0
1.8
MPY RESOLUTION TEST CHART
NATIONAL BUREAU OF STANDARDS - 1963 - A

effective coupling of the field to the quantized system remains constant over the entire frequency domain while in the latter, as the level separation ω increases, successive higher photon transitions are more weakly coupled to the applied sinusoidal field. For this reason perturbation expansions up to tenth order in β have adequately described frequency shifts for this latter experiment, even when β is quite large. However, when the coupling strength β remains constant and relatively large over the entire frequency domain, a theoretical analysis becomes increasingly difficult due to strong overlap between multiphoton resonances.

The formal results of Section 3.7, for the temporal phase averaged, the phase/time averaged and the damped averaged induced transition probabilities, will now be employed to extract explicit results for the two level system under the different experimental conditions outlined above. To further emphasize the generality of this formal method we will study, in addition, the effect of a static field $\mathcal{E}^{\circ}$, applied parallel to the oscillating field, on the multiphoton spectra under both types of experimental conditions. The magnetic analogue to this experiment has been carried out recently by Yabusaki, Murakami and Ogawa [72] who employ two mutually perpendicular static magnetic fields, one of which splits the Zeeman sublevels of the Cesium atom, while the other, in combination with a radiofrequency field of fixed frequency ν, induces magnetic dipole transitions between the two substates. Further discussion of this experiment and the above authors' theoretical results will be postponed until Section 4.3 where it will be demonstrated that both the electric and magnetic dipole problems are intimately related as far as the solution to the time dependent Schroedinger equation is concerned.

The steady state induced transition probability $\bar{P}_{22}$, see equation 3.7.6, for the two level nondegenerate system is shown in Figures 4.3(a),(b) as a function of frequency ν for the two coupling strengths β =0.25 and 0.769. These choices of β are made to compare with the results of Shirley [13] and to contrast with those of Gush

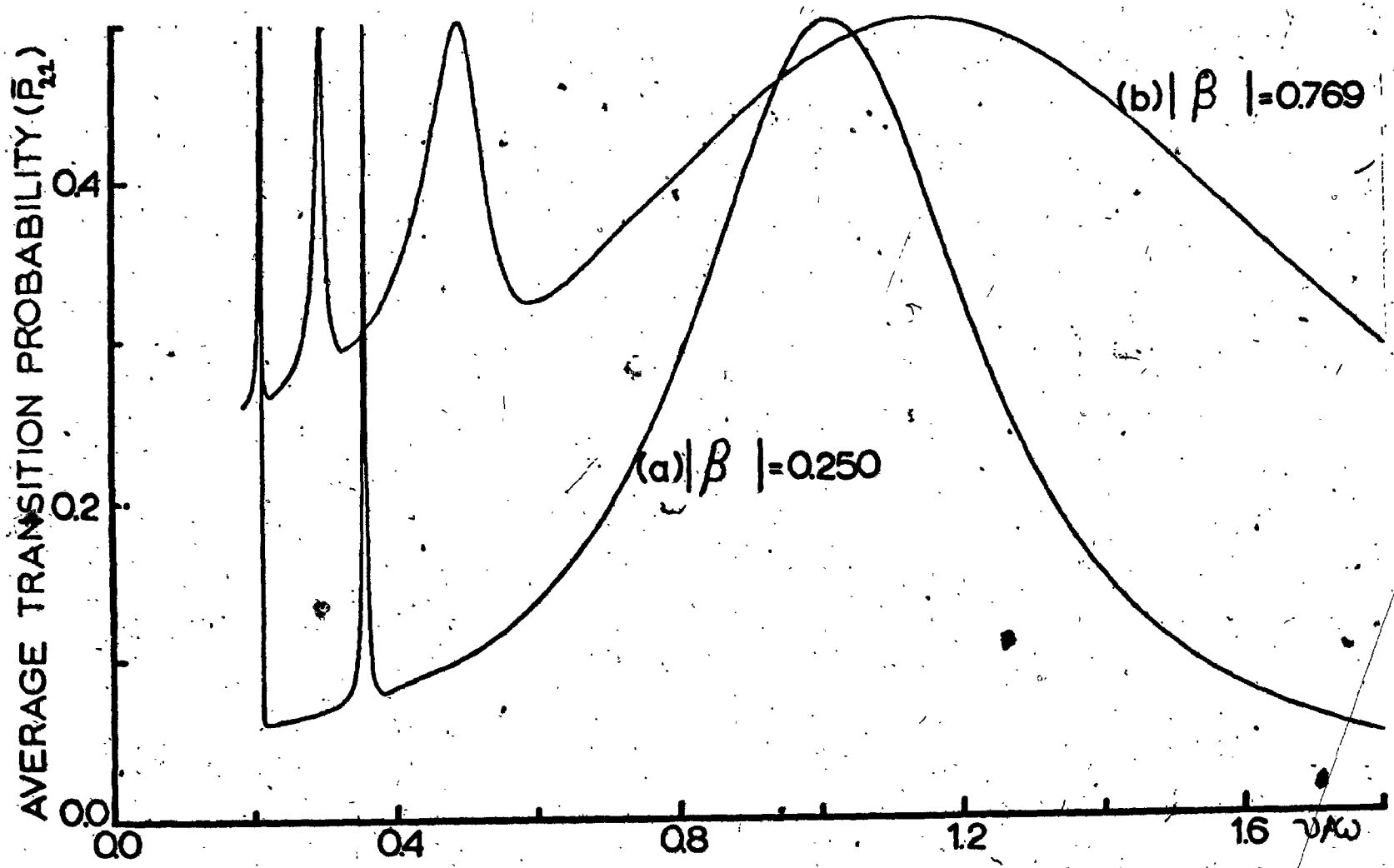

Figure 4.3. The phase averaged steady state induced transition probability, $\bar{P}_{22}$, as a function of frequency ν, in units of ω, for (a) $\beta = 0.25$ (includes the 1,3,5-photon peaks) and (b) $\beta = 0.769$ (includes the 1,3,5,7-photon peaks). Numerical values of the other parameters employed in this calculation are; $|a_1(0)|^2 = 1$, $\omega = E_2 - E_1 = 1.0$; $E_1 = -\frac{1}{2}$, $E_2 = \frac{1}{2}$, $\mu_{12} = 1.0$.

and Gush [15] who vary the level separation ω and hold ν constant. The multiphoton resonances corresponding to successively higher odd photon transitions 1,3,5 (1,3,5,7) photon peaks for β =0.25(0.769) have undergone huge shifts relative to the positions predicted by either the rotating field approximation or simple perturbation theory (that is $\omega, \omega/3, \omega/5$ etc...) and each resonance peaks at $\bar{\rho}_{22}$ =.5 due to the neglect of damping effects. Also evident in these plots is an increasing asymmetry in the individual resonance line shapes as β increases showing a deviation from the symmetric Lorenzian lineshape predicted by the rotating field approximation , see Chapter 2. While both the positions and widths of the resonance peaks are evident from the multiphoton spectra of Figures 4.3(a) and (b), they can easily be determined directly from plots of the characteristic exponents, Δ_j , of the Floquet solution, see equation 3.5.20, as a function of frequency ν, without having to evaluate the induced transition probability from equation 3.7.6.

The original interpretation of these characteristic exponent plots was made by Besset, Horowitz, Messiah and Winter [20] who studied their behaviour for an N-level system via the rotating field approximation. These authors identify a real transition between states i and j as occurring at the frequency ν for which the difference $|\Delta_1^R - \Delta_2^R|$ is a minimum, where Δ_i^R are the characteristic exponents for the Rabi solution, see below. For the two state system the identification of Δ_1^R and Δ_2^R is easy if the Rabi results in equation 2.4.3 are written in the Schroedinger representation in Floquet form, see equation 3.5.14;

$$\begin{pmatrix} a_1(t) \\ a_2(t) \end{pmatrix} = \begin{pmatrix} \gamma_- \exp[-i\nu t/2] & \gamma_+ \exp[-i\nu t/2] \\ -\frac{|\mu\mathcal{E}|}{2\alpha}\exp[i\nu t/2] & \frac{|\mu\mathcal{E}|}{2\alpha}\exp[i\nu t/2] \end{pmatrix} \begin{pmatrix} \exp[i\Delta_1^R t] & 0 \\ 0 & \exp[i\Delta_2^R t] \end{pmatrix} \times \begin{pmatrix} 1 & 1 \\ 1 & 1 \end{pmatrix} \begin{pmatrix} a_1(0) \\ a_2(0) \end{pmatrix} \qquad 4.2.6$$

where $\gamma_\pm = \frac{1}{2}(1 \pm \Omega/\alpha)$; $\alpha = \sqrt{\Omega^2 + |\mu\mathcal{E}|^2}$, $\Omega = \nu - \omega$ and

$$\Delta_2^R = -(E_1 + E_2)/2 \pm \tfrac{1}{2}\sqrt{\Omega^2 + |\mu\mathcal{E}|^2}. \qquad 4.2.7$$

The sum and difference of these characteristic exponents Δ_j^R , j=1,2, becomes

$$\Delta_1^R + \Delta_2^R = -(E_1+E_2)$$
$$\Delta_1^R - \Delta_2^R = \sqrt{\Omega^2+(\mu\mathcal{E})^2} \quad . \qquad 4.2.8$$

If the Rabi lineshape formula, see equation 2.4.6, is now written directly in terms of Δ_j^R , we obtain

$$\bar{\rho}_{22} = \frac{(\mu\mathcal{E})^2}{2(\Delta_1^R-\Delta_2^R)^2} \equiv \frac{(\mu\mathcal{E}^2)}{2[(\nu-\omega)^2+(\mu\mathcal{E})^2]} \quad . \qquad 4.2.9$$

where $|\mu\mathcal{E}|$ is a direct measure of the width at half maximum of the resonance profile in the Rabi approximation. Thus, when $|\Delta_1^R - \Delta_2^R|$ is a minimum $(\nu=\omega)$, $\bar{\rho}_{22}$ is a maximum and this corresponds to the peak in the spectral profile, see Chapter 2. It is also evident from equation 4.2.9 that $|\Delta_1^R - \Delta_2^R|$ at its minimum value is a direct measure of the half width of the resonance profile, that is

$$|\Delta_1^R - \Delta_2^R| = |\mu\mathcal{E}| \qquad 4.2.10$$

Since any physical property of the system derives directly from the density matrix $\underline{\rho}(t)$, through the trace prescription of equation 3.6.3, the occurrence only of the difference $(\Delta_1^R - \Delta_2^R)$, see equation 4.2.6, in this result indicates that such properties depend only on the energy difference $\omega(\equiv(E_2-E_1))$, see equation 4.2.8, and not on the individual magnitudes of E_1, E_2 making their choice arbitrary. Indeed equation 4.2.7 shows that the term $-(E_1+E_2)/2$ acts as an absolute energy reference point for the frequency dependent characteristic exponents Δ_j^R and can be conveniently chosen to be zero by setting $E_1=-\frac{\omega}{2}, E_2=\frac{\omega}{2}$. The above choice of a zero energy reference point will prove particularly convenient when the characteristic exponents Δ_j for the exact solution are computed, see below, and Shirley [13].

As the exact solution and the Rabi formula must agree in the weak field limit for $\nu\sim\omega$ we would expect the characteristic exponents Δ_j derived in the formal method of Chapter 3 to be related to Δ_j^R in this limit. Indeed a general expression for the sum of the exact Δ_j's has already been obtained, see equation 3.5.19 , which is directly analgous to the result of equation 4.2.8 for $(\Delta_1^R+\Delta_2^R)$, and which,

for this two state system becomes

$$E_1 + E_2 = -(\Delta_1 + \Delta_2)\nu \quad , \mathrm{mod}(\nu) \qquad 4.2.11$$

Thus in the weak field limit, for $\nu \sim \omega$ we obtain

$$(\Delta_1 + \Delta_2)\nu \simeq \Delta_1^R + \Delta_2^R \quad , \mathrm{mod}(\nu) \qquad 4.2.12$$

Equations 4.2.11 and 4.2.12 suggest that plots of the characteristic exponents* Δ_j for the exact solution can be used to locate resonance maxima and the shifts of these resonances from the positions predicted by the usual perturbation theory result, see equation 2.3.21, or the rotating field approximation [13,58]. The power of such characteristic exponent plots both for locating resonance positions and determining their respective halfwidths** will be demonstrated explicitly for the two level system in this and the following sections, see for example Figures 4.4-4.5, and for multilevel systems in Chapter 5.

The choice of an absolute energy reference point of zero, see equation 4.2.11, ensures that $\Delta_1 = -\Delta_2$, mod$(\nu/2)$, thereby yielding the following simple symmetric periodic relationship between the multiple values of Δ_j, see equation 3.5.20, that is

$$\Delta_j' = \Delta_j + n/2 \qquad n = 0, \pm 1, \pm 2, \cdots \qquad 4.2.13$$

where Δ_j corresponds to the smallest value of Δ_j' $(n=0)$. As was pointed out in the previous chapter, this multivaluedness of the characteristic exponents arises directly from equations 3.5.19 and 3.5.20 through the arctangent function and from equation 4.2.11, see Shirley [13,58]. Coupled with equation 4.2.13 one can visualize

---

* Note that the multiplicative factor ν must be included in any physical interpretation of the characteristic exponents. However as we are studying their behaviour as a function of ν over a wide frequency domain it will be more convenient to plot the Δ_j's rather than $\nu\Delta_j$, see Section 4.4.

** As a halfwidth is defined only for a symmetric lineshape, the increasing asymmetry of the resonance profiles as β increases makes such a term become redundant, see Figures 4.3 and 4.5. However, $2\nu|\Delta_1 - \Delta_2|$ still provides an estimate of the width of the profile.

infinitely many branches [13,58] of Δ_j (specified by the value of n) lying above and below one another and where the values of Δ_j are bounded by the branch lines $n \pm 1/2$. Due to the simple periodic relation between the characteristic exponents Δ_j, their plots in each branch are identical so that we need concern ourselves only with a single branch.

The above characteristic exponents also appear in more recent fully quantized studies, by Cohen-Tannoudji and Haroche [71] and Yabusaki et al [72,73], of the magnetic interactions of a spin 1/2 system coupled directly to a general static magnetic field and a strong radiofrequency field. It can be demonstrated, see Section 4.3, that the energies of the fully quantized system, in units of ν, computed to tenth order in perturbation theory, coincide precisely with the characteristic exponents Δ_j derived from the Floquet solution in the semiclassical model. In the plots of these energies of the total system of atom and static and r.f fields, real transitions occur at the points at which these energies or characteristic exponents Δ_j, approach but do not touch the branch lines $n/2$; such points are labelled "anti-crossings" and these determine the positions of the resonance maxima. Twice the distance from such an "anti-crossing" to the nearest branchline is proportional* to the "half width" of the respective transition, for example see equation 4.2.10. In addition the points at which Δ_j crosses these branch lines are termed "level crossings" and such points correspond to degeneracies in the energies $\nu\Delta_j$. Such degeneracies can be removed by applying a static electric field $\mathcal{E}^\circ$ or magnetic field $\mathcal{B}^\circ$, which converts these level crossings to anti-crossings thereby inducing additional transitions in the system, see Sections 4.2.3 and 4.3 for electric and magnetic cases respectively.

---

* The actual halfwidth is given by the quantity $\nu|\Delta_1 - \Delta_2|$ when it is a minimum. In the interpretation of a frequency sweep experiment this definition must be used to determine the precise location of the anti-crossing since ν is not held constant.

The interpretation of the characteristic exponent plots in the previous paragraph will be adopted in discussing results for the two level system, while the interpretation by Besset et al [20] will be used when multilevel systems are considered in the next chapter. Both approaches are clearly equivalent** and the above choices are dictated by convenience.

The characteristic exponents Δ_j corresponding to the induced transition probabilities shown in Figure 4.3(a),(b) are plotted over the same frequency domain ω in Figure 4.4(a),(b). From these plots the multiphoton resonances 1,3,5(1,3,5,7) in Figures 4.3(a),(b) occur at the anti-crossings A_1, A_3, A_5 (A_1, A_3, A_5, A_7) in Figures 4.4(a),(b) respectively. The level crossings (n=2,4,6,8) are also indicated in these plots where the subscript n in A_n, refers to an n-photon allowed transition while in L_n, it refers to a forbidden n-photon transition. As the coupling strength β increases the precise position of the anti-crossing A_1 is not obvious and this indicates the very large broadening of the single photon maximum. These plots also show how successive higher photon peaks encroach upon one another as the frequency ω approaches the static limit $\omega = 0$.

Figure 4.5(a),(b) show the multiphoton spectrum and its accompanying characteristic exponent plot in the strong coupling region (β=2.0). Comparing Figures 4.4 and 4.5 we can draw the following conclusions regarding the behaviour of these spectra as a function of β. As β increases all of the resonance peaks shift

---

** The interpretation of the characteristic exponents Δ_j used by Cohen-Tannoudji and Haroche[71] remains valid as long as the condition $\epsilon_1 + \epsilon_2 = 0$ is satisfied, this implies that $\Delta_1 = -\Delta_2$.

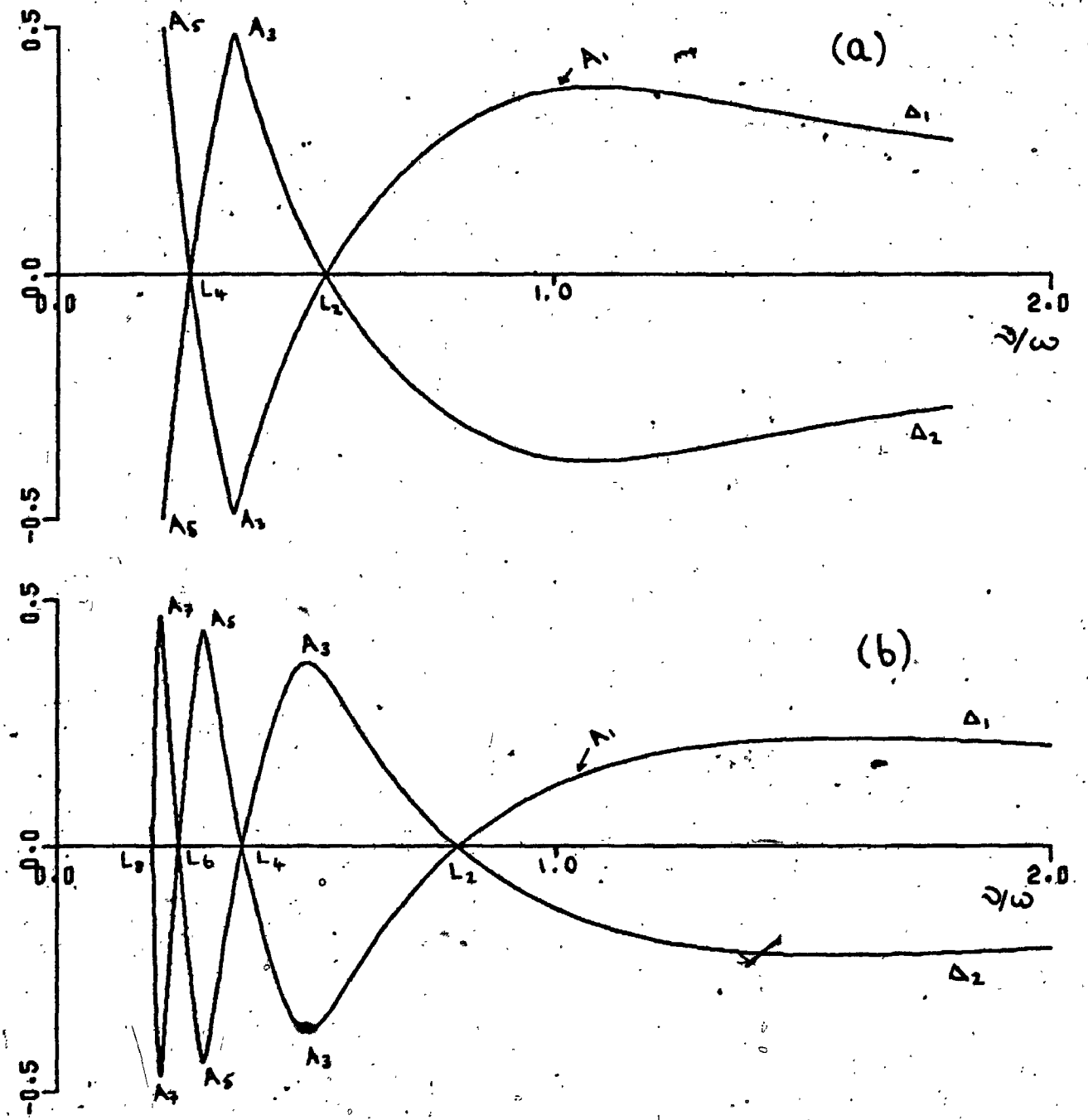

Figure 4.4. Plots of the characteristic exponents Δ_1 and Δ_2 corresponding to $\bar{P}_{22}$ in Figure 4.3 and over the same frequency domain. (a) $\beta = 0.25$, (b) $\beta = 0.769$. A_n correspond to the "anti-crossings" signifying an allowed n-photon transition while L_n correspond to the "level-crossings" which signify a "forbidden" n-photon transition.

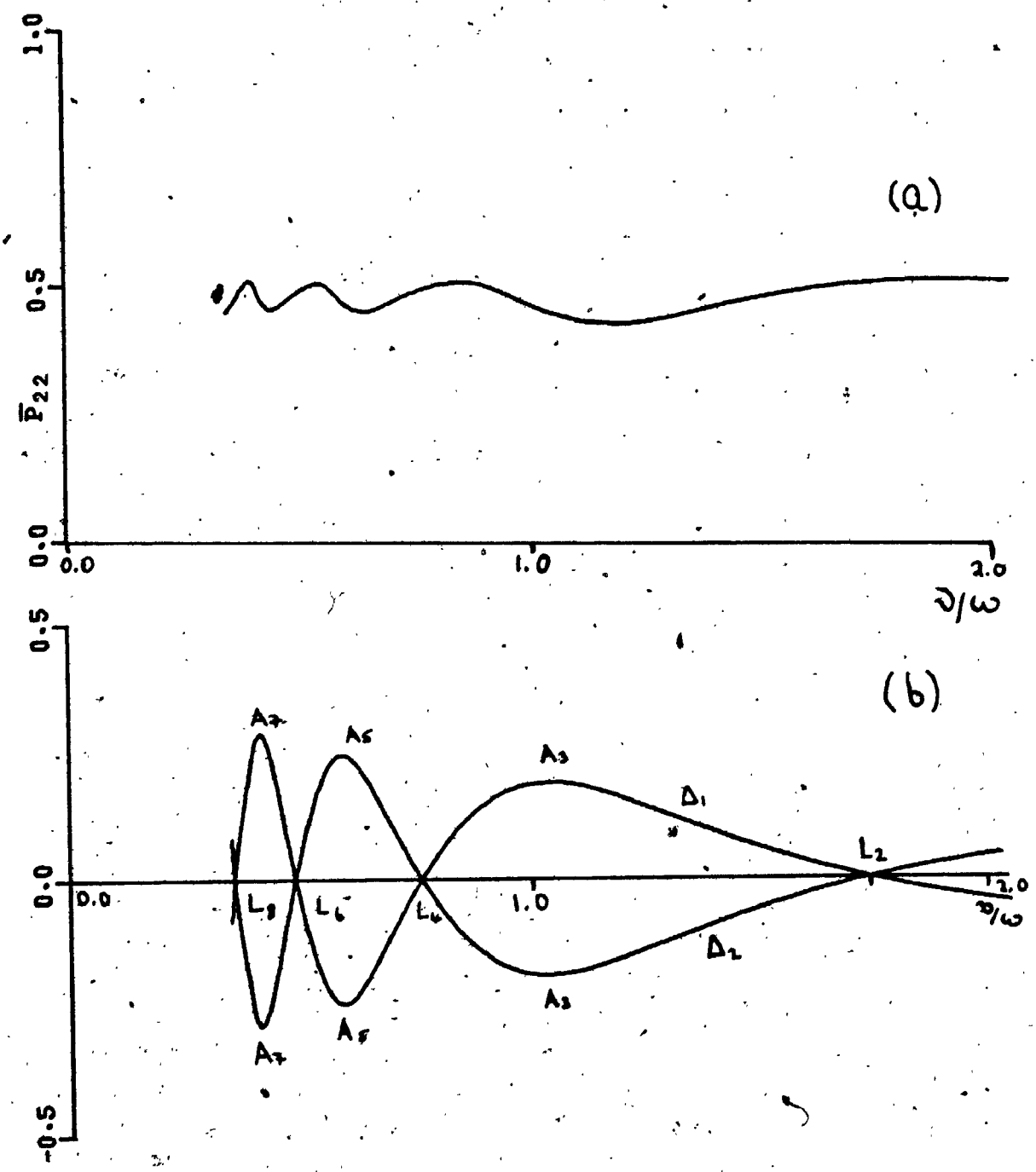

Figure 4.5. (a) The phase averaged steady state induced transition probability, $\bar{P}_{22}$, for $\beta = 2.0$. (b) The accompanying characteristic exponent plots. The numerical values of the other parameters used to generate this figure are the same as in the preceding two figures except that = 2.0.

towards higher frequency ν until finally in the strong coupling region (β=2.0) there is such a strong overlap between neighbouring resonances that the entire spectrum approaches $\bar{P}_{22}$=.5 at which point $\bar{P}_{11} = \bar{P}_{22}$=0.5 and all the transitions are saturated. The characteristic exponent plots also reflect this behaviour with the level crossings L_n moving along the zero line to higher frequencies. The gradual approach of the anti-crossings to the zero line reflects the broadening of the n-photon resonances and the asymptotic coupling limit ($\beta \to \infty$) at which the n-photon transitions completely vanish is represented by the value of β for which A_n reaches the zero line (that is Δ_1 and Δ_2 are degenerate).

Next we consider the temporal behaviour of the phase averaged induced transition probability $\bar{P}_{11}(t) = 1 - \bar{P}_{22}(t)$ for frequencies ν lying on the resonance maxima in the multiphoton spectra of Figures 4.3(a) and (b). Figures 4.6 and 4.7 show $\bar{P}_{11}(t)$, see equation 3.7.3, for these frequencies over a finite number of "periods" of its slowly varying part (long time scale). Even for these intermediate values of β the sinusoidal pattern for the single photon transition predicted for $\bar{P}_{11}(t)$ by the Rabi formula begins to breakdown, resulting in a more complicated aperiodic pattern, compare Figures 4.6(a) and 4.7(a), which indicates that the anti-resonant terms ignored in the Rabi approximation become increasingly important as β increases. The effect of increasing β is even more dramatic for the higher photon induced transition probabilities, see Figures 4.6 and 4.7, where complicated oscillatory patterns occur over the "period" of the slowly varying part of $\bar{P}_{11}(t)$. The period of these undulations lies close to the period of the oscillatory perturbation (short time scale) $t \sim \pi/\nu$ and their amplitudes increase with increasing β. These undulations arise from the pronounced dependence of the phase dependent induced transition probability, $\rho_{11}(t,\delta)$ on the phase δ of the applied sinusoidal field. This phase dependence is shown explicitly over one period of the Hamiltonian in Figures 4.8 and 4.9 for two representative phases ($\delta = 0, \pi/2$) and for the coupling parameters β and frequencies ν of Figures 4.6 and 4.7. It is clear from these results that the differences in induced transition rates, $\partial/\partial t\, \rho_1(t,\delta)$, for the

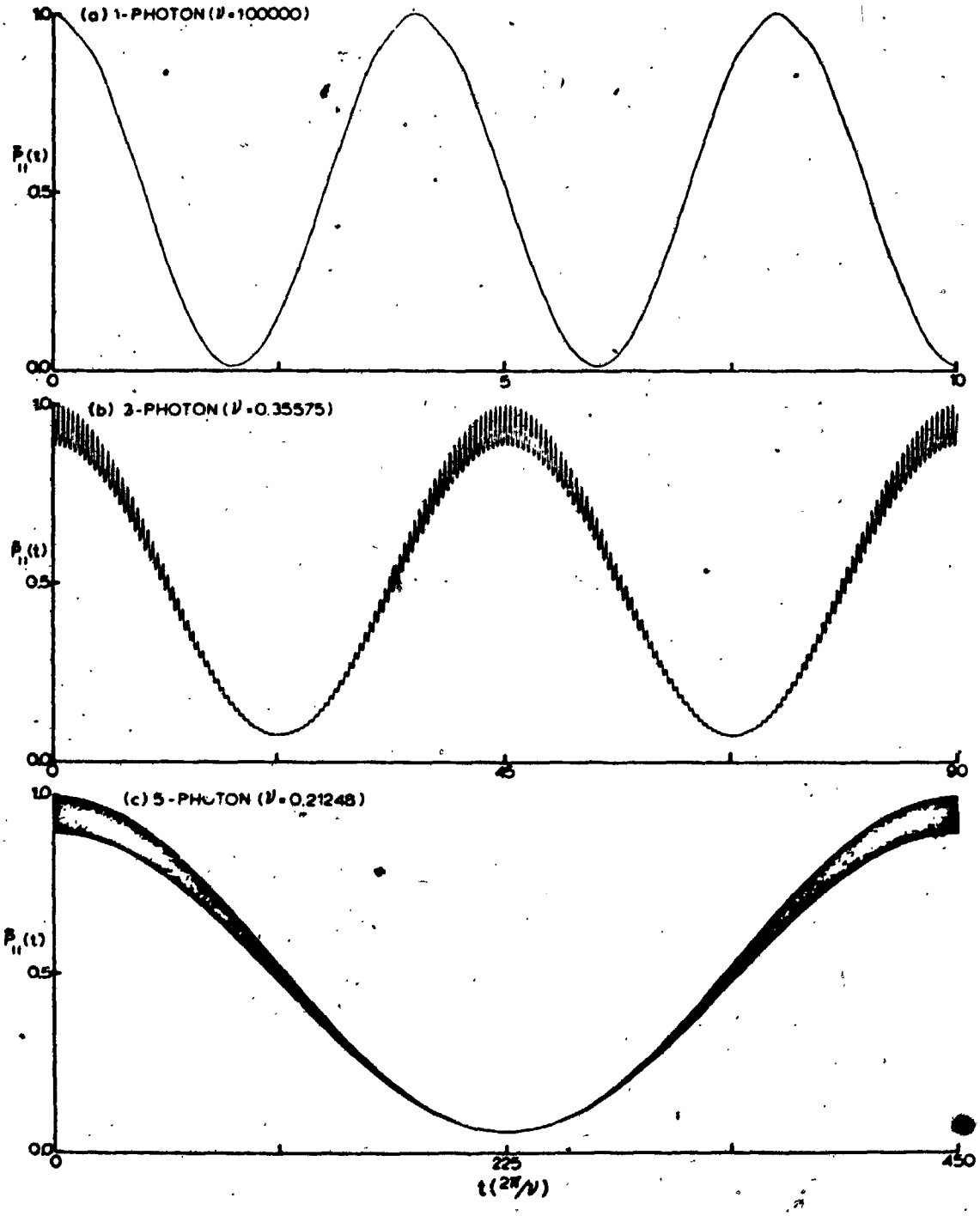

Figure 4.6. The phase averaged induced transition probabilities, $\bar{P}_{11}(t)$, corresponding to frequencies ν associated with the resonance maxima of Figure 4.3(a); $\beta = 0.25$. Figure 4.6(c) appears as a dark background, as the graphical scale is too small to resolve the oscillatory pattern. $\bar{P}_{11}(t)$ is shown as a function of t over a finite number of cycles. Here time, t, is in units of $(2\pi/\nu)$.

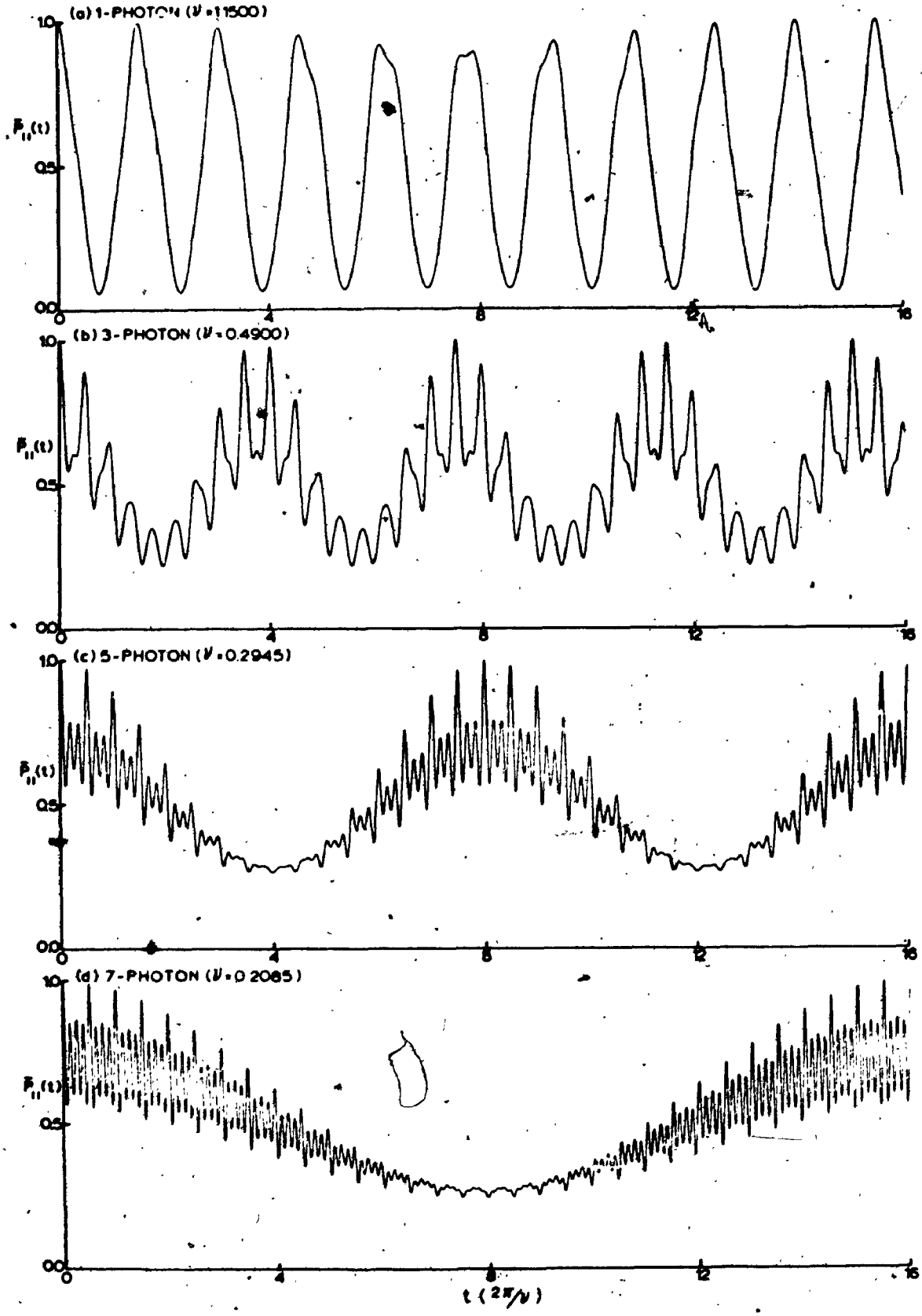

Figure 4.7. The phase averaged induced transition probabilities, $\bar{P}_{11}(t)$, corresponding to frequencies ν associated with the resonance maxima of Figure 4.3(b); $\beta = 0.769$.

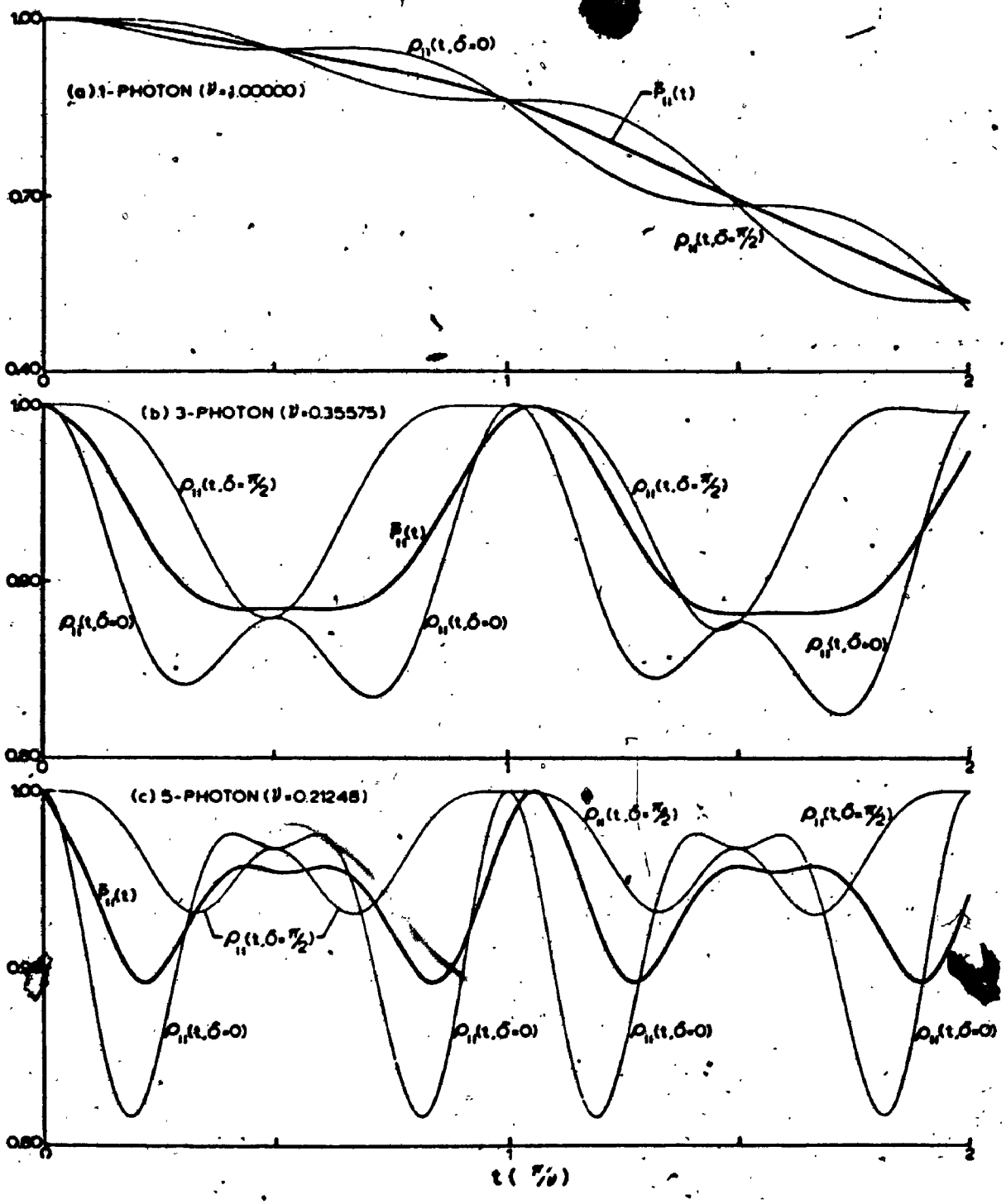

Figure 4.8. The phase dependent induced transition probability, $\rho_{11}(t,\delta)$, for $\delta = 0$ and $\delta = \pi/2$ as a function of time over one period of the Hamiltonian for $\beta = 0.25$ and the frequencies associated with the three resonance maxima of Figure 4.3(a). Enlarged portions of the corresponding plots of the phase averaged induced transition probability, $\bar{P}_{11}(t)$, versus t given in Figure 4.6(a), (b) and (c) are included for comparative purposes. Here t is in units of (π/ν).

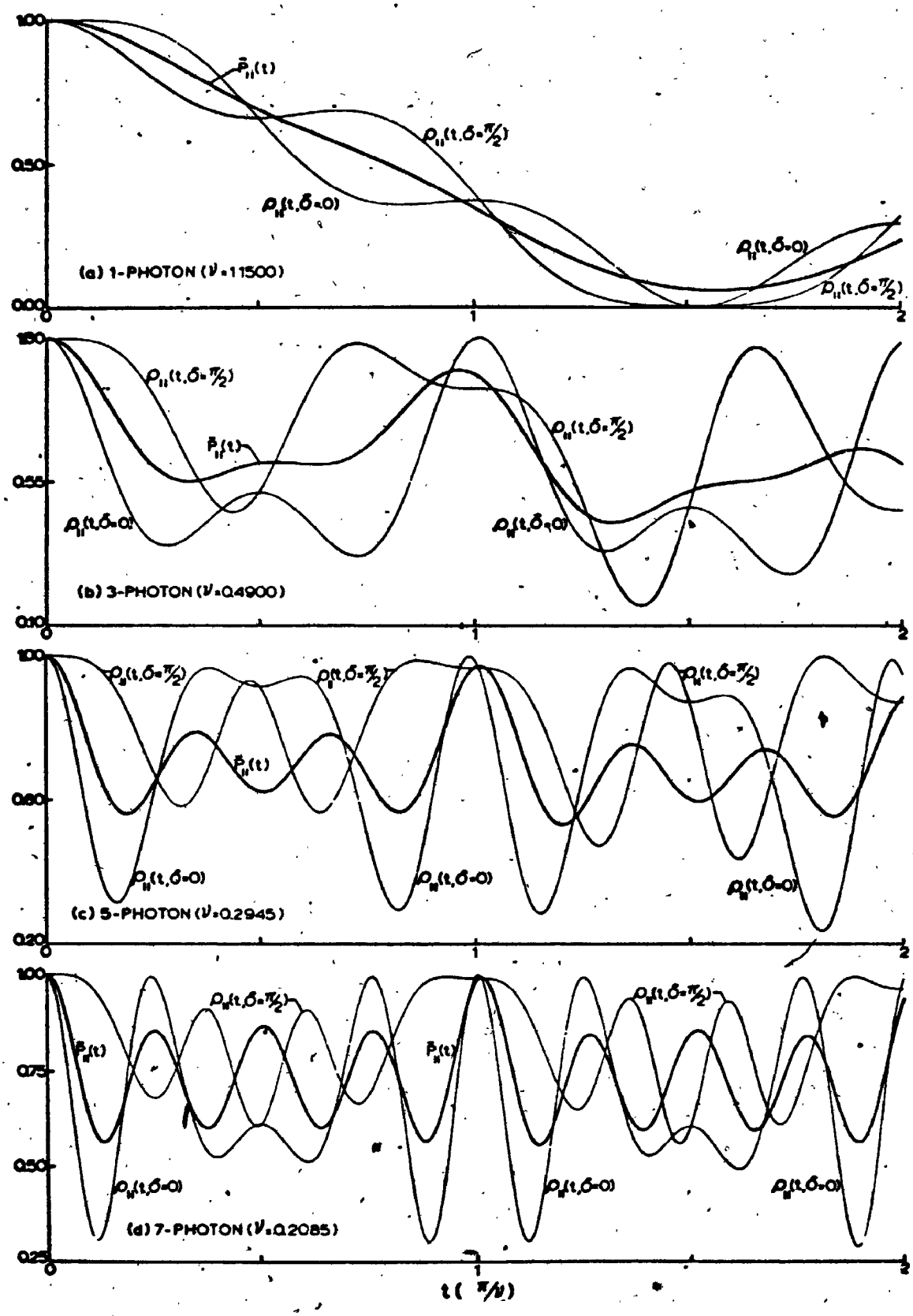

Figure 4.9. The phase dependent induced transition probability, $\rho_{11}(t,\delta)$, for $\delta = 0$ and $\delta = \pi/2$ over one period of the Hamiltonian for $\beta = 0.769$ and for frequencies ν associated with the four resonance, maxima of Figure 4.3(b). Enlarged portions of the corresponding plots of $\bar{P}_{11}(t)$ versus t given in Figure 4.7(a),(b),(c) and (d) are also shown for comparative purposes.

sudden ($\delta=0$) versus the slow ($\delta=\pi/2$) "switching on" of the applied perturbation becomes more pronounced (1) as β increases for a particular multiphoton transition and (2) for higher relative to lower multiphoton transitions for fixed β. The former effect suggests, see also the discussion above for the single photon case, that the retention of only "resonant" terms in the representation of $\bar{P}_{11}(t)$ for fairly large values of β will lead to incorrect results for all multiphoton transitions. The latter effect on the other hand suggests that there is a strong nonlinear dependence of the higher photon transitions on the field intensity $I \propto |\mu\mathcal{E}|^2$ the transition probability for a n-photon transition being proportional to $|\mu\mathcal{E}|^{2n}$ [38].

The effects of damping on the multiphoton spectra of Figures 4.3(a) and (b), are shown in Figures 4.10 and 4.11 where the damped phase averaged induced transition probability $\bar{P}_{22}^{\tau}$ is plotted, see equation 3.7.10, for three different values of the relaxation constant τ for $\beta=.25$ and .769 respectively. These choices of τ were made to damp out certain phase averaged induced transition probabilities $\bar{P}_{11}(t)$ in Figures 4.6 and 4.7 for different multiphoton transitions before steady state oscillations can set in; thus for example, τ is chosen in Figure 4.10(b) so that $\bar{P}_{11}(t)$ for the 5-photon transition damps out before there is any significant accumulation of transition probability for the excited state (that is the resonance vanishes) while the 3-photon peak has reduced to $\sim 1/2$ its undamped height. The systematic drop off in the higher relative to the lower photon resonance maxima for fixed τ is caused by the increase in the long time period of $\bar{P}_{11}(t)$ for the higher photon transitions, see Figure 4.6. Thus the actual observation of these multiphoton resonances in any experiment will depend critically on relaxation effects. In Figure 4.11 the damped multiphoton spectra become more complicated than in Figure 4.10, because the slowly varying "periods" of successive higher photon induced transition probabilities $\bar{P}_{11}(t)$ begin to approach the same limit, compare Figure 4.6 with 4.7.

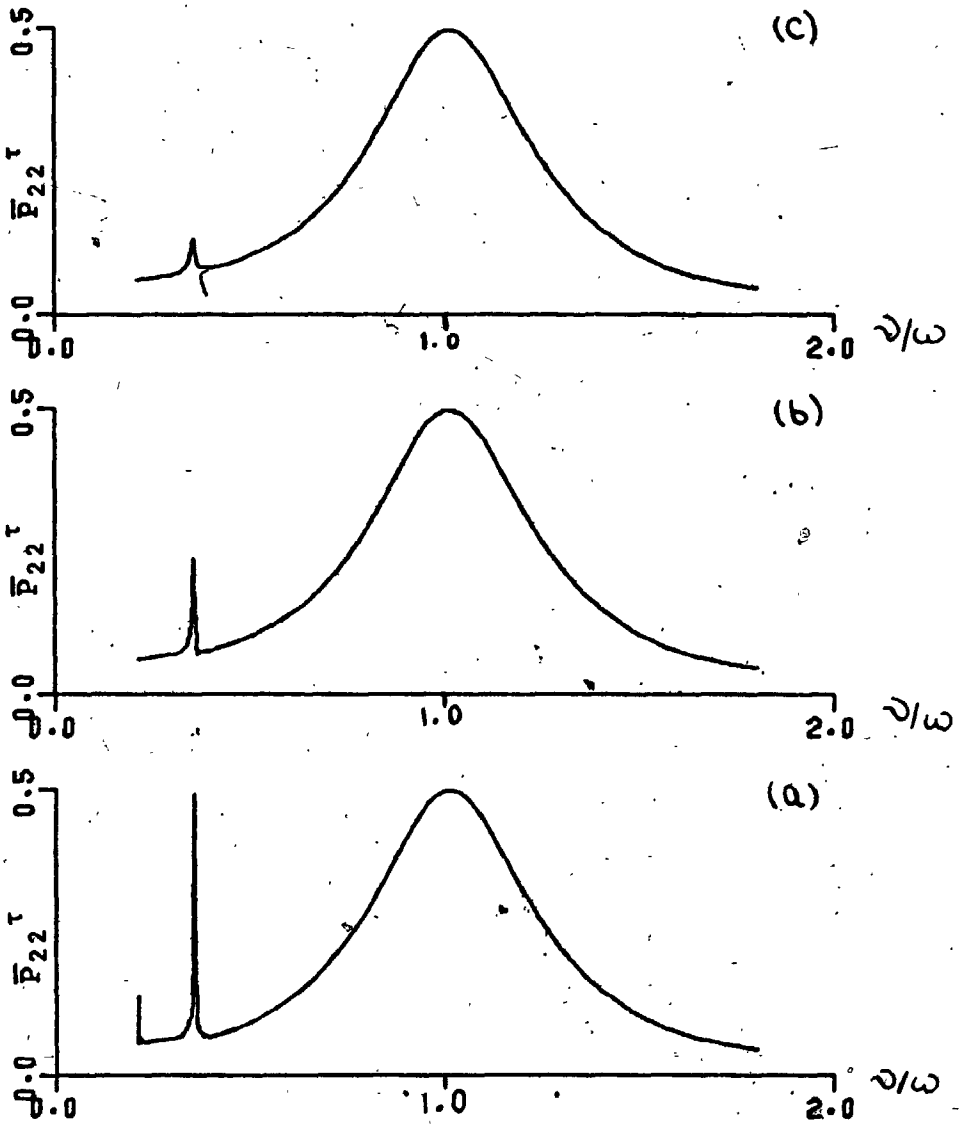

Figure 4.10. The damped phase averaged induced transition probability, $\bar{P}_{22}^{\tau}$, for $\beta = 0.25$ over the same frequency domain and for the same parameters as in Figure 4.3(a). (a) $\tau = 10^3$ (b) $\tau = 10^2$ (c) $\tau = 50$. These choices of τ were made to cut off $\bar{P}_{22}(t)(\equiv(1 - \bar{P}_{11}(t))$, see Figure 4.6) at different stages before steady state oscillations set in.

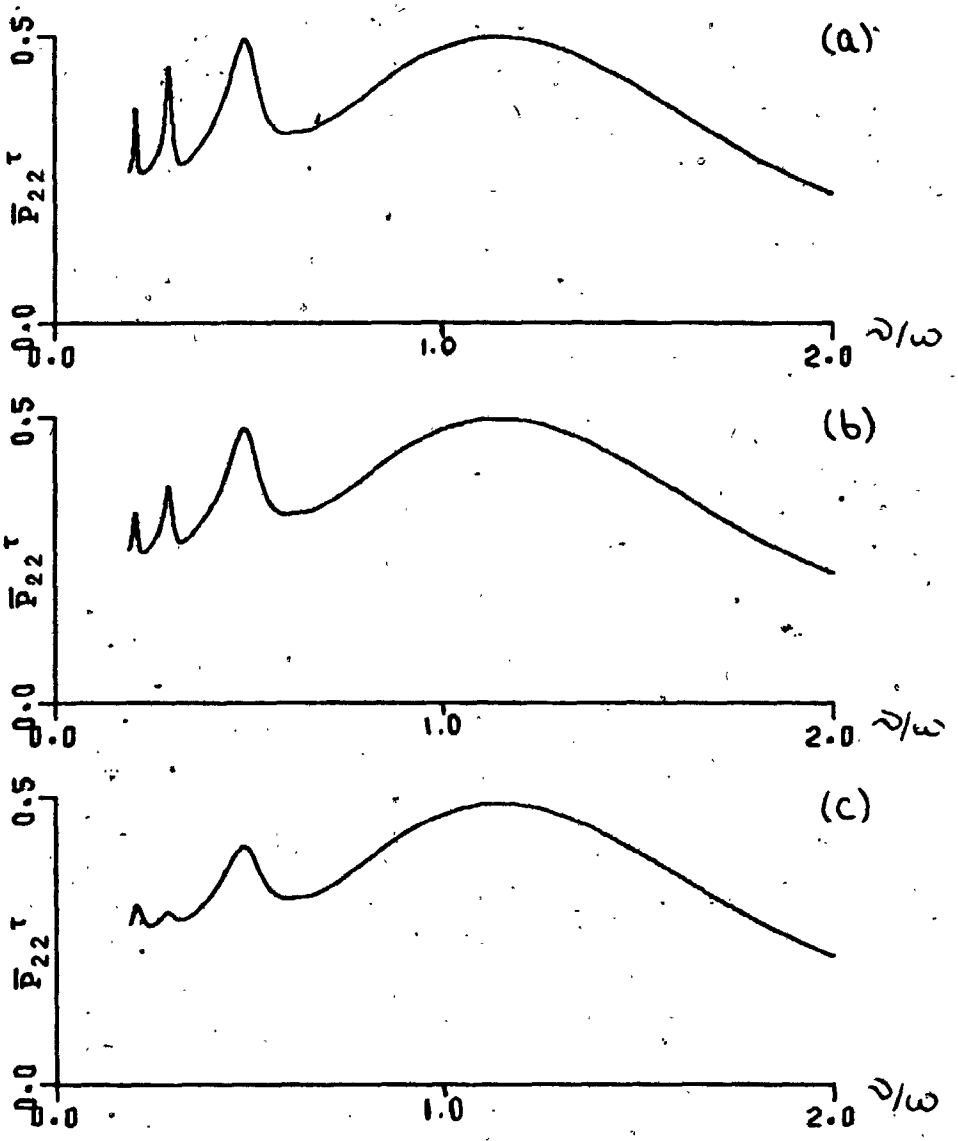

Figure 4.11. The damped phase averaged induced transition probability, $\bar{P}_{22}^{\tau}$, for $\beta = 0.769$ over the same frequency domain and for the same parameters as in Figure 4.3(b). (a) $\tau = 10^2$, (b) $\tau = 50$, (c) $\tau = 10$. Again the choices of τ were dictated by the oscillatory behaviour of $\bar{P}_{22}(t)(\equiv(1 - \bar{P}_{11}(t))$, see Figure 4.7.

Before concluding this section we refer briefly to a recent article by Ahmad [21] which alludes to the fact that a discrepancy exists between his result for the average transition probability and that obtained by Shirley [13] when the applied field is exactly on resonance ($\nu = \omega$). It is easy to show, using the formal method developed in Chapter 3, that Ahmad has in fact calculated $\bar{P}_{12}(\delta)$ for $\delta = 0$, see equation 3.7.5, rather than $\bar{P}_{22}$ which corresponds to the phase average of $\bar{P}_{22}(\delta)$. Figure 4.12 shows $\bar{P}_{22}(\delta)$ for three representative phases $\delta = 0, \pi/4, \pi/2$ along with $\bar{P}_{22}$, for $\nu = \omega$, as a function of the coupling parameter β. The oscillatory behaviour of $\bar{P}_{22}(0)$ coincides precisely with Ahmad's description of the average transition probability over this coupling strength range and the values of β at which his computed transition probability again equals 0.5 ($\beta/2 \sim 1.23$–1.24 and 2.07) coincide precisely with the points at which $\bar{P}_{22}(0)$ crosses the line 0.5. This figure shows rather dramatically the strong dependence of the time averaged induced transition probability $\bar{P}_{22}(\delta)$ on the phase δ of the applied sinusoidal field in the intermediate-strong coupling domains. It is also clear from this figure that the phase averaged steady state induced transition probability $\bar{P}_{22}$, which corresponds to Shirley's physical observable, never exceeds 1/2. The oscillatory behaviour of $\bar{P}_{22}$ below 0.5 is indicative of the fact that successive higher photon resonance maxima are being shifted to higher frequencies past the point $\nu = \omega$, in the frequency domain, as β increases and for example Figure 4.12 shows that when $\beta/2$ increases to ~ 1.23, the three photon resonance peak has shifted to $\nu = \omega$ in the frequency domain while when $\beta/2 \simeq 2.07$ the five photon resonance peak has been shifted to this frequency.

Other treatments [16–18, 21–24] of the two level system, with the exception of Shirley [13] and Gush and Gush [15], have not taken the effects of phase averaging into account in evaluating induced transition probabilities in the intermediate-strong coupling regions.

Figure 4.12. The phase dependent steady state induced transition probability, $\bar{P}_{22}(\delta)$, for $\delta = 0, \pi/4, \pi/2$ as a function of the coupling parameter β for $\nu = \omega$. Included for comparative purposes is the phase average of $\bar{P}_{22}(\delta)$ which corresponds to the physically observed steady state induced transition probability, $\bar{P}_{22}$. The numerical values of the other parameters employed in generating this figure are; $|a_1(0)|^2 = 1$, $\nu = \omega = 1.0$, $E_1 = -2.0$, $E_1 = -1.0$, $\mu_{12} = 1.0$. The abscissa in this figure is in units of $\beta/2$ to compare with Ahmad's [21] definition of his coupling parameter $S(\equiv \beta/2)$.

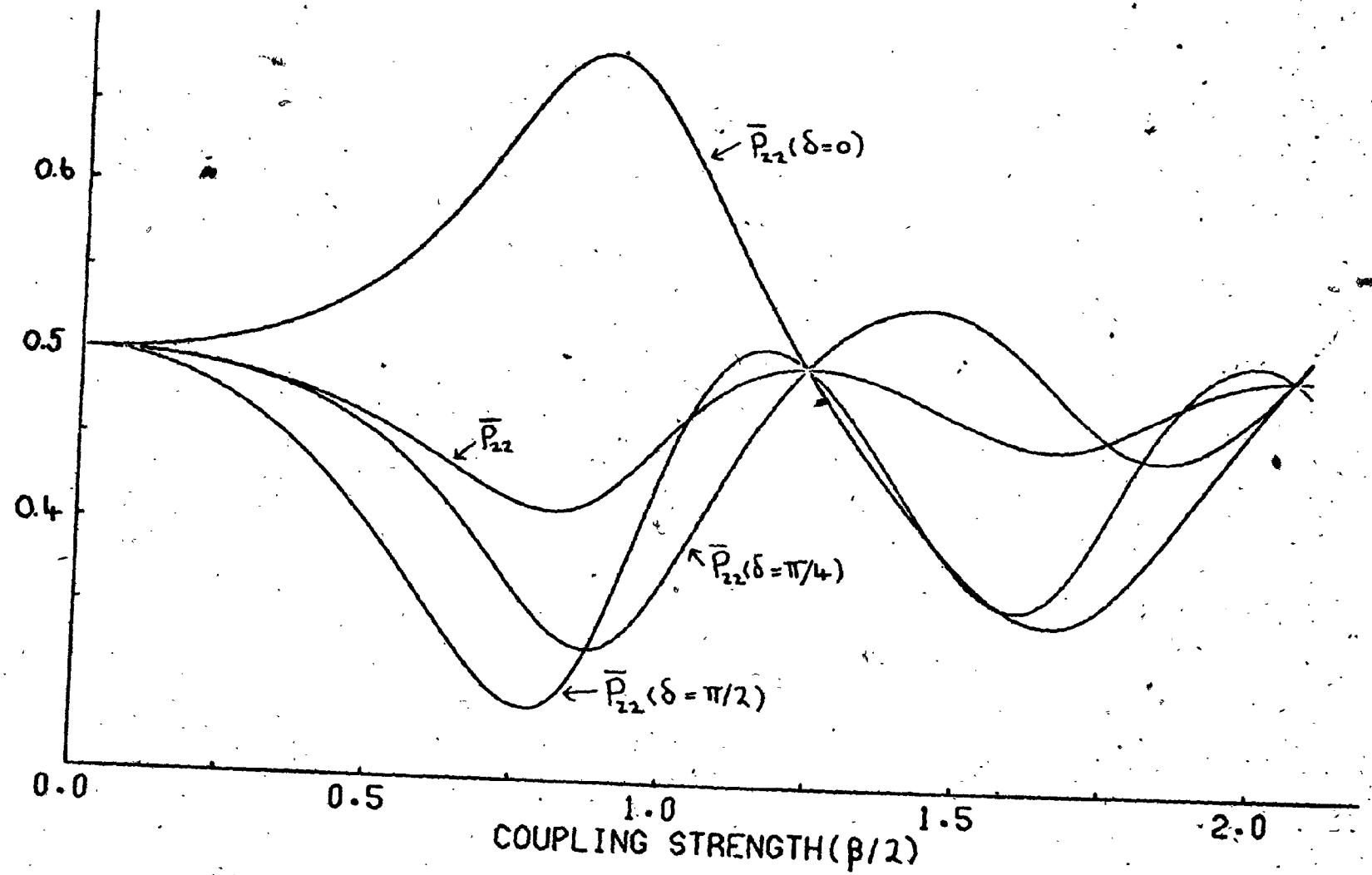
$\bar{P}_{22}(\delta=0)$
$\bar{P}_{22}$
$\bar{P}_{22}(\delta=\pi/4)$
$\bar{P}_{22}(\delta=\pi/2)$
0.6
0.5
0.4
0.0
0.5
1.0
1.5
2.0
COUPLING STRENGTH(β/2)

4.2.3 EFFECT OF A STATIC STARK FIELD ON THE TWO LEVEL MULTIPHOTON SPECTRA.

The inclusion of a static field $\mathcal{E}^\circ$ parallel to the applied sinusoidal field, $\mathcal{E}\cos(\omega t+\delta)$, introduces a number of interesting features in the multiphoton spectra of the previous section. The static field $\mathcal{E}^\circ$ will mix the two states of the system so that, in effect, the oscillating field is inducing transitions between two states of mixed parity [36]. Thus both odd and even photon transitions will be allowed in this system, see Chapter 2. The total Hamiltonian for the system becomes

$$H(r,t) = H_0(r) - \mu_z[\mathcal{E}^\circ + \mathcal{E}\cos(\omega t+\delta)] \qquad 4.2.14$$

The Hamiltonian still retains its periodic property and the system of coupled differential equations describing the interaction is given by

$$i\frac{\partial}{\partial t}\begin{pmatrix}a_1(t)\\a_2(t)\end{pmatrix} = \begin{pmatrix}E_1 & -\mu_{12}\mathcal{E}^\circ\\ -\mu_{21}\mathcal{E}^\circ & E_2\end{pmatrix}\begin{pmatrix}a_1(t)\\a_2(t)\end{pmatrix} - \mathcal{E}\cos(\omega t+\delta)\begin{pmatrix}0 & \mu_{12}\\ \mu_{21} & 0\end{pmatrix}\begin{pmatrix}a_1(t)\\a_2(t)\end{pmatrix} \qquad 4.2.15$$

The formal method developed earlier still applies to the solution of equation 4.2.15. However the symmetry over adjoining π intervals is lost due to the presence of nonzero off diagonal elements in the $\underline{\underline{E}}$ matrix, see Chapter 3 and Appendix A2, and the matching power series solution must be employed on the entire $[0,2\pi]$ domain.

In the absence of the oscillating field equation 4.2.15 can be solved in closed form by employing standard Laplace transform techniques discussed in Appendix B. The solution, $\hat{\underline{a}}(t)$, to 4.2.15 when $\mathcal{E}=0$ is given by

$$\hat{\underline{a}}(t) = \gamma^{-1}\exp[-i(E_1+E_2)t/2]\,\hat{\underline{\underline{S}}}(t)\,\underline{a}(0) \qquad 4.2.16$$

where $\hat{\underline{\underline{S}}}(t)$ is a unitary matrix,

$$\hat{\underline{\underline{S}}}(t) = \begin{pmatrix}[\gamma\cos\tfrac{1}{2}\gamma t + i\omega\sin\tfrac{1}{2}\gamma t] & 2i\mu_{12}\mathcal{E}^\circ\sin\tfrac{1}{2}\gamma t\\ 2i\mu_{21}\mathcal{E}^\circ\sin\tfrac{1}{2}\gamma t & [\gamma\cos\tfrac{1}{2}\gamma t - i\omega\sin\tfrac{1}{2}\gamma t]\end{pmatrix} \qquad 4.2.17$$

and

$$\gamma = \sqrt{\omega^2+4|\mu_{12}\mathcal{E}^\circ|^2}\quad ;\quad \omega = E_2-E_1 \qquad 4.2.18$$

Inspection of equations 4.2.16–4.2.18 shows that $\hat{\underline{a}}(t)$ has

exponential terms oscillating at the frequencies

$$q_{A}^{S} = (E_1+E_2)/2 \pm 1/2\,\gamma \qquad 4.2.19$$

and in the limit that both states are degenerate, $\omega \to 0$, we recover the familiar expression for the Stark splitting of the original degenerate pair of states [36],

$$q_{\pm} = E_0 \pm \mu_{12}\mathcal{E}^0 \quad ; \; E_0 = E_1 = E_2 \; . \qquad 4.2.20$$

Equation 4.2.19 therefore represents the more general Stark splitting of two nondegenerate states and its close resemblence to the characteristic exponents Δ_2^R of the Rabi solution (replace Ω^2 by ω^2 in equation 4.2.7) indicates that the characteristic exponents $q_{\pm}$ (or Δ_2^R) represent the energies of the two state system when perturbed by a static (or rotating) field. After some straightforward manipulations using equations 4.2.16-4.2.18 the total wavefunction $\Psi(r,t)$ can be written in the form

$$\Psi(r,t) = \Psi_S \exp[-i q_S t] + \Psi_A \exp[-i q_A t] \qquad 4.2.21$$

where Ψ_S and Ψ_A, corresponding to the eigenvalues q_S and q_A, diagonalize the Hamiltonian

$$H(r,t) = H_0(r) - \mu_z \mathcal{E}^0 \qquad 4.2.22$$

Here

$$\Psi_S = C_1\phi_1(r) + C_2\phi_2(r)$$
$$\Psi_A = C_3\phi_1(r) + C_4\phi_2(r)$$

and

$$C_1 = \gamma^{-1}[(-\omega/2+\gamma/2)\,a_1(0) + \mu_{12}\mathcal{E}^0 a_2(0)]$$
$$C_2 = \gamma^{-1}[(\omega/2+\gamma/2)\,a_2(0) + \mu_{12}\mathcal{E}^0 a_1(0)]$$
$$C_3 = \gamma^{-1}[(\omega/2+\gamma/2)\,a_1(0) - \mu_{12}\mathcal{E}^0 a_2(0)]$$
$$C_4 = \gamma^{-1}[(-\omega/2+\gamma/2)\,a_2(0) - \mu_{12}\mathcal{E}^0 a_1(0)] \qquad 4.2.23$$

and in the limit $\omega \to 0$

$$\Psi(r,t) \to \Psi_- \exp[i q_- t] + \Psi_+ \exp[i q_+ t] \qquad 4.2.24$$

where

$$\Psi_{\pm} = 1/2\left[a_1(0)\left(\phi_1(r) \pm \phi_2(r)\right) + a_2(0)\left(\phi_1(r) \pm \phi_2(r)\right)\right]$$
$$= 1/2\left(a_1(0) + a_2(0)\right)\left(\phi_1(r) \pm \phi_2(r)\right)$$

One can now visualize that the oscillating field, in equation 4.2.15, is inducing transitions between two stationary states Ψ_S and Ψ_A of mixed parity and with respective energies a_S and a_A. Rather than use equation 4.2.15 directly, the problem could be solved by expanding the total wavefunction $\Psi(r,t)$ in the representation which diagonalizes the new stationary state Hamiltonian given by equation 4.2.22, that is [36,75,76]

$$\Psi(r,t) = a_S(t)\,\Psi_S(r) + a_A(t)\,\Psi_A(r) \qquad 4.2.25$$

In this representation the coupled differential equations become

$$i\frac{\partial}{\partial t}\begin{pmatrix} a_S(t) \\ a_A(t)\end{pmatrix} = \begin{pmatrix} a_S & 0 \\ 0 & a_A\end{pmatrix}\begin{pmatrix} a_S(t) \\ a_A(t)\end{pmatrix} - \mathcal{E}\cos(\omega t+\delta)\begin{pmatrix} \mu_{SS} & \mu_{SA} \\ \mu_{AS} & \mu_{AA}\end{pmatrix}\begin{pmatrix} a_S(t) \\ a_A(t)\end{pmatrix} \qquad 4.2.26$$

where

$$\langle\Psi_S|\mu_z|\Psi_S\rangle = \mu_{SS} = 2C_3C_4\mu_z,\ \langle\Psi_A|\mu_z|\Psi_A\rangle = \mu_{AA} = 2C_1C_2\mu_{12}$$

$$\langle\Psi_S|\mu_z|\Psi_A\rangle = \mu_{SA} = (C_1C_4+C_2C_3)\mu_{12} = \mu_{AS}$$

In the limit that $\omega\to 0$, $\mu_{SA}\to\mu_{\mp}\to 0$ and equation 4.2.26 can be integrated directly to yield the solution to the two level degenerate system in an oscillating field, see Section 4.1. As equation 4.2.26 provides no particular computational advantage over equation 4.2.15, we will employ the latter in actual calculations. Equation 4.2.26 will be particularly useful however in interpreting the results that follow.

The effect of the static Stark field $\mathcal{E}^o$ on the multiphoton spectra of Figures 4.3(a) and (b) is shown in Figures 4.13(a)-4.14(a) and Figures 4.15(a)-4.16(a), respectively, for two values of the static field coupling parameter $\delta = 2|\mu_{12}\mathcal{E}^o|/\omega = 0.2, 1.0$. Both even and odd photon transitions can now occur as the original states $\phi_1(r)$ and $\phi_2(r)$ are partially mixed by the static field $\mathcal{E}^o$, see Chapter 2. The occurrence of even photon transitions (2,4,6...) in these spectra is further illustrated by the accompanying characteristic exponent plots, see Figures 4.13(b)-4.14(b) and 4.15(b)-4.16(b), where the "level crossings" L_n (n even) in Figures 4.4(a) and 4.4(b), respectively, have now changed to "anti-crossings" A_n signifying the occurrence of a real transition at these frequencies. Again the

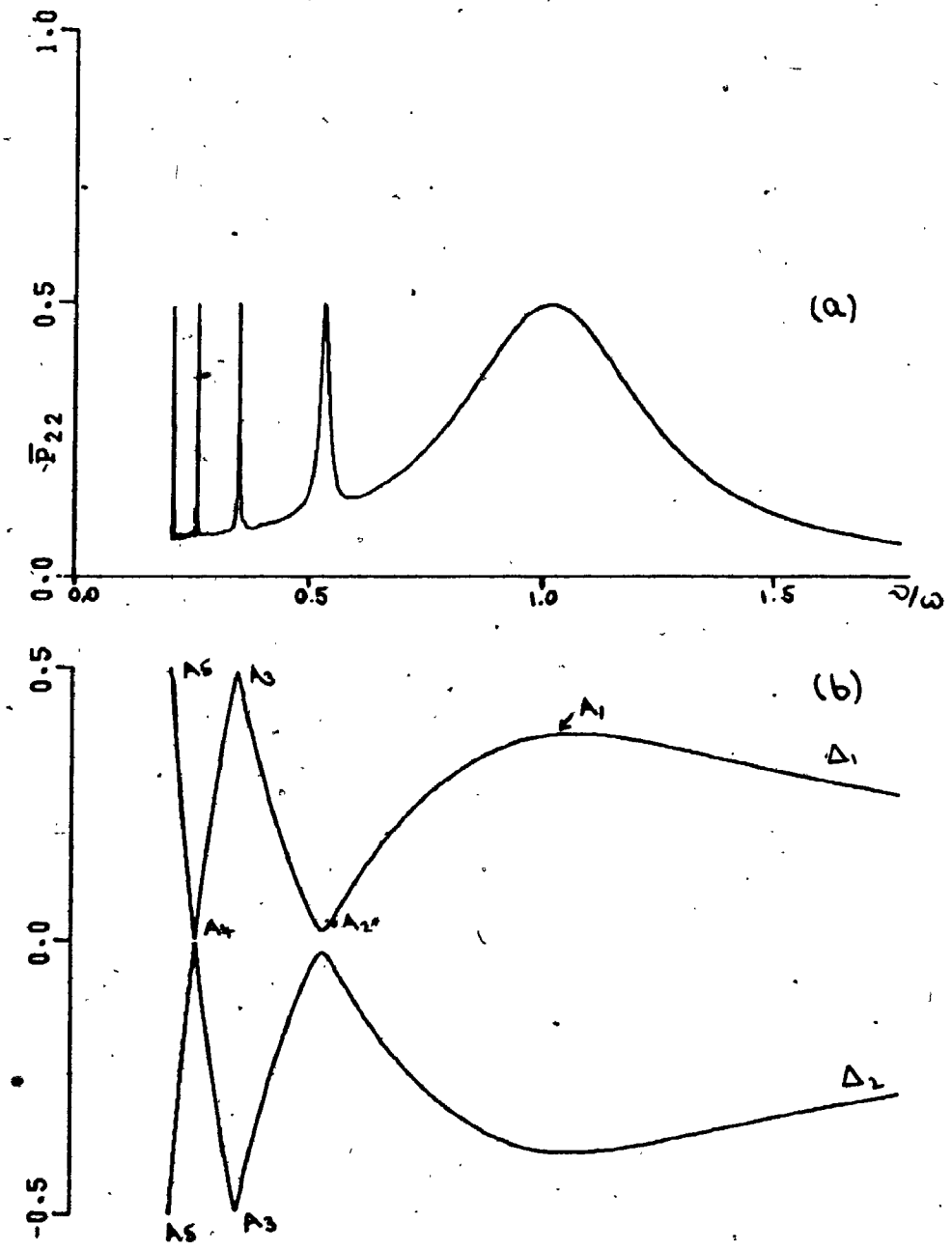

Figure 4.13. The phase averaged steady state induced transition probability, $\bar{P}_{22}$, and the accompanying characteristic exponent plots as a function of frequency ν for the static stark coupling parameter $\delta = 2|\mu_{12}\mathcal{E}^0|/\omega = 0.2$ and for $\beta = 0.25$. All n-photon transitions (n = 1,2,3,4 and 5 are shown in the figure) occur at the positions of the "anti-crossings" A_n. All other parameters needed to generate Figures 4.13 - 4.14 are the same as used to generate Figure 4.3(a).

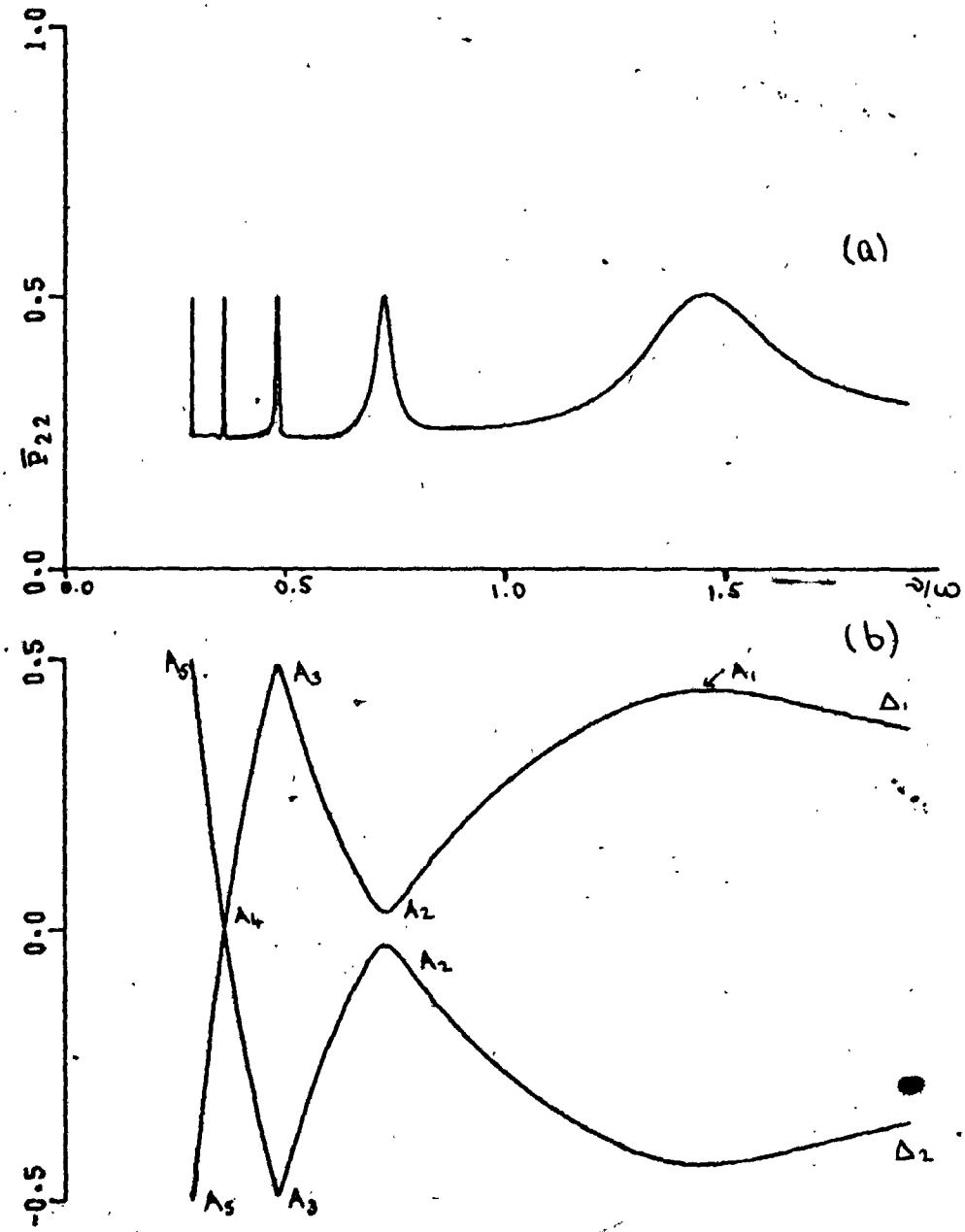

Figure 4.14. The phase averaged steady state induced transition probability, $\bar{P}_{22}$, and the accompanying characteristic exponent plots for the static stark field coupling parameter $\delta = 1.0$. The remainder of the parameters are precisely the same as used in Figure 4.13.

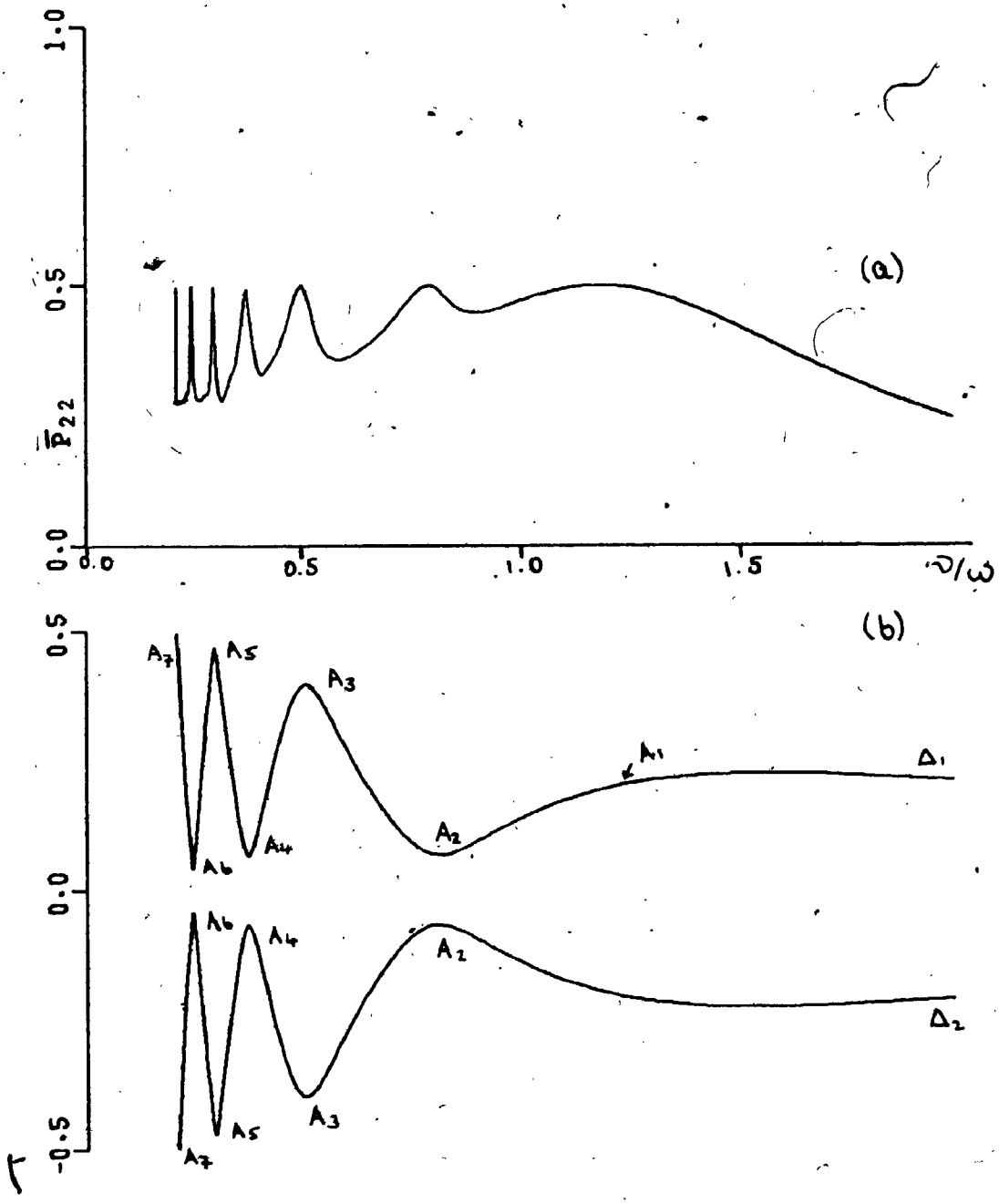

Figure 4.15. The phase averaged steady state induced transition probability, $\bar{P}_{22}$, and the accompanying characteristic exponent plots as a function of frequency ν for the static stark field coupling parameter $\delta = 0.2$ and for $\beta = 0.769$. This figure shows the leading eight n-photon resonances (A_n, n = 1,2,3,4,5,6,7,8). The remaining parameters used to generate this figure and Figure 4.16 are the same as used for Figure 4.3(b).

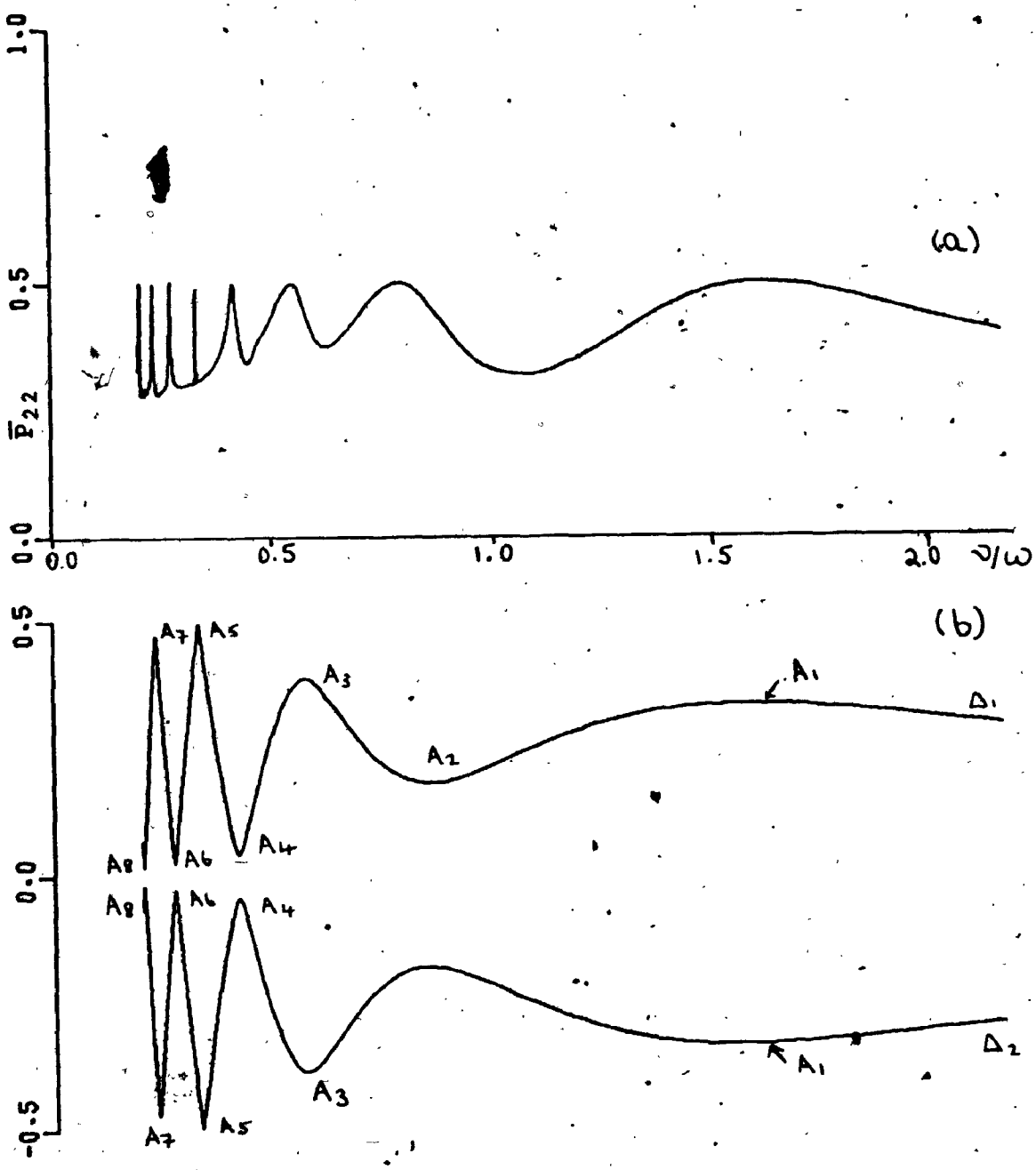

Figure 4.16. The phase averaged steady state induced transition probability, $\bar{P}_{22}$, with its accompanying characteristic exponent plots as a function of frequency ν for $\delta = 1.0$ and $\beta = 0.769$.

precise location of these "anti-crossings" A_n as a function of frequency ν is given by the minimum in the quantity $\nu|\Delta_1-\Delta_2|$ or, equivalently, the frequency times twice the distance of closest approach to a branch line $(0,\pm 1/2)$, see the previous section. Increasing the static Stark field $\mathcal{E}^\circ$ shifts the resonance peaks to higher frequencies (Compare Figures 4.13(a) with 4.14(a) and 4.15(a) with 4.16(a)) and increases further the background to these resonances. The constant background to these resonances, for fixed $\mathcal{E}^\circ$, arises from the frequency independent contribution to the induced transition probability $\bar{P}_{22}$. In the absence of the oscillating field $\bar{P}_{22}$ can be obtained from equations 4.2.16-4.2.18 and is given by.

$$\bar{P}_{22} = 2|\mu_{12}\mathcal{E}^\circ|/[\omega^2 + 4|\mu_{12}\mathcal{E}^\circ|^2], \mathcal{E}=0, a_1(0)=1. \qquad 4.2.27$$

Increasing the static field $\mathcal{E}^\circ$ further causes this background to increase and ultimately reach 0.5, thereby suppressing all resonances; compare, for example, Figure 4.13(a) with 4.14(a).

Transitions in this two state nondegenerate system may also be monitored by holding the amplitude $\mathcal{E}$ and frequency ν of the oscillating field fixed while Stark tuning the states through a resonance by varying the static field $\mathcal{E}^\circ$. Such Stark tuning techniques are commonly employed in situations where, due to technical limitations, the oscillating field frequency ν cannot be readily swept [11]. The typical experimental set up is indicated in Figure 4.17(a) where the fixed oscillating field frequency ν is slightly greater than the unperturbed level separation ω so that a relatively small change in $\mathcal{E}^\circ$ is required to shift the levels into resonance*, see equation 4.2.19 and equation 4.2.28 that follows. Figure 4.18(a)

---

* A similar Stark tuning experiment could be carried out for higher photon transitions with the oscillating field frequency ν slightly greater than the q-photon transition frequency ω/q. To obtain a full multiphoton spectrum at a single frequency ν would require such a large variation in $\mathcal{E}^\circ$ that most of the spectrum would completely saturate.

Figure 4.17. The level configurations employed to investigate stark tuning experiments on two level systems. (a) The two level non-degenerate system where the level separation ω is slightly less than the fixed frequency ν of the sinusoidal field. The actual numerical values of the parameters used in calculations on this system are; $\omega = E_2 - E_1 = 0.45$, $E_1 = -0.5$, $E_2 = -0.05$, $\nu = 0.5$ and $\mu_{12} = 1.0$ (b) Stark tuning experiment on two degenerate levels ($\omega = 0$). For convenience we choose $E_0 = 0$ here and the remaining parameters are the same as in (a). (c) Stark tuning of near degenerate levels. The condition $\nu >> \omega$ is imposed for this model, see equation 4.2.28. Actual values of the parameters used for calculations on this system are; $\omega = 0.01$, $E_1 = 0.0$, $E_2 = -0.01$, $\nu = 0.5$, and $\mu_{12} = 1.0$. For the definition of the symbols +, -, S and A in (b) and (c), see the main text.

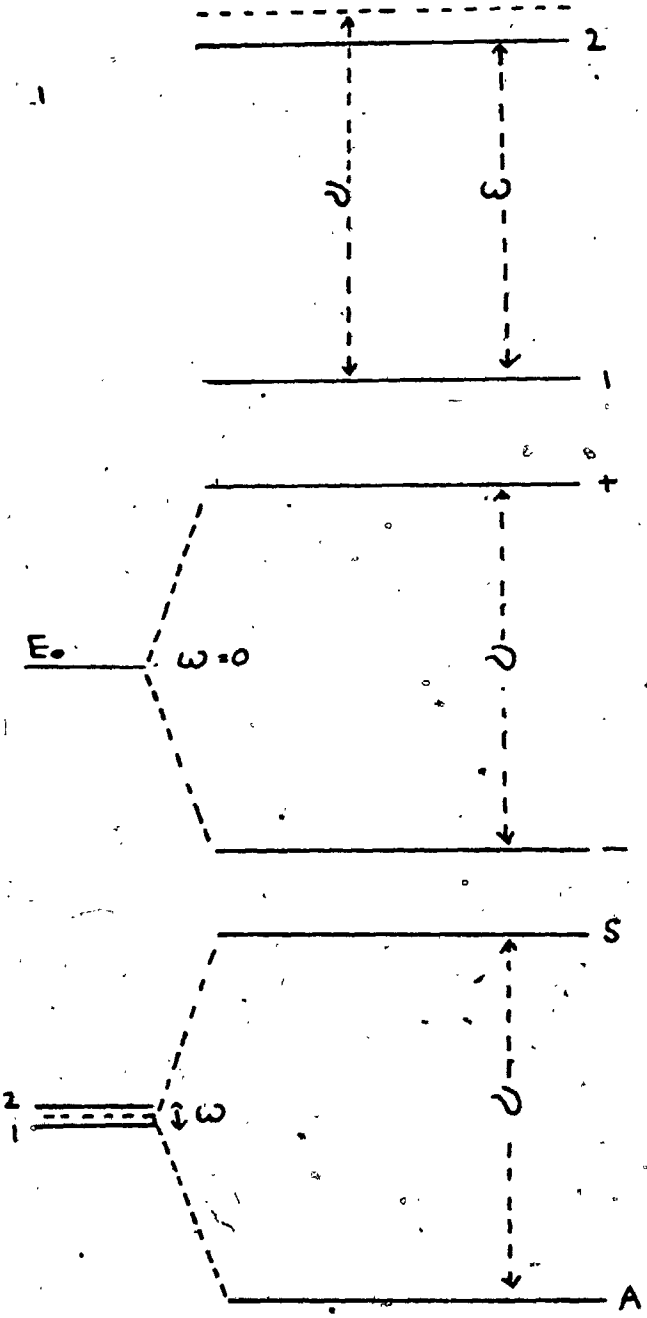
2
1
(a)
+
E₀
ω=0
(b)
S
2
1
ω
(c)
A

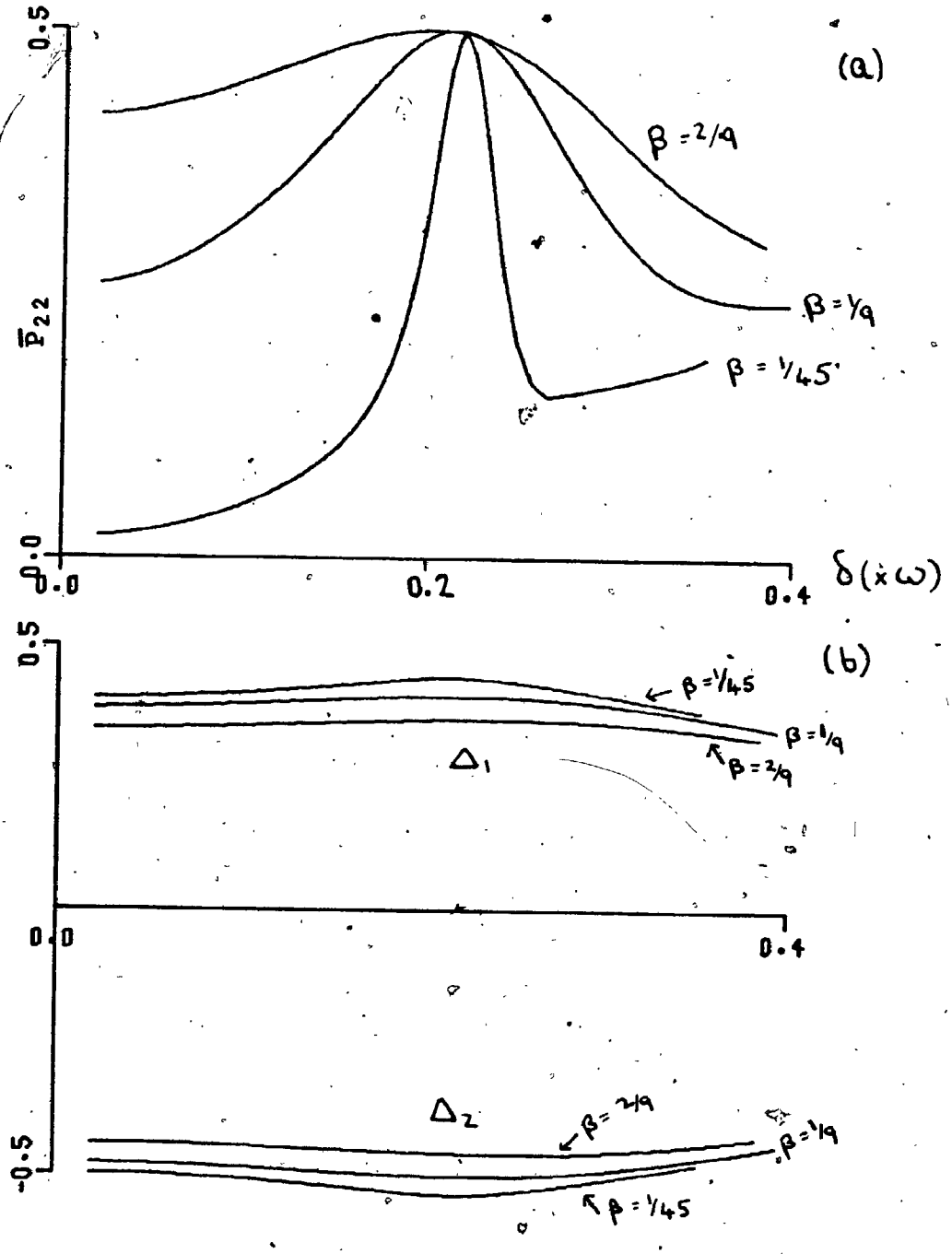

Figure 4.18. The phase averaged steady state induced transition probability, $\bar{P}_{22}$, for the stark tuning experiment shown in Figure 4.17(a), as a function of δ, in units of ω^{-1}, for the three values of the coupling parameter $\beta = 1/45, 1/9, 2/9$. The single photon resonance is explicitly shown in (a) and (b) contains the accompanying characteristic exponent plots.

and (b) shows $\bar{\rho}_{22}$ along with its accompanying characteristic exponent plots for $\nu/\omega = 10/9$ as a function of $\delta (= 2|\mu_{11}\mathcal{E}^0|/\omega)$ for three values of $\beta = 1/45\ ,\ 1/9\ ,\ 2/9$ for the above experiment. For the weaker oscillating field $\beta = 1/45$ the increased background on the high Stark tuned side (larger δ) of the single photon profile is due to the relatively large static field $\mathcal{E}^0$ required to tune through the resonance. If the ratio ν/ω lies closer to unity (that is the frequency ν lies closer to the level separation ω) the entire profile would become more symmetric, relative to the results of Figure 4.18(a), as smaller values of $\mathcal{E}^0$ would be required to bring the system into resonance. On the other hand, for larger values of $\beta (= 1/9, 2/9)$ the strong competition between the large oscillating field $\mathcal{E}$ and the large static field $\mathcal{E}^0$ causes the resonance profiles to saturate more symmetrically, see Figure 4.18(a) . The accompanying characteristic exponent plots reflect this saturation by starting to level off to constant values as β increases, so that the location of the "anti-crossing" A_1 becomes less distinct. The Stark tuning experiment described in Figure 4.17(a) indicates that even for weak oscillating fields saturation effects by the static field can be important unless the ratio ν/ω is close to unity, see Figure 4.18(a). If we ignore resonance shifts due to the oscillating field (Dynamic Stark shift) the resonance condition for Stark tuning is given by, see Equation 4.2.19

$$\nu \simeq \Delta q_\nu = q_{V_S} - q_{V_A} = \omega\sqrt{1+\delta^2} \qquad 4.2.28$$

Thus if $\nu \sim \omega$ the entire profile can be Stark tuned by a small variation in static field $\mathcal{E}^0$ (or δ).

Finally, we investigate the situation in which $\nu \gg \omega$ which would correspond to the Stark tuning of degenerate($\omega = 0$), see Figure 4.17(b) , or near degenerate, see Figure 4.17(c) , states in the presence of an oscillating field of fixed frequency ν and amplitude $\mathcal{E}$. To satisfy the resonance condition, given by equation 4.2.28, will require a large variation in $\delta(\mathcal{E}^0)$, since $\nu \gg \omega$, and hence we expect that saturation effects will dominate over most of the Stark tuning domain. It is convenient at this stage to write explicitly the

dipole matrix element μ_{AS} coupling the Stark tuned states. This is obtained by substituting equation 4.2.23 into equation 4.4.26 and by using the initial condition $a_1(0)=1$, $a_2(0)=0$;

$$\mu_{AS} = \omega|\mu_{12}\mathcal{E}^0|^2/\gamma^2 \qquad 4.2.29$$

From this result it is clear that in the limit $\omega \to 0$, $\mu_{AS} \to \mu_{\pm} = 0$ and there is no coupling between the static Stark tuned states ψ_+ and ψ_-. The plots of the characteristic exponents Δ_1 and Δ_2 which coincide with q_+ and q_- when $E_1 + E_2 = 0$, for the Stark tuning of an initially degenerate system are shown in Figure 4.19 as a function of $\Delta q = q_+ - q_- = 2|\mu_{12}\mathcal{E}|$. In these plots no "anti-crossings" occur, but a series of "level-crossings" L_n occur at $\Delta q = n\nu$ where $n=0,1,2,\ldots$ and $\nu \gg \omega$ is fixed; there are no transitions induced by the oscillating field so the transition probabilities $\bar{P}_{22} = \bar{P}_{11} = 0.5$ irrespective of the imposed initial conditions due to the complete mixing of $\phi_1(r)$ and $\phi_2(r)$ by the static Stark field $\mathcal{E}^0$. The results of Figure 4.19 are independent of the size of the oscillating field which is a manifestation of the fact that there is no coupling whatsoever between the Stark split states if $\omega = 0$.

If both states are initially near degenerate that is $\omega \sim 0$, see Figure 4.17(c), there will be a finite but small coupling between the Stark split states and a series of interesting resonances are observed at $\Delta q = n\nu$. Figure 4.20(a) shows the phase averaged steady state induced transition probability $\bar{P}_{22}$ as a function of Δq, subject to the initial conditions* $a_1(0)=1$, $a_2(0)=0$, for a number of values of the coupling parameter $\beta = |\mu_{12}\mathcal{E}|/\omega$; this figure includes the first two resonances at $\Delta q = \nu$ and $\Delta q = 2\nu$. While transitions between $\phi_1(r)$

---

* The amplitude of these resonances depends on the imposed initial conditions and if we choose $a_1(0) = a_2(0) = 0.5$ the resonances are not observed at all. The greater the difference in population of the near degenerate states the greater the amplitude of the resonance. As a rough guide, for example, we have found that if the $\Delta a = a_1(0) - a_2(0) > 0$ the maximum amplitude of the dip at $\Delta q = \nu$ is $\sim \Delta a/3$.

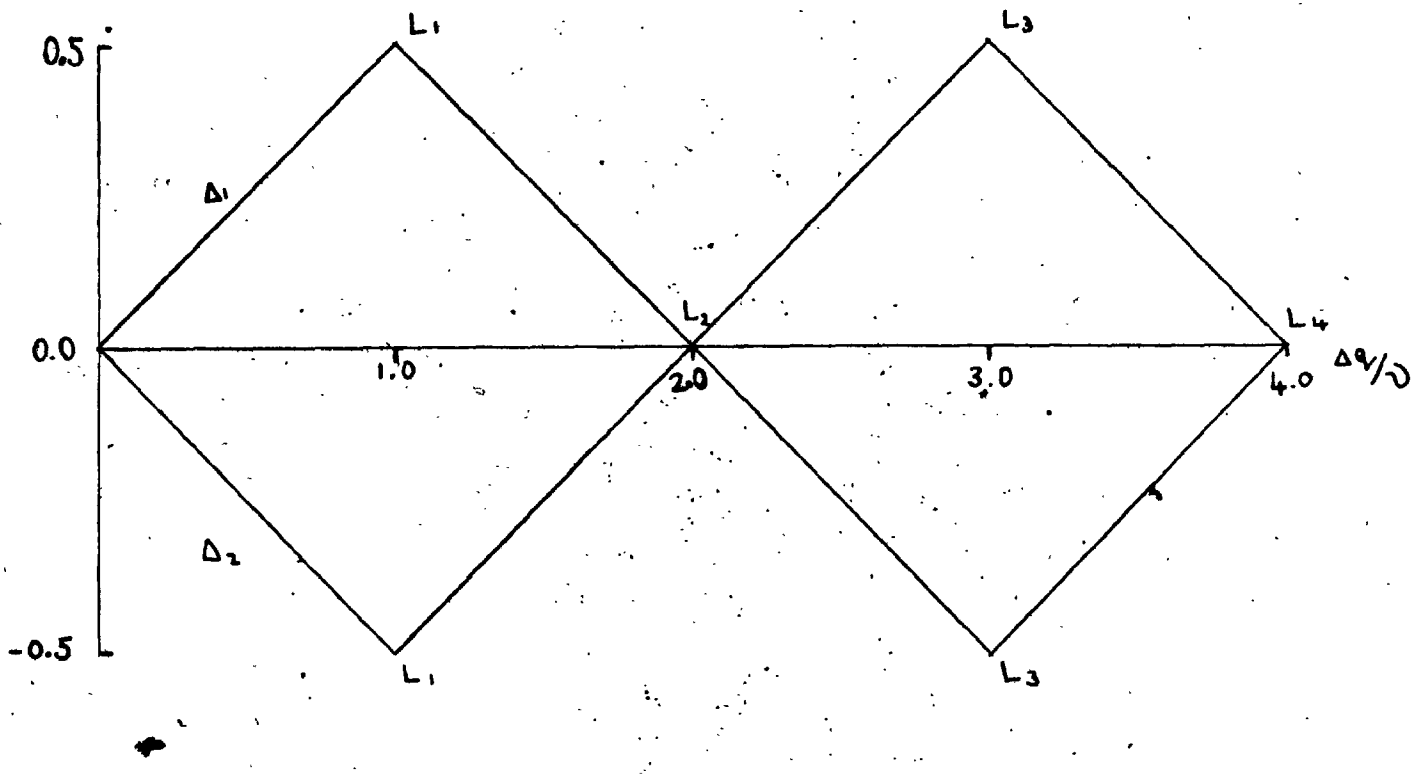

Figure 4.19. The characteristic exponent plots Δ_j for the stark tuning of two degenerate levels as a function of the tuned level separation Δq, see Figure 4.17(b). There are no transitions in this system ($\bar{P}_{22} = \bar{P}_{11} = 0.5$) as signified by the occurrence only of "level crossings" L_n at the transition values of $\Delta q = q_+ - q_- = 2|\mu_{12}\varepsilon^0|$. Here Δq is in units of ν.

Figure 4.20(a). Resonance dips ($\bar{P}_{22}$) for the stark tuning (as a function of $\Delta q/\nu$) of the near degenerate levels shown in Figure 4.17(c). Each spectrum corresponds to a different value of the coupling strength parameter β. These dips occur at $\Delta q = n\nu$, see equation 4.2.28 for $n = 1$.

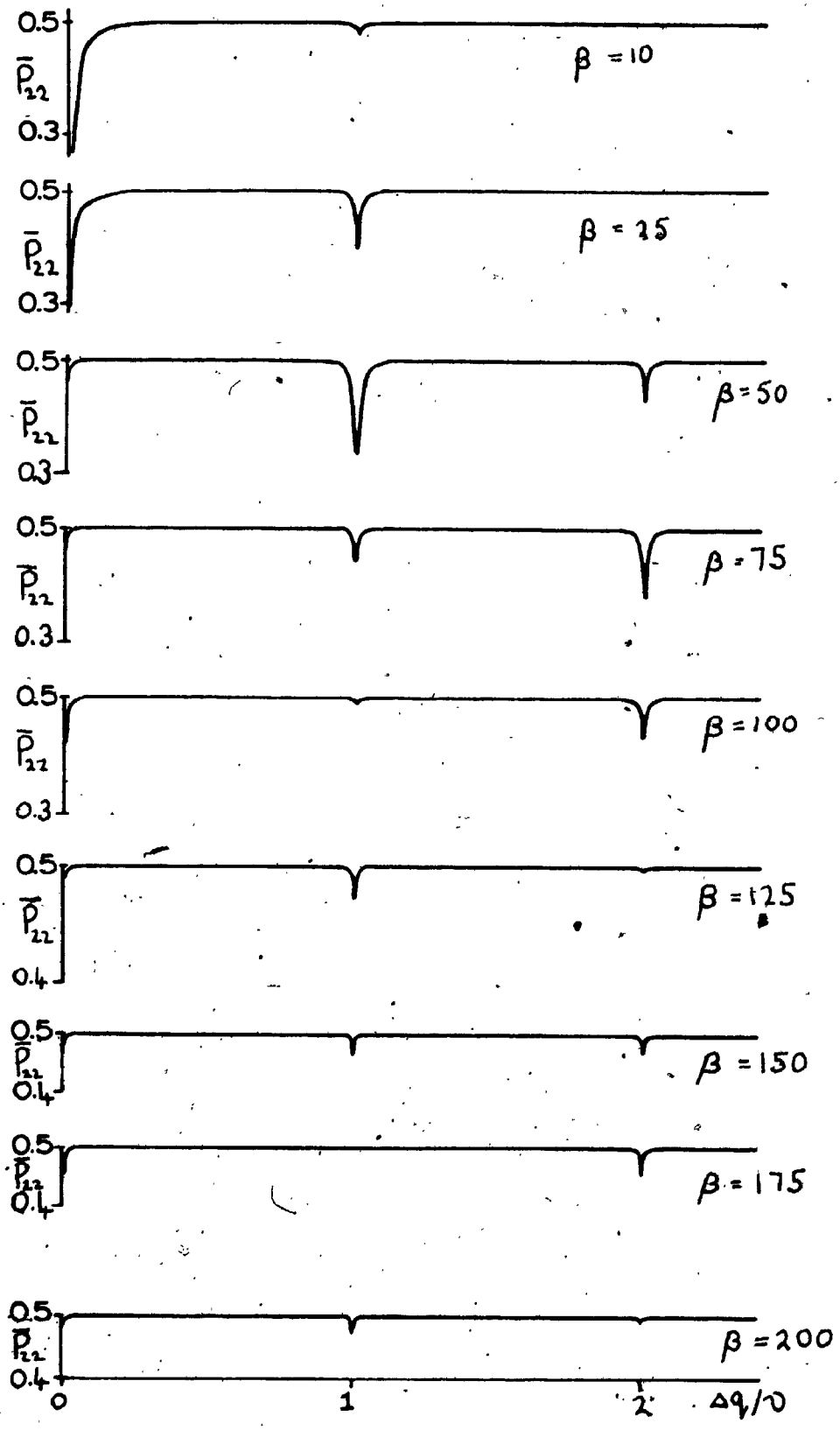
0.5
$\bar{P}_{22}$
0.3
β = 10
β = 25
β = 50
β = 75
β = 100
β = 125
0.4
β = 150
β = 175
β = 200
0
1
2
Δq/v

and $\phi_2(r)$ are completely saturated ($\bar{P}_{11} = \bar{P}_{22} = 0.5$) by both the strong static Stark and oscillating fields over most of the Stark tuning domain, a series of very sharp dips** occur in $\bar{P}_{22}$ at $\Delta q = n\nu$. The dip in $\bar{P}_{22}$ at low static and oscillating fields, see Figure 4.20(a) for β =10 and 25 as $\Delta q \to 0$, is indicative of the fact that the transition $1 \to 2$ is not saturated for such field strengths. These resonances differ from the conventional resonances discussed in this chapter, see Sections 4.2 and 4.3, in that they do not broaden or shift with increasing oscillating field amplitude $\mathcal{E}$. Pegg and Series [77] in an elegant treatment of the analogous magnetic resonance experiment (see the following section for the relevant Hamiltonian) predicted that such resonances occur at integer multiples of $|\gamma B_{0x}|$ and identified them with a beating between the oscillating magnetic field, $B_{1x}\cos(\nu t+\delta)$, and the natural oscillations of the magnetically tuned (by $B_{0x} \gg B_{0z}$) system. These authors explicitly deal with the resonant case for the magnetic resonance experiment and suggest formally how the problem may be treated for arbitrary values of $|\gamma B_{0x}|$.

The oscillatory behaviour of the resonance minima evident in Figure 4.20(a) as a function of oscillating field amplitude $\mathcal{E}$, is also evident in the characteristic exponent plots of Δ_j shown as a function of Δq for β =10, 50 and 100, in Figure 4.20(b). Unlike the conventional resonances discussed earlier the "anti-crossings" A_n do not shift or broaden as a function of β but instead undergo small oscillations in the vicinity of the branch lines $0, \pm 0.5$ at the resonance positions $\Delta q = n\nu$. In the asymptotic limit $\beta \to \infty$ these "anti-crossings" A_n change to "level-crossings" L_n , as in Figure 4.9, signifying that the system has become degenerate. Figure 4.21(a) and (b) shows in detail the oscillatory behaviour of both the resonance minima and widths as a function of β , for n=1 and n=2, respectively, corresponding to the spectra in Figure 4.20(a). The relatively high symmetry of the resonances is displayed in Figure 4.22

** These resonances are observed as dips in $\bar{P}_{22}$ due to the imposed initial conditions, $a_1(0) = 1$, $a_2(0) = 0$ and because $\bar{P}_{22}$ cannot exceed 0.5.

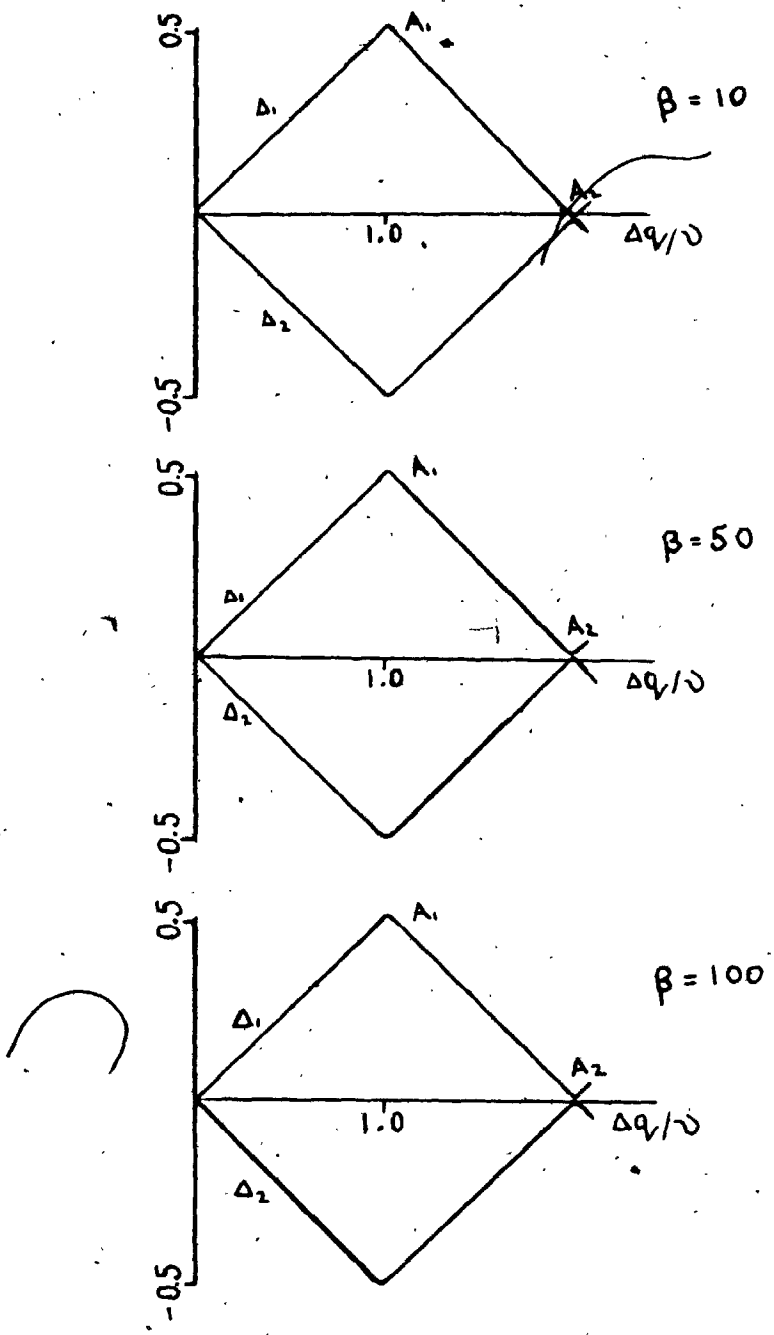

Figure 4.20(b) shows the characteristic exponent plots (Δj) for β = 10, 50 and 100 with the "anti-crossings" A_1 and A_2 included. The oscillatory behaviour of A_n is not very evident in this figure as a result of the extremely narrow resonance widths, see however Figure 4.21(b).

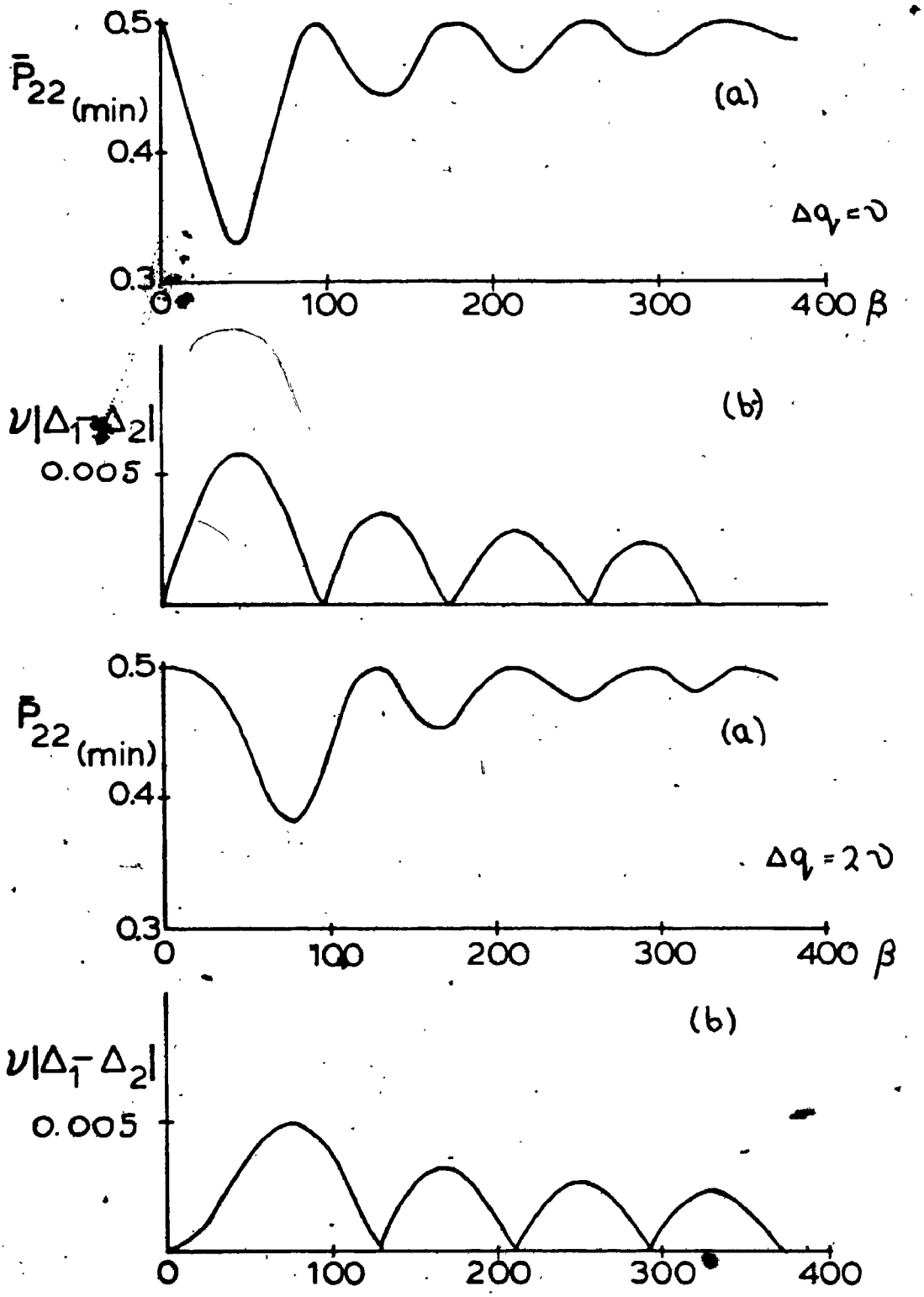

Figure 4.21. (a) The oscillatory behaviour of $\bar{P}_{22}$ at the first and second resonance minima ($\Delta q = \nu$ and 2ν) in Figure 4.20(a), as a function of coupling strength β. (b) The behaviour of the width at half maximum, $\nu|\Delta_1 - \Delta_2|_{min}$, of these resonances over the same coupling domain.

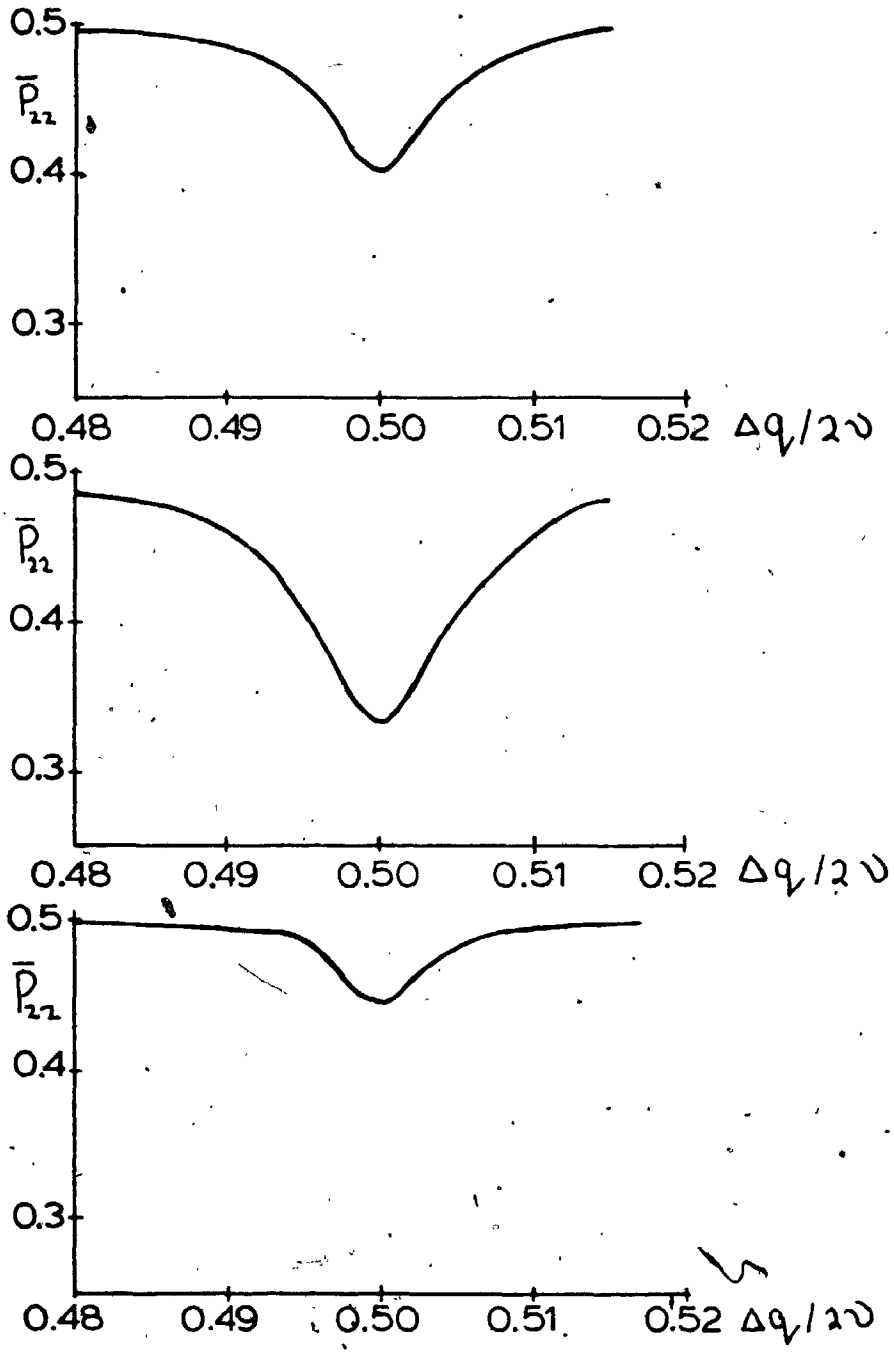

Figure 4.22. Enlargements of the resonances corresponding to $\Delta q = \nu$ in Figure 4.20(a) for the three values of the coupling strength parameter β = 25, 50 and 75.

where the three resonances corresponding to $\Delta q = \nu$ for at β =25,50 and 75 are "blown up". Finally in Figure 4.23 we show that a simple linear relation exists between the resonance width, which is given by a minimum in $\nu|\Delta_1 - \Delta_2|$ occurring at an anti-crossing A_n, and the near degenerate level separation ω; this figure corresponds to the first minimum in $\bar{P}_{22}$ as a function of β, shown for $\Delta q = \nu$ in Figure 4.21. Thus

$$\nu|\Delta_1 - \Delta_2| = \text{Constant} \times \omega . \qquad 4.2.30$$

The results leading to equation 4.2.30 suggest the possibility that Stark tuning experiments of the type just discussed for near degenerate states could be employed to measure both the electric dipole matrix element μ_{12} and the level separation ω, if the constant in equation 4.2.30 is determined by using a system with a known near degenerate level separation. Also as pointed out in the footnote on page 107 the amplitude of the resonance minima will depend critically on the relative populations of the near degenerate levels. In many real situations, however, more than two near degenerate levels can be present in a narrow spectral region and the theoretical analysis would have to be extended to include their contributions. It is interesting to note that the analgous treatment for the magnetic resonance experiment yields the Lande g factor, which is the magnetic analogue of μ_{12}, as discussed by Pegg and Series [77] and Chapman [78]; in this situation ω is the known Zeeman splitting.

4.3 INDUCED TRANSITION PROBABILITIES FOR THE TWO LEVEL SYSTEM IN A SINUSOIDAL MAGNETIC FIELD.

Magnetic interactions in a two level system have received considerable experimental and theoretical attention over the past twenty years and were the first systems in which multiphoton transitions were observed experimentally [5,6]. The purpose of this brief section will be to show that as far as the solution to the time dependent problem is concerned, both magnetic and electric interactions are intimately related. It will also be demonstrated

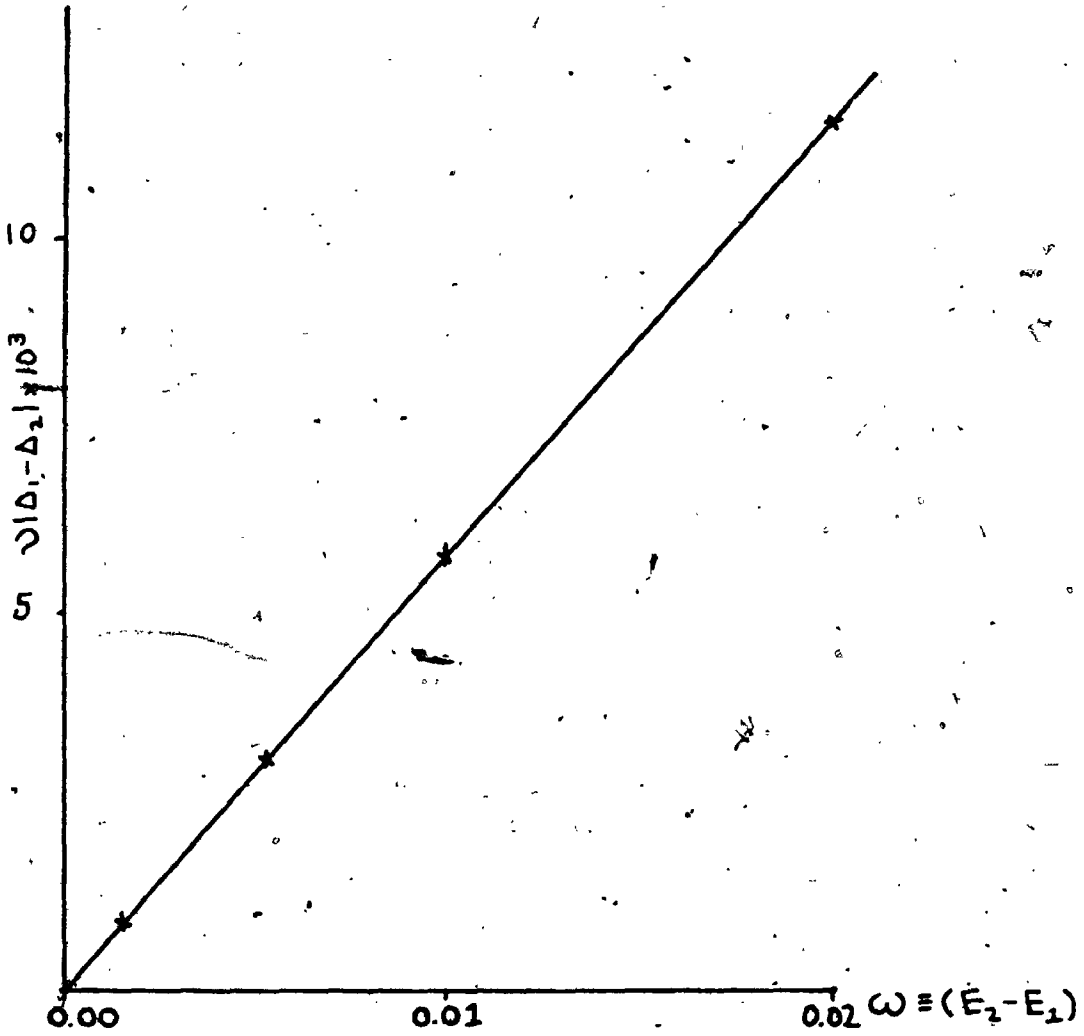

Figure 4.23. The linear relationship between the resonance width at half maximum ($\nu|\Delta_1-\Delta_2|$) and the near degenerate level separation ω, for $\beta = 50$ in Figure 4.20(a).

that the ν_{Δ_0} obtained here through a semi-classical treatment coincide precisely with the energies of the fully quantized Hamiltonian recently obtained by Yabusaki, Murakami and Ogawa [72,74].

As a specific example we consider a spin 1/2 system perturbed by two mutually perpendicular static magnetic fields, B_{0x} and B_{0z}, and a strong radiofrequency field of amplitude B_{1x} [72,74,77]. The system is initially degenerate and the static magnetic field B_{0z} splits the degenerate pair into the magnetic substates $|+1/2\rangle$ and $|-1/2\rangle$. The Hamiltonian representing this interaction is given by [70]

$$H_0' = -\gamma B_{0z} I_z \qquad 4.3.1$$

where γ is the "gyromagnetic ratio" and I_z is the z-component of the nuclear angular momentum operator with eigenvalues $\pm 1/2$. The two level system therefore consists of two states $|+1/2\rangle$ and $|-1/2\rangle$ with respective energies $E_\pm = \pm \frac{1}{2}|\gamma B_{0z}|$. Application of an oscillating Radiofrequency field $B_{1x}\cos(\nu t+\delta)$ perpendicular to B_{0z} induces magnetic dipole transitions between the two spin 1/2 states* and for complete generality we include a static magnetic field B_{0x} parallel to B_{1x} which effectively mixes both states through an allowed magnetic dipole interaction. The total Hamiltonian for this system now becomes

$$H(r,t) = H_0(r) - \gamma\left[B_{0z} I_z + \left(B_{0x} + B_{1x}\cos(\nu t+\delta)\right) I_x\right] \qquad 4.3.2$$

where $H_0(r)$ represents the unperturbed Hamiltonian, with energy E_0, corresponding to the energy of the initially degenerate spin half states.

The coupled differential equations describing the time evolution of this system become ($|+1/2\rangle \equiv 2$, $|-1/2\rangle \equiv 1$)

$$i\frac{\partial}{\partial t}\begin{pmatrix} a_1(t) \\ a_2(t) \end{pmatrix} = \begin{pmatrix} E_1 & -\mu_{12}B_{0x} \\ -\mu_{21}B_{0x} & E_2 \end{pmatrix}\begin{pmatrix} a_1(t) \\ a_2(t) \end{pmatrix} - B_{1x}\cos(\nu t+\delta)\begin{pmatrix} 0 & \mu_{12} \\ \mu_{21} & 0 \end{pmatrix}\begin{pmatrix} a_1(t) \\ a_2(t) \end{pmatrix} \qquad 4.3.3$$

where we have chosen $E_0 = 0$, $\mu_{12} = -\gamma\langle -1/2|I_x|+1/2\rangle = \mu_{21}$ and

---

* Both fields must be mutually perpendicular to satisfy the magnetic dipole selection rules; that is $\langle +1/2|I_x|-1/2\rangle \neq 0$ [70].

$E_1 = -\frac{1}{2}|\gamma B_{oz}|, E_2 = \frac{1}{2}|\gamma B_{oz}|$. Equations 4.3-3 and 4.2.15 have precisely the same form showing the intimate connection between electric dipole and magnetic dipole experiments. If, for example, the static magnetic field B_{oz}, the oscillating field amplitude B_{1x} and its frequency ν are held constant while the static magnetic field B_{ox} is varied, we have the same situation as in the Stark tuning experiment described in the previous section and the results for both experiments are identical. On the other hand if B_{oz}, B_{ox} and B_{1x} are held constant while the frequency ν of the oscillating field is swept, the results are identical to those obtained for the frequency spectrum of a two level system in a fixed static Stark field, see Figures 4.13-4.16.

In a recent calculation, Yabusaki, Murakami and Ogawa used a quantized field approach, developed earlier by Cohen-Tannoudji and Haroce [73], to calculate the energies of the total system as a function of the two static magnetic fields B_{oz} and B_{ox}, while holding the amplitude B_{1x} and frequency ν of the strong ($|\gamma B_{1x}| \sim 1$) radiofrequency field constant. Their infinite quantized Hamiltonian matrix, which is analgous to Shirley's Floquet matrix, was truncated to a 40x40 matrix and diagonalized to obtain the energies accurate to tenth order in perturbation theory. These energy plots as a function of B_{oz} and B_{ox} were then employed to locate various resonances in the system. These authors point out that these fully quantized energy calculations cannot provide any information regarding the intensity and lineshapes of the various resonances and they return to numerically solving the semiclassical density matrix equations to calculate the multiphoton spectra [72].

Figure 4.24(a) and (b) shows the characteristic exponent plots, Δ_j as a function of $|\gamma B_{oz}|/\nu$ (ω_1/ω in Yabusaki's notation), with $|\gamma B_{1x}|/\nu(\omega_1/\omega)$ =1(2),2(4),4(8) for $|\gamma B_{ox}|(\omega_{11})=0$ and $|\gamma B_{ox}|$ $=0.45\nu(0.9\omega)$, respectively. Yabusaki et al give the quantized energy plots for $|\gamma B_{1x}|/\nu(\omega_1/\omega) = 1(2), 2(4), 4(8)$ for $|\gamma B_{ox}|(\omega_{11}) = 0$ in their Figure 4 and for $|\gamma B_{1x}|/\nu(\omega_1/\omega) = 1(2), 2(4)$ for $|\gamma B_{ox}| = 0.45\nu$ in their Figure 7. Direct comparison with Figures 4.24(a) and (b) shows

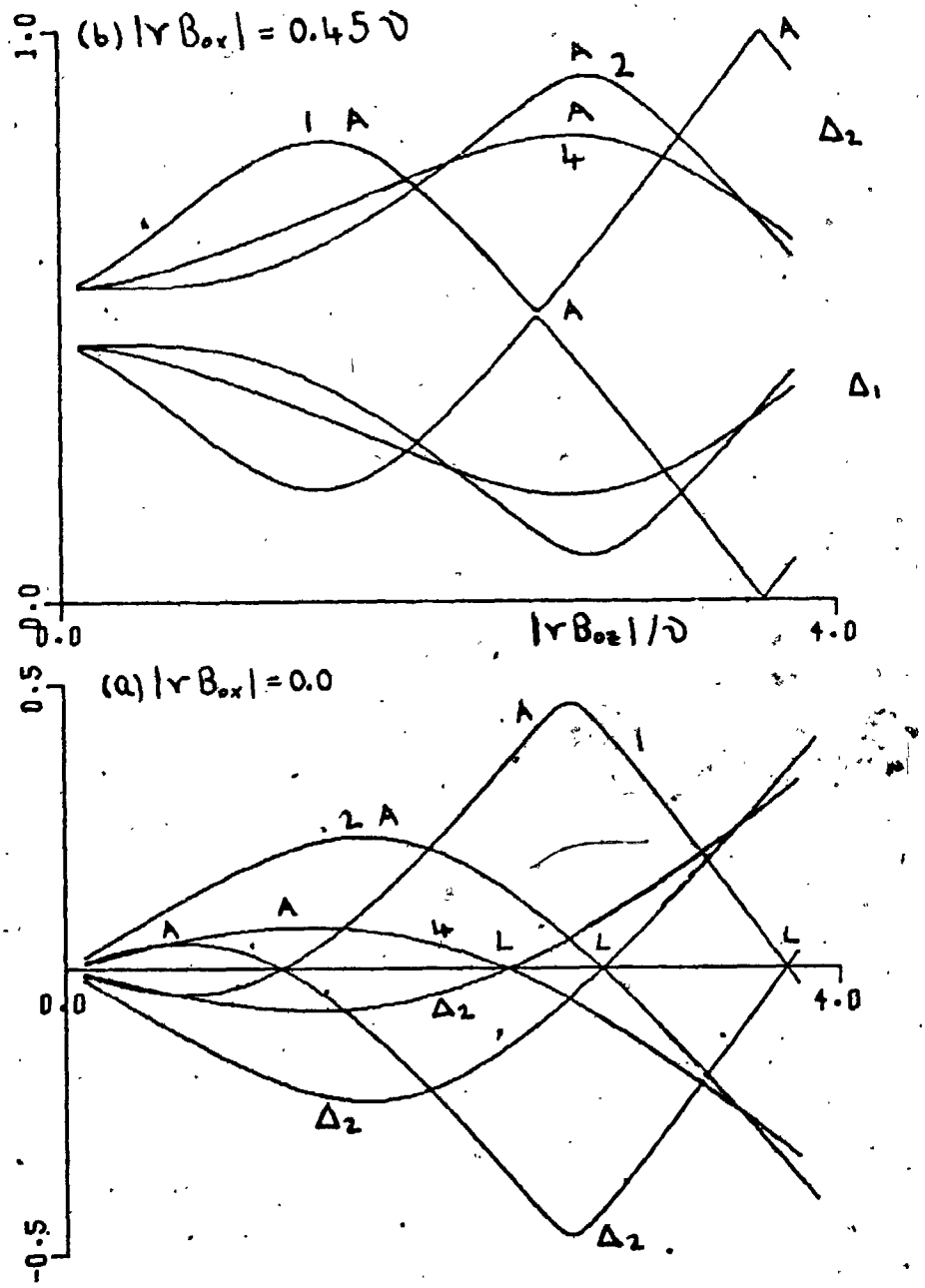

Figure 4.24. Characteristic exponent plots Δj as a function of magnetic level tuning ($|\gamma B_{oz}|/\nu$). (a) Plots of Δj for $|\gamma B_{ox}| = 0$ and $|\gamma B_{1x}|/\nu$ = 1,2 and 4. (b) Plots of Δj for $|\gamma B_{ox}| = 0.45\nu$ and $|\gamma B_{1x}|/\nu$ = 1,2 and 4. The curves are labelled by the appropriate values of $|\gamma B_{1x}|/\nu$. "Anti-crossings" are indicated by A while "level crossings" are indicated by L.

that the $\nu\Delta_j$ correspond precisely to their quantized energies. Such a correspondence for these coupling strengths is not surprising as Shirley [13,58] has demonstrated that the semiclassical and quantum treatments should coincide when the photon number N in the quantized field is large. Unlike the method of Yabusaki et al[72], the formal method of solution developed in Chapter 3 provides both the energies ($\nu\Delta_j$) and multiphoton spectra without recourse to a second calculation.

The multiphoton spectra ($\bar{P}_{22}$), subject to the initial conditions $a_1(0)=1$, $a_2(0)=0$, corresponding to the characteristic exponent plots in Figure 4.24(a) and (b) are shown as a function of $|\gamma B_{0z}|/\nu$ in Figures 4.25(a) and (b), respectively. In the absence of the parallel static magnetic field ($|\gamma B_{0x}|=0$ only odd photon transitions can occur at the positions of the "anti-crossings" A, see Figure 4.24(a), and the resonances corresponding to these odd photon transitions are shown in Figure 4.25(a) for the three values of $|\gamma B_{1x}|/\nu$ in Figure 4.24(a). The strong coupling strengths employed in these calculations are reflected in the very broad resonances, which are approaching complete saturation as the oscillating field strength increases (compare both the spectra and corresponding Δ_j plots for $|\gamma B_{1x}|/\nu=1,2$ and 4). In the presence of the static magnetic field ($|\gamma B_{0x}| = 0.45\nu$) the "level-crossings" L in Figure 4.24(a), corresponding to the forbidden even photon transitions in Figure 4.25(a), have now become "anti-crossings" A signifying the occurrence of even photon transitions in Figure 4.25(b). These resonance peaks again occur precisely at the "anti-crossings" A whose position corresponds to a minimum in $\nu|\Delta_1-\Delta_2|$ as a function of $|\gamma B_{0z}|/\nu$. The behaviour of these resonances and characteristic exponents (quantized energies) is discussed in detail by Yabusaki et al [72,74].

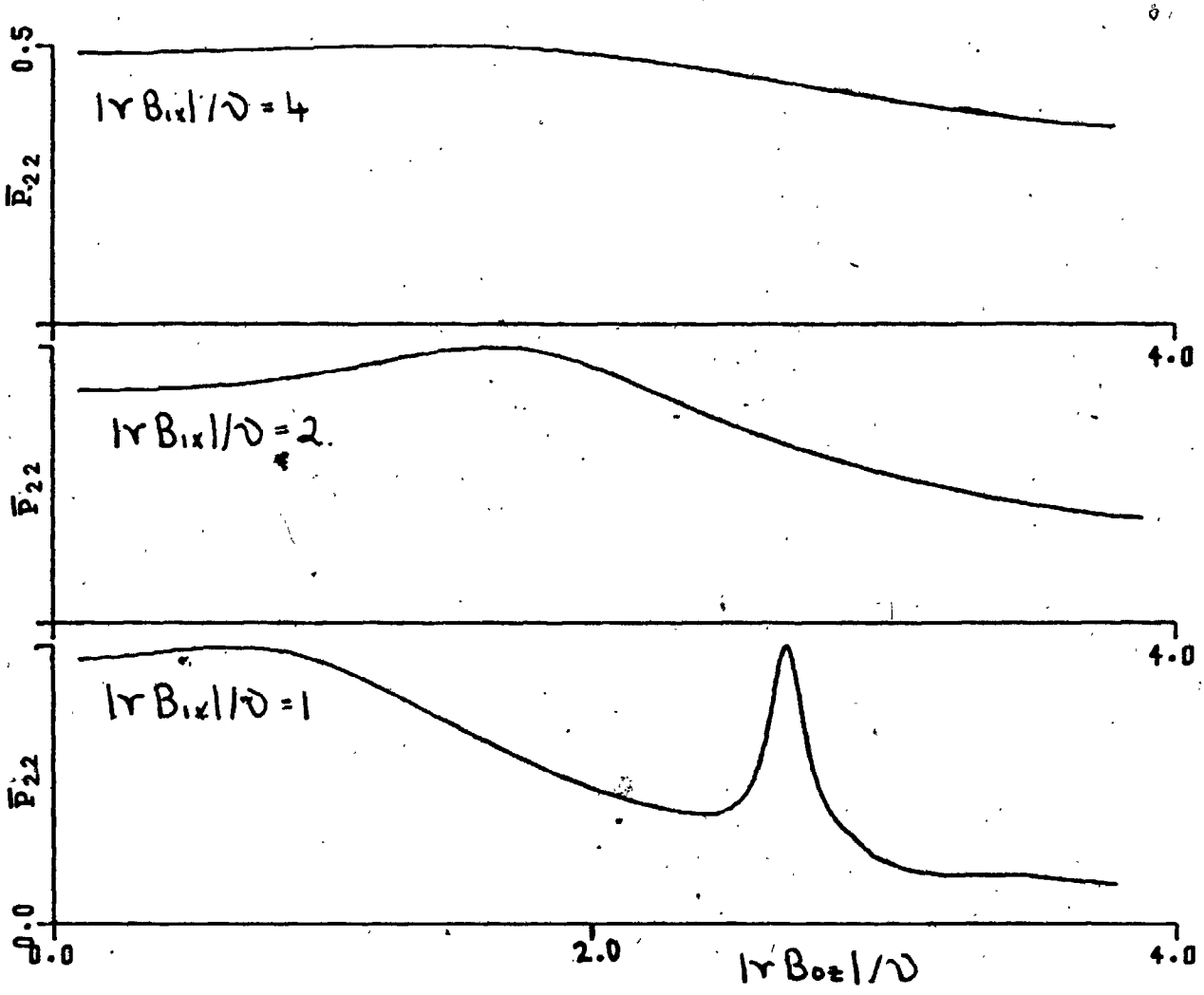

Figure 4.25(a). The phase averaged steady state induced transition probability, $\bar{P}_{22}$, over the same magnetic tuning domain ($|\gamma B_{oz}|/\nu$) and for the same parameters as in Figure 4.24(a).

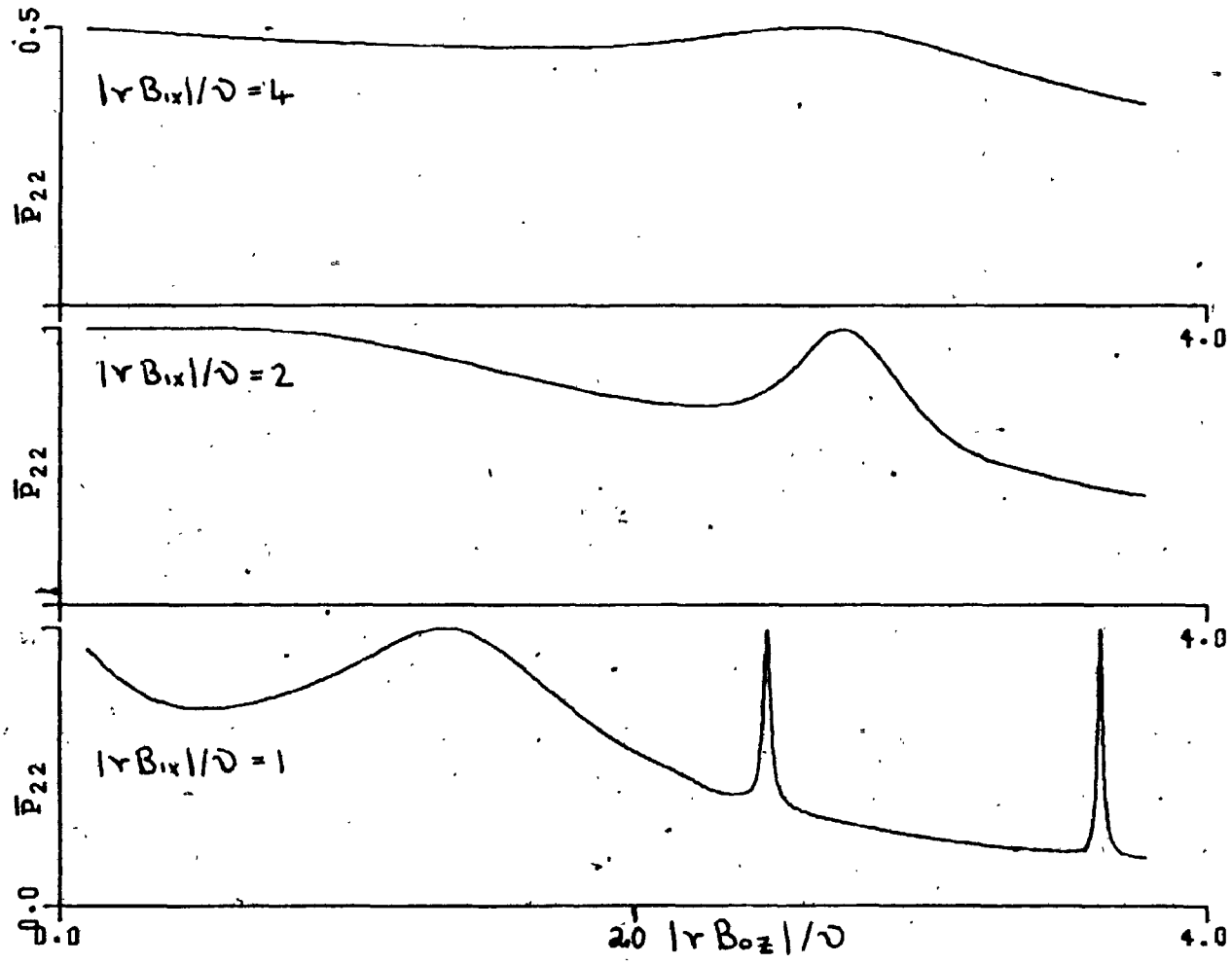

Figure 4.25(b). The phase averaged steady state induced transition probability, $\bar{P}_{22}$, over the same magnetic tuning domain and for the same parameters as in Figure 4.24(b).

4.4 BEHAVIOUR OF THE CHARACTERISTIC EXPONENTS IN THE NEIGHBOURHOOD OF A RESONANCE.

The behaviour of the characteristic exponents Δ_i in the neighbourhood of a resonance has led to some confusion in the literature recently [21]. Besset, Horowitz, Messiah and Winter [20] in their approximate rotating field analysis of the N-level system, see Section 4.2 , note that as a resonance between two states $\phi_i(r)$ and $\phi_j(r)$ is approached by sweeping over the frequency domain ν, the characteristic exponents Δ_i and Δ_j approach one another and "anti-cross" at the resonance frequency.* They note in addition that (1) as the resonance is traversed the two characteristic exponents Δ_i and Δ_j suddenly interchange identity ($\Delta_i \leftrightarrow \Delta_j$) and (2) both $\nu\Delta_i$ and $\nu\Delta_j$ closely mirror the behaviour of the perturbed stationary state energies and are approximately equal to E_i and E_j far off resonance if the oscillating field is sufficiently weak. This change over in identity however is compensated for by a corresponding change in their accompanying eigenvectors $\underline{S}_i$ and $\underline{S}_j$, see Besset et al and Chapter 3, with the result that any physical property being evaluated is unaffected. Autler and Townes [14], in their analysis of the two level system as a function of frequency ν, also observed a very complicated behaviour and accredited this behaviour to the skipping from one solution to another of the infinitely many allowed solutions ($\Delta_j' = \Delta_j + n/2$, $n = 0, \pm 1, \cdots$) occurring in the problem, see Section 4.2. These authors remark that all of these solutions contain the same physical information so that which ones are chosen in an actual calculation is basically quite arbitrary.

The two level characteristic exponents Δ_1 and Δ_2 plotted in the earlier sections of this chapter were well-behaved and continous ($\Delta_1 \leftrightarrow \Delta_2$) over the entire frequency domain and showed none of the above behaviour as a function of ν. The reason for this lay solely in the choice of energy reference ($E_1 + E_2 = 0$), see Section 4.2 and Shirley [13], and we shall now demonstrate explicitly that the apparent discontinuity arising from the sudden interchange of identity of Δ_1 and Δ_2 ($\Delta_1 \leftrightarrow \Delta_2$) is nonphysical and indeed whether or not

it occurs will depend critically on the choice of $(E_1 + E_2)$. Figures 4.26(a) and (b) show the single photon profiles for the two experimental situations commonly encountered in magnetic resonance spectroscopy**, namely (a) sweeping with frequency ν of the oscillating field while keeping $|\gamma B_{oz}|$ fixed, see equation 4.3.2 with $B_{ox}=0$, for three values of $|\gamma B_{1x}|/\omega = 0.1$, 0.25 and 0.5 and (b) magnetically tuning the levels by varying the perpendicular static magnetic field B_{oz} (again $B_{ox}=0$) while keeping ν fixed for three values of $|\gamma B_{1x}|/\nu = 0.1$, 0.25 and 0.5. The spectra in Figure 4.26(a) were calculated with four different values of $(E_1 + E_2)$, holding $\omega = E_2 - E_1$ fixed, for each individual value of $|\gamma B_{1x}|/\omega$ while those in Figure 4.26(b) represent three different values of $(E_1 + E_2)$, holding ν fixed, for each value of $|\gamma B_{1x}|/\nu$, see below. As expected these spectra are independent of the choice of $(E_1 + E_2)$ for any given value of $|\gamma B_{1x}|/\omega$ or $|\gamma B_{1x}|/\nu$, see Section 4.2. On the other hand the characteristic exponents Δ_α depend strongly on the choice of $(E_1 + E_2)$, see what follows.

Initially we confine our attention to the behaviour of the characteristic exponents Δ_α, as a function of $(E_1 + E_2)$, for the frequency spectra of Figure 4.26(a). Figure 4.27(a) shows these characteristic exponents as a function of ν for $|\gamma B_{1x}|/\omega = 0.1$, 0.25 and 0.5 and for $(E_1 + E_2) = 0$ which corresponds to the energy choice made in all the earlier calculations in this chapter. These plots are

---

* The precise location of the "anti-crossing" and hence the resonance frequency is determined from the minimum in the quantity $\nu|\Delta_1 - \Delta_2|$. For the frequency sweep spectrum the "anti-crossings" A_n are so sharp in general as a function of ν that a minimum in $\nu|\Delta_1 - \Delta_2|$ coincides graphically with the minimum in $|\Delta_1 - \Delta_2|$.

** Figure 4.26(a) also corresponds to the electric dipole case when ν_e is swept for $\beta = 0.1, 0.25$, and 0.5. In Figure 4.26(a) E_1, E_2 refer to the energies of the magnetic substates split by B_{oz} which is held constant. In Figure 4.26(b) E_1 and E_2 are initially degenerate with common energy $E_o = (E_1 + E_2)/2$ and are tuned by B_{oz}.

Figure 4.26. (a) $\bar{P}_{22}$ as a function of frequency ν for three values of the coupling parameter $|\gamma B_{1x}|/\omega = 0.1$, 0.25 and 0.5 and with $|\gamma B_{ox}| = 0$. The numerical values of the parameters used in this calculation are $\omega = 1.0$, $\gamma = 1.0$ and four different choices of E_1 and E_2, consistent with the given value of $\omega = E_2 - E_1$ but yielding different values for the energy reference $(E_1 + E_2)$. The individual values of E_1 and E_2 are specified in Figures 4.27 - 4.29 and the results for $\bar{P}_{22}$ are independent of $(E_1 + E_2)$.
(b) $\bar{P}_{22}$ as a function of magnetic tuning ($|\gamma B_{oz}|$) for fixed frequency ν and for $|\gamma B_{1x}|/\nu = 0.1$, 0.25 and 0.5 with $|\gamma B_{ox}| = 0$. In this calculation $\nu = 1.0$, $\gamma = 1.0$ and three different choices of energy reference $(E_1 + E_2)$, now given by the initial degenerate value $E_0 = (E_1 + E_2)/2$, are made which yield identical spectra. The individual values of E_1 and E_2 are given in Figure 4.30.

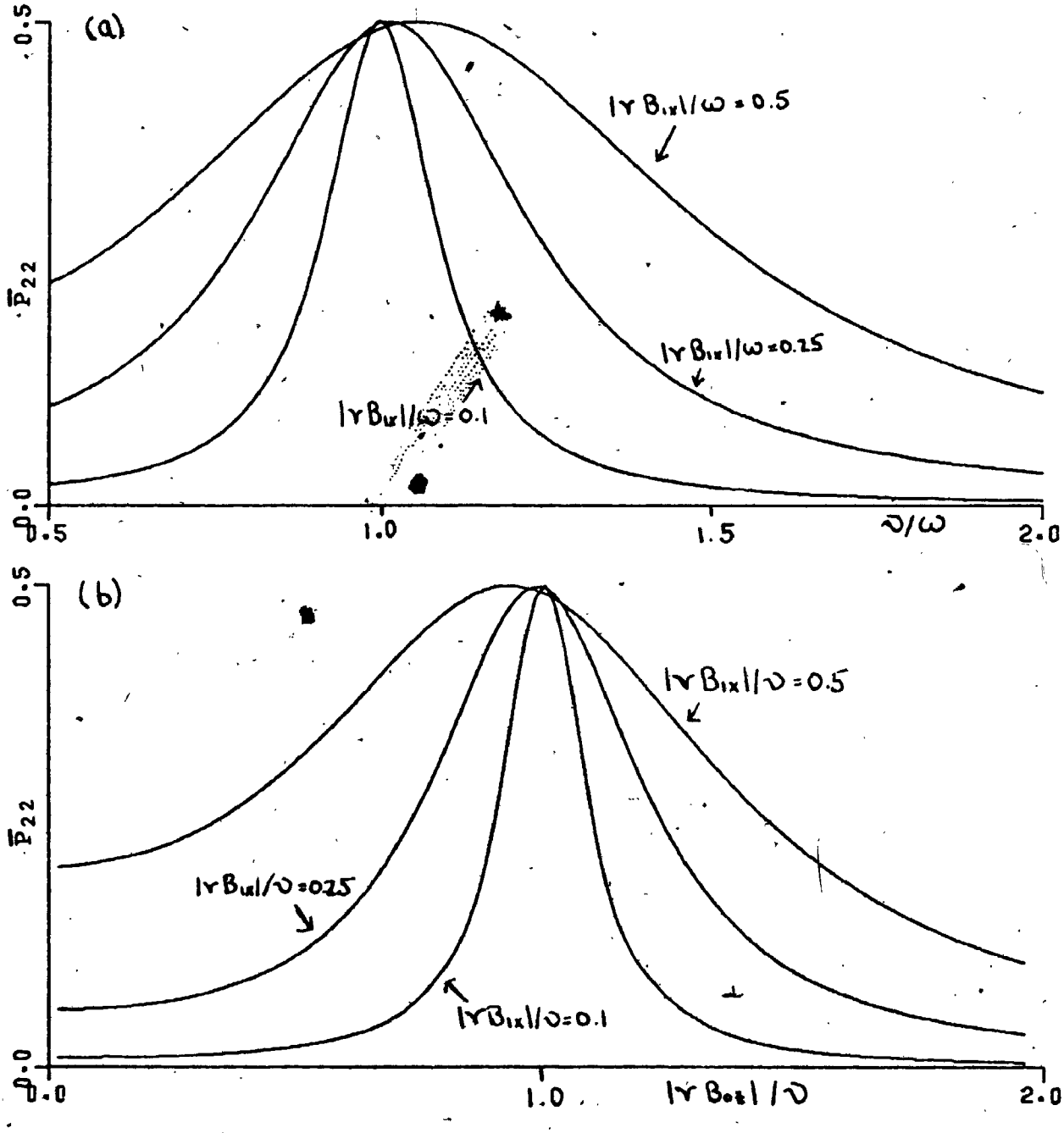
(a)
0.5
0.0
$\bar{P}_{22}$
$|\gamma B_{ix}|/\omega = 0.5$
$|\gamma B_{ix}|/\omega = 0.25$
$|\gamma B_{ix}|/\omega = 0.1$
0.5
1.0
1.5
2.0
ν/ω
(b)
0.5
0.0
$\bar{P}_{22}$
$|\gamma B_{ix}|/\nu = 0.5$
$|\gamma B_{ix}|/\nu = 0.25$
$|\gamma B_{ix}|/\nu = 0.1$
0.0
1.0
2.0
$|\gamma B_{0z}|/\nu$

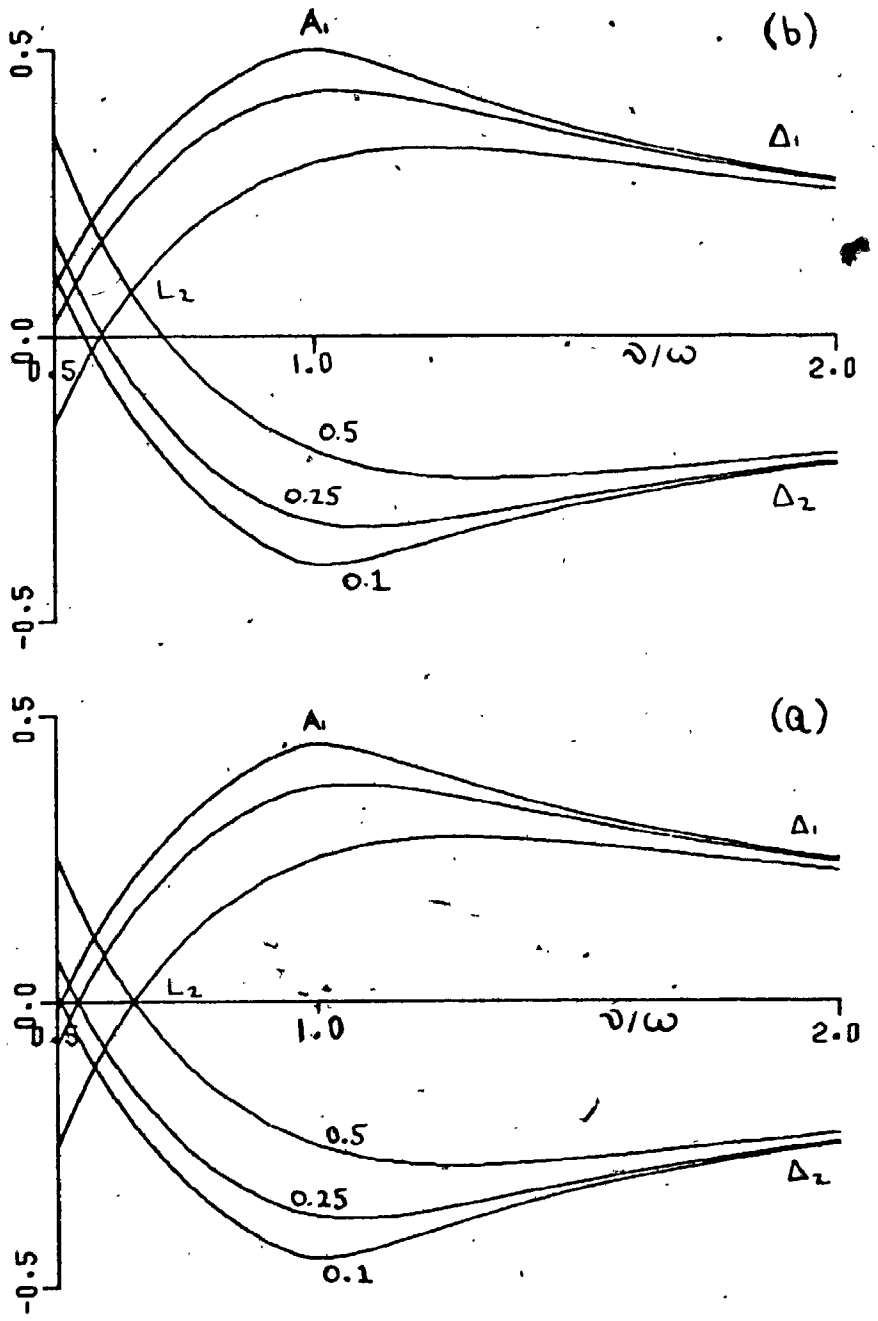

Figure 4.27. (a) The characteristic exponent (Δj) plots corresponding to the frequency spectra in Figure 4.26(a) for $|\gamma B_{1x}|/\omega = 0.1$, 0.25 and 0.5 and for the choice of energy reference $(E_1 + E_2) = 0.0$; $E_1 = -0.5$, $E_2 = 0.5$. (b) The Δj plots for the same parameters as in (a) except that $(E_1 + E_2) = -0.1$; $E_1 = -0.55$, $E_2 = 0.45$. The general location of the "level-crossing" L_2 and "anti-crossing" A_1 are indicated on the figure.

symmetric about the line $-(E_1+E_2)/2$ which represents the zero energy reference point* and also coincides precisely with the line 0. In these plots there is no interchange of identity by Δ_1 and Δ_2 ($\Delta_1 \Leftrightarrow \Delta_2$) and the "anti-crossing" ** A_n coincides precisely with the resonance maxima in Figure 4.26(a) with the "level-crossings" L_n occurring on the zero branchline at the forbidden two photon transition frequency. Figure 4.27(b) shows the plots of Δ_1 and Δ_2 for $(E_1+E_2)=-0.1$ for the same values of $|\gamma B_{1x}|/\omega$ and ν. While these plots are still fairly symmetric about the energy reference point $-(E_1+E_2)/2 = .05$, particularly to the high frequency side of A_1, the "level-crossing" is displaced from this energy reference line; the positions of A_1, L_2 are unchanged as a function of frequency. It should also be noted that the displacement of the energy reference point $-(E_1+E_2)/2$ off the zero branch line has caused the characteristic exponent Δ_1, for $|\gamma B_{1x}|/\omega = .1$ to cross over at $\nu \sim \omega$ into the lower half of the next highest branch [0.5, 1.5].

This crossing of the branch line should not be confused with an interchange of identity ($\Delta_1 \Leftrightarrow \Delta_2$) as this value of Δ_1 cannot represent the smooth continuation of the Δ_2 curve.** It does however indicate the sort of complex behaviour that can arise if a non-zero energy reference point in choosen for the problem.

---

* This energy reference point is a natural choice for plots of the Δ_j's as it occurs in the characteristic exponents for the Rabi solution, that is $\Delta_{1,2}^R = -(E_1+E_2)/2 \mp \sqrt{\Omega^2+|\mu_{12}\mathcal{E}|^2}$, see equation 4.2.7, which in turn coincides with $\nu\Delta_{1,2}$ in the weak oscillating field limit.

** The arctangent function, see equation 3.5.20, returns values lying in the branch [-0.5, 0.5]. As the Δ_1 curve crosses the branch line 0.5 into the next highest branch [0.5, 1.5] the arctangent function returns a numerical value of $\Delta_1' = -.4999$ when $\nu \sim \omega$; $\Delta_1 = \Delta_1' + 1$. This value for Δ_1' represents the continuation of the Δ_1' curve in the upper half of the lower branch [-1.5, -0.5].

Figure 4.28 shows plots of Δ_j for $|\gamma B_{12}|/\omega = 0.1$, 0.25, and 0.5 respectively, for $(E_1+E_2) = -1.8$ which corresponds to an energy reference point of $-(E_1+E_2)/2 = 0.9$ located in the branch $[0.5,1.5]$ and lying below the nearest branch line at 1.0; the plots of Δ_1 and Δ_2 are restricted to $[-0.5,0.5]$ due to the properties of the arctangent function, see equation 3.5.20. The behaviour of the characteristic exponents Δ_j is now drastically altered from their symmetric behaviour in the previous figures. It should perhaps be emphasised at this point that the computed spectra of Figure 4.26(a), for any given value of $|\gamma B_{12}|/\omega$ are identical for all choices of (E_1+E_2). While both the "anti-crossing" A_1 and "level-crossing" L_2 are still evident in these spectra, and occur at the same values of υ, the plots are becoming extremely complicated and begin to lose their interpretive value.* For the first time we observe that Δ_1 and Δ_2 begin to interchange identity ($\Delta_1 \leftrightarrow \Delta_2$) at different points in the frequency domain but not at $\upsilon \sim \omega$. Closer inspection of these plots shows that an interchange of identity ($\Delta_1 \leftrightarrow \Delta_2$) occurs in the region where $|\Delta_1| \simeq |\Delta_2|$ indicated by broken lines in the figures. An interchange of identity at the "level-crossing" L_2 also occurs as this corresponds to a real degeneracy ($\Delta_1 = \Delta_2$) in the system. Because of our choice of energy reference the condition $|\Delta_1| = |\Delta_2|$ cannot be fulfilled in the region $\upsilon \sim \omega$** and hence no interchange of identity occurs at this point ($\Delta_1 \not\leftrightarrow \Delta_2$). This interchange of identity can be visualized as the jumping from one solution to another of the infinitely many periodic solutions for the problem [13,14] or,

---

* In these plots, see Figures 4.28 and 4.29, the characteristic exponent curves cross the branch lines at ± 0.5 and could be continued smoothly into the neighbouring branches by using the periodicity relation given by equation 4.2.13.

** It should be recalled that the single photon resonance in the neighbourhood of $\upsilon \sim \omega$ requires that $\upsilon|\Delta_1 - \Delta_2|$ be a minimum [20] which specifies the precise location of the "anti-crossing" A_1. However it is clear from Figure 4.28 that $\Delta_1 \neq \Delta_2$ in this region and the condition $|\Delta_1| = |\Delta_2|$ cannot be satisfied.

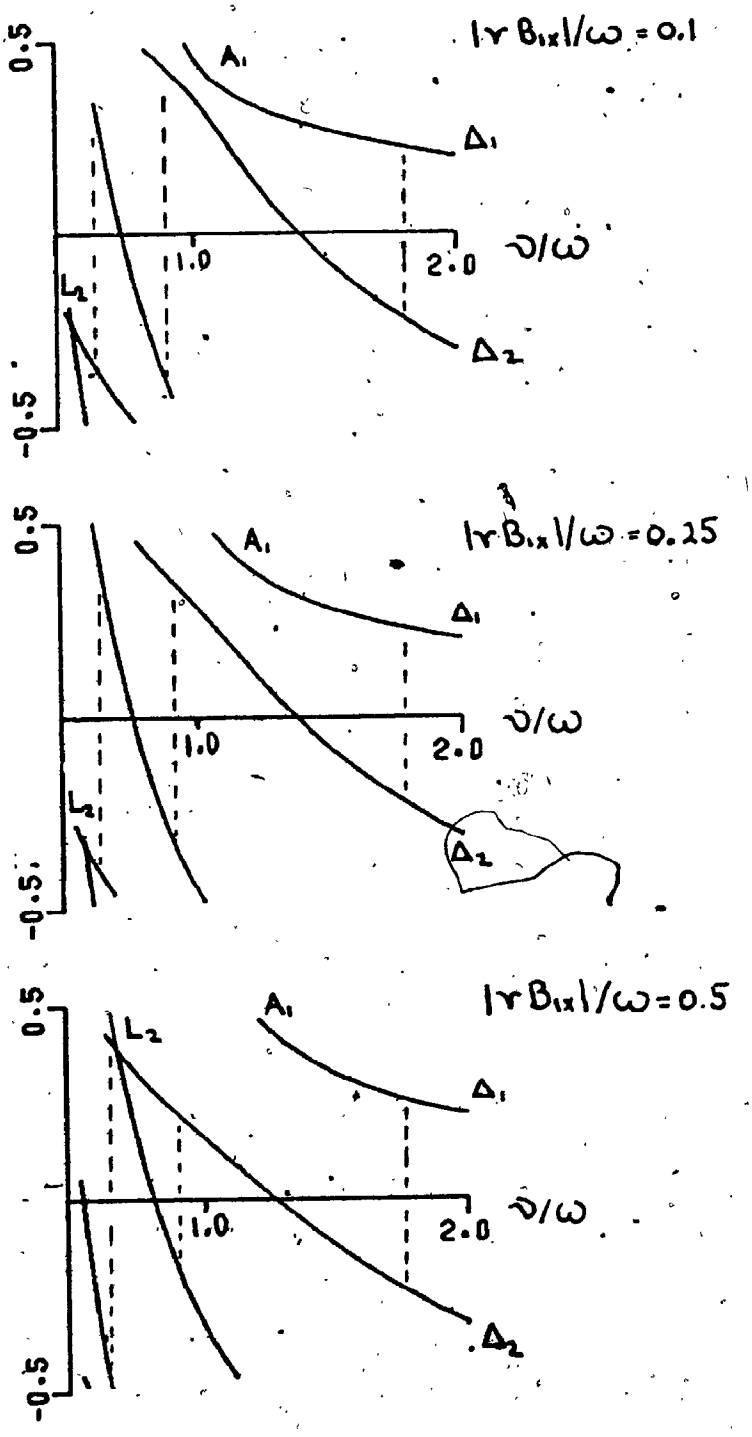

Figure 4.28. The characteristic exponent plots corresponding to Figure 4.26(a) except that $(E_1 + E_2) = -1.8$; $E_1 = -1.4$, $E_2 = -0.4$. The points in the frequency domain at which the Δj's interchange identity are shown by dashed lines.

equivalently, the jumping from one branch to another of the infinitely many adjoining branches $n \pm 1/2$, $n = 0, \pm 1, \pm 2, \ldots$. As the arctangent function, see equation 3.5.19, can only return the values for Δ_1 and Δ_2 in the branch [-0.5,0.5] it is not surprising that the choice of energy reference point $-(E_1+E_2)/2$ in some other branch leads to such complicated behaviour.

Finally, we choose $(E_1+E_2) = -3$ in Figure 4.29 so that the energy reference point $-(E_1+E_2)/2 = 1.5$ lies precisely on a branch line. Although the behaviour of Δ_1 and Δ_2 is as complicated as in Figure 4.28 the condition $|\Delta_1| = |\Delta_2|$ is satisfied at $\upsilon = \omega$ and an interchange of identity ($\Delta_1 \leftrightarrow \Delta_2$) occurs precisely at this point. It should be noted however that this interchange of identity also occurs at other points where $|\Delta_1| = |\Delta_2|$ is satisfied. It is important to note that a change in identity of the Δ_j does not imply a resonance, see [20].

Next we study the behaviour of the Δ_j's for the magnetic tuning experiment, see Figure 4.26(b), which has received considerable attention in recent years [6,7,17,18,56,57]. Ahmad [21] used this example to argue that Shirley's [13] result for $\bar{P}_{22}$, see Section 4.2, was invalid at the point $\upsilon = \omega$. It has been demonstrated in Section 4.2 that the quantity computed by Ahmad does not correspond to $\bar{P}_{22}$. In this magnetic tuning experiment the two states are initially degenerate with a common energy E_0 which corresponds to $(E_1+E_2)/2$. Figure 4.30(a),(b) and (c) shows the characteristic exponent plots as a function of $|\delta B_{02}|/\upsilon$ for the three spectra in Figure 4.26(b) ($|\delta B_{1x}|/\upsilon$ = 0.1,0.25,0.5) for three values of the energy reference point $-(E_1+E_2)/2$ =0,1.4,1.0 (E_0 =0,-1.4,-1.0). These plots, unlike the previous ones for frequency sweeping, retain their symmetry for all choices of ($E_1 + E_2$) except that the choice of $-(E_1+E_2)/2 = 1.4$ has displaced the energy reference line downwards by 0.1. In Figure 4.30(a) Δ_1 and Δ_2 do not interchange identity at any point in the tuning domain, including the point $\upsilon = \omega$ involved in Ahmads criticism of Shirley. Although displaced from the nearest branch line (1.5) in Figure 4.30(b) both Δ_1 and Δ_2 still retain their symmetry about the

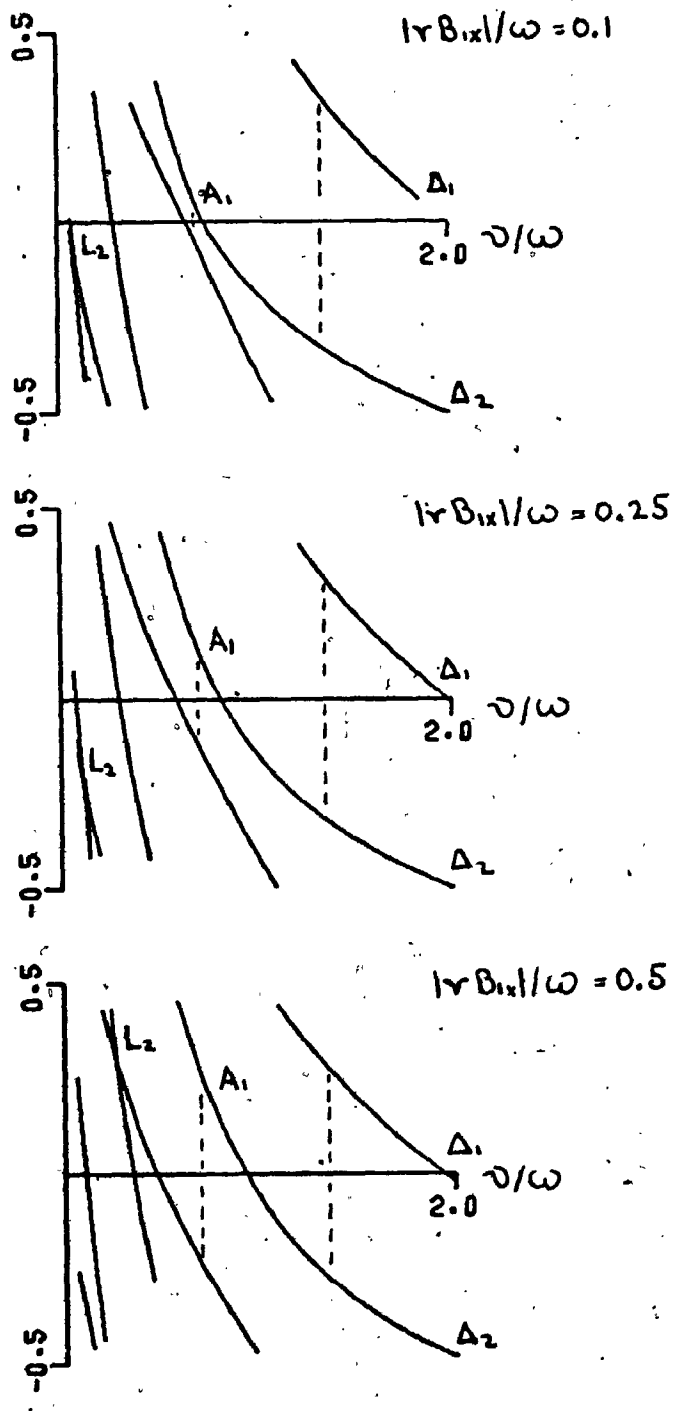

Figure 4.29. The characteristic exponent plots corresponding to Figure 4.26(a) with $(E_1 + E_2) = -3.0$; $E_1 = -2.0$, $E_2 = -1.0$. The interchange of identity ($\Delta_1 \leftrightarrow \Delta_2$) occurs at the dashed lines.

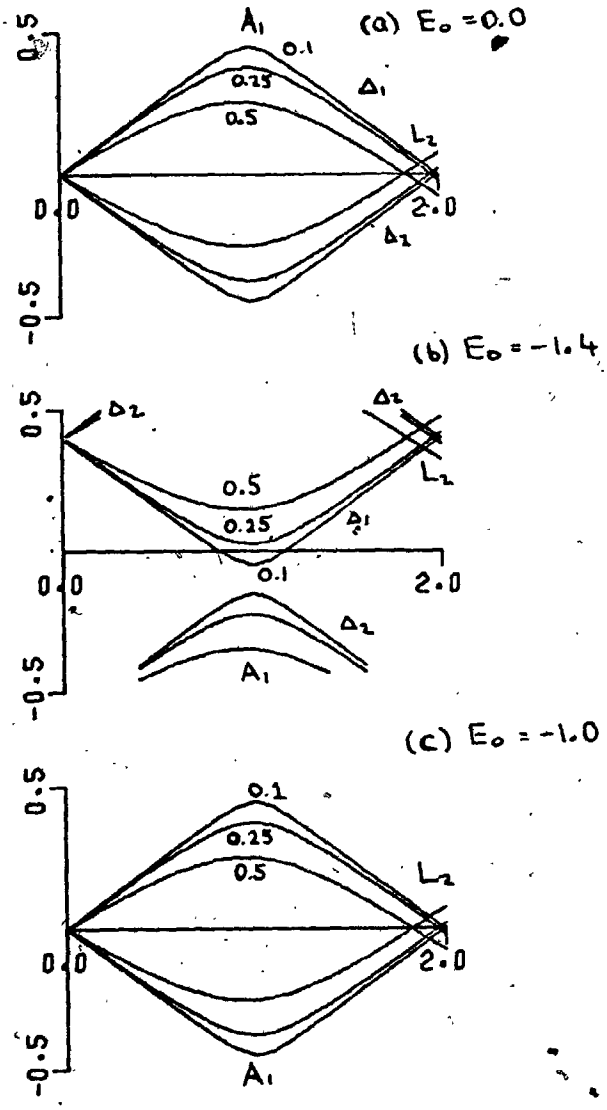

Figure 4.30. Characteristic exponent plots, for the Zeeman tuning experiment for which the spectra are shown in Figure 4.26(b). (a) $E_0 = 0.0$ (b) $E_0 = -1.4$ and (c) $E_0 = -1.0$. (the Δ_j's interchange identity at random in this figure but are plotted as continuous curves). The curves are labelled by the numerical values of $|\gamma B_{1x}|/\nu$.

zero energy reference point $[-(E_1+E_2)/2 = 1.4$ in the branch $[0.5,1.5]$; or $[-(E_1+E_2)/2 = 0.4$ in the branch $[-0.5,0.5]$ in Figure 4.30(b)] and again as the condition $|\Delta_1| = |\Delta_2|$ cannot be satisfied at any point except at the "level-crossing" L_2, where $\Delta_1 = \Delta_2$, no interchange of identity can occur except at L_2. Because of the periodic relationship between the characteristic exponents in adjoining branches the Δ_2 curves in the lower half of the branch $[-0.5,0.5]$, in Figure 4.30(b), are identical to those in the lower half of the branch $[0.5,1.5]$, that is $\Delta_2' = \Delta_2 + 1$. As a result of this periodic relationship the characteristic exponent plots, if viewed about the energy reference line $-(E_1+E_2)/2 = 0.4$, are precisely the same as those plotted about the energy reference line $-(E_1+E_2)/2 = 0$ in Figure 4.30(a). Thus the Δ_2 curves in the lower half of the branch indicated in the upper half of the branch $[-0.5,0.5]$, can be continued across the branch line 0.5 into the Δ_2' curves in the lower half of the branch $[0.5,1.5]$. Finally the plots of Δ_1 and Δ_2 appear to be precisely the same in Figure 4.30(c) as in Figure 4.30(a) where we have chosen the energy reference point to lie on the branch line, that is $-(E_1+E_2)/2 = 1.0$. These plots differ however in that Δ_1 and Δ_2 appear to change identity ($\Delta_1 \longleftrightarrow \Delta_2$) at random over the entire tuning domain because the condition $|\Delta_1| = |\Delta_2|$ is satisfied everywhere. This interchange of identity ($\Delta_1 \longleftrightarrow \Delta_2$) does not occur in Figure 4.30(a) due to the choice of energy reference point.

From the preceding results the behaviour of the characteristic exponents Δ_j for the frequency sweep and magnetic tuning experiments can be summarized as follows. Most importantly, we have demonstrated explicitly that the interchange of identity ($\Delta_1 \longleftrightarrow \Delta_2$) is nonphysical and can be made to occur at different points by an artificial change in the total energy reference (E_1+E_2). The choice of (E_1+E_2) has a profound effect on the behaviour of Δ_j for the frequency tuning experiment and unless (E_1+E_2) is confined to the branch $[-0.5,0.5]$ an extremely complicated behaviour of the characteristic exponents results, see [14]. This complicated behaviour can be rationalized by the following simple qualitative argument. In Figure 4.27(a) the individual energies E_1 and E_2 are

equal in magnitude and as $\nu\Delta_1$ and $\nu\Delta_2$, and also Δ_1 and Δ_2, closely mirror the behaviour of these energies when perturbed by the oscillating field we would expect the behaviour of Δ_1 and Δ_2 to be smooth, continous and symmetric. In Figure 4.27(b) these energies differ slightly in magnitude with the result that their plots become slightly distorted. In Figures 4.28 and 4.29 E_1 and E_2 differ considerably in magnitude with the result that the zero energy reference point $-(E_1+E_2)/2$ occurs in the branch [0.5,1.5]. As a resonance is approached both Δ_1 and Δ_2 must undergo such large changes in magnitude to achieve the minimum value of $\nu|\Delta_1-\Delta_2|$ that they can jump from one branch to another. For the magnetic tuning experiment however, the actual energies E_δ are being linearly varied by the static magnetic field B_{oz}. This linear variation is also exhibited by the characteristic exponents Δ_1 and Δ_2 except in the region of a resonance where they "anti-cross". The fact that Δ_1 and Δ_2 appear to randomly interchange identity ($\Delta_1 \longleftrightarrow \Delta_2$) as a function of $|\gamma B_{oz}|/\nu$ in Figure 4.30(c) again indicates that the energy reference point $-(E_1+E_2)/2$ does not occur in the branch [-0.5,0.5].

At this point we refer briefly to Ahmad's [21] recent criticism of Shirley's result which is based on his claim that the characteristic exponents are discontinous precisely at the point $\nu=\omega$. An apparently singular expansion, see Equation (29)[13], for the characteristic exponent q (in Ahmad's notation) leads this author to argue that the characteristic exponents are discontinous at the point $\nu=\omega$ and hence cannot be used to compute $\bar{P}_{22}$ precisely at this point via Shirley's equation (26), which involves a derivative of q with respect to ω. It should be noted that Shirley does not use this equation to determine q, but in fact determines it directly from an exact numerical integration of the time dependent Schroedinger equation and as he also chooses $(E_1+E_2)=0$ in all his calculations his characteristic exponents will agree with those presented in Figure 4.30(a). This choice of energy reference, that is $(E_1+E_2)=0$ requires that $q_{\nu_1} = -q_{\nu_2}$, or $\nu\Delta_1 = -\nu\Delta_2$ in our notation, and hence the expansion for q in Shirley's equation (29) can be seen to represent the distinct root q_{ν_1} on one side of the resonance and q_{ν_2}

on the other side[79]. The characteristic exponent plot presented by Ahmad as an incorrect view of their behaviour (Ahmad's Figure 2) coincides precisely with the exact Δ_j's plotted in Figure 4.30(a). As was demonstrated in Section 4.2, the characteristic exponent plots of Figure 4.30(a) coincide precisely with the quantized energies computed recently by Yabusaki et al [72,74].

The behaviour of the characteristic exponents Δ_j in the neighbourhood of higher photon resonances will also depend critically on the choice of $(E_1 + E_2)$. As long as this choice is confined to the branch [-0.5,0.5] plots of the Δ_j's remain very informative and will provide accurate frequency shifts and "widths" for various n-photon resonances. The results for the two level system presented above also suggest that such characteristic exponent plots will be well behaved and informative for multilevel systems as long as we confine the energy sum $\sum_{j=1}^{N} E_j$ to within the branch [-0.5,0.5]. In Chapter 5 such multilevel characteristic exponent plots will be used to map out more complicated spectra and will be shown to provide accurate frequency shifts and widths for the various resonances occurring in thes spectra.

CHAPTER 5

MULTILEVEL SYSTEMS

The two level system discussed in Chapter 4 has given us a deeper insight into the complex interactions between radiation and matter. Even this simple system has previously been difficult to analyse in the strong coupling region [13,14] as discussed briefly in Section 4.1. The source of this difficulty is the counter rotating component of the oscillating field, its presence being accounted for previously [13,17,18,56,57] in the weak and intermediate coupling regions through perturbation corrections up to tenth order, while in the strong coupling region some form of direct numerical solution of the original differential equations has been required [13,14,58]. If, in a transition between two states, there are neighbouring states coupled directly to either one of them, one would intuitively expect that the nonresonant interactions with such states might be the same order of magnitude of, or even greater than, the nonresonant interaction between the original two states [12,80,81,82]. In such situations these nonresonant interactions must be quantitatively accounted for and in this chapter the formal method developed in Chapter 3 will be employed to study a number of model multilevel systems. In Section 5.4, for example, we will see that resonance shifts in complicated systems can be accounted for through the inclusion of a relatively small number of neighbouring states coupled directly to the initial and final states involved in the transition.

Another important feature of this chapter is to examine the behaviour of the characteristic exponents Δ_j ,see equation 3.5.20, for some of these model systems. These characteristic exponents Δ_j were identified earlier with the quantized energies of the total

system of atom and perturbing fields, see Chapter 4. Their plots will prove particularly useful in mapping out complicated spectra, providing both the shifts and "widths" of individual resonances without having to compute the multiphoton spectra.

5.1 THREE LEVEL SYSTEM CONTAINING AN EXCITED DEGENERATE PAIR OF STATES

The three level system shown in Figure 5.1(a), interacting with a sinusoidal field of arbitrary amplitude $\mathcal{E}$ and frequency υ, should exhibit a number of additional interesting features absent from the simple two level nondegenerate system dealt with in Chapter 4. For example, the presence of an excited degenerate pair of states, $\phi_2(r)$ and $\phi_3(r)$, of opposite parity and coupled directly to one another via the dipole matrix element μ_{23}, should have a profound effect on the multiphoton spectrum of this system particularly when the coupling is large. This type of system will be considered explicitly here, choosing the ground state $\phi_1(r)$ to have the same parity as $\phi_3(r)$, see Figure 5.1(a). For this configuration the eigenvalue matrix $\underline{\underline{E}}$, the dipole matrix $\underline{\underline{\mu}}$ and the state amplitude vector $\underline{a}(t)$ in the coupled differential equations, 3.1.4, are given by

$$\underline{\underline{E}} = \begin{pmatrix} E_1 & 0 & 0 \\ 0 & E_2 & 0 \\ 0 & 0 & E_3 \end{pmatrix}, \quad \underline{\underline{\mu}} = \begin{pmatrix} 0 & \mu_{12} & 0 \\ \mu_{21} & 0 & \mu_{23} \\ 0 & \mu_{32} & 0 \end{pmatrix}, \quad \underline{a}(t) = \begin{pmatrix} a_1(t) \\ a_2(t) \\ a_3(t) \end{pmatrix} \qquad 5.1.1$$

where $E_2 = E_3 = E_0$. In order to keep the discussion of this system completely general we define the dimensionless parameters

$$\beta_{12} = |\mu_{12}\mathcal{E}| / \omega \qquad 5.1.2$$

where $\omega = E_0 - E_1$ and

$$\alpha = |\mu_{23}| / |\mu_{12}| \qquad 5.1.3$$

Since we will consider transitions from the nondegenerate ground state to the excited degenerate pair, the parameter β_{12} will provide a rough measure of the strength of such transitions while α is a measure of the relative couplings between the individual states within the system. In the discussions that follow we choose* $\alpha = 4$ and β_{12} will be varied.

---

* This choice of α agrees with the ratio $|\mu_{2s,2p}| / |\mu_{1s,2p}|$ in the H atom.

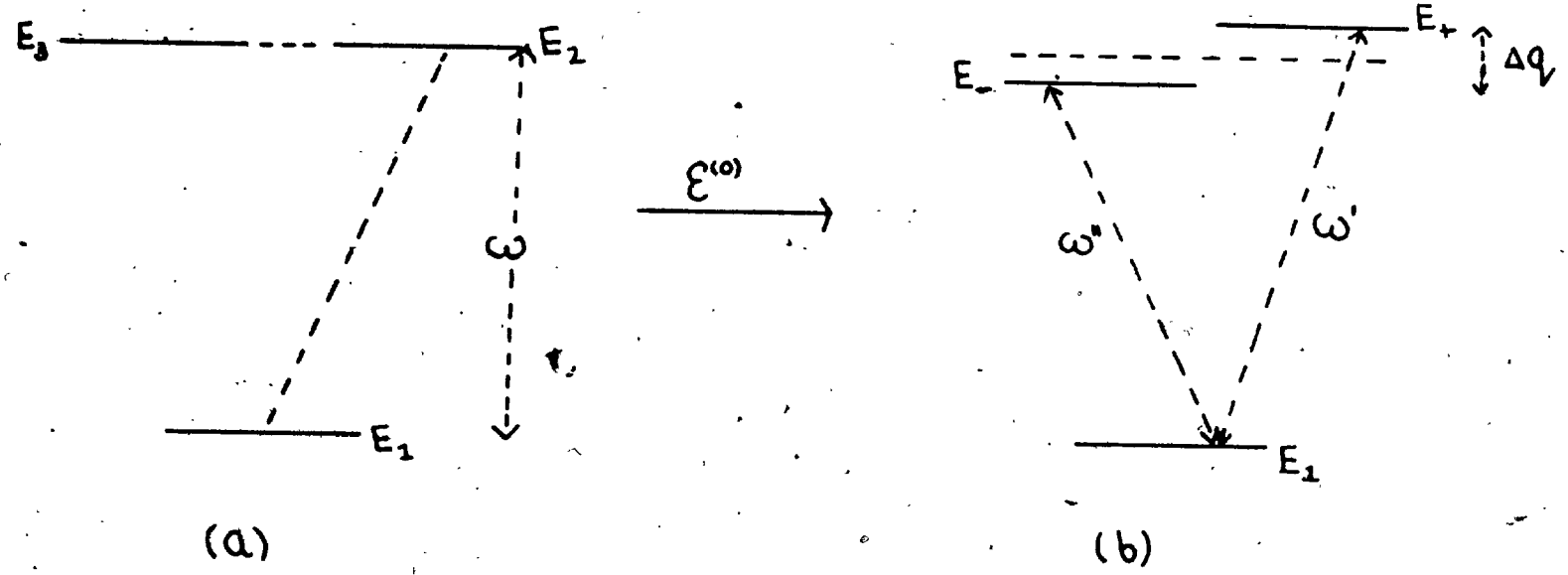

Figure 5.1 (a) The three level configuration employed to study the effects of degeneracy on induced transition probabilities. Both $\phi_1(r)$ and $\phi_3(r)$ are coupled directly to $\phi_2(r)$ of opposite parity. (b) The effect of an applied static Stark field on the level configuration in (a). Numerical values of the parameters used in subsequent calculations on these systems are given explicitly in the relevant figures.

Before proceeding to discuss this three level system in detail a comment will be made regarding the representation used to solve the problem. In analogy with the two-level system discussed in Section 4.1 , one may employ the original representation given by equation 5.1.1 or, alternatively, a representation generated by first diagonalizing the time dependent perturbation $V(r,t)$ with respect to the original degenerate states $\phi_2(r)$ and $\phi_3(r)$ to yield $\phi_+(r)$, $\phi_-(r)$ and $\phi_1(r)$ as the new unperturbed states. In the perturbation treatment of the problem [36] the latter representation must be employed as the original representation leads to singular perturbation expansions. In this new representation the exact coupled differential equations describing the evolution of the system in Figure 5.1(a) are modified so that the new dipole matrix $\underline{\underline{\mu}}$ and state amplitude vector $\underline{a}(t)$ in equation 3.1.4 become

$$\underline{\underline{\mu}} = \begin{pmatrix} 0 & \mu_{1+} & \mu_{1-} \\ \mu_{+1} & \mu_{++} & 0 \\ \mu_{-1} & 0 & \mu_{--} \end{pmatrix} \quad , \quad \underline{a}(t) = \begin{pmatrix} a_1(t) \\ a_+(t) \\ a_-(t) \end{pmatrix} \qquad 5.1.4$$

where

$$\mu_{1\pm} = \langle \phi_1(r) | \mu_z | \phi_\pm(r) \rangle \quad , \quad \mu_{\pm\pm} = \langle \phi_\pm(r) | \mu_z | \phi_\pm(r) \rangle$$

$$\phi_\pm(r) = (\phi_2(r) \pm \phi_3(r))/\sqrt{2} \quad , \quad a_\pm(t) = (a_2(t) \pm a_3(t)) \qquad 5.1.5$$

For the reasons discussed earlier, see Section 4.2.3 and Appendix A.2, the form of the matrix $\underline{\underline{\mu}}$ in equation 5.1.4 necessitates that the matching power series expansion be continued up to 2π , whereas in the original representation, given by equation 5.1.1, it can be terminated at π. As the solutions obtained are very accurate over the period of the Hamiltonian $H(r,t)$, which coincides with the period of oscillation of the degenerate state amplitudes $a_2(t)$ and $a_3(t)$, see equation 4.1.7, both representations should provide equally accurate results and this has been demonstrated explicitly by numerical calculation. Thus an added advantage of the formal method of solution developed herein is that degeneracies in multilevel systems require no special consideration, so that the more symmetric and computationally more convenient representation given by equation 5.1.1 can be used throughout.

5.1.1 MULTIPHOTON FREQUENCY SPECTRUM OF THE THREE LEVEL SYSTEM IN FIGURE 5.1(a).

The phase averaged steady state induced transition probability, $(1-\bar{P}_{11}) = (\bar{P}_{22}+\bar{P}_{33})$, subject to the initial conditions $a_1(0)=1$, $a_2(0)=a_3(0)=0$, is plotted in Figure 5.2(a),(b),(c) over a wide frequency domain for the following values of the coupling parameter β_{12} = 0.075, 0.15 and 0.25, respectively. Both even and odd photon transitions occur in this system due to the parity selection rules, see Chapter 2. For the weaker coupling strength (β_{12} = 0.075) the spectrum shows the expected pattern, with individual resonances peaking at 0.5, indicating that the system is effectively behaving as a two level system with an excited state of mixed parity [9]. On increasing β_{12} however, this pattern begins to gradually breakdown and the higher photon resonances begin to exceed 0.5 until eventually, for β_{12} = 0.25, only the single photon resonance peak remains close to 0.5. This behaviour is indicative of the fact that the radiation is being partially trapped in the excited degenerate pair and that this trapping is more effective for higher photon transitions. As $(1-\bar{P}_{11})$ is the sum of the individual induced transition probabilities $\bar{P}_{22}$ and $\bar{P}_{33}$, a study of their behaviour as a function of frequency υ should be particularly enlightening. Figure 5.3 (a), (b) and (c) shows plots of $\bar{P}_{22}$ and $\bar{P}_{33}$, whose sum comprise the multiphoton spectra in Figure 5.2 (a),(b) and (c), respectively. If the individual transitions $(\phi_1 \rightarrow \phi_2)$ and $(\phi_1 \rightarrow \phi_3)$ occurred independently of one another we would expect that the multiphoton spectra for $\bar{P}_{22}$ would contain only odd photon (1,3,5...)transitions while the spectrum for $\bar{P}_{33}$ would contain only even photon (2,4,6...) transitions. However; it is obvious from Figure 5.3 that for the values of β_{12} chosen here the oscillating field gives rise to a dynamic Stark mixing of the degenerate pair. Such a dynamic Stark mixing arises from the nonresonant interaction of the oscillating field with the degenerate states, see equation 4.1.6, and as a result it is much weaker than the static Stark mixing which essentially involves a resonant interaction, with a field of zero frequency interacting with a pair of degenerate

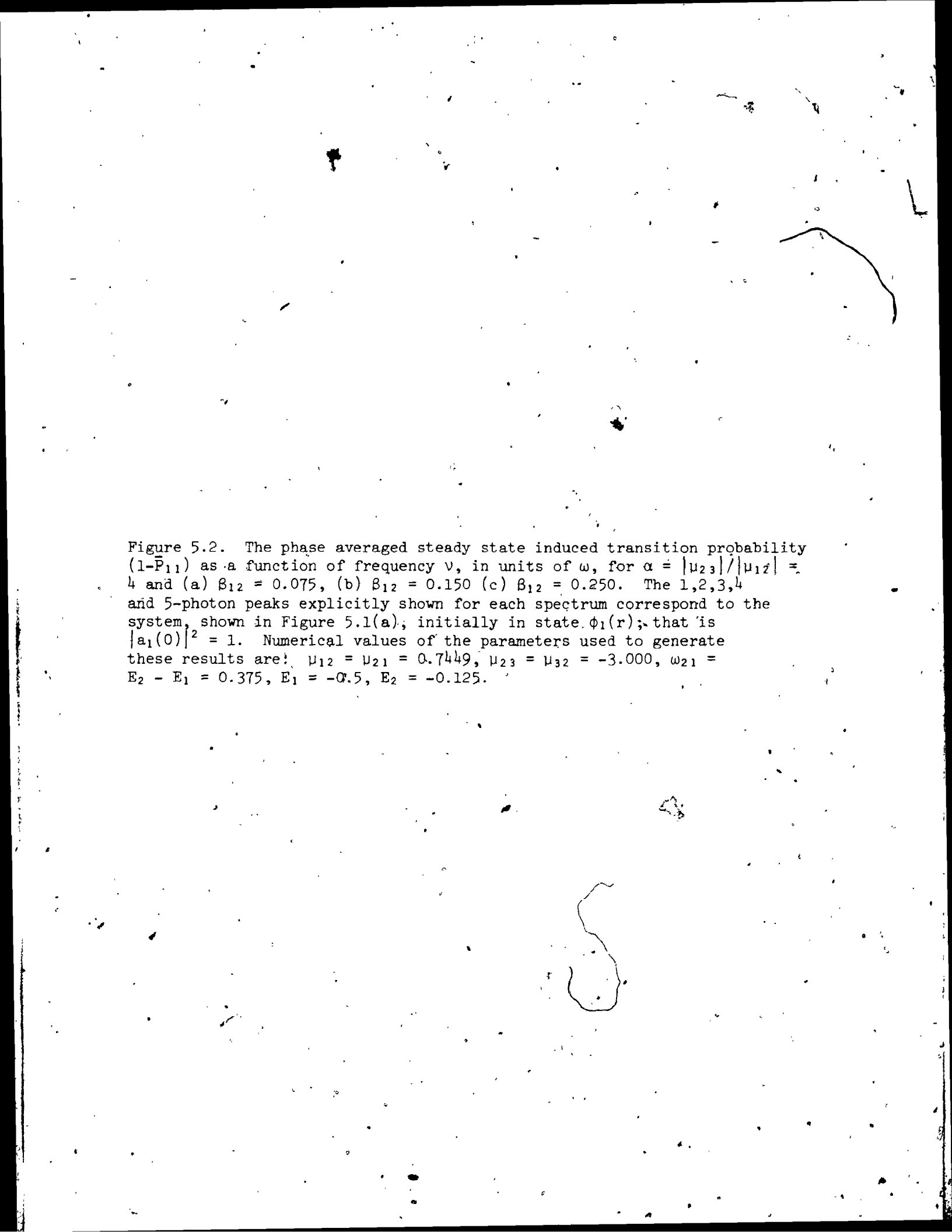

Figure 5.2. The phase averaged steady state induced transition probability $(1-\bar{P}_{11})$ as a function of frequency ν, in units of ω, for $\alpha = |\mu_{23}|/|\mu_{12}| = 4$ and (a) $\beta_{12} = 0.075$, (b) $\beta_{12} = 0.150$ (c) $\beta_{12} = 0.250$. The 1,2,3,4 and 5-photon peaks explicitly shown for each spectrum correspond to the system, shown in Figure 5.1(a), initially in state $\phi_1(r)$; that is $|a_1(0)|^2 = 1$. Numerical values of the parameters used to generate these results are: $\mu_{12} = \mu_{21} = 0.7449$, $\mu_{23} = \mu_{32} = -3.000$, $\omega_{21} = E_2 - E_1 = 0.375$, $E_1 = -0.5$, $E_2 = -0.125$.

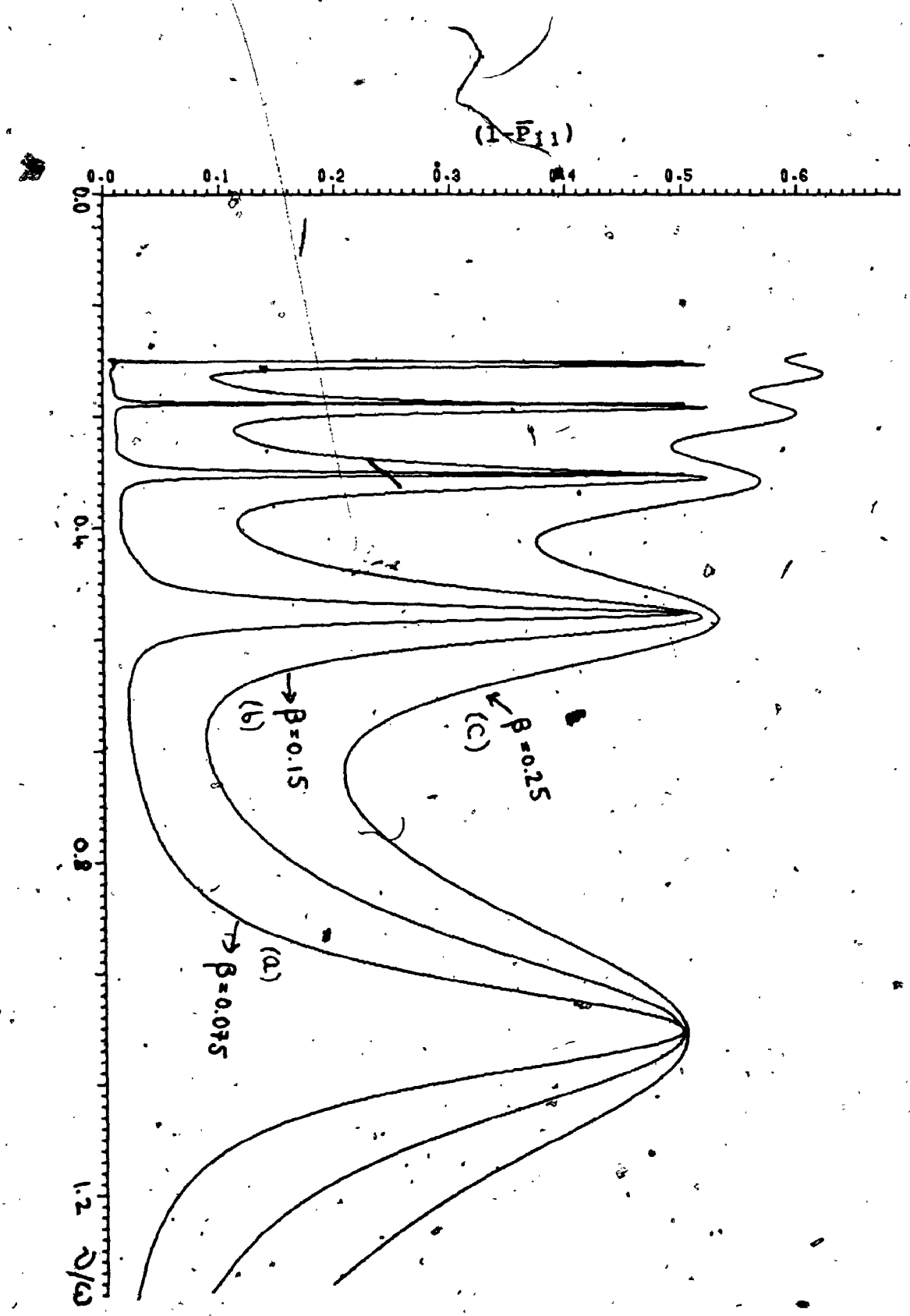
$(1-\bar{P}_{11})$
0.0
0.1
0.2
0.3
0.4
0.5
0.6
0.0
4.0
8.0
12
ω/ω_c
(a) β=0.075
(b) β=0.15
(c) β=0.25

Figure 5.3 The phase averaged steady state induced transition probabilities $\bar{P}_{22}$ and $\bar{P}_{33}$ as a function of frequency ν, in units of ω, for the same parameters as in Figure 5.2(a), (b) and (c). (a) $\bar{P}_{22}$ and $\bar{P}_{33}$ for $\beta_{12} = 0.075$, (b) $\bar{P}_{22}$ and $\bar{P}_{33}$ for $\beta_{12} = 0.150$ and (c) $\bar{P}_{22}$ and $\bar{P}_{33}$ for $\beta_{12} = 0.250$.

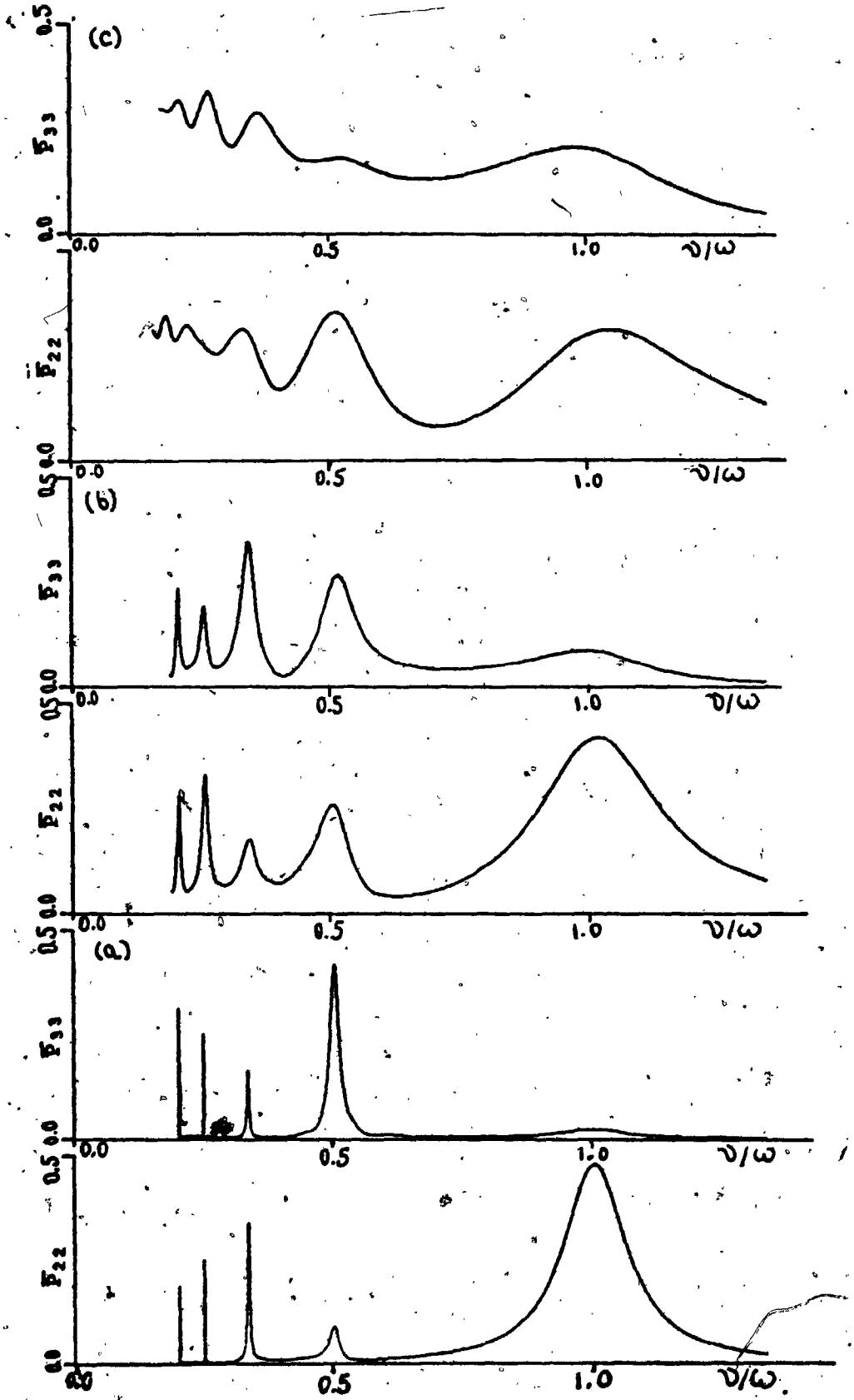
(c)
F_{33}
F_{22}
(b)
F_{33}
F_{22}
(a)
F_{33}
F_{22}
0.0
0.5
1.0
ν/ω

states, see Chapter 4.

Thus while this mixing is evident for β_{12} =0.075, see Figure 5.3(a), where the so called "forbidden" transitions are clearly occurring in both $\bar{P}_{22}$ and $\bar{P}_{33}$, the mechanism of resonant population transfer between the ground state $\phi_1(r)$ and the excited states still dominates over the competing mechanism of population transfer between the degenerate states $\phi_2(r)$ and $\phi_3(r)$ via dynamic Stark mixing. Hence the spectrum in Figure 5.2(a) still retains the characteristics of a two level system with an excited state of mixed parity. Also evident in Figure 5.3(a) is the fact that so-called "forbidden" transitions become increasingly important for the higher photon resonances, which is not surprising as the frequency ν of the oscillating field is moving toward the static limit, $\nu = 0$, as one proceeds to the higher photon resonances. As β_{12} is increased, both mechanisms of population transfer become equally important, until eventually for β_{12} =0.25 radiation trapping in the excited degenerate pair is occurring over most of the frequency domain. This trapping is even more evident in Figures 5.3(b) and (c), where $(\bar{P}_{22} + \bar{P}_{33})$ exceeds 0.5, indicating population inversion in the excited state. The fact that this population inversion is greater for successive higher photon transitions is due to the fact that their induced transition rate decreases as a result of its nonlinear dependence on $|\mu_{12}\mathcal{E}|$ and hence allows the trapping mechanism between the degenerate pair to compete more effectively.

The phase averaged induced transition probabilities, $\bar{P}_{11}(t)$, $\bar{P}_{22}(t)$ and $\bar{P}_{33}(t)$, corresponding to frequencies ν lying on the three photon resonance maxima corresponding to β_{12} =0.075, 0.15

---

*Of course the spectrum for $\bar{P}_{33}$ is only observable because of the presence of $\phi_2(r)$ of opposite parity. However, for sufficiently weak coupling strength, $\phi_2(r)$ should behave solely as a virtual state coupling $\phi_1(r)$ to $\phi_3(r)$, so that there should be no population transfer to it.

and 0.25 in Figures 5.2(a),(b),(c) are shown over a number of cycles of their "slowly varying" part in Figure 5.4(a),(b) and (c) respectively. Their behaviour in the time domain is a further indication of the increased trapping of population in the excited states as β_{12} increases. For β_{12} =0.075 the induced transition probability $\bar{P}_{11}(t)$ oscillates between 1 and 0 in the same manner as in the simple two level nondegenerate system dealt with in Chapter 4; for the three photon resonance the state ϕ_3 becomes less important as β_{12} decreases. However, as β_{12} increases, the oscillatory behaviour of $\bar{P}_{11}(t)$ begins to deviate from that expected for a simple two-level system. While the induced transition probability $\bar{P}_{33}(t)$ should be negligible for weak couplings, these figures show that its contribution increases rapidly in the intermediate coupling region and for β_{12} =0.15 $\bar{P}_{33}(t)$ is already greater in magnitude than $\bar{P}_{22}(t)$ [compare Figures 5.4(a),(b),(c) and Figures 5.3(a),(b),(c)].

Figures 5.5(a),(b) and 5.6(a),(b) show the multiphoton spectra for β_{12} =0.1 and 0.25 along with their characteristic exponent plots over the same frequency domain.* As pointed out by Besset et al [20], these characteristic exponents closely mirror the behaviour of the original unperturbed energies E_j between the various resonances. Thus, for example, in Figure 5.5(b) two of the characteristic exponents Δ_2 and Δ_3, associated with the degenerate pair of states E_2 and E_3, remain near degenerate between resonances and each in turn "anti-crosses" with the third characteristic exponent Δ_1 as an odd photon (basically $1\rightarrow 2$) or even photon (basically $1\rightarrow 3$) resonance is traversed. For example, as the two photon resonance (A_2) is

---

*The characteristic exponents Δ_j flip identity at various points in the frequency domain but as already demonstrated this flip over in identity is non-physical, see Section 4.4, and does not affect the physical results. For this reason they will be plotted so that they mirror the behaviour of the original unperturbed energies E_j in the presence of the oscillatory field.

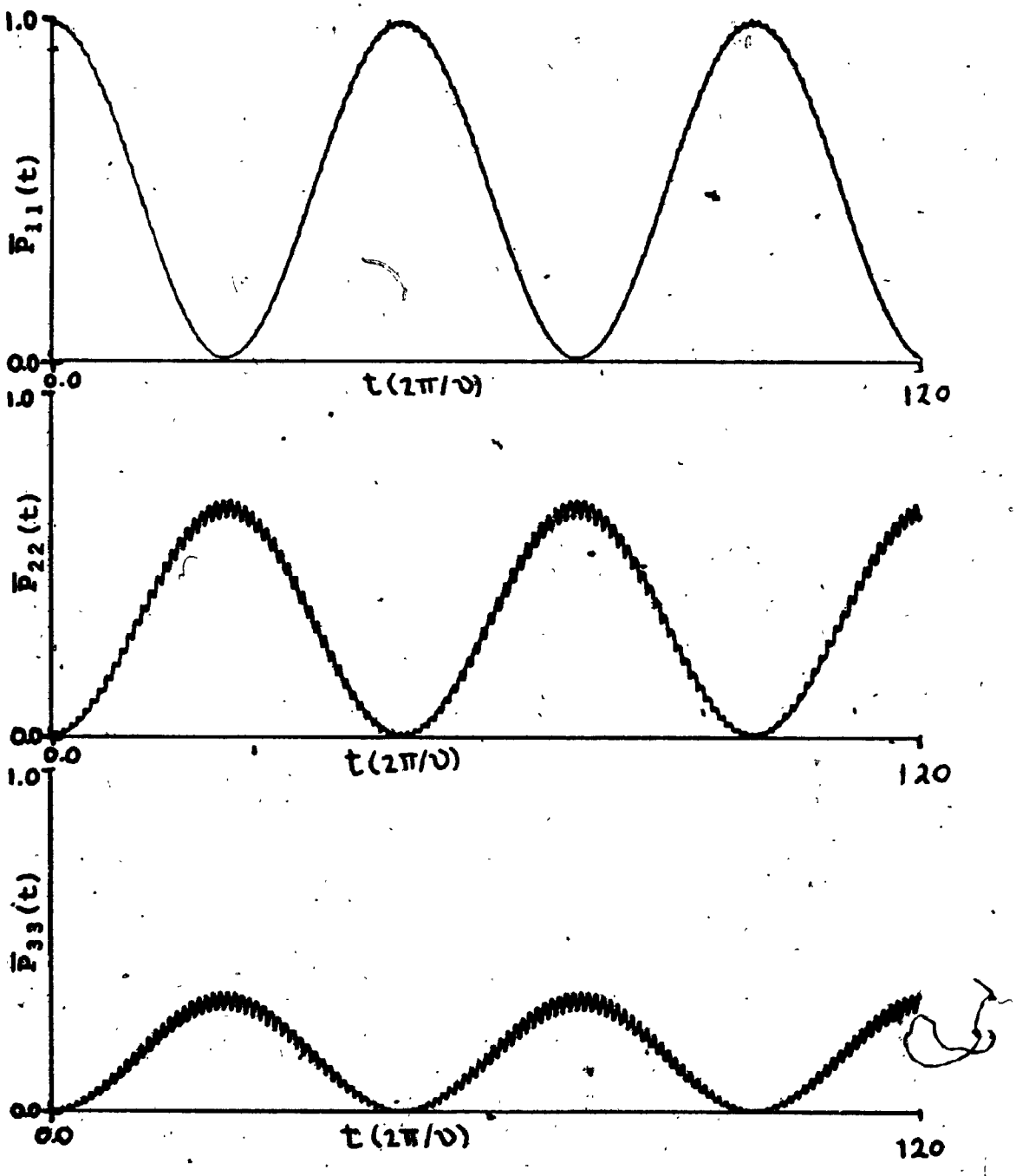

Figure 5.4(a) The phase averaged induced transition probabilities, $\bar{P}_{11}(t)$, $\bar{P}_{22}(t)$ and $\bar{P}_{33}(t)$ as a function of t, in units of $2\pi/\nu$, corresponding to the frequency $\nu = 0.1257$ lying on the three photon, maximum in Figure 5.2(a).

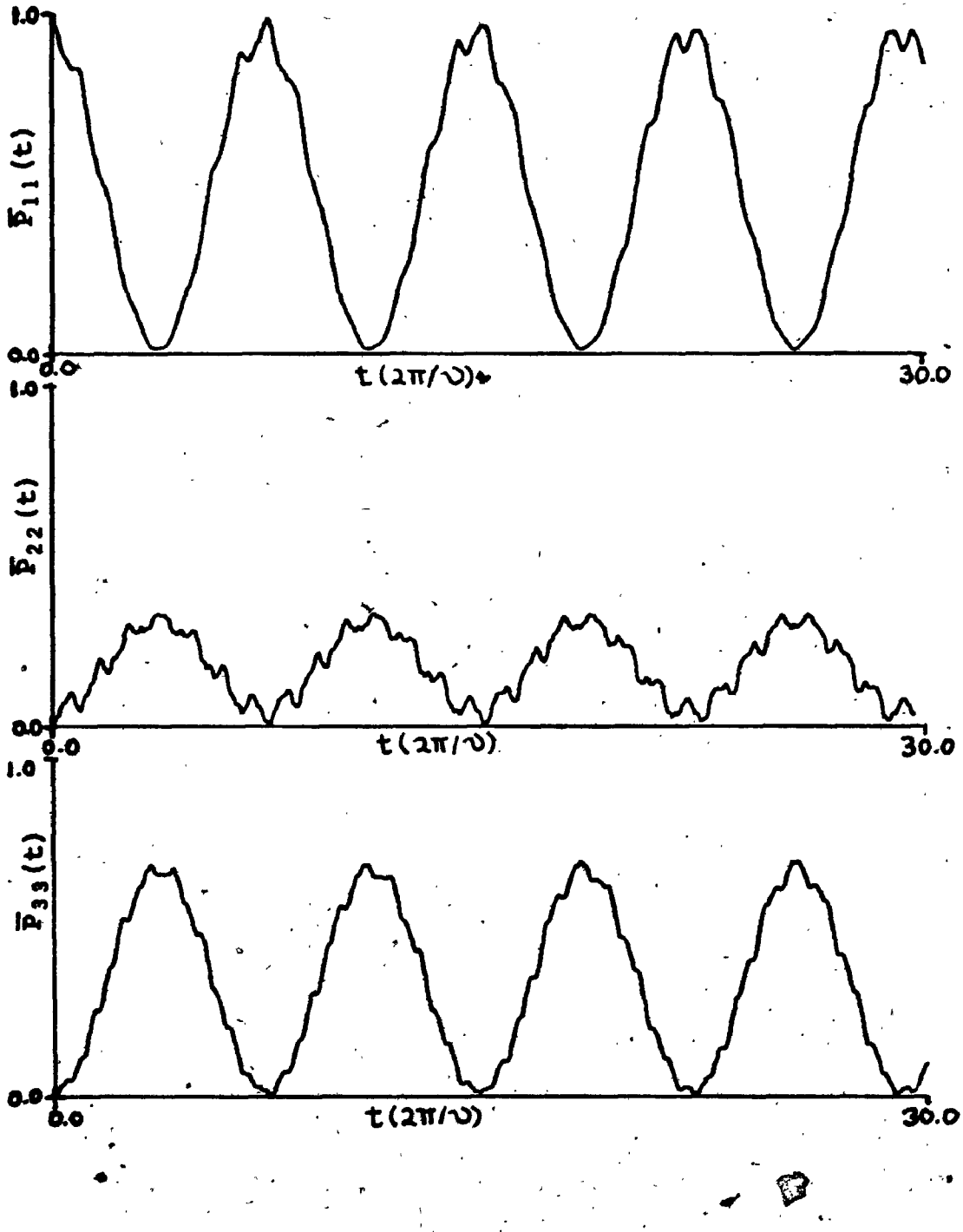

Figure 5.4(b) The phase averaged induced transition probabilities, $\bar{P}_{11}(t)$, $\bar{P}_{22}(t)$ and $\bar{P}_{33}(t)$, as a function of t, in units of $2\pi/\nu$, corresponding to the frequency $\nu = 0.1275$ lying on the three photon resonance maximum in Figure 5.2(b).

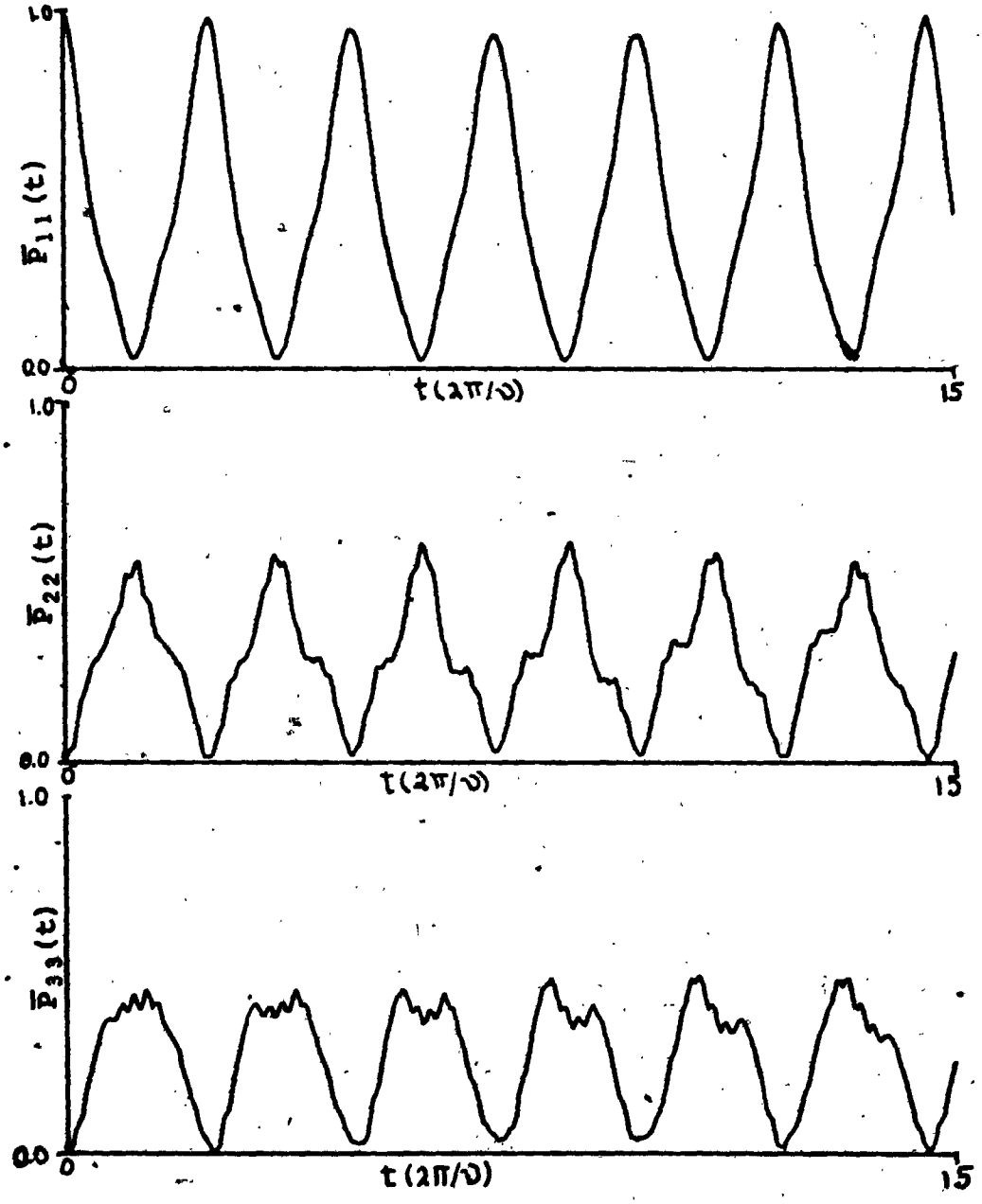

Figure 5.4(c) The phase averaged induced transition probabilities $\bar{P}_{11}(t)$, $\bar{P}_{22}(t)$ and $\bar{P}_{33}(t)$, as a function of t, in units of $2\pi/\nu$, corresponding to the frequency $\nu = 0.1305$ lying on the three photon resonance maximum in Figure 5.2(c).

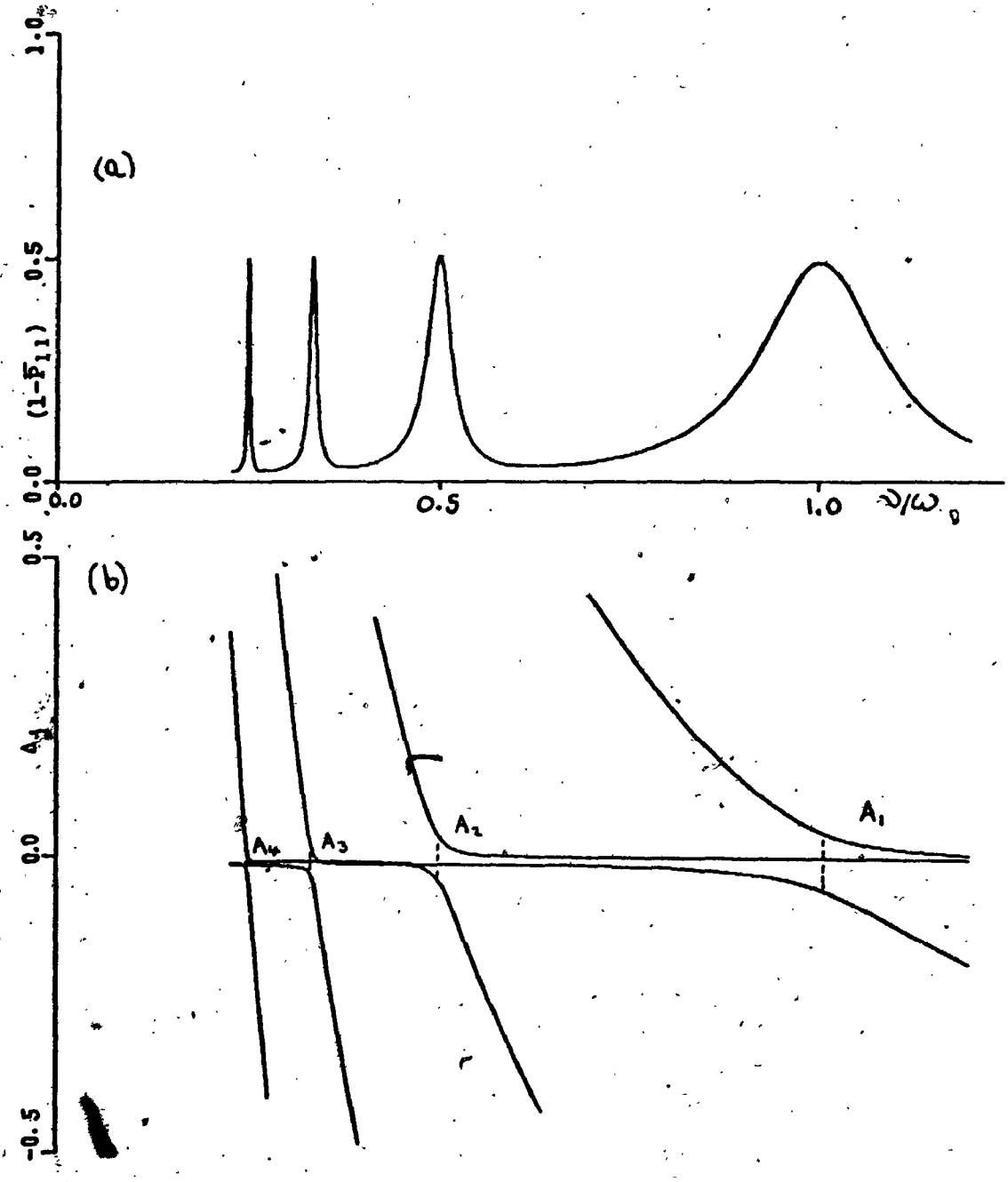

Figure 5.5. The phase averaged steady state induced transition probability $(1 - \bar{P}_{11})$ and the accompanying characteristic exponent (Δj) plots as a function of frequency ν for $\alpha = 4$, $\beta_{12} = 0.1$ and subject to the initial conditions $|a_1(0)|^2 = 1$. The occurrence of an n-photon resonance in Figure 5.5(a) is signified by the presence of an "anti-crossing" A_n between two of the three characteristic exponents Δj in Figure 5.5(b). Numerical values of the parameters used to generate these results are; $\omega = E_0 - E_1 = 0.5$, $E_1 = -0.5$, $E_0 = E_3 = E_2 = 0.0$, $\mu_{12} = 1.0$ and $\mu_{23} = 4.0$.

traversed, the characteristic exponents Δ_1 and Δ_3 anti-cross in Figure 5.5(b), while Δ_2 remains essentially unperturbed. The "anti-crossing" points A_n for the transition $i \rightarrow j$ occur at the minima in the quantity $\nu|\Delta_i - \Delta_j|$, see Section 4.2 for discussion, and correspond precisely to the resonance maximum of the appropriate n-photon transition in the accompanying spectra. In Figure 5.6(a),(b) the effect of strong coupling on the degenerate pair is dramatically illustrated in the characteristic exponent plots. With the exception of the single photon transition region, all three characteristic exponents Δ_j are strongly perturbed, indicating a strong coupling between the degenerate pair $\phi_2(r)$ and $\phi_3(r)$, which manifests itself in the accompanying multiphoton spectrum where trapping of the radiation in the excited state is evident. Now, for example, as the two photon resonance is traversed in Figure 5.6(b), the third characteristic exponent Δ_2 no longer remains unperturbed. This shows clearly that as β_{12} increases, the two degenerate states $\phi_2(r)$ and $\phi_3(r)$ begin to lose their identity due to dynamic Stark mixing. The periodic relationship between the characteristic exponents Δ_j, see Section 4.2, in neighbouring branches (for example [0.5,1.5],[-0.5,-1.5]) is also evident from Figures 5.5(b) and 5.6(b), where whenever Δ_j crosses a branch line either at 0.5 or -0.5, it reappears immediately in the other half of the branch at -0.5 or 0.5, respectively

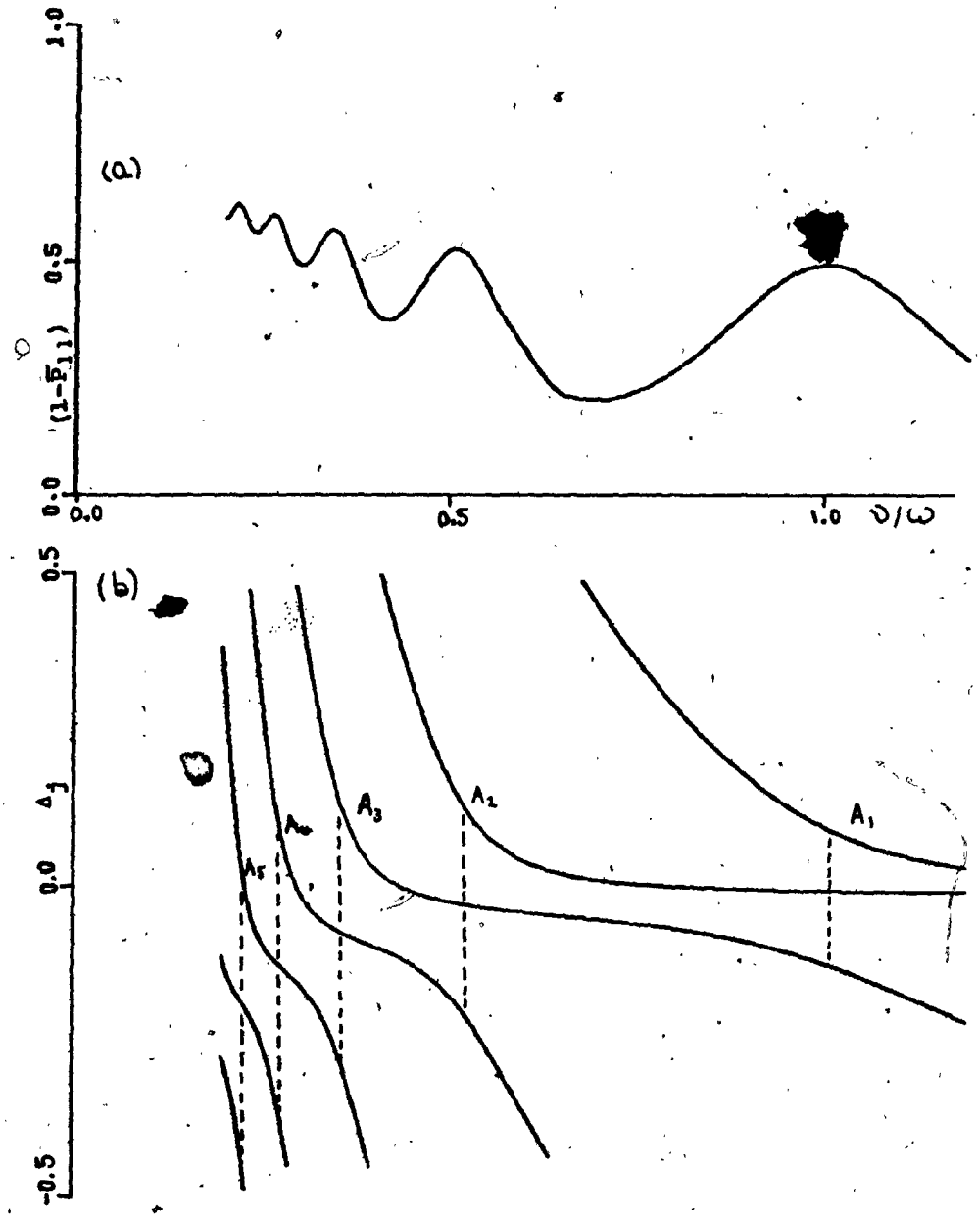

Figure 5.6. The phase averaged steady state induced transition probability $(1 - \bar{P}_{11})$ and the accompanying characteristic exponent plots as a function of frequency ν for $\beta_{12} = 0.25$. The remainder of the parameters used to generate this figure are the same as for Figure 5.5.

5.1.2 EFFECT OF A STATIC STARK FIELD ON THE MULTIPHOTON SPECTRUM OF THE SYSTEM IN FIGURE 5.1(a).

When a static Stark field $\mathcal{E}^\circ$ is applied to the system in Figure 5.1(a), the degenerate states $\phi_2(r)$ and $\phi_3(r)$ are strongly mixed and split into two states $\phi_\pm(r)\,(\equiv(\phi_2 \pm \phi_3)/\sqrt{2})$ of mixed parity. Assuming that the third state $\phi_1(r)$ is sufficiently remote from the degenerate pair, the splitting of the mixed states is approximately given by, see Chapter 4,*

$$\Delta q \simeq 2|\mu_{23}\mathcal{E}^\circ| \qquad 5.1.6$$

If an oscillating field of amplitude $\mathcal{E}$ is now swept over the same frequency domain as in the previous section, we would expect to observe a series of multiphoton resonances (even and odd) at the approximate transition frequencies $\omega, \omega/2, \omega/3, \cdots$ and $\omega'', \omega''/2, \omega''/3, \cdots$ corresponding to the transitions $\phi_1(r) \to \phi_+(r)$ and $\phi_1(r) \to \phi_-(r)$, respectively, see Figure 5.1(b). The differential equations describing the time evolution of this system are given by equation 3.1.4 with the dipole and state amplitude matrices given by equation 5.1.1 and the matrix $\underline{\underline{E}}$ becomes

$$\underline{\underline{E}} = \begin{pmatrix} E_1 & -\mu_{12}\mathcal{E}^\circ & 0 \\ -\mu_{21}\mathcal{E}^\circ & E_2 & -\mu_{23}\mathcal{E}^\circ \\ 0 & -\mu_{32}\mathcal{E}^\circ & E_3 \end{pmatrix} \qquad 5.1.7$$

The phase averaged steady state induced transition probability $(1-\bar{P}_{11})$ and its accompanying characteristic exponent plots Δ_j for the three level configuration of Figure 5.1(b), subject to the initial conditions $a_1(0)=1$, $a_2(0)=a_3(0)=0$, is plotted for $\beta_{12}=0.1$ and $\alpha=4$ in Figure 5.7(a),(b)-5.9(a),(b) for three values of the ratio $\gamma=\mathcal{E}^\circ/\mathcal{E}$ (that is $\gamma=0.1,0.2,0.3$). The presence of the static Stark field $\mathcal{E}^\circ$

---

*The physical interpretation of the above results will be made on the basis of the $(\phi_1, \phi_\pm)$ diagonal representation, whereas actual calculations are carried out in the original (ϕ_1, ϕ_2, ϕ_3) representation for the reasons discussed earlier, see Section 5.1.

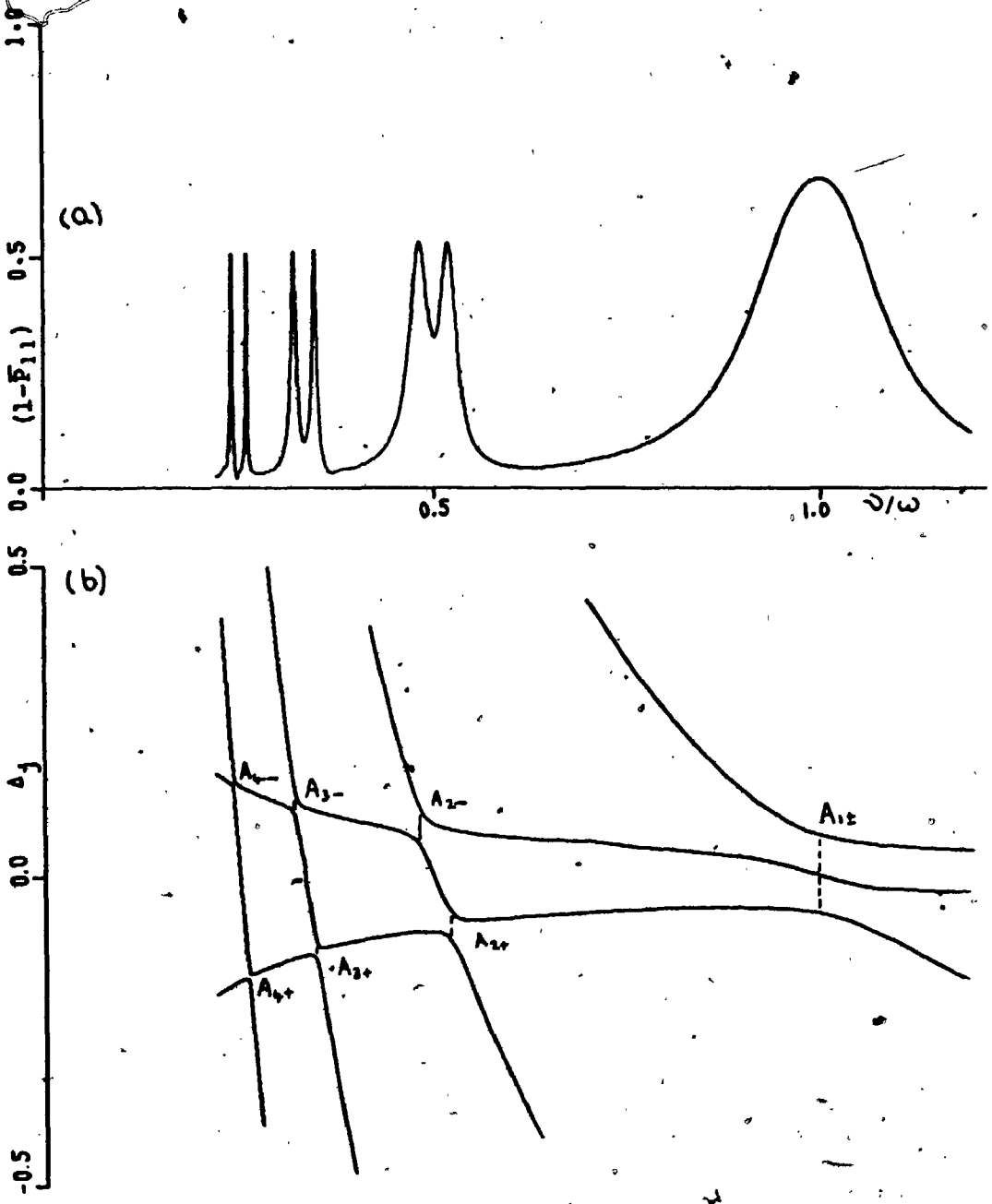

Figure 5.7. The phase averaged steady state induced transition probability $(1 - \bar{P}_{11})$ and the accompanying characteristic exponent plots as a function of frequency ν for the relative field strength parameter $\gamma = \mathcal{E}^{\circ}/\mathcal{E} = 0.1$; see Figure 5.1(b). Otherwise the same parameters as used to generate Figure 5.5 are employed here. The "anti-crossings" $A_{n\pm}$ refer, respectively, to the allowed n photon transitions between the initially populated ground state and the Stark split excited $\pm$ states shown in Figure 5.1(b).

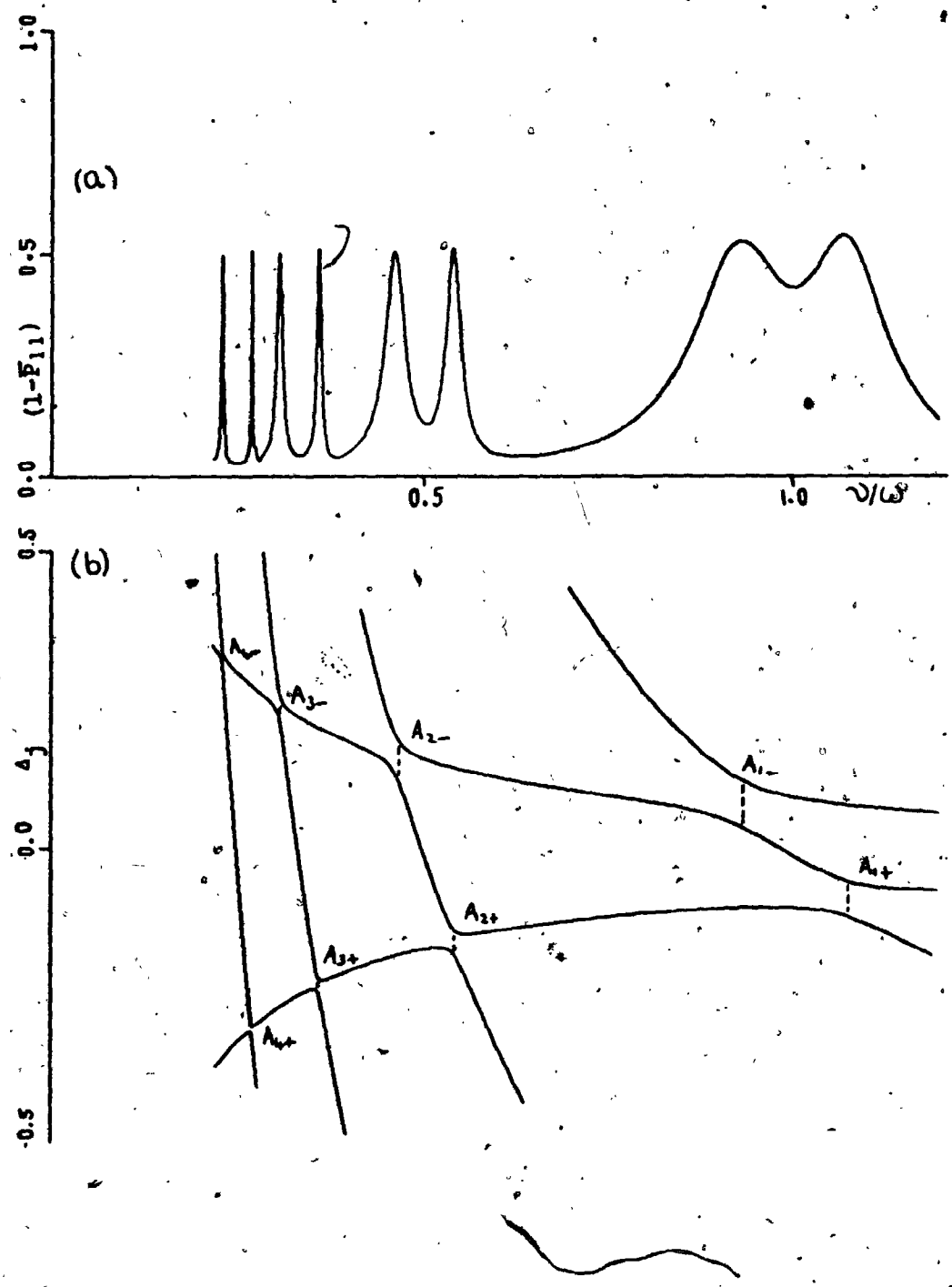

Figure 5.8. The phase averaged steady-state induced transition probability $(1 - \bar{P}_{11})$ and the accompanying characteristic exponent plots for the relative field strength parameter $\gamma = 0.2$ and for the same parameters as in Figure 5.7.

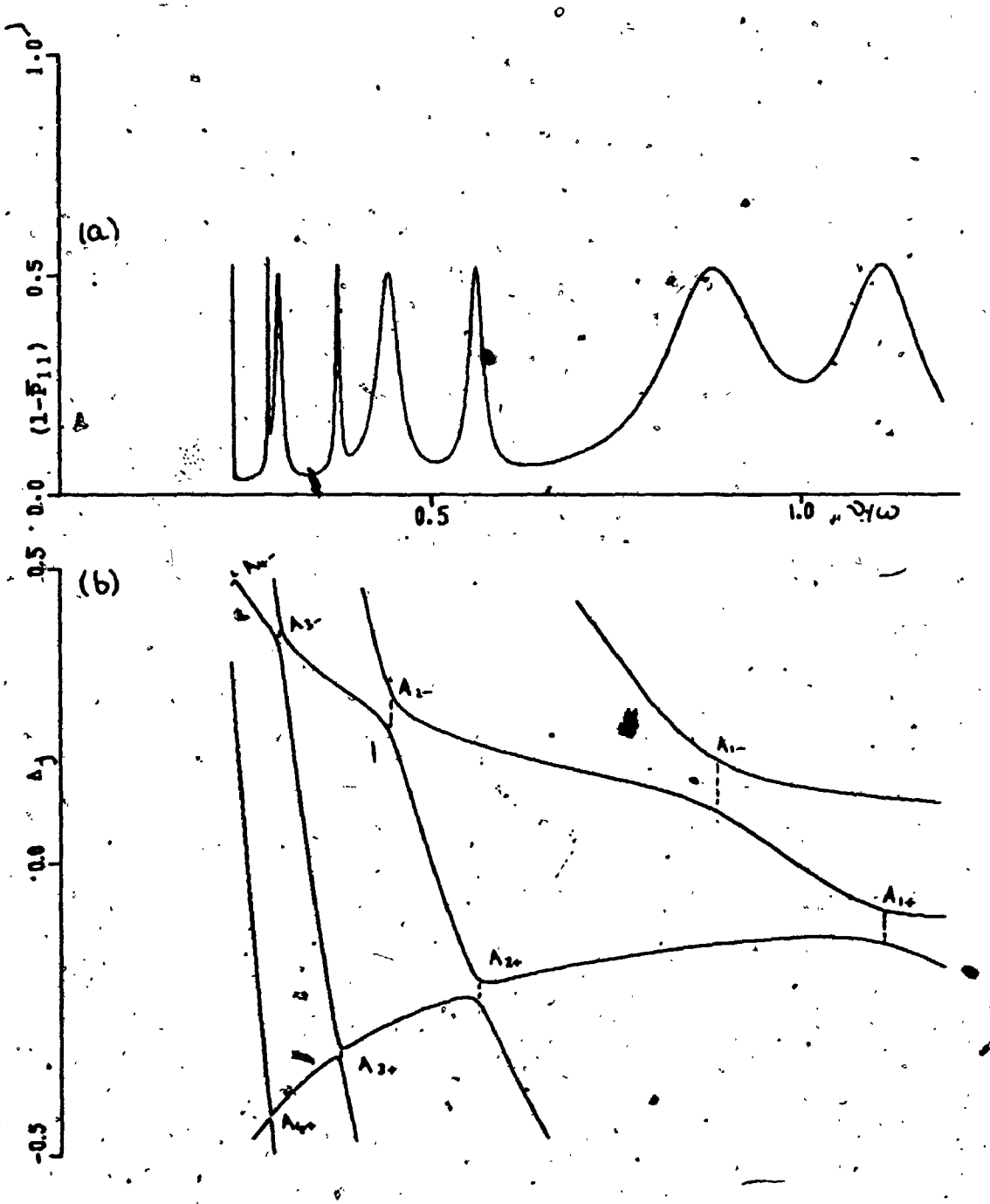

Figure 5.9. The phase averaged steady state induced transition probability $(1 - \bar{P}_{11})$ and the accompanying characteristic exponent plots for the relative field strength parameter $\gamma = 0.3$ and the same parameters as in Figure 5.7.

is evident from the splitting of each n-photon resonance peak (1,2,3 and 4) into two components displaced to either side of the original resonance position when $\mathcal{E}^{\circ}=0$ [Compare with Figure 5.5(a)]. For the weaker static Stark field, $\gamma=0.1$, only the three and four photon profiles are appreciably split; the two photon profile is only partially split and the original single photon peak is not split at all. Increasing the Stark field ($\gamma=0.2,0.3$) causes all profiles to split until finally for $\gamma=0.3$ the high frequency component of the four photon doublet and the low frequency component of the three photon doublet begin to overlap. In each case the low frequency component of each doublet is broader than its high frequency counterpart, which is in agreement with the relative order of magnitudes of the coupling parameters $\beta_{1-} > \beta_{1+}$ [$(\beta_{1-}/\beta_{1+}) = \omega'/\omega'' > 1$; β_{12} is the coupling parameter when $\mathcal{E}^{\circ}=0$ or $\omega'=\omega''=\omega$]. The splitting of each n-photon doublet when resolved, is approximately given by $\Delta q/n$ as suggested by Figure 5.1(b).

The characteristic exponent plots accompanying these spectra, see Figures 5.7(b)-5.9(b), provide a dramatic illustration of the effect of the static Stark field $\mathcal{E}^{\circ}$ on the multiphoton spectra corresponding to $\mathcal{E}^{\circ}=0$. The near degeneracy between resonances of the two characteristic exponents Δ_2 and Δ_3 in Figure 5.5(b) is gradually broken as the Stark field is increased (Compare Figure 5.5(b) with 5.7(b)-5.9(b)). The appearance of a doublet at the single photon transition frequencies is signified by the gradual change from a degenerate pair of "anti- crossings" $A_{1\pm}$ in Figure 5.7(b) to two neighbouring split "anti- crossings" in Figures 5.8(b) and 5.9(b). In these plots the "anti-crossings", $A_{n\pm}$, occur in pairs at the precise frequencies at which the two components of each n-photon transition occur. The greater magnitude of $|\Delta_0 - \Delta_1|$ at each low frequency component is indicative of the greater "width" of this component.

Finally, the effect of damping on the multiphoton spectra of Figures 5.7(a) - 5.9(a) is shown in Figure 5.10(a),(b),(c), respectively, where the damped phase averaged induced transition probability $(1-\bar{P}_{11}^{\tau})$, see equation 3.7.10, is plotted over the same

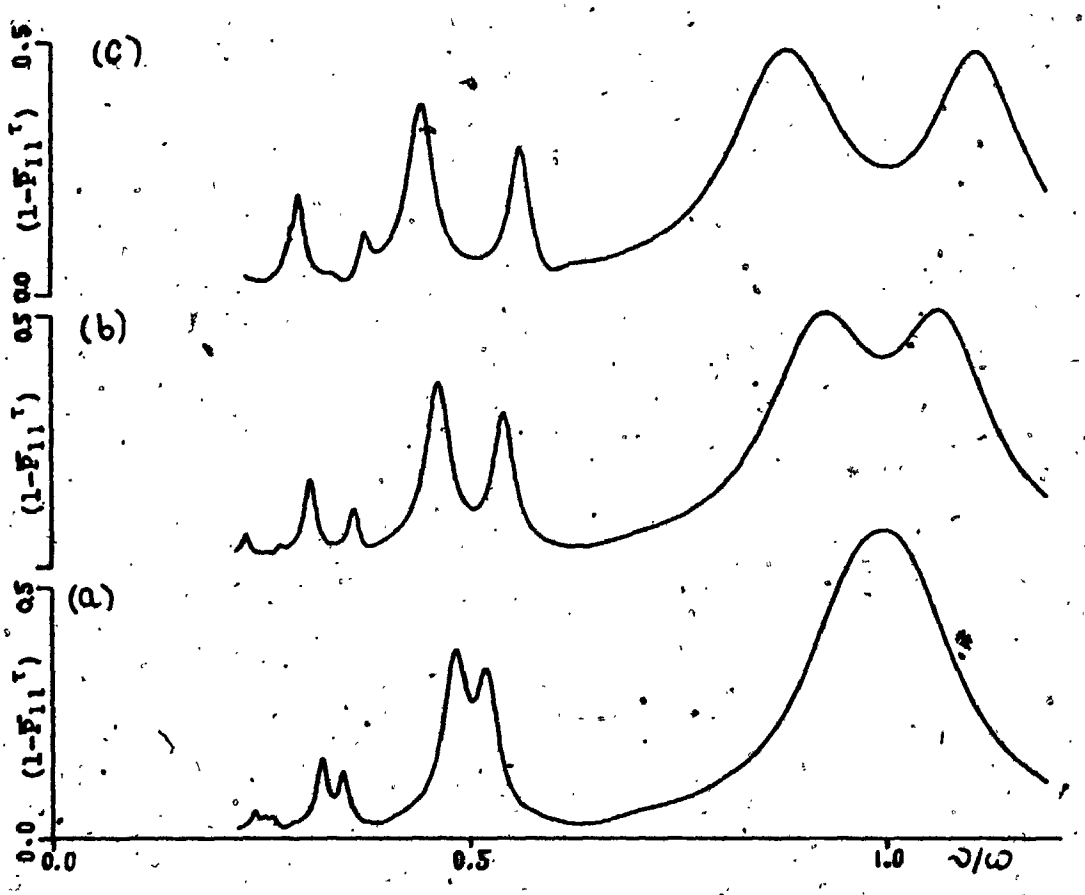

Figure 5.10. The damped phase averaged induced transition probability $(1 - \bar{P}_{11}^{\tau})$ as a function of frequency ν for the damping constant $\tau = 10^3$. (a) The damped version of Figure 5.7(a), (b) the damped version of Figure 5.8(a) and (c) the damped version of Figure 5.9(a).

frequency domain for* $\tau = 100$. In all of these spectra the damped lower frequency component of each doublet is higher than its high frequency counterpart and the difference in their relative heights increases as the static Stark field $\mathcal{E}^0$ increases. This behaviour indicates that each low frequency component saturates more readily in agreement with the relative order of magnitudes of the coupling parameters $\beta_{1-} > \beta_{1+}$, see also Figure 5.1(b).

5.2 THE EFFECT OF STARK MIXING ON AN EXCITED NONDEGENERATE STATE

In the three level system discussed in the previous section, the presence of even a weak static Stark field caused a strong mixing and splitting of the excited degenerate pair of states. The splitting of the excited mixed states $\phi_+(r)$ and $\phi_-(r)$ was reflected in the splitting of the n-photon resonances which was approximately given by $\Delta q / n$. The question naturally arises as to how such a static Stark field might affect the excited pair of states $\phi_2(r)$ and $\phi_3(r)$ if they are initially nondegenerate. To answer this question we study the three level configuration in Figure 5.11 as a function of static Stark field $\mathcal{E}^0$ for fixed values of $\beta = |\mu_{12}\mathcal{E}|/\omega$ and $\alpha = |\mu_{23}\mathcal{E}|/|\mu_{12}\mathcal{E}| = 3$, over the frequency domain encompassing the single photon profile $(1 \to 2)$. For this configuration we again choose the states $\phi_2(r)$ and $\phi_3(r)$ to have the same parity so that in effect we have displaced $\phi_3(r)$ upwards and $\phi_2(r)$ downwards from their positions in Figure 5.1(a). If we ignore the effect of the ground state $\phi_1(r)$ and the oscillatory electric field, we can regard the excited states $\phi_2(r)$ and $\phi_3(r)$ as being mixed and further split by the applied static field $\mathcal{E}^0$. The energy splitting between the resulting states is then given by, see Section 4.2.3,

---

* The above choice of τ was made to damp the two photon doublet to approximately two thirds its undamped height.

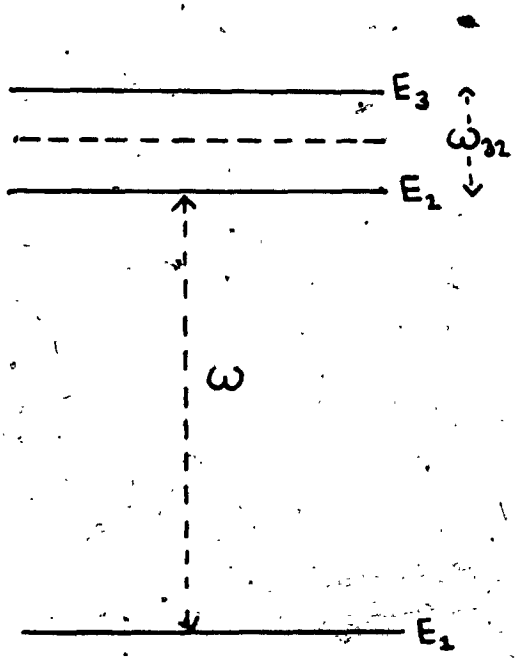

Figure 5.11. The three level configuration employed to study the effect of Stark mixing on an originally nondegenerate excited state. Numerical values of the parameters used in subsequent calculations on this level configuration are; $\omega = E_2 - E_1 = 0.45$, $\omega_{32} = E_3 - E_2 = 0.10$, $E_1 = -0.5$, $E_2 = -0.05$, $E_3 = 0.05$, $\mu_{12} = 1$, $\mu_{23} = 3$, $\mu_{13} = 0$, $\alpha = 3$ and $\beta = 1/9$. These values are used to generate Figures 5.12(a) -(e) for different values of the static Stark field $\mathcal{E}^0$.

$$\Delta\eta \sim \omega_{32}\sqrt{1+\delta^2} \qquad 5.2.1$$

where $\omega_{32}=(E_3-E_2)$ and $\delta = 2|\mu_{23}|\mathcal{E}^0/\omega_{32}$ Equation 5.2.1 will prove useful in a qualitative discussion of the results that follow..

The phase averaged steady state induced transition probability $(1-\bar{P}_{11})$ for $\beta=1/9$ and $\alpha=3$ is plotted in Figures 5.12 (a),(b),(c) and (d) along with its accompanying characteristic exponent plots $\sigma(\Delta_j)$ for $\delta = 0.0, 0.3, 0.6$ and 3.0 , ($\gamma = \mathcal{E}^0/\mathcal{E} = 0.0, 0.1, 0.2$ and 1.0) respectively; $\gamma = \mathcal{E}^0/\mathcal{E}$ is the relative field strength parameter. In the absence of the static Stark field $\mathcal{E}^0$, see Figure 5.12(a), one observes the single photon profile for the transition $(1\to2)$ slightly shifted to higher frequency $(\nu/\omega \sim 1.01)$ from its unperturbed position at $(\nu/\omega = 1.0)$, see Figure 5.11. In the accompanying characteristic exponent plots an "anti-crossing" A_1 occurs at this resonance peak position, while a "level crossing" L'_1 occurs at the forbidden single photon $(1\to3)$ transition frequency; of course the $(1\to3)$ two photon transition is allowed and would be observed if we swept with frequency ν in the neighbourhood of $(E_3-E_1)/2$, see also Figure 5.12(d). Introducing a weak static Stark field ($\gamma=0.1, \delta=0.3$), see Figure 5.12(b), causes a sharp single photon resonance to appear on the high frequency wing of the $(1\to2)$ single photon profile at the $(1\to3)$ single photon transition frequency. The occurrence of this single photon transition is also reflected in the accompanying characteristic exponent plots where the "level crossing" L'_1 in Figure 5.12(a) has now changed to an "anti-crossing" A'_1 . This high frequency single photon transition arises from the partial mixing of state $\phi_2(r)$ with state $\phi_3(r)$ of opposite parity and qualitatively, using $\delta=0.3$ in equation 5.2.1, we would expect the separation between both single photon peaks to be approximately $\Delta\eta \sim 0.231$. The actual peak separation is ~ 0.187, indicating that the ground state $\phi_1(r)$ acts to supress the excited state splittings.

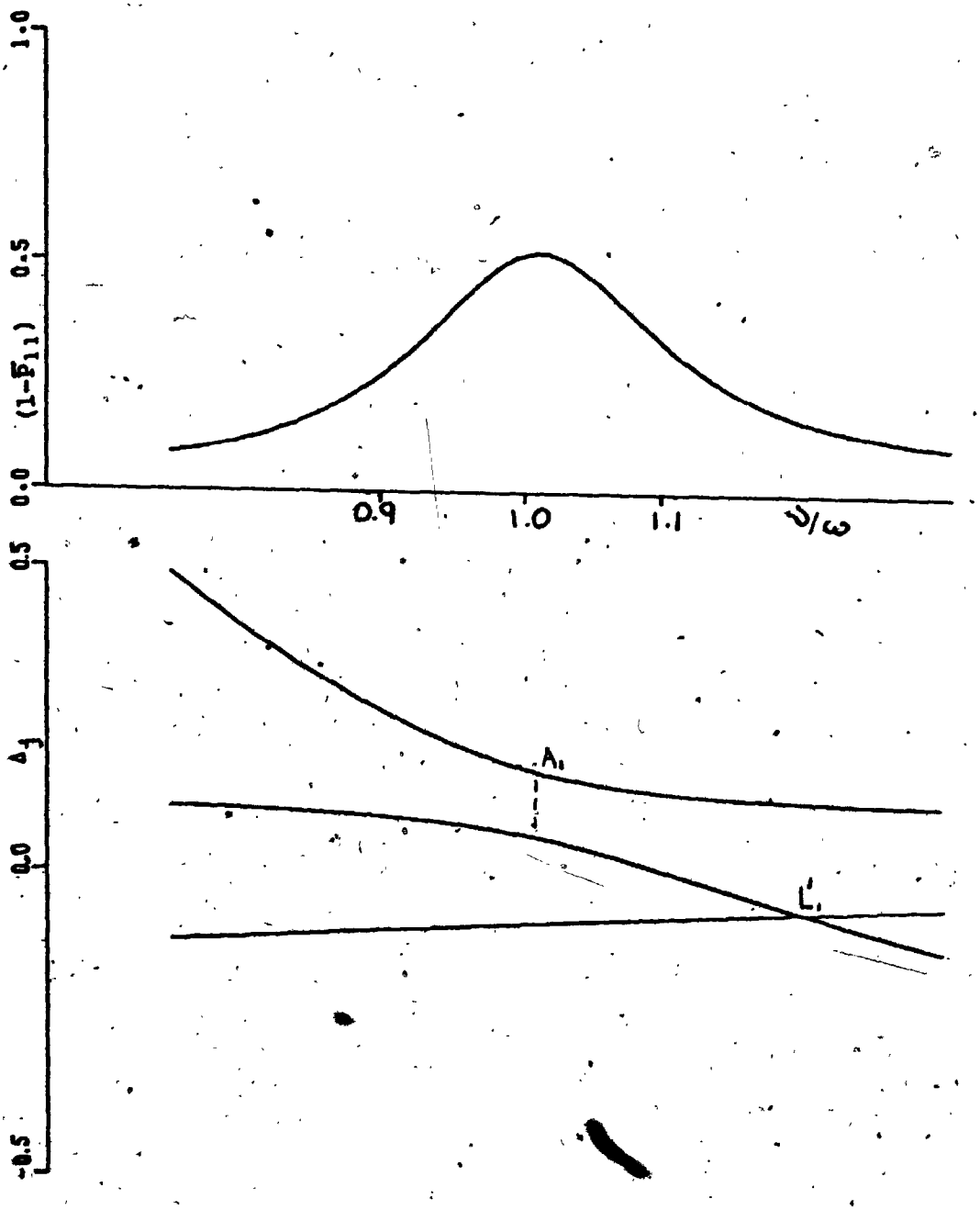

Figure 5.12(a) The phase averaged steady state induced transition probability $(1 - \bar{P}_{11})$ and the accompanying characteristic exponent plots as a function of frequency ν for $\beta = |\mu_{12}\xi|/\omega = 1/9$, $\alpha = |\mu_{23}|/\mu_{12}| = 3$, $\delta = 2|\mu_{23}\xi^0|/\omega = 0$ and $\gamma = \xi^0/\xi = 0$. The "allowed" single photon transition occurs at the position of the "anti-crossing" A_1 and the "level crossing" L_1' corresponds to the forbidden 1-3 single photon transition.

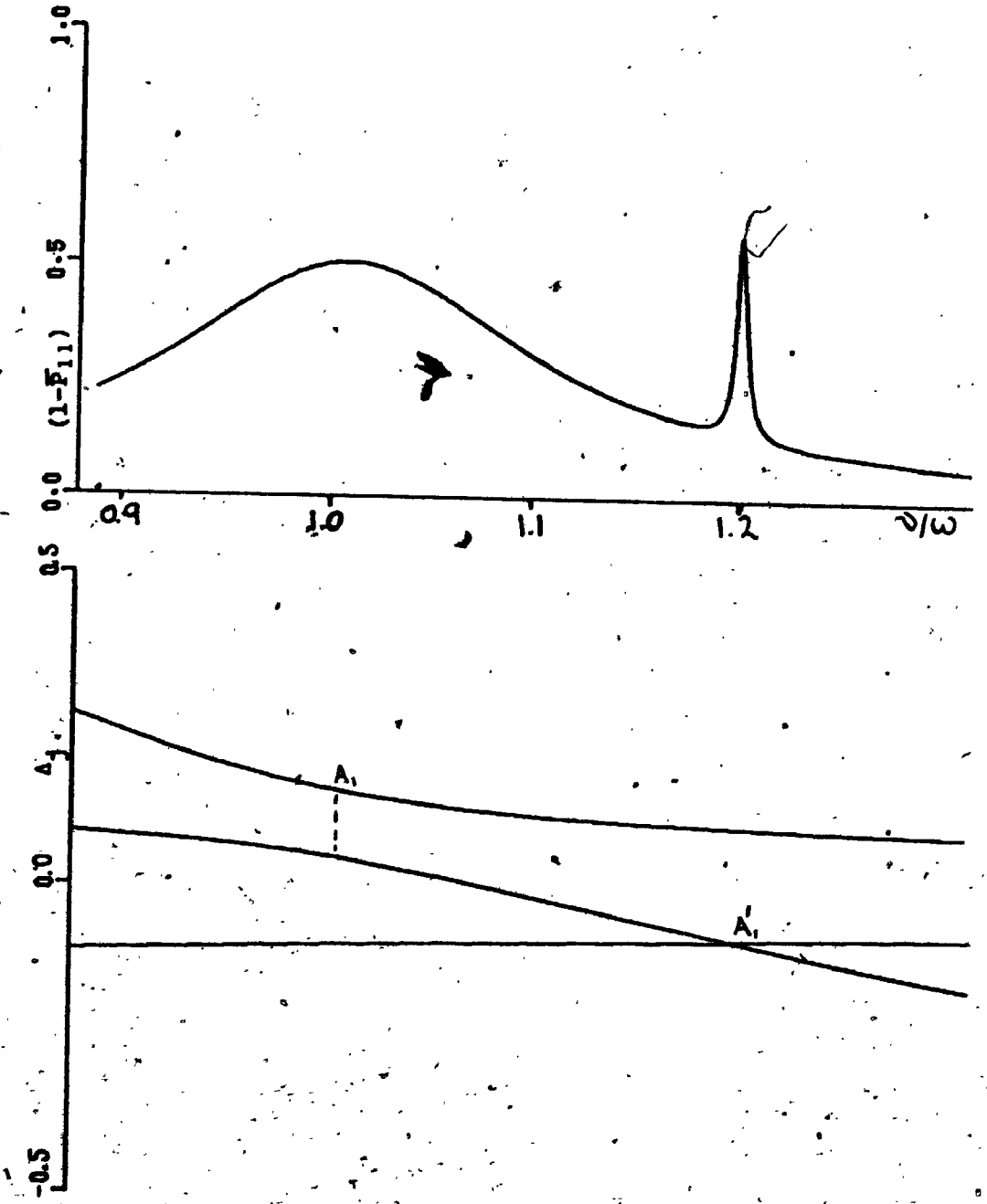

Figure 5.12(b) The phase averaged steady state induced transition probability $(1 - \bar{P}_{11})$ and the accompanying characteristic exponent plots as a function of frequency ν for $\delta = 0.3$, $\gamma = 0.1$ and β and α have the same values as in Figure 5.12(a). The appearance of a sharp single photon resonance is signified by the occurrence of the "anti-crossing" A_1'.

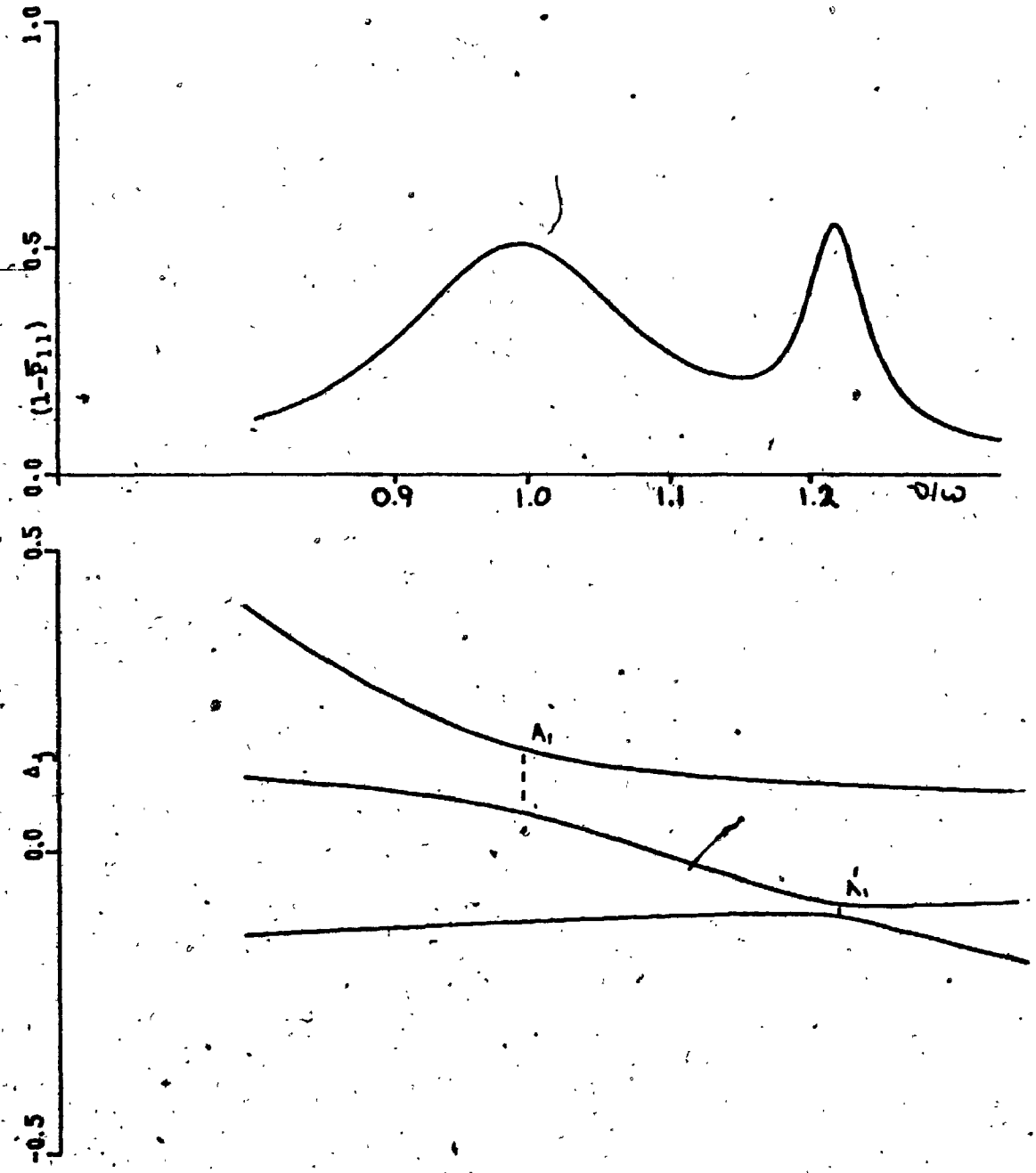

Figure 5.12(c) The phase averaged steady state induced transition probability $(1 - \bar{P}_{11})$ and the accompanying characteristic exponent plots, as a function of frequency ν for $\delta = 0.6$, $\gamma = 0.2$ and α and β are the same as in Figure 5.12(a). The broadening of the (1→3) single photon resonance is also evident from the increased width of the anti-crossing at A_1' (Compare with Figure 5.12(b)).

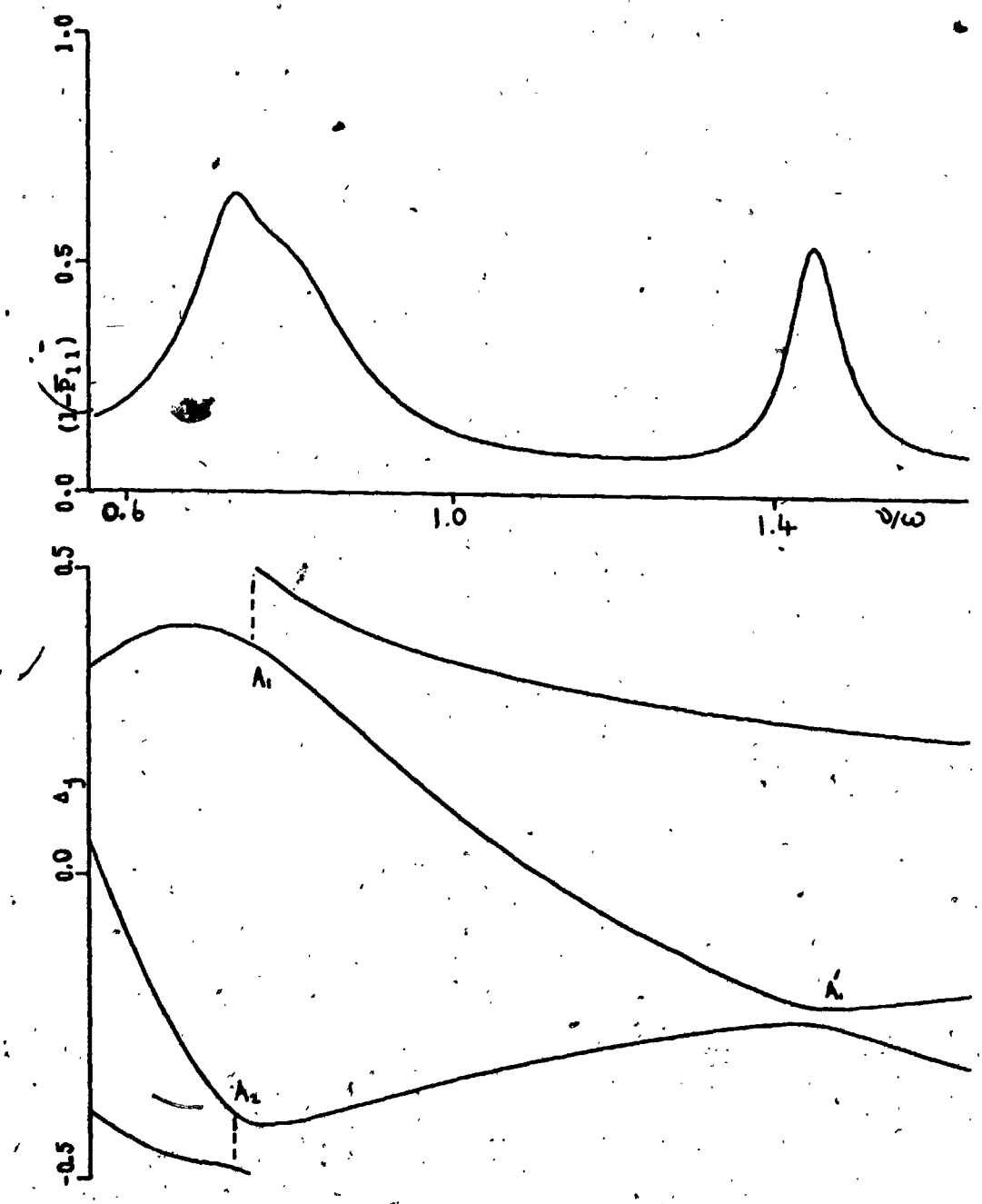

Figure 5.12(d) The phase averaged steady state induced transition probability $(1 - \bar{P}_{11})$ and the accompanying characteristic exponent plots as a function of frequency ν for $\delta = 3.0$, $\gamma = 1.0$ and the same values of α and β as in Figure 5.12(a). The bump on the low frequency single photon profile at A_1 arises from overlap with the high frequency two photon profile at A_2.

Increasing the static Stark field $\mathcal{E}^{\circ}$ (Compare Figures 5.12(b) and 5.12(c) increases the degree of mixing of the excited states and this is reflected in the increased width of the high frequency profile and the slightly increased splitting of the resonance peaks. Again equation 5.2.1 with $\delta = 0.6$ would predict a splitting $\Delta\eta \sim 0.26$, whereas the actual splitting ~ 0.22. Finally, Figure 5.12(d) shows the spectrum for $\delta = 3.0 (\gamma = 1.0)$ with its accompanying characteristic exponent plot. The asymmetry of the low frequency peak arises from the overlap of the high frequency component of the two photon doublet, see Section 5.1 and below, with the low frequency single photon profile. Figure 5.12(e) shows this overlap region at a lower value of (=.) just before they overlap completely, while the characteristic exponent plots in this figure show both "anti-crossings" A_2 and A_1 before they merge at approximately the same frequency; see Figure 5.12(d). Again the splittings of the single photon profiles in Figure 5.12(d) is still given approximately by $\Delta\eta$ in equation 5.2.1.

The behaviour exhibited in the single photon spectra as a function of γ and δ discussed above, should be observed for all higher photon transitions with the "forbidden" n-photon resonance occurring on the high frequency side of the allowed n-photon transition for n odd and on the low frequency side for n even, see Figure 5.11. Thus, for example, the high frequency two photon profile appearing in Figure 5.12(d) is the original allowed (1→3) two photon transition. Also the splittings of each n-photon pair should be given approximately by $\Delta\eta/n$, see Section 5.1.

5.3 INTERFERENCE EFFECTS BETWEEN A TWO PHOTON TRANSITION AND NEIGHBOURING SINGLE PHOTON TRANSITIONS IN A THREE LEVEL NONDEGENERATE SYSTEM.

The three level nondegenerate system shown in Figure 5.13, where the intermediate state $\phi_2(r)$ of opposite parity to $\phi_1(r)$ and $\phi_3(r)$ lies almost midway between these states, was initially suggested as the optimum configuration for which a two photon transition could be

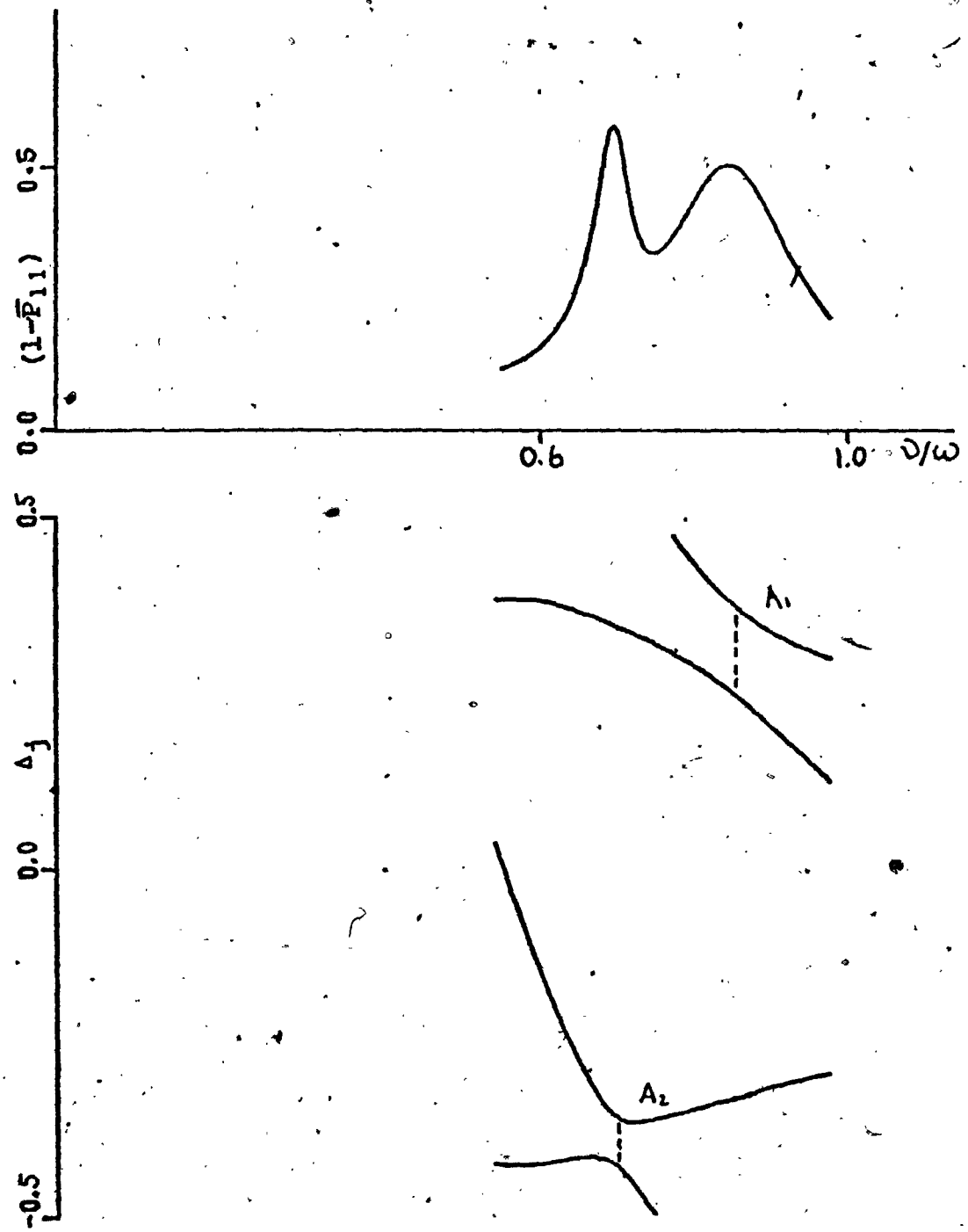

Figure 5.12(e) The phase averaged steady state induced transition probability $(1 - \bar{P}_{11})$ and the accompanying characteristic exponent plots as a function of frequency ν for $\delta = 2.4$, $\gamma = 0.8$ and α and β are the same as in Figure 5.12(a). This figure shows the overlap region between the low frequency single photon profile at A_1 and the high frequency two photon profile at A_2 for a slightly smaller value of δ than employed in Figure 5.12(d).

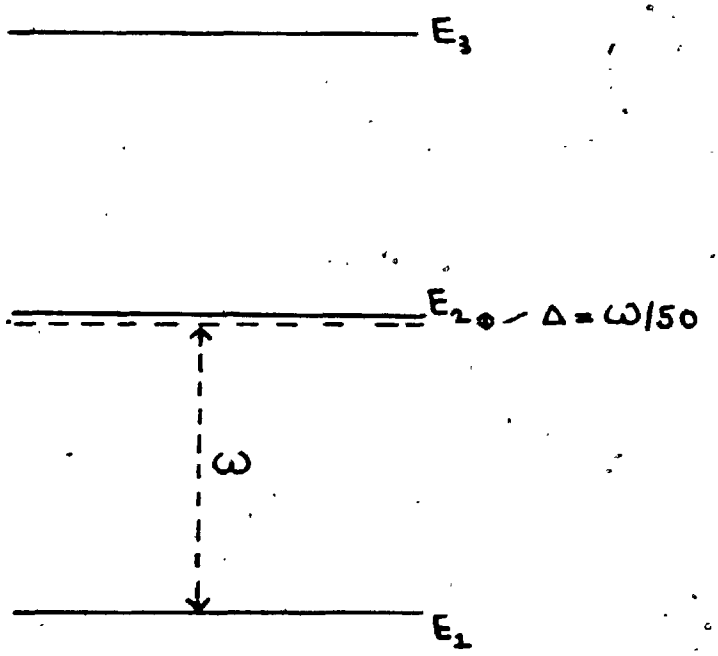

Figure 5.13. The three level configuration employed to study interference effects between a two photon transition (at $\nu \sim \omega$) and two neighbouring single photon transitions (at $\nu \sim E_2 - E_1$ and $\nu \sim E_3 - E_2$). Numerical values of the parameters used in subsequent calculations on this level configuration are (see Figures 5.14 - 5.16); $\omega = (E_3 - E_1)/2 = 0.5$, $E_1 = -0.5$, $E_2 = \Delta = 0.01$, $E_3 = 0.5$, $\mu_{12} = \mu_{23} = 1$, $\mu_{13} = 0$. These values are used to generate Figures 5.14 - 5.16 for different values of the applied sinusoidal field amplitude .

observed at optical frequencies [29].* The two photon transition in this system will be observed at the approximate frequency

$$\nu \sim (E_3 - E_1)/2 = \omega \qquad 5.3.1$$

and the deviation of the state $\phi_2(r)$ from this central frequency is given by

$$\Delta = (\omega - (E_3 - E_2)) \; . \qquad 5.3.2$$

The closeness of the frequencies of the allowed $(1\rightarrow2)$ and $(2\rightarrow3)$ single photon transitions to the two photon transition frequency suggests that for sufficiently high oscillating field amplitude $\mathcal{E}$ interference effects between the two photon resonance profile and one or both the single photon profiles should be important. In analogy with the earlier model systems we define a relative coupling strength parameter $\beta = |\mu\mathcal{E}|/\omega$, where we have chosen $\mu_{12} = \mu_{23} = \mu$ for convenience and in addition we define the parameter $\eta = |\mu\mathcal{E}|/\Delta$, which will provide a measure of the interference effect.

The phase averaged steady state induced transition probability $(1 - \bar{P}_{11})$, subject to the initial conditions $a_1(0)=1$, $a_2(0) =$, $a_3(0) = 0$, is plotted as a function of frequency ν, along with its accompanying characteristic exponents Δ_j, in Figures 5.14(a),(b) and 5.16(a),(b) for $\Delta = 0.01\omega$ and for $\beta =$ 0.01, 0.02 and 0.04 ($\eta = 0.5$, 1.0 and 2.0), respectively. The above choice of the parameters β and η is based on our knowledge that the approximate width of a single photon profile is $|\mu\mathcal{E}|$, see Section 4.2.2, so that at $\eta = 1$ we should expect appreciable overlap between the single photon $(1\rightarrow2)$ and two photon $(1\rightarrow3)$ profiles. In Figure 5.14(a) where $\beta = 0.01$ and $\eta = 0.5$ both resonances are still well resolved and the characteristic exponents Δ_j in Figure 5.14(b) reflect this behaviour with the "anti-crossings" A_2 and $A_1^{1\rightarrow2}$ well separated. Increasing the oscillating field amplitude $\mathcal{E}$, see Figure 5.15, so that $\beta = 0.02$ and $\eta = 1.0$ causes both resonances to overlap appreciably. The accompanying

---

* Dimensionless notation will be retained in discussing this system as the results can be scaled to any spectral region.

Figure 5.14. The phase averaged steady state induced transition probability $(1 - \bar{P}_{11})$ and the accompanying characteristic exponent plots, for the level configuration specified in Figure 5.13, as a function of frequency ν for $\beta = |\mu|/\omega = 0.01$, $\eta = |\mu|/\Delta = 0.5$ and subject to the initial conditions $|a_1(0)|^2 = 1$. The "anti-crossings" $A_1^{1\to 2}$ and $A_1^{2\to 3}$ in Figure 5.14(b) coincide with the 1→2 and 2→3 single photon transition frequencies while A_2 coincides with the 1→3 two photon transition frequency. Only the 1→2 single photon and 1→3 two photon transition appear in Figure 5.14(a), see text for details.

3 3

OF /DE

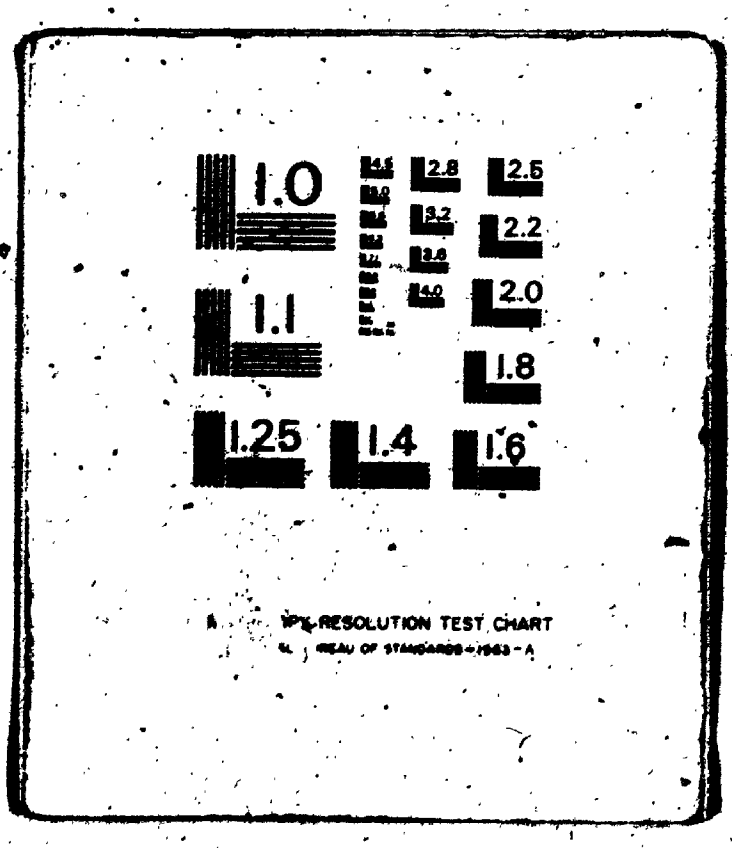

ARC-274

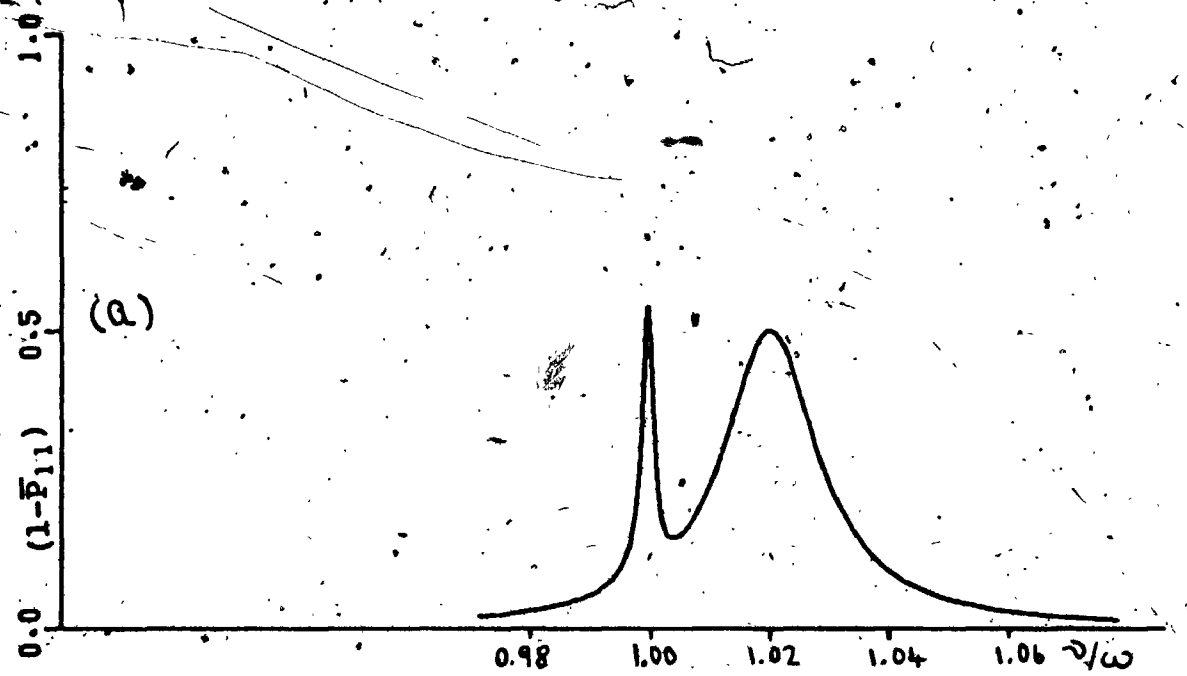
(a)
1.0
0.5
0.0
$(1-\bar{P}_{11})$
0.98
1.00
1.02
1.04
1.06
ν/ω

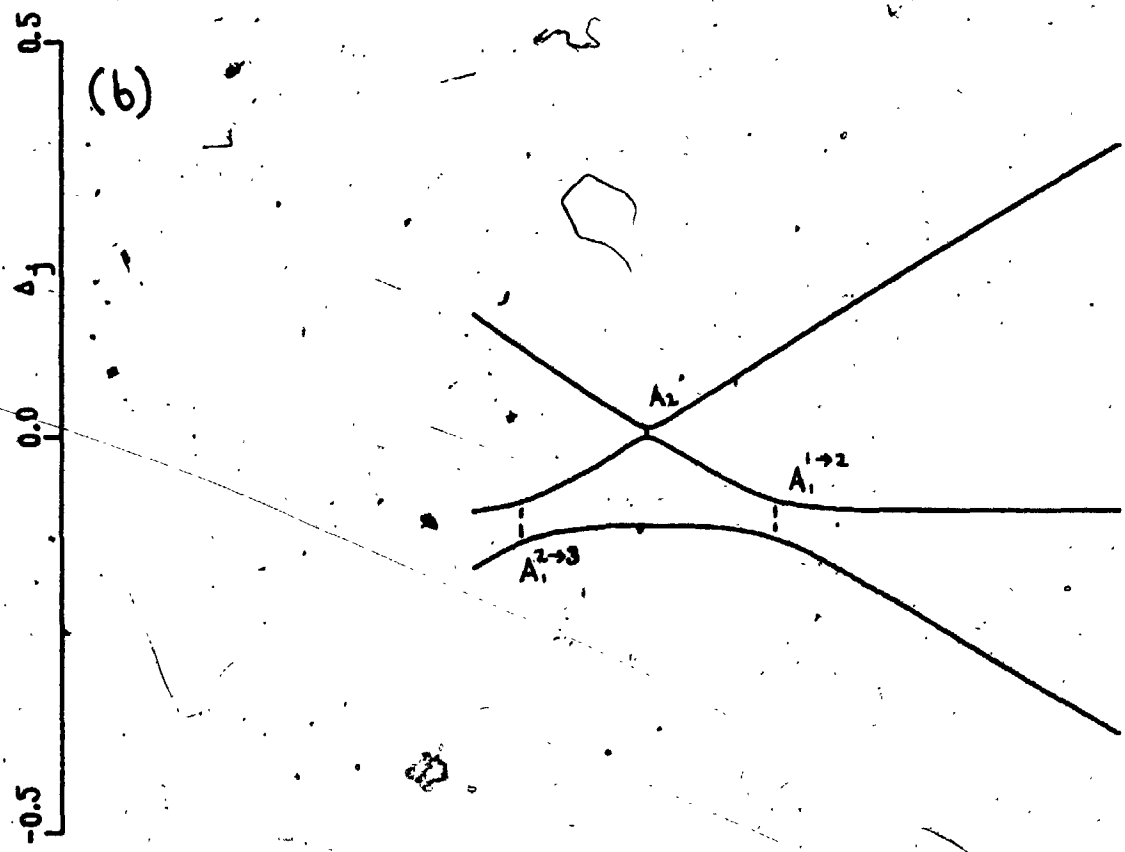
(b)
0.5
0.0
-0.5
Δ_j
A_2
$A_1^{1\to 2}$
$A_1^{2\to 3}$

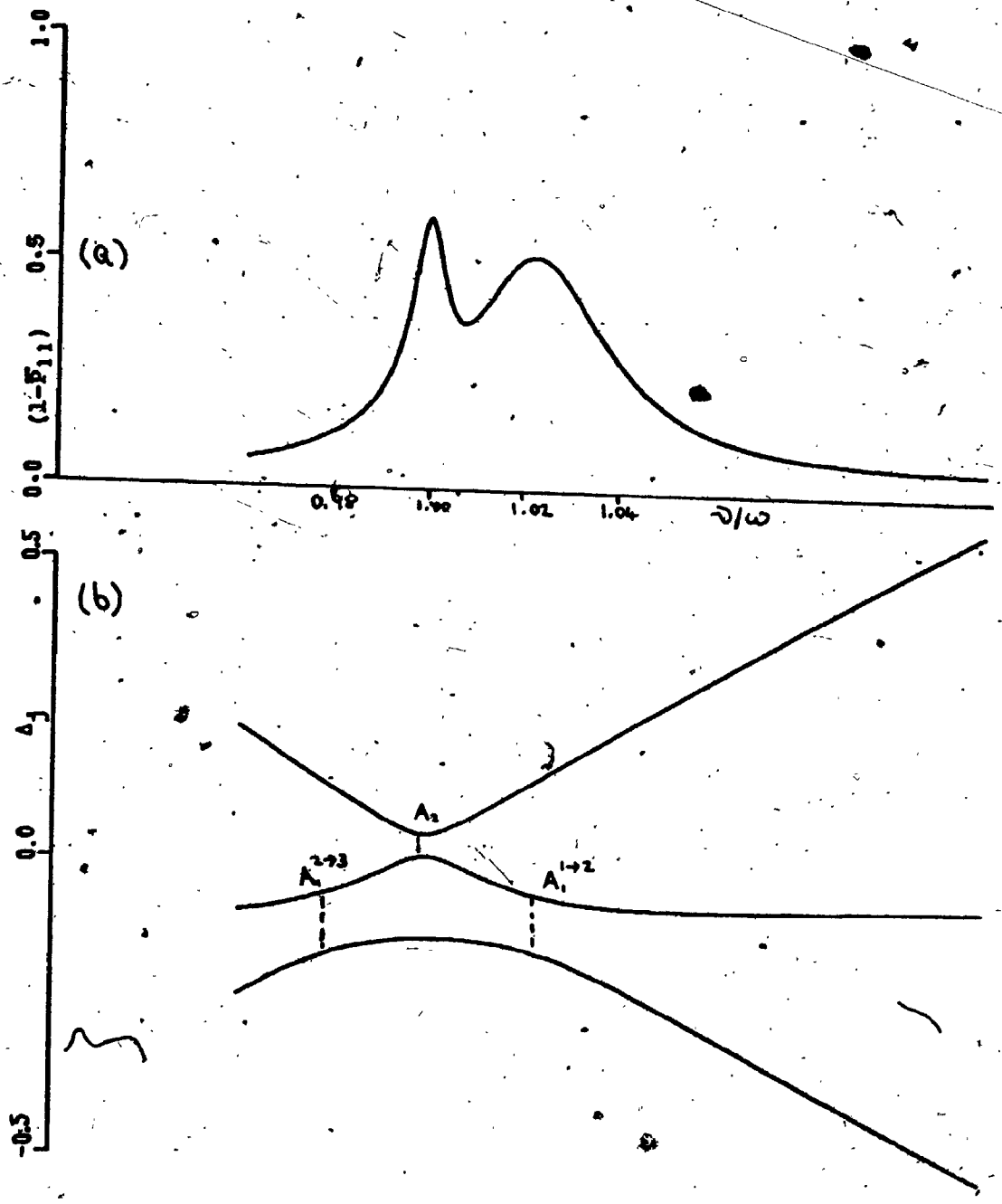

Figure 5.15. The phase averaged steady state induced transition probability $(1 - \bar{P}_{11})$ and the accompanying characteristic exponent plots as a function of frequency ν for $\beta = 0.02$ and $\eta = 1$.

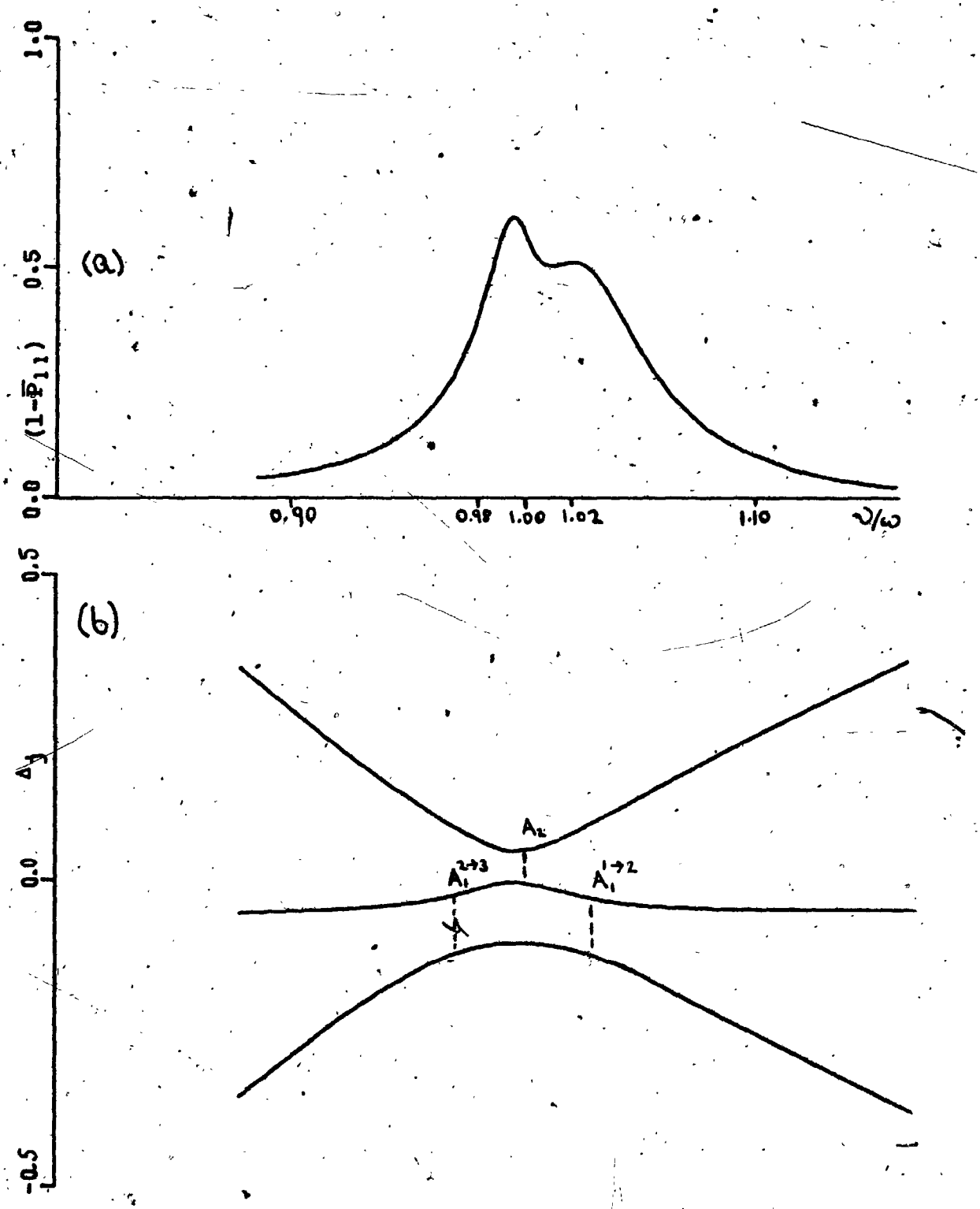

Figure 5.16. The phase averaged steady state induced transition probability $(1 - \bar{P}_{11})$ and the accompanying characteristic exponent plots as a function of frequency ν for $\beta = 0.04$ and $\eta = 2$. The increasing overlap of the two photon and single photon profiles as a function of increasing field amplitude $\mathcal{E}$ is evident also from the gradual merging of the "anti-crossings" on going from Figures 5.14 - 5.16.

characteristic exponents again reflect this partial overlap with a clear distinction between the two photon "anti-crossing" A_2 and the neighbouring single photon "anti-crossing" $A_1^{1\to 2}$ becoming less obvious. Finally in Figure 5.16(a) both resonance profiles have almost completely merged ($\beta = 0.04, \eta = 2.0$) and the "anti-crossings" in Figure 5.16(b) are becoming very broad and less distinct as a function of .

Because of the imposed initial conditions on the system the $(2\to 3)$ single photon transition although "allowed", as is clearly evident from the presence of the "anti-crossing" $A_1^{2\to 3}$ in the above figures, is very weak; its approximate position is given by $\nu/\omega = 0.98$. Such a transition can only occur if the state $\phi_2(r)$ is appreciably populated at this $(2\to 3)$ transition frequency and this $1\to 2\to 3$ two step single photon transition should occur for large oscillating field strengths. However, for these values of β, no distinction can be made between the $1\to 2\to 3$ single photon and $1\to 3$ two photon mechanism for populating $\phi_3(r)$. The plot of $\bar{P}_{21}$ given in Figure 5.17 may be useful in distinguishing between these two mechanisms.

The above results indicate, as expected, that in order to observe a distinct two photon resonance experimentally, for this level system there will be an upper limit on the oscillating field strength $\mathcal{E}$ set by the parameter η (or β). Also if the deviation of the state $\phi_2(r)$ from the midway separation increases a corresponding increase in β would be required to observe such interference effects.

5.4 FREQUENCY SHIFTS DUE TO NONRESONANT INTERACTIONS WITH NEIGHBOURING STATES.

As discussed in Section 5.1, the presence of neighbouring states coupled directly to the initial and/or final states involved in a particular transition can make a major contribution to the frequency shift of the resonance profile. The purpose of this section is to illustrate how the formal method developed in Chapter 3 can be employed to evaluate quantitatively such frequency shifts. We will confine our attention to the two photon transition in two typical

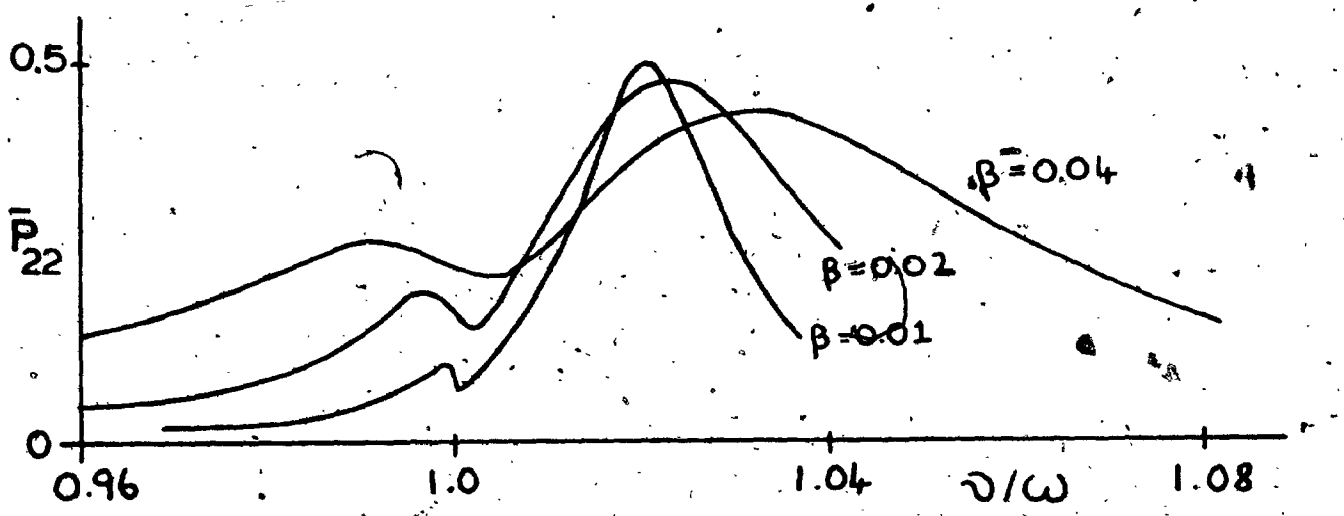

Figure 6.17. The phase averaged steady state induced transition probability $\bar{P}_{22}$ as a function of frequency ν for $\beta = 0.01$, 0.02 and 0.04 ($\eta = 0.5$, 1.0 and 2.0) for the same initial conditions and parameters as in Figures 5.14 - 5.16.

level configurations* and we expect that similar trends should be observed either at single photon or higher photon transition frequencies. The two photon transition is particularly important as Doppler broadening, which is important at optical frequencies, can be effectively eliminated [53,83] by using oppositely directed laser beams.

5.4.1 TWO PHOTON TRANSITION FROM A NONDEGENERATE GROUND STATE TO AN EXCITED DEGENERATE PAIR OF STATES.

The basic three level configuration has already been dealt with in Section 5.1, see Figure 5.1(a), where the multiphoton spectrum has been presented for different values of the coupling strength parameter β_{12}. We now study how the two photon transition ($1 \rightarrow 3$) in this basic system is affected by the inclusion of extra nonresonant states ($\phi_4(r)$ $\phi_5(r)$, $\phi_6(r)$) coupled directly to $\phi_1(r)$ and $\phi_3(r)$. The full level configuration is shown in Figure 5.18(a)** with the absolute energies

---

* In recent years, the two photon transition at optical frequencies has been extensively studied experimentally [83,84,85], particularly in the alkali metals. In these systems there are many neighbouring states present so nonresonant interactions will be very important [12,80,81,82].

** This configuration corresponds to the H-atom level configuration with the two photon transition occurring between $\phi_{1s}(\phi_1)$ and $\phi_{2s}(\phi_3)$ via the $\phi_{2p}(\phi_2)$ state in the original study in Section 5.1. The remaining states (ϕ_4, ϕ_5, ϕ_6) correspond to the three next lowest p-states ($\phi_{3p}, \phi_{4p}, \phi_{5p}$), respectively. Secondary couplings of other s and d states (even parity) through these p states (odd parity) do not to contribute significantly to the two photon frequency shift for the field strengths considered here.

Figure 5.18. The two model multilevel configurations used to study the importance of neighbouring states on the frequency shifts of the two photon resonance profile. Convergent results are obtained for both models on including a total of six states. (a) The basic configuration in this model involves the three states $\phi_1(r)$, $\phi_2(r)$ and $\phi_3(r)$ with the excited pair $\phi_2(r)$ and $\phi_3(r)$ degenerate and of opposite parity. The two photon transition occurs between states $\phi_1(r)$ and $\phi_3(r)$ of the same parity. Numerical values of the parameters employed in subsequent calculations on this level configuration are [35] (see Figures 5.19 - 5.21); $\omega = E_0 - E_1 = 0.375$, $E_1 = -0.5$, $E_2 = E_3 = E_0 = -0.125$, $E_4 = -0.5556(-1)$, $E_5 = -0.3125(-1)$, $E_6 = -0.2(-1)$, $\mu_{12} = 0.7449$, $\mu_{14} = 0.2983$, $\mu_{15} = 0.1758$, $\mu_{16} = 0.1205$, $\mu_{32} = -3$, $\mu_{34} = 1.7695$, $\mu_{35} = 0.7405$, $\mu_{36} = 0.4468$ and the dipole matrix elements coupling the remaining states are zero. (b) The basic configuration in this model involves the nondegenerate states $\phi_1(r)$, $\phi_2(r)$ and $\phi_3(r)$ but now the state $\phi_2(r)$ lies between the states $\phi_1(r)$ and $\phi_3(r)$ which are directly involved in the two photon transition. Numerical values of the parameters employed in subsequent calculations on this level configuration are [83a] (see Figures 5.22 - 5.24); $\omega = E_3 - E_1 = 0.1173427$, $E_1 = -0.1889593$, $E_2 = -0.111606$, $E_3 = -0.716166(-1)$, $E_4 = -0.509608(-1)$, $E_5 = -0.292111(-1)$, $E_6 = -0.189310(-1)$, $\mu_{12} = 2.5194$, $\mu_{14} = 0.2269$, $\mu_{15} = -0.8319(-1)$, $\mu_{16} = 0.4634(-1)$, $\mu_{32} = 1.4276$, $\mu_{34} = 5.7165$, $\mu_{35} = 0.6739$, $\mu_{36} = 0.2721$ and the dipole matrix elements coupling the remaining states are zero.

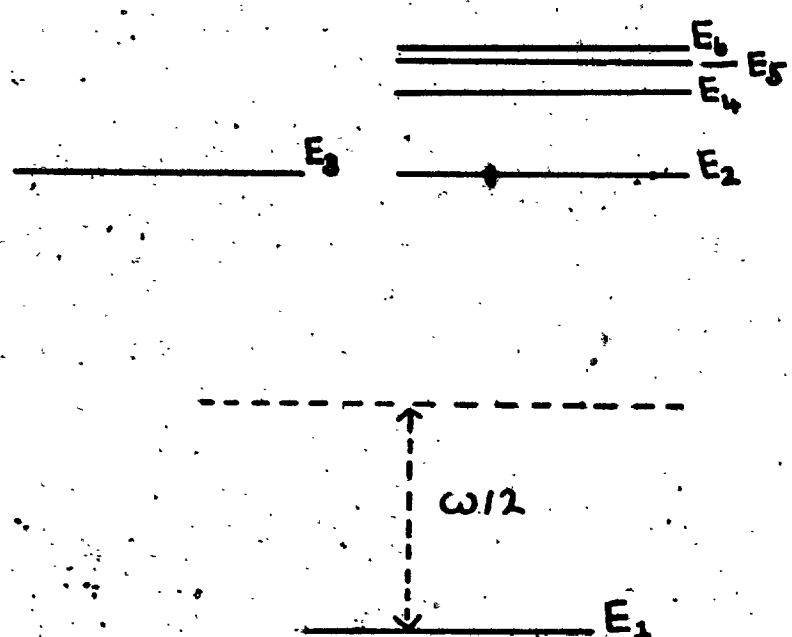

(a)

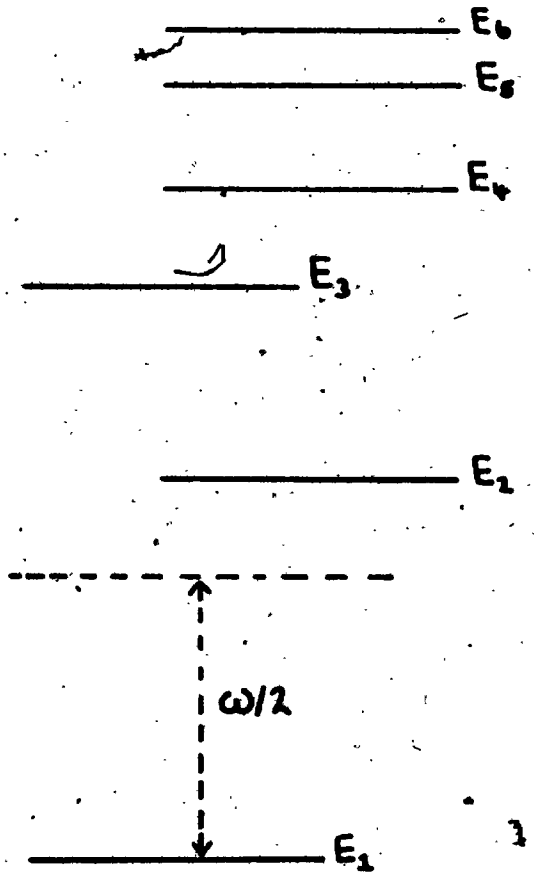

(b)

$(E_1, E_2, E_3, E_4, E_5, E_6)$ indicated. The dipole matrix $\underline{\mu}$ for this six level configuration is, see equation 3.1.4,

$$\underline{\mu} = \left(\begin{array}{c|c|c|c|c|c} 0 & \mu_{12} & 0 & \mu_{14} & \mu_{15} & \mu_{16} \\ \mu_{21} & 0 & \mu_{23} & 0 & 0 & 0 \\ 0 & \mu_{32} & 0 & \mu_{34} & \mu_{35} & \mu_{36} \\ \hline \mu_{41} & 0 & \mu_{43} & 0 & 0 & 0 \\ \hline \mu_{51} & 0 & \mu_{53} & 0 & 0 & 0 \\ \hline \mu_{61} & 0 & \mu_{63} & 0 & 0 & 0 \end{array}\right) \qquad 5.4.1$$

The broken lines indicate the actual $\underline{\mu}$ matrices used in the calculations starting with the 3x3 matrix representing the basic three level configuration, studied in Section 5.1, and succesively including the additional states $(\phi_4(r), \phi_5(r), \phi_6(r))$ one at a time. The actual numerical values of the dipole matrix elements used in these calculations are also indicated in Figure 5.18(a). This system will be discussed in terms of absolute energies and field strengths due its complexity; the final results however can be scaled to any spectral region.

Figures 5.19(a) - 5.21(a) show the two photon profile $(1-\bar{P}_{11})$ for the basic three level system $(\phi_1(r), \phi_2(r), \phi_3(r))$ in Figure 5.18(a), as a function of frequency detuning $(\nu-\omega/2)$ for the following oscillating field amplitudes $\mathcal{E} = 1\times10^{-5}$, 1×10^{-4} , 1×10^{-3} , respectively. These choices* of field amplitudes $\mathcal{E}$ were made since they span the wide range of intermediate to very high intensity laser sources [46]. As expected, the two photon resonance peak is shifted to high frequency from the position predicted by the simple perturbation

---

* Higher field amplitudes $\mathcal{E}$ could easily be employed in the above calculation but for the configuration of Figure 5.18(a) the resonance maximum exceeds 0.5 when $\mathcal{E} = 1\times10^{-2}$ suggesting that population leakage to neighbouring states becomes important. Under these conditions $(1-\bar{P}_{11})$ can exceed 0.5, see Section 5.1, for these model calculations.

Figure 5.19 The phase averaged steady state induced transition probability $(1 - \bar{P}_{11})$ as a function of frequency detuning $(\nu - \omega/2)$ for the level configuration of Figure 5.18(a) and for $\mathcal{E} = 1 \times 10^{-5}$.
The four two photon profiles appearing in this figure represent calculations with a different number of states included, see equation 5.4.1. (a) $\phi_1(r)$, $\phi_2(r)$ and $\phi_3(r)$, (b) $\phi_1(r)$, $\phi_2(r)$, $\phi_3(r)$ and $\phi_4(r)$, (c) $\phi_1(r)$, $\phi_2(r)$, $\phi_3(r)$, $\phi_4(r)$ and $\phi_5(r)$, (d) $\phi_1(r)$, $\phi_2(r)$, $\phi_3(r)$, $\phi_4(r)$, $\phi_5(r)$ and $\phi_6(r)$.

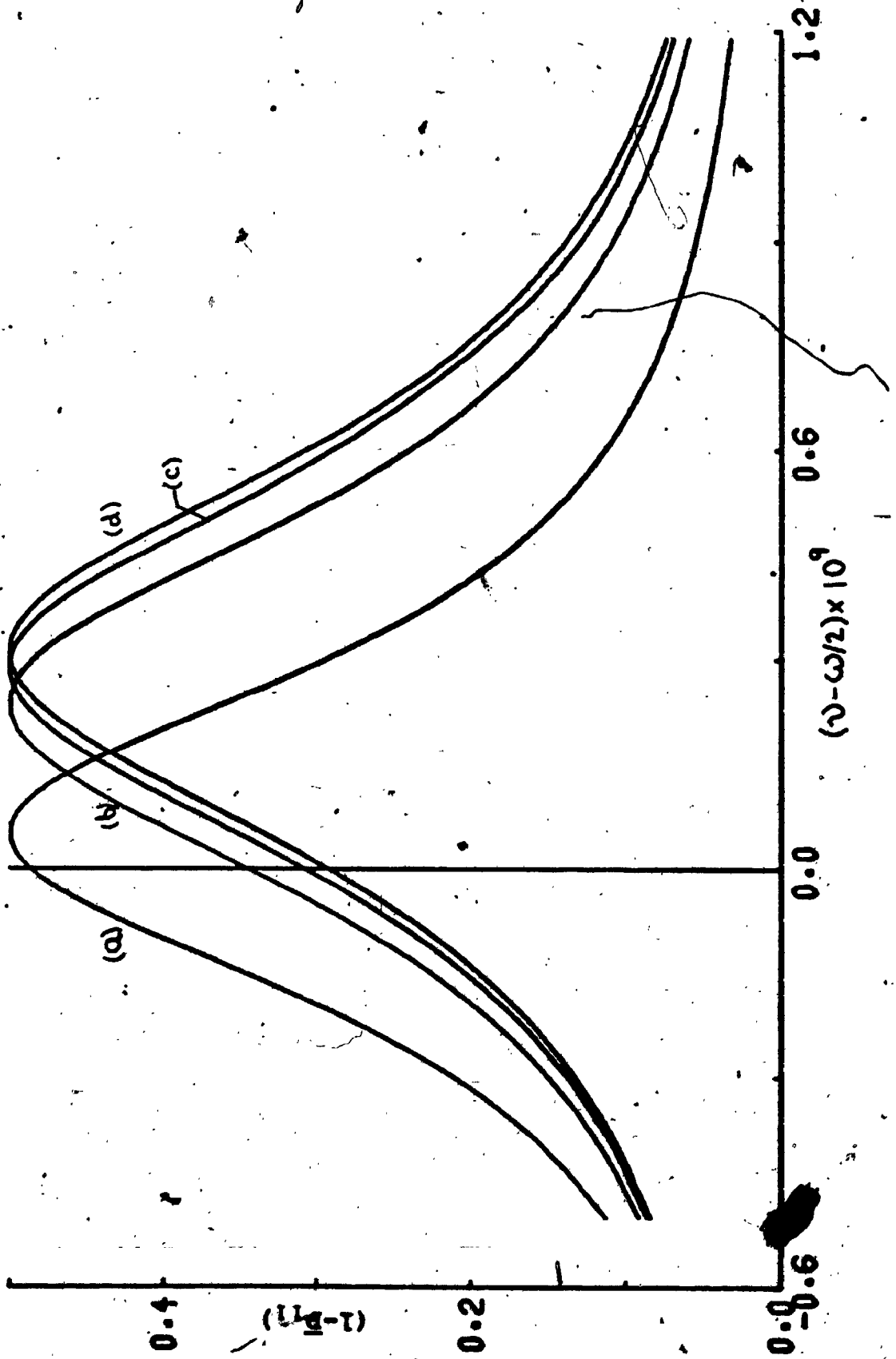
(a)
(b)
(c)
(d)
0.4
0.2
0.0
-0.6
0.0
0.6
1.2
$(1-\bar{B}_{11})$
$(\nu-\omega/2)\times 10^9$

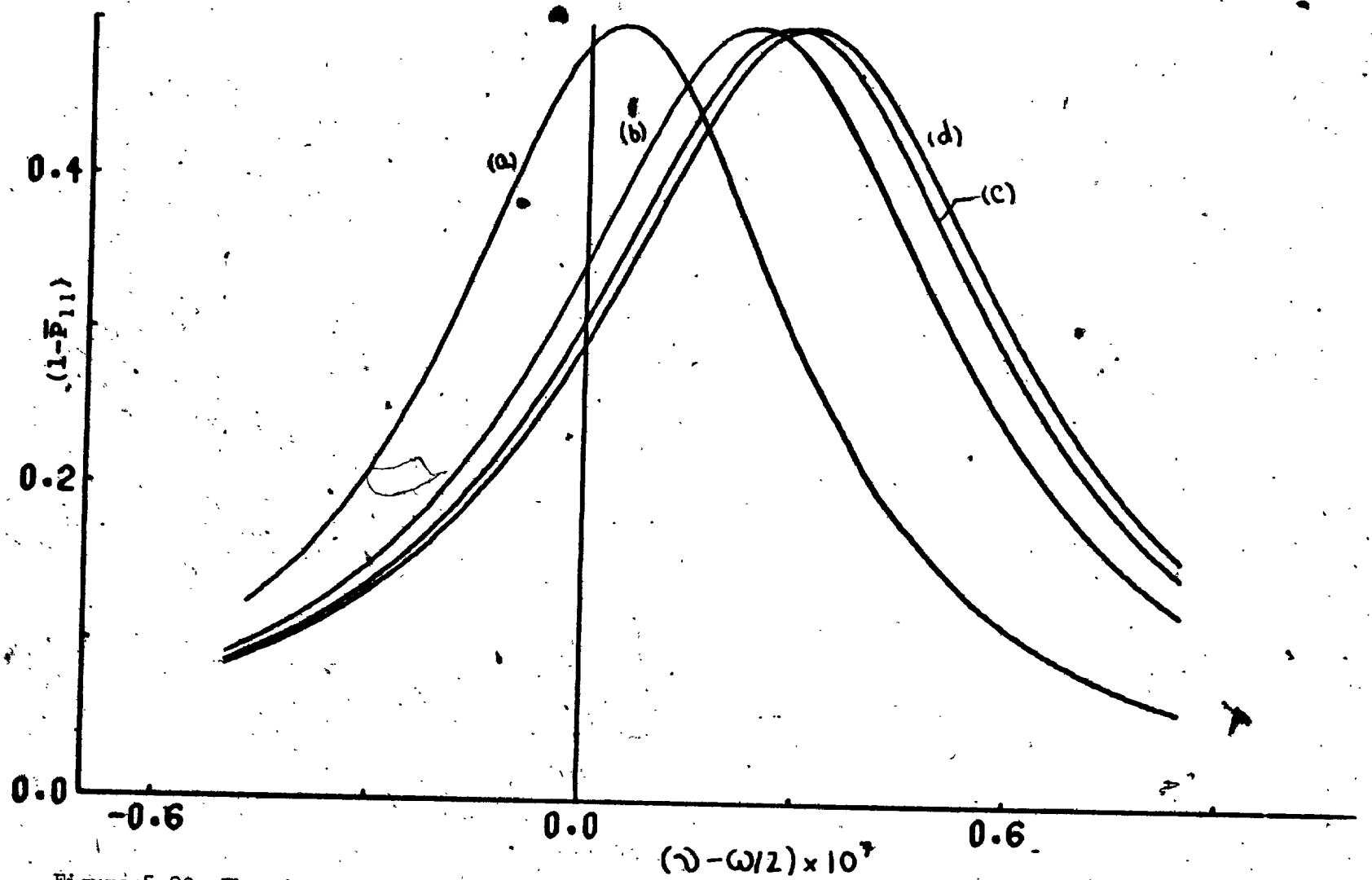

Figure 5.20 The phase averaged steady state induced transition probability $(1 - \bar{P}_{11})$ as a function of frequency detuning $(\nu - \omega/2)$ for $\mathcal{E} = 1 \times 10^{-4}$ and the same parameters as in Figure 5.18(a). The two photon profiles labelled (a)-(d) represent the systematic inclusion of 3-6 states in the calculation, see Figure 5.19.

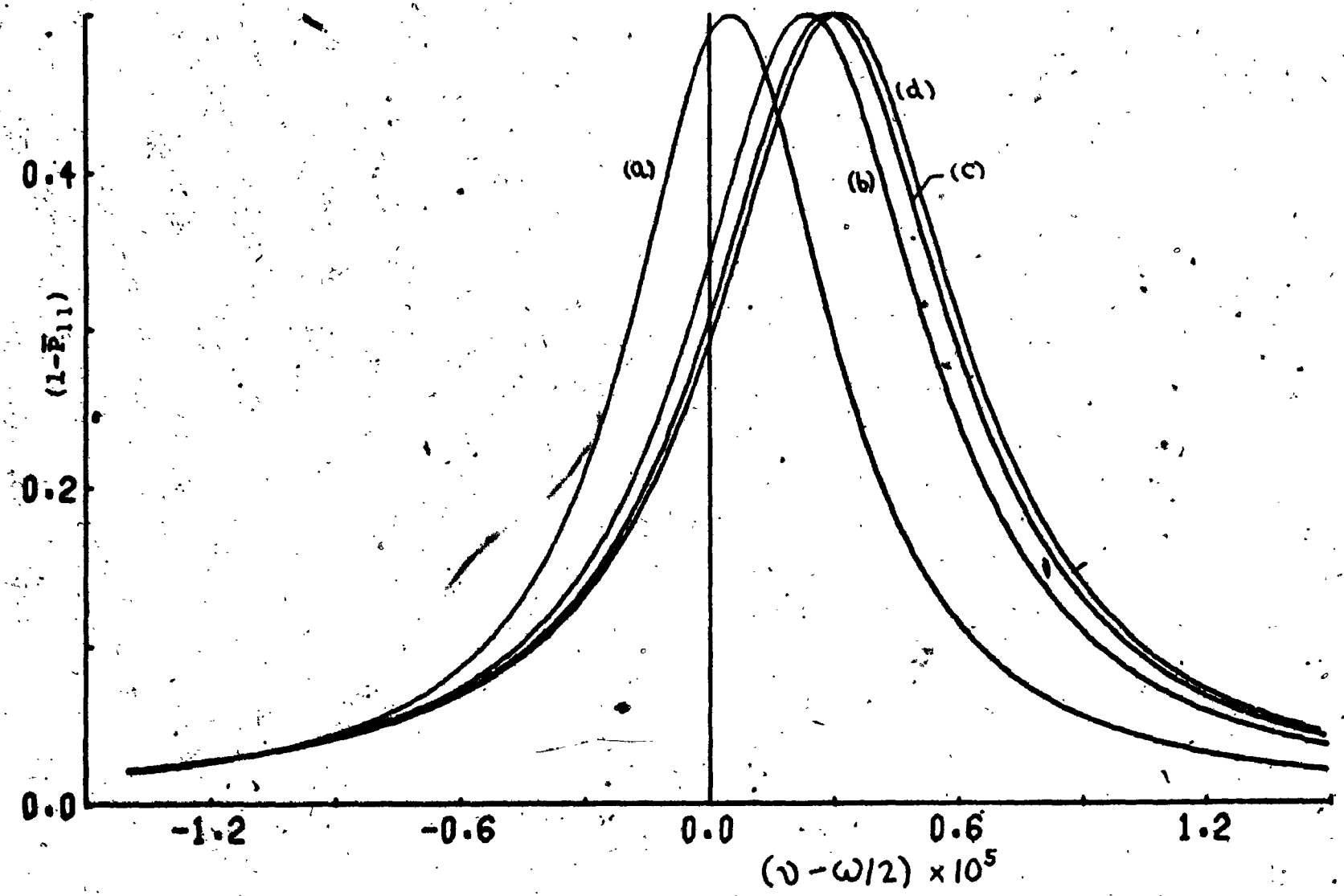

Figure 5.21 The phase averaged steady state induced transition probability $(1 - \bar{P}_{11})$ as a function of frequency detuning $(\nu - \omega/2)$ for $\mathcal{E} = 1 \times 10^{-3}$ and for the same parameters as in Figure 5.18(a). The two photon profiles labelled (a)-(d) represent the systematic inclusion of 3-6 states in the calculation, see Figure 5.19.

result, see Chapter 2, (that is $(\nu-\omega/2)=0$). The numerical values of these frequency shifts are given in Table II. Figures 5.19(b),(c),(d) - 5.21(b),(c),(d) show the effect of successively including the states ϕ_4, ϕ_5, ϕ_6 on the basic three level configuration (ϕ_1, ϕ_2, ϕ_3). The additional state $\phi_4(r)$ increases the frequency shift by a factor of ~ 5 (see Table II and compare Figures 5.19(a)-5.21(a) with Figures 5.19(b)-5.21(b),) while the shift converges rapidly on including $\phi_5(r)$ and $\phi_6(r)$, see Figures 5.19(c),(d)-5.21(c),(d). It is interesting to note that for any fixed number of states, see Table II, the frequency shift remains linear in field intensity $I(\alpha\mathcal{E}^2)$, see [38]. The widths of these profiles are essentially unaffected by these nonresonant states, but broaden uniformly as a function of increasing field amplitude $\mathcal{E}$ for a fixed number of states.

5.4.2 TWO PHOTON TRANSITION FROM A NONDEGENERATE GROUND STATE TO A NONDEGENERATE EXCITED STATE.

The full level configuration is shown in Figure 5.18(b) along with the absolute values of the energies E_i and dipole matrix elements μ_{ij}.* The dipole matrix $\underline{\underline{\mu}}$ for this system has the same structure as given by equation 5.4.1. The basic three level system (ϕ_1, ϕ_2, ϕ_3) in this configuration, see Figure 5.18(b), is intermediate between the three level configuration discussed in Section 5.3, see Figure 5.13, and that discussed in the previous subsection, see Figure 5.18(a).

---

* This configuration corresponds to the Na atom level configuration with the two photon transition occurring between the ground state $(1s)^2(2s)^2(2p)^6 3s^2S\,(\phi_1(r))$ and the excited state $(1s)^2(2s)^2(2p)^6 4s^2S\,(\phi_3)$. The states $\phi_2, \phi_4, \phi_5, \phi_6$ are the four lowest $(1s)^2(2s)^2(2p)^6 np^2P$ states ($\phi_{3p}, \phi_{4p}, \phi_{5p}, \phi_{6p}$) and the higher s and d states do not contribute to the frequency shift, see before.

TABLE II. (a) Resonance frequency shifts ($\nu_{Res} - \omega/2$) for the level configuration shown in Figure 5.18(a). These results exhibit the effect of successively including nonresonant states in the calculation for three values of the applied sinusoidal field amplitude . (b) The corresponding results for the level configuration shown in Figure 5.18(b).

	(a)		(b)	
Number of states included		$(\nu_{Res} - \omega/2)^*$		$(\nu_{res} - \omega/2)^*$
$\phi_i(r)$, i=1-3	1×10^{-5}	5.0×10^{-11}	1×10^{-6}	3.7×10^{-11}
	1×10^{-4}	5.0×10^{-9}	1×10^{-5}	3.7×10^{-9}
	1×10^{-3}	5.0×10^{-7}	1×10^{-4}	3.7×10^{-7}
$\phi_i(r)$, i=1-4	1×10^{-5}	2.4×10^{-10}	1×10^{-6}	9.3×10^{-11}
	1×10^{-4}	2.4×10^{-8}	1×10^{-5}	9.3×10^{-9}
	1×10^{-3}	2.4×10^{-6}	1×10^{-4}	9.3×10^{-7}
$\phi_i(r)$, i=1-5	1×10^{-5}	2.8×10^{-10}	1×10^{-6}	9.6×10^{-11}
	1×10^{-4}	2.8×10^{-8}	1×10^{-5}	9.6×10^{-9}
	1×10^{-3}	2.8×10^{-6}	1×10^{-4}	9.6×10^{-7}
$\phi_i(r)$, i=1-6	1×10^{-5}	3.1×10^{-10}	1×10^{-6}	9.8×10^{-11}
	1×10^{-4}	3.1×10^{-8}	1×10^{-5}	9.8×10^{-9}
	1×10^{-3}	3.1×10^{-6}	1×10^{-4}	9.8×10^{-7}

*These frequency shifts were estimated from the resonance maxima of the corresponding two photon profiles in Figures 5.19-5.24.

The two photon profile for the basic three level system (ϕ_1, ϕ_2, ϕ_3) is shown in Figures 5.22(a)-5.24(a) as a function of frequency detuning $(\nu-\omega_{12})$ for the following values of the oscillating field amplitude** $\mathcal{E} = 1\times10^{-6}$, 1×10^{-5}, 1×10^{-4}. Again the frequency shift increases linearly with field intensity I ($\propto \mathcal{E}^2$), see Table II and Figures 5.22(a)-5.24(a). Addition of the state ϕ_4 increases the shift by a factor ~ 2.5 (see Table II, compare Figures 5.22(a)-5.24(a) with 5.22(b)-5.24(b)) while the frequency shift converges very rapidly on including the additional states ϕ_5 and ϕ_6, see Figures 5.22(c),(d)-5.24(c),(d). As in the previous subsection the frequency shift remains linear as a function of field intensity I for any fixed number of states, see Table II.

The results of the above two calculations show explicitly that although the relative rate of convergence of the resonance frequency shift depends critically on individual level configurations, quantitative results for such shifts can be obtained by including a finite number of nonresonant states. In a recent article Wong, Garrison and Einwohner [46], using "multiple time scales" perturbation theory, arrived at a similar conclusion regarding the resonance frequency shift for a two photon transition between vibrational states in the HF molecule. These authors discuss the limitations and restrictions on their method as a function of an effective coupling parameter $\beta = |\bar{\mu}\mathcal{E}|/(\omega_{12})$ where $\bar{\mu}$ represents an average of all nonzero dipole matrix elements in the calculation.

** For this level configuration the two photon profile became distorted and $(1-\bar{P}_{11})$ exceeded 0.5 when $\mathcal{E} = 1\times10^{-3}$ was employed.

Figure 5.22 The phase averaged steady state induced transition probability $(1 - \bar{P}_{11})$ as a function of frequency detuning $(\nu - \omega/2)$ for the level configuration of Figure 5.18(b) and for $\mathcal{E} = 1 \times 10^{-6}$. The four two photon profiles labelled (a)-(d) represent calculations with a different number of states included. (a) $\phi_1(r)$, $\phi_2(r)$ and $\phi_3(r)$, (b) $\phi_1(r)$, $\phi_2(r)$, $\phi_3(r)$ and $\phi_4(r)$, (c) $\phi_1(r)$, $\phi_2(r)$, $\phi_3(r)$, $\phi_4(r)$ and $\phi_5(r)$ and (d) $\phi_1(r)$, $\phi_2(r)$, $\phi_3(r)$, $\phi_4(r)$, $\phi_5(r)$ and $\phi_6(r)$.

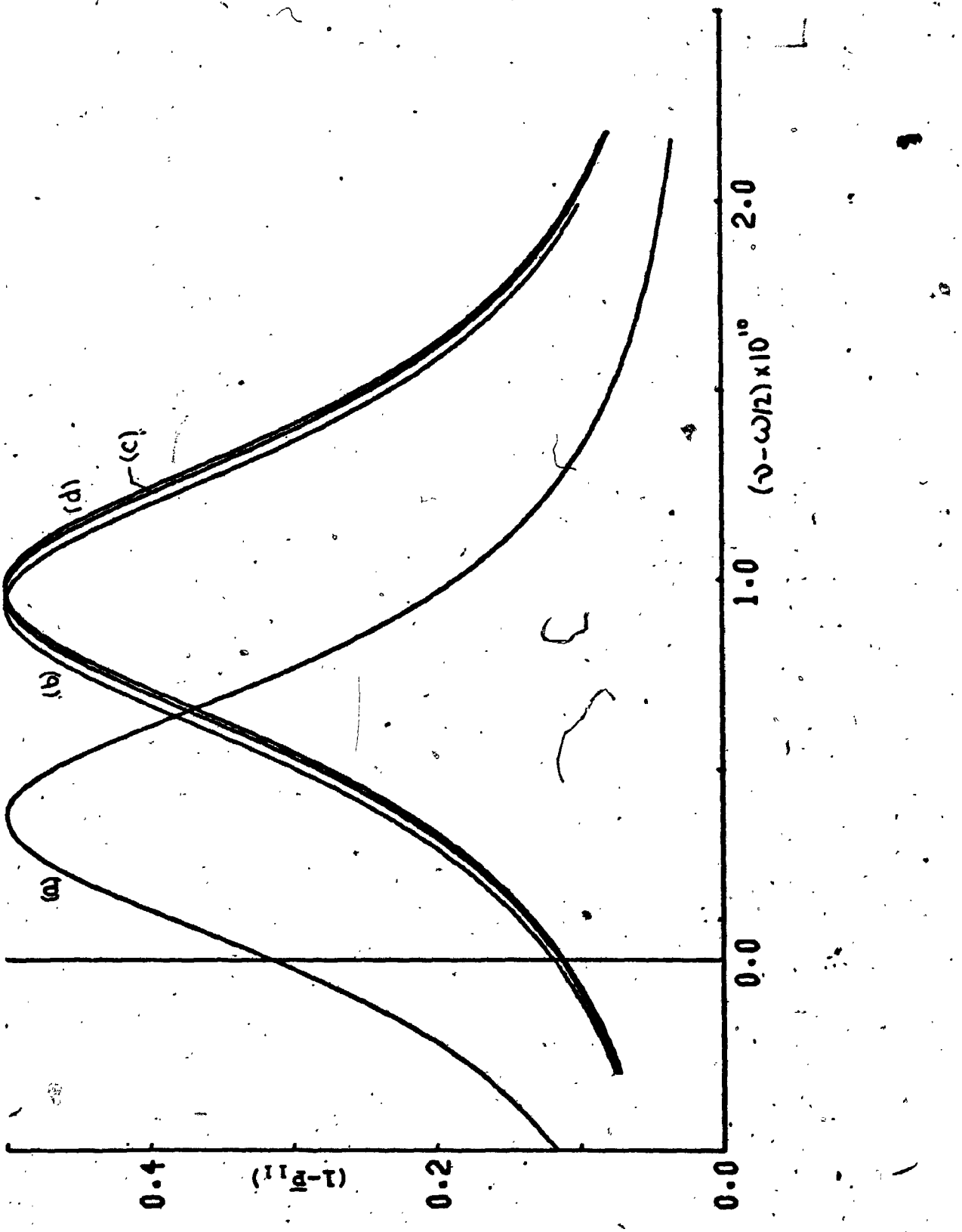
0.0
0.2
0.4
$(1-\bar{P}_{11})$
0.0
1.0
2.0
$(\omega-\omega_0)\times10^{10}$
(a)
(b)
(c)
(d)

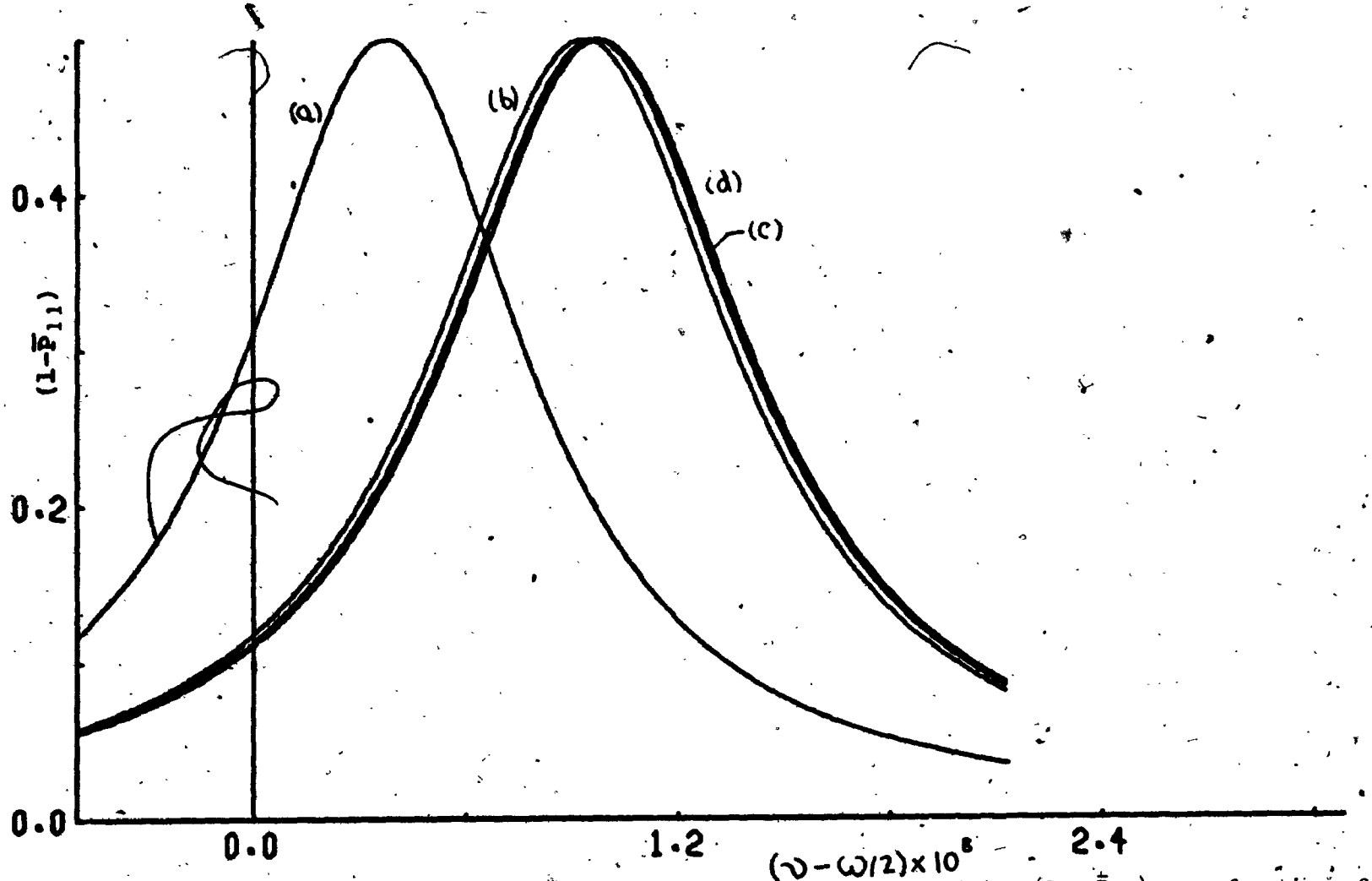

Figure 5.23 The phase averaged steady state induced transition probability $(1 - \bar{P}_{11})$ as a function of frequency detuning $(\nu - \omega/2)$ for $\mathcal{E} = 1 \times 10^{-5}$ and the same parameters as in Figure 5.18(b). The two photon profiles labelled (a)-(d) represent the systematic inclusion of 3-6 states in the calculation, see Figure 5.22.

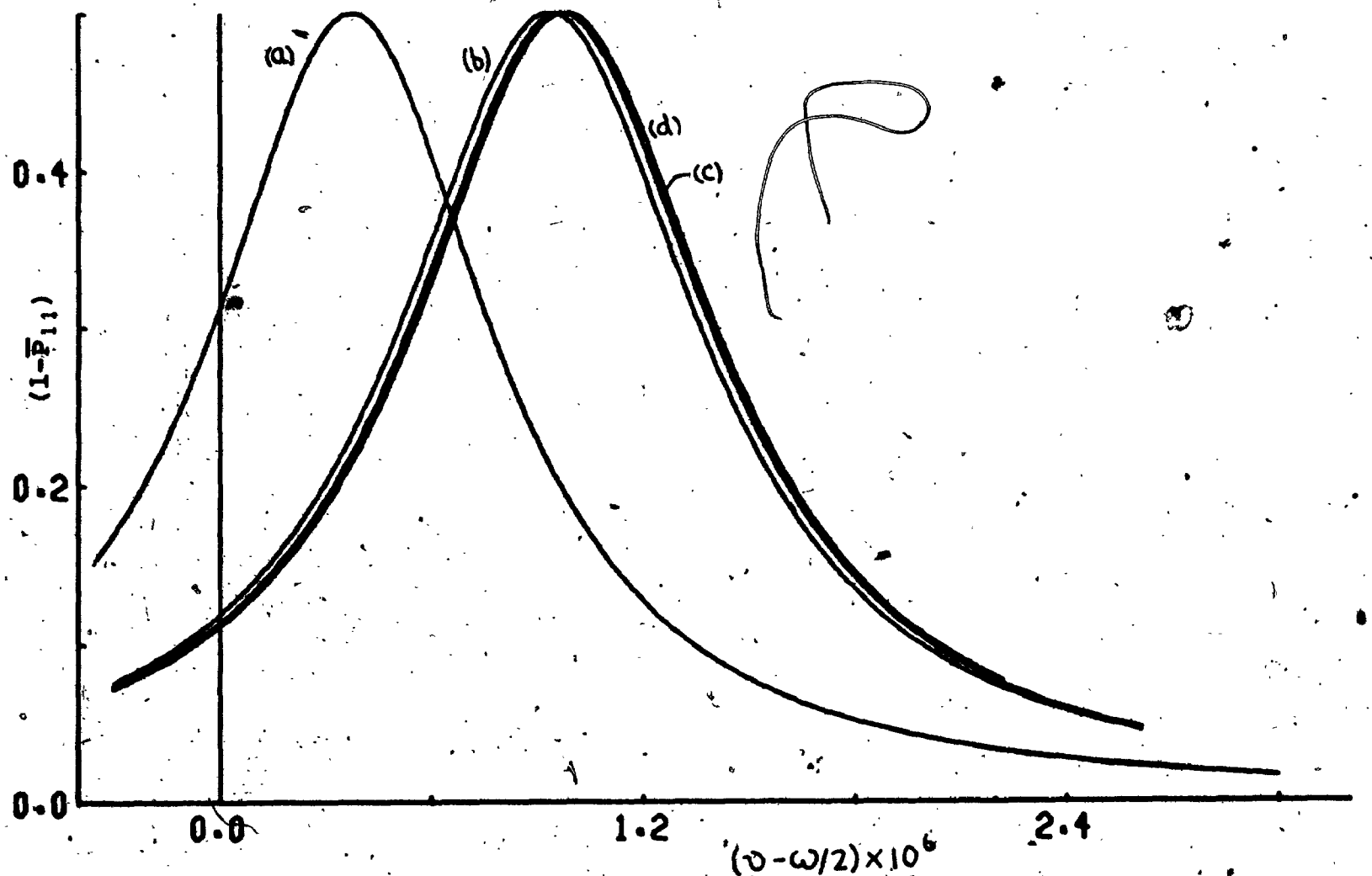

Figure 5.24 The phase averaged steady state induced transition probability $(1 - \bar{P}_{11})$ as a function of frequency detuning $(\nu - \omega/2)$ for $\xi = 1 \times 10^{-4}$ and the same parameters as in Figure 5.18(b). The two photon profiles labelled (a)-(d) represent the systematic inclusion of 3-6 states in the calculation, see Figure 5.22.

CHAPTER 6
CONCLUSIONS

The main emphasis of this work has been to present an accurate means of constructing the exact wavefunction $\Psi(r,t)$, representing the solution to the problem of a sinusoidal field, of arbitrary amplitude, frequency and phase interacting with an N-level quantum system of arbitrary configuration, via the dipole approximation. The formalism in Chapter 3, however, is equally applicable to problems involving any periodic Hamiltonian satisfying

$$H(r,t) \equiv H(r,t+T) \qquad 6.1.1$$

The formal analysis can be extended to include higher multipole interactions in a straightforward manner.

While providing very accurate solutions on the time domain for a sinusoidal field of well defined phase, the exact wavefunction $\Psi(r,t)$, when transformed to Floquet form, provides a convenient representation for the accurate evaluation of phase and/or time averaged properties of the quantum system plus external field(s). The important role played by the phase δ of the applied sinusoidal field as the coupling strength parameter $\beta = |\mu\mathcal{E}|/\omega$ approaches unity is readily apparent within the present treatment and leads to a clarification of an apparent discrepancy between some recent work[21] and the earlier work of Shirley[13]. Indeed, the physical significance of the phase δ when computing physical properties in the strong coupling region has not been considered by several authors recently [16,18,21,23,24].

The direct application of the formal method of solution, developed in Chapter 3, has been illustrated by evaluating induced transition probabilities and their phase and/or time averages for a two level system in Chapter 4 and for a number of model multilevel

systems in Chapter 5. In particular, the usefulness of plots of the characteristic exponents of the Floquet solution in mapping out complicated spectra and in evaluating multiphoton resonance frequency shifts has been explicitly demonstrated in these chapters. A direct coincidence between the characteristic exponents and the quantized energies computed recently by Yabusaki et al[72,74] for a two level system has also been demonstrated in Section 4.3 and leads to an interpretation of the characteristic exponents, in general, as energies of the N-level quantum system plus external field(s), see also [20]. The present work, to our knowledge, represents the first occasion on which the behaviour of the characteristic exponents has been investigated in the strong coupling region for more than two levels. It should be emphasised also that degeneracies pose no particular problem within the formalism used here.

An experimental verification of some of the theoretical results presented in Chapters 4 and 5 could best be made at radiofrequencies due to the wide tunability [4-7] of radiofrequency sources and the low field amplitudes required [4-7] to achieve β values close to unity. An increased use of "fast atomic beam multiphoton radiofrequency spectroscopy" for precision measurement of fine structure level separations in hydrogeniclike systems has been suggested recently by Brandenberger , Lundeen and Pipkin[90]. These authors measure fine structure separations in He^+ using such techniques and a quantitative verification of their experimental results using the formal method developed in this thesis should be particularly useful. In particular, as the relative populations of the fine structure levels in this experiment are poorly understood[90], it may be possible to theoretically determine them by a simple readjustment of the initial condition array $Q_2(0)$ until the experimental spectra are reproduced. This could aid in the interpretation of such experiments and in the understanding of relative level populations in atomic beam experiments. The very high field amplitudes required at optical frequencies to observe many of the effects discussed in Chapters 4 and 5 for $\beta \gtrsim 1$ suggests that multiphoton ionization effects will become predominant in these experiments. Recent evidence[91] however,

suggests that the ionization process in the presence of a very strong optical field is relatively slow so that a possibility exists of carrying out the entire experiment with ultra short ($\leq 10^{-12}$ sec.) optical pulses before appreciable population leakage to other states can occur. The effects of static Stark and Zeeman mixing on the multiphoton spectra as discussed in Chapters 4 and 5 should be observable particularly at radio and microwave frequencies.

Although the method of solution has been explicitly demonstrated by evaluating induced transition probabilities, any other property could have been investigated, see Section 3.6. One such property of particular interest is the polarisation induced in the quantum system by the strong sinusoidal field. This property is of particular importance in Laser theory[39] and recent experiments with intense laser pulses [1,3,11] suggest a need for the accurate evaluation of this quantity on the time domain.

Finally, some useful formulae for the transition rates and power absorbed and emitted, which are exact within the rotating field approximation, are presented in Appendix B for three level quantum systems resonantly coupled to two classical oscillating fields. These formulae are derived by using a Laplace transform method initially developed by Freed[32] and his method is extended to include relaxation effects. The exact rotating field solutions derived in Appendix B can be used to investigate situations where both fields are comparable in magnitude and represent a considerable improvement on recently derived approximate rotating field results[33,89].

APPENDIX A

A.1 CONVERGENCE OF THE MATRIX POWER SERIES EXPANSION GIVEN BY EQUATION 3.3.1

A sufficient condition for the convergence, as a function of γ, of the power series matrix expansion, given by equation 3.3.1, is that the individual elements within the matrix $\underline{Q}_\ell$ converge [86]. Closer inspection of the recurrence relationship for $\underline{Q}_\ell$, see equation 3.3.7, shows that these matrix coefficients are real or pure imaginary as ℓ is even or odd respectively. Therefore, a test on convergence can be made by evaluating the ratio $|q^{ij}_{\ell+2}/q^{ij}_{\ell}|$ at each stage of the recursive evaluation, where q^{ij}_{ℓ} is the ij-th element of the matrix $\underline{Q}_\ell$. This ratio is checked for each ij element until the specified convergence is achieved which corresponds to $\ell_{max} = K$ in equation 3.3.1.

In virtually all of the calculations carried out in this work the maximum computational efficiency was achieved by restricting the number of terms retained to ensure convergence to the range $K \sim 25-50$. This restriction in turn required that the generalized recurrence relations, given by equation 3.2.12, be employed over expansion subintervals ranging from $\pi/2 - \pi/10$ for intermediate to very strong coupling β. As a rough guide for all the calculations in this thesis, convergence to 16 significant figures could readily be obtained using a $\pi/2 - \pi/4$ expansion subinterval for $\beta \leq 0.25$ while for $\beta > 0.25$ a $\pi/8 - \pi/10$ expansion subinterval was needed.

A.2 SYMMETRY RELATION FOR THE ITERATIVE SOLUTION OVER ADJOINING π-INTERVALS.

In Section 3.3 it was indicated that a simple symmetry, see equation 3.3.4 , exists between the matrices $\underline{\underline{f}}(\gamma)$ and $\underline{\underline{g}}(\gamma)$ on adjoining π-intervals when all the diagonal elements of the matrix $\underline{\underline{M}}$ and off-diagonal elements of the matrix $\underline{\underline{E}}$, which occur in equation* 3.2.7 are zero. In any other situation the matching power series solution, given by equation 3.2.6, must be continued up to $\theta = 2\pi$. To demonstrate how this symmetry arises the leading five (NxN) expansion matrices $\underline{\underline{Q}}_\ell$ occurring in equation 3.3.6 are written out explicitly in terms of the matrices $\underline{\underline{E}}$ and $\underline{\underline{M}}$;

$$\underline{\underline{Q}}_0 = \underline{\underline{I}} \quad , \quad \underline{\underline{Q}}_1 = \frac{1}{\nu}\left[\underline{\underline{E}} + (-1)^{n+1}\varepsilon\underline{\underline{M}}\right]$$

$$\underline{\underline{Q}}_2 = -\frac{1}{\nu^2}\left\{\left[\underline{\underline{E}}^2 + \varepsilon^2\underline{\underline{M}}^2\right] + (-1)^{n+1}\varepsilon\left[\underline{\underline{E}}\underline{\underline{M}} + \underline{\underline{M}}\underline{\underline{E}}\right]\right\}$$

$$\underline{\underline{Q}}_3 = \frac{1}{\nu^3}\left\{\left[\underline{\underline{E}}^3 + \varepsilon^2\left(\underline{\underline{E}}\underline{\underline{M}}\underline{\underline{M}} + \underline{\underline{M}}\underline{\underline{E}}\underline{\underline{M}} + \underline{\underline{M}}\underline{\underline{M}}\underline{\underline{E}}\right)\right] + (-1)^{n+1}\varepsilon\left[\underline{\underline{E}}\underline{\underline{E}}\underline{\underline{M}} + \underline{\underline{E}}\underline{\underline{M}}\underline{\underline{E}} + \underline{\underline{M}}\underline{\underline{E}}\underline{\underline{E}} + \varepsilon^2\underline{\underline{M}}\underline{\underline{M}}\underline{\underline{M}} + \nu^2\underline{\underline{M}}\right]\right\}$$

$$\underline{\underline{Q}}_4 = \frac{1}{\nu^4}\left\{\left[\underline{\underline{E}}^4 + \varepsilon^2\left(\underline{\underline{E}}\underline{\underline{E}}\underline{\underline{M}}\underline{\underline{M}} + \underline{\underline{E}}\underline{\underline{M}}\underline{\underline{E}}\underline{\underline{M}} + \underline{\underline{E}}\underline{\underline{M}}\underline{\underline{M}}\underline{\underline{E}} + \underline{\underline{M}}\underline{\underline{E}}\underline{\underline{E}}\underline{\underline{M}} + \underline{\underline{M}}\underline{\underline{E}}\underline{\underline{M}}\underline{\underline{E}} + \underline{\underline{M}}\underline{\underline{M}}\underline{\underline{E}}\underline{\underline{E}} + \varepsilon^2\left(\underline{\underline{M}}^4 - \nu^2\underline{\underline{M}}^2\right) + \nu_2^2\underline{\underline{M}}^2\right)\right] + (-1)^{n+1}\varepsilon\left[\underline{\underline{E}}\underline{\underline{E}}\underline{\underline{E}}\underline{\underline{M}} + \underline{\underline{E}}\underline{\underline{E}}\underline{\underline{M}}\underline{\underline{E}} + \underline{\underline{E}}\underline{\underline{M}}\underline{\underline{E}}\underline{\underline{E}} + \underline{\underline{M}}\underline{\underline{E}}\underline{\underline{E}}\underline{\underline{E}} + \nu_2^2\underline{\underline{E}}\underline{\underline{M}} + \varepsilon^2\left(\underline{\underline{E}}\underline{\underline{M}}\underline{\underline{M}}\underline{\underline{M}} + \underline{\underline{M}}\underline{\underline{E}}\underline{\underline{M}}\underline{\underline{M}} + \underline{\underline{M}}\underline{\underline{M}}\underline{\underline{E}}\underline{\underline{M}} + \underline{\underline{M}}\underline{\underline{M}}\underline{\underline{M}}\underline{\underline{E}} - \nu^2\underline{\underline{M}}\underline{\underline{E}}\right)\right]\right\} \qquad \text{A.2.1}$$

The phase factor $(-1)^{n+1}$ accompanies only odd powers of the matrix $\underline{\underline{M}}$ in the expressions for $\underline{\underline{Q}}_\ell$ while the matrix $\underline{\underline{E}}$ and all its higher powers are diagonal and they are not multiplied by this phase factor. Each matrix power series coefficient $\underline{\underline{Q}}_\ell$ can therefore be represented as the sum of two resultant matrices $\underline{\underline{A}}_\ell$ and $\underline{\underline{B}}_\ell$ where $\underline{\underline{B}}_\ell$ is multiplied by the phase factor $(-1)^{n+1}$, that is

---

* The arguments that follow also hold for the general recurrence relation, given by equation 3.2.12, where the phase factor $(-1)^{n+1}$ is replaced by terms involving $\cos\alpha$ and $\sin\alpha$.

$$\underline{Q}_\ell = \underline{A}_\ell + (-1)^{n+1} \underline{B}_\ell \qquad \text{A.2.2}$$

If the condition $A_\ell^{ij} \neq 0$ implies $B_\ell^{ij} = 0$ holds, the matrix $\underline{Q}_\ell$ in adjoining π-intervals, that is $[0,\pi]$ and $[\pi, 2\pi]$, corresponding to $n=0$ and $n=1$ respectively, will differ only in that the elements q_ℓ^{ij} corresponding to nonzero B_ℓ^{ij} change sign and hence equation 3.3.4 follows. However, if $A_\ell^{ij} \neq 0$ implies $B_\ell^{ij} \neq 0$ the phase factor will be scrambled in the resulting matrix elements q_ℓ^{ij} and the simple symmetry relation breaks down. Therefore to show the symmetry relationship between the matrices $\underline{f}(x)$ and $\underline{g}(x)$, given by equation 3.3.4, it is necessary only to demonstrate that the elements of the resultant matrices $\underline{A}_\ell$ and $\underline{B}_\ell$ whose structure is determined by even and odd powers of the matrix $\underline{\mu}$, respectively, satisfy the condition $A_\ell^{ij} \neq 0$ implies $B_\ell^{ij} = 0$.

As an example we consider a three level system interacting with an oscillating field. The dipole matrix $\underline{\mu}$ for this interaction is given by *

$$\underline{\mu} = \begin{pmatrix} 0 & \mu_{12} & 0 \\ \mu_{21} & 0 & \mu_{23} \\ 0 & \mu_{32} & 0 \end{pmatrix} \qquad \text{A.2.3}$$

The leading two powers of $\underline{\mu}$ are adequate to display the structures of the matrices $\underline{A}_\ell$ and $\underline{B}_\ell$ in equation A.2.2. Writing these structures out explicitly

$$\underline{\mu}\,\underline{\mu} = \begin{pmatrix} X & 0 & X \\ 0 & X & 0 \\ X & 0 & X \end{pmatrix}, \quad \underline{\mu}\,\underline{\mu}\,\underline{\mu} = \begin{pmatrix} 0 & X & 0 \\ X & 0 & X \\ 0 & X & 0 \end{pmatrix} \qquad \text{A.2.4}$$

where X denotes a nonzero element. Obviously, all higher even powers of $\underline{\mu}$ have the same structure as $\underline{\mu}\,\underline{\mu}$ while all higher odd powers have the same structure as $\underline{\mu}$. Referring back to equation A.2.1 and A.2.2

---

* The dipole selection rules ensure that one of the off-diagonal matrix elements of $\underline{\mu}$ must be zero, as one state $\phi_1(r)$ of definite parity cannot simultaneously couple with two states $\phi_2(r)$ and $\phi_3(r)$ of multually opposite parities. While we have arbitrarily chosen $\mu_{13} = 0$ the following results hold in general for states of definite parity.

we see that the matrix $\underline{\underline{A}}_\ell$ has the same structure as $\underline{\mu}\,\underline{\mu}$ while $\underline{\underline{B}}_\ell$ has the same structure as $\underline{\mu}$ and hence the condition $A_\ell^{ij} \neq 0 \Rightarrow B_\ell^{ij} = 0$ holds.

An important exception to the above symmetry relation occurs when a static electric or magnetic field applied parallel to the oscillating field is included in the perturbation term $V(r,t)$. This additional field introduces nonzero off-diagonal elements into the $\underline{\underline{E}}$ matrix, see Sections 4.2 and 4.3, which scrambles the phase dependent elements in the resultant matrices; that is $A_\ell^{ij} \neq 0$ does not imply $B_\ell^{ij} = 0$. In this situation the matrix $\underline{\underline{q}}(\gamma)$ must be constructed by a power series expansion on the $[\pi, 2\pi]$ interval, see Section 3.3.

A.3 NUMERICAL ANALYSIS

Equations 2.2.3 for the state amplitudes $b_j(t)$ in the interaction representation were numerically integrated using a fourth order Runge Kutta method [30] to provide an independent check on the power series and iterative solutions developed in Sections 3.2-3.4. For economic reasons these numerical solutions were confined to a few two and three model level systems and the very small grid size ($\Delta t \sim .01$) required to provide comparable accuracy to the power series method restricted these solutions to short ranges of the independent variable t in equation 2.2.3. In all cases studied the numerical solution agreed with the power series solution to the number of significant figures to which the numerical result was reliable, that is $\Delta t^4 \sim 10$ significant figures.

The Runge Kutta method was also employed to directly integrate equation 2.2.3 when the perturbation term $V(r,t)$ represents two oscillating fields of arbitrary amplitudes $\mathcal{E}_1$ and $\mathcal{E}_2$, frequencies ν_1 and ν_2, and phases δ_1 and δ_2, respectively.

$$V(r,t) = -\mathcal{E}_1 \mu_z \cos(\nu_1 t + \delta_1) - \mathcal{E}_2 \mu_z \cos(\nu_2 t + \delta_2) \qquad \text{A.3.1}$$

No in depth investigation of the phase dependence of both fields on the computed transition probabilities has been carried out as the computational labour necessary to phase average the final results would be prohibitive. Instead we have studied the solutions, $|b_j(t)|^2$, for several three level configurations for four combinations of the relative phases, namely $[\delta_1, \delta_2] = [0,0]$, $[0, \pi/2]$, $[\pi/2, 0]$ and $[\pi/2, \pi/2]$. The results, as expected, depend critically on the relative strengths of the dipolar couplings between the various levels, but qualitatively the same behaviour is observed as for the single field case. The matching power series method should provide a much more efficient means for studying solutions to two field problems as a function of time for large field strengths $\mathcal{E}_1$ and $\mathcal{E}_2$, but no satisfactory method appears to be available for the extraction of phase and phase/time averaged properties from these solutions, except in the special case that both frequencies ν_1 and ν_2 are commensurable; $\nu_1/\nu_2 = S$, S a rational number. In this situation the Hamiltonian is periodic and the formal method of Chapter 3 can be directly employed.

Finally, for illustrative purposes, the induced transition probabilities $|b_j(t)|^2$, evaluated by using the Runge Kutta procedure, for the interaction of two oscillating fields given by equation A.3.1 with the three level configuration given in Figure A.1, are shown over a number of cycles in Figure A.2(a). This configuration corresponds to Wallaces [31] Figure 3 for "Resonance Raman scattering". For comparative purposes, the induced transition probabilities obtained by Wallace using a non hermitian Hamiltonian are included in Figure A.2(b). These results correspond to this authors' Figure 5 and are non physical for the same reasons as discussed for his treatment of the two level system in Section 4.2.1. In the calculation of [31] the non-self adjoint nature of the treatment has led to the neglect of reabsorption by the initial state and reemission from the final state; this can be seen graphically by comparing Figures A.2(a) and A.2(b). The rotating field treatment of this problem is the self adjoint analogue of the approach used in [31] and contains these important reabsorption and reemission terms.

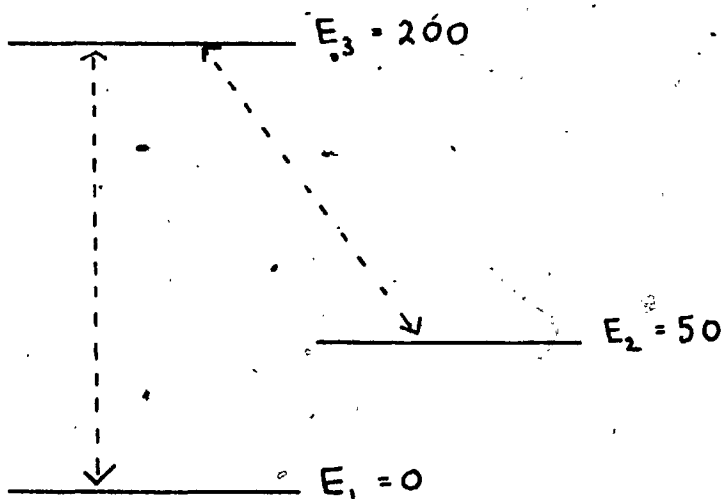

Figure A.1. The three level configuration employed by Wallace to study "Resonance Raman scattering". The absolute values of the energies used in subsequent calculations on this system are indicated in the figure.

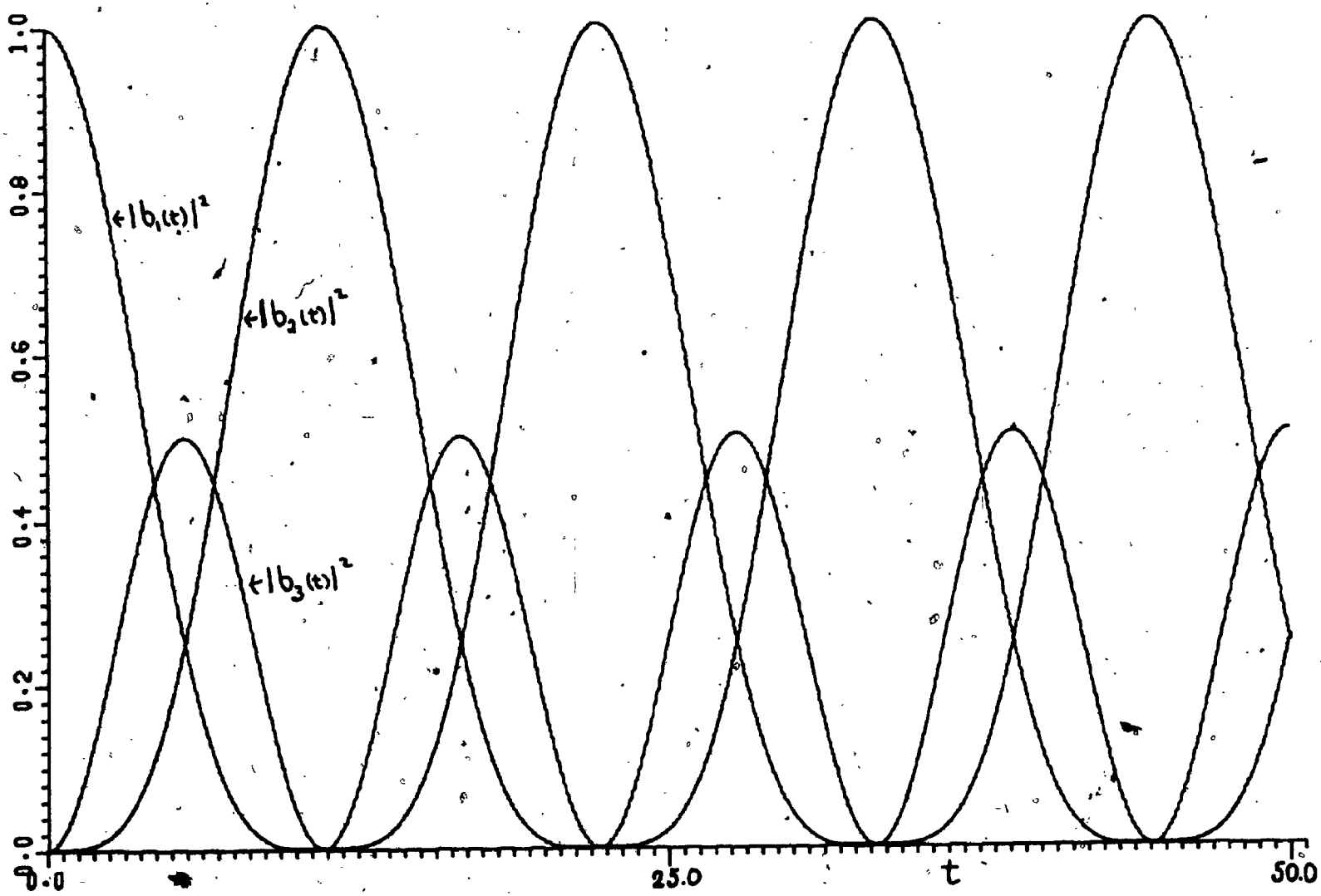

Figure A.2(a) The exact induced transition probabilities $|b_j(t)|^2$, $j = 1,2,3$, as a function of time for the level configuration shown in Figure A.1. The initial conditions on this system are $b_1(0) = 1$, $b_2(0) = b_3(0) = 0$ and the numerical values of the dipole coupling energies are: $\mu_{13}\mathcal{E}_1 = 0.2$, $\mu_{23}\mathcal{E}_2 = 0.2$.

Figure A.2(b) Wallaces [31] corresponding nonphysical results for the same parameters as in Figure A.2(a).

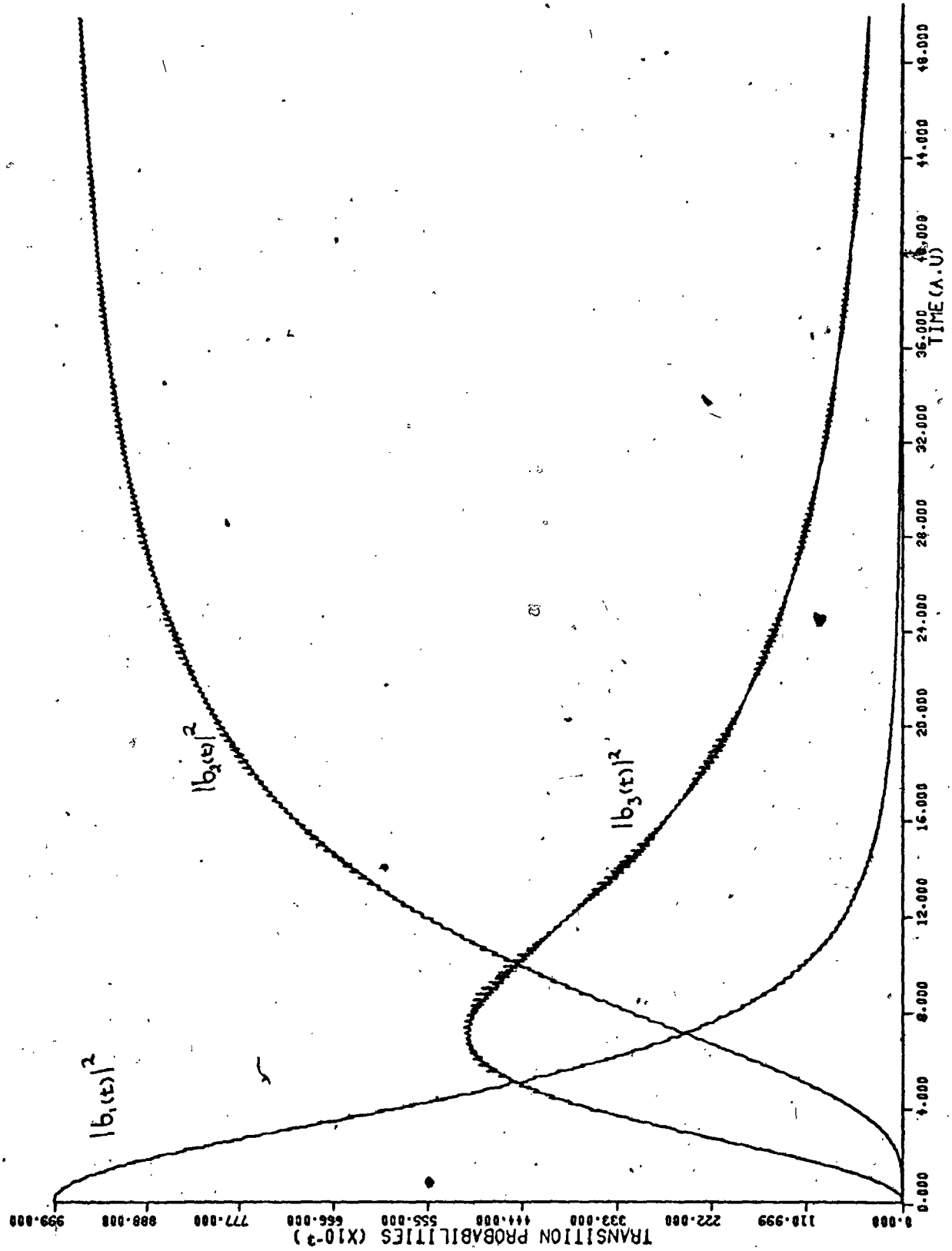
TRANSITION PROBABILITIES (X10-3)
0.000
110.999
222.000
333.000
444.000
555.000
666.000
777.000
888.000
999.000
0.000
4.000
8.000
12.000
16.000
20.000
24.000
28.000
32.000
36.000
40.000
44.000
48.000
TIME(A.U)
$|b_1(t)|^2$
$|b_2(t)|^2$
$|b_3(t)|^2$

The integrands appearing in the phase and time integrals, given by equations 3.7.5 and 3.7.6 (or 3.7.9 and 3.7.10 for their damped counterparts), were so well-behaved for all of the systems studied in Chapters 4 and 5 that a simple numerical quadrature, using Simpson's 2/3 rule [30], required approximately 10 to 20 grid points to yield final results accurate to 5 to 10 significant figures. The need for so few grid points is particularly encouraging as the evaluation of the double integral over phase and time (equations 3.7.5 and 3.7.6) becomes the major time consuming process in the computational procedure when $N \geq 4$ where N specifies the number of levels in the system under consideration. The rate of convergence of the numerical quadrature is not strongly dependent on the coupling strength parameter $\beta = |\mu\mathcal{E}|/\omega$ (see Chapters 4 and 5) so that accurate results are still obtained with the same range of grid points even if $\beta > 1$.

All of the spectra presented in this thesis were generated by fitting a cubic spline [87] to the computed discrete points. Approximately 10 to 15 points were needed to fit an individual resonance peak while the remainder of the frequency (or tuning domain) required a lower density of points.

The following computational times represent a very rough guide to the central processor times required to compute the integral matrix, $\mathbf{F}(\beta)$, $0 \leq \beta \leq 2\pi$, in double precision to sixteen figure accuracy.

N - levels	C.P. time per point
2	~ 7 c.p.s.
5	~ 50 c.p.s.
6	~ 80 c.p.s.

These timings were made on a Control Data CYBER 73 machine. A rough estimate of the timings for the evaluation of the phase and time averages, given by equations 3.7.6 and 3.7.10, can be obtained by multiplying the above times by a factor of 3/2.

APPENDIX B

ROTATING FIELD APPROXIMATION

In Section 2.4, the two level system interacting resonantly with an oscillating field was treated within the rotating field approximation and the generalization of this approximation by Freed [32] was very briefly mentioned. The purpose of this appendix is twofold, namely, (i) to demonstrate explicitly, by examples, how this approximation can be applied to situations for which it remains valid and (ii) to derive explicit expressions which represent an improvement to corresponding approximate transition rate and power expressions derived previously by Roberts and Fortson [33] and Javan [34], respectively. In deriving the results the formal procedure developed by Freed [32] will be followed closely and extended to include the radiative widths of individual levels. Initially we briefly review Freed's method of solution for a general N-level nondegenerate system coupled resonantly to one or more applied oscillating fields; the explicit method of solution depends on the energy level configuration, see examples that follow. Here, for complete generality, the radiative widths $\gamma_j/2$ of the individual levels $\phi_j(r)$ making up the system are included in the treatment. The basic set of coupled differential equations in the interaction representation which need to be solved via the rotating field approximation are given by equation 2.2.3 with the perturbation $V(r,t)$ in this equation now representing one or more oscillating fields * that is

---

* The phase dependence is again ignored as it cancels out in any final physical result derived through the rotating field approximation.

$$V(r,t) = -\mu_z \sum_{j=1}^{2} \mathcal{E}_j \cos \nu_j t = -\frac{\mu_z}{2} \sum_{j=1}^{2} \mathcal{E}_j \left[\exp[i\nu_j t] + \exp[-i\nu_j t] \right] \qquad \text{B.1.1}$$

As the rotating field approximation can only describe resonant or near resonant interactions, the frequencies ν_j of the oscillating fields must lie close to the allowed transition frequencies within the multilevel system. Thus one of the two exponential terms in equation B.1.1 will be resonant with a particular transition while the second term will be nonresonant and can be ignored, see Section 2.4.

B.1. THE LAPLACE TRANSFORM METHOD OF SOLUTION

The initial step involved in applying the rotating field approximation is to drop all nonresonant terms from the coefficients multiplying the $b_j(t)$ in the differential equations given by equation 2.2.3 . Next, we seek a "phase factoring" transformation [13;58] which will remove the time dependence from the remaining coefficients. This is achieved by the following transformation*, see Freed [32],

$$b_j(t) = C_j(t) \exp[i\alpha_j t] \qquad \text{B.1.2}$$

where the phases α_j are suitably chosen to remove this time dependence. The resulting differential equations for the new amplitudes $C_j(t)$ can be written as follows in matrix form

$$i \frac{\partial}{\partial t} \underline{\underline{C}}_j(t) = \underline{\underline{H}} \, \underline{\underline{C}}(t) \qquad \text{B.1.3}$$

$\underline{\underline{H}}$ is a constant NxN matrix whose form depends on the configuration of the N-level system. Explicit forms for $\underline{\underline{H}}$ will be given in the following sections. The coupled differential equations for $C_j(t)$ can be transformed to a set of simultaneous algebraic equations by using the following properties [54] of the Laplace transform

---

* This transformation is analgous to Shirley's "phase factoring" method [13,58].

$$\mathcal{L}\left(\frac{d}{dt}C_j(t)\right) = s\mathcal{L}(C_j(t)) - C_j(0) \qquad B.1.4$$

where

$$\mathcal{L}(C_j(t)) = \int_0^\infty \exp[-st]\, C_j(t)\, dt \equiv M_j(s)$$

The inverse Laplace transform $\mathcal{L}^{-1}(M_j(s))$ formally involves a contour integration in the complex plane but for our purposes $\mathcal{L}^{-1}(M_j(s))$ is either tabulated or has a well known representation in terms of partial fractions, see later and [54]. Following Freed [32] we set $g_j(0) = C_j(0)$ where $C_j(0)$ are the initial conditions on the system. The set of algebraic equations resulting from the Laplace transform of equation B.1.3 are conveniently written in matrix notation as follows,

$$-i\underline{\underline{g}} = (\underline{\underline{H}} - \lambda\underline{\underline{I}})\,\underline{\underline{M}}(s) \;, \quad \lambda \equiv is \qquad B.1.5$$

The matrix equation B.1.5 needs to be inverted to solve for $\underline{\underline{M}}(s)$ subject to the initial conditions specified by the constant matrix $\underline{\underline{g}}$; that is

$$\underline{\underline{M}}(s) = (\underline{\underline{H}} - \lambda\underline{\underline{I}})^{-1}\underline{\underline{g}} = -i\,\underline{\underline{D}}(\lambda)\,\underline{\underline{g}} \qquad B.1.6$$

where

$$D_{ij}(\lambda) = \langle \underline{\underline{H}} - \lambda\underline{\underline{I}} \rangle^{ji} / \det(\underline{\underline{H}} - \lambda\underline{\underline{I}}) \qquad B.1.7$$

where $\langle \underline{\underline{H}} - \lambda\underline{\underline{I}} \rangle^{ji}$ denotes the ji-th co-factor [32,63] of the matrix $(\underline{\underline{H}} - \lambda\underline{\underline{I}})$. Once the eigenvalues λ_j (or equivalently roots of the polynomial in λ) have been found the elements $D_{ij}(\lambda)$ can be written as

$$D_{ij}(\lambda) = \langle \underline{\underline{H}} - \lambda\underline{\underline{I}} \rangle^{ji} / \prod_{k=1}^{N} (\lambda - \lambda_k) \qquad B.1.8$$

Finally, the amplitudes $C_j(t)$ are obtained from the inverse Laplace transform of equation B.1.6 which can readily be evaluated by using the following partial fraction representation of the inverse Laplace transform*

---

* The notation used in equation B.1.9 is due to Freed [32] and the symbol Δ_n , which is the partial fraction representation of the inverse Laplace transform, should not be confused with the similar symbol used to represent the characteristic exponents Δ_j in the main text.

$$\mathcal{L}^{-1}\left(\frac{\lambda^n}{\prod_{j=1}^{N}(\lambda-\lambda_j)}\right) = -i\sum_{j=1}^{N}\left\{\lambda_j^n \exp[-i\lambda_j t]/\prod_{k\neq j=1}^{N}(\lambda_j-\lambda_k)\right\} \equiv -i\Delta_n \qquad \text{B.1.9}$$

The use of these partial fractions expansions will be made clear in the applications that follow. If $N>3$ the determinant in equation B.1.7 will need to be evaluated numerically in general unless the symmetry of the problem allows the NxN matrix $\underline{\underline{H}}$ to be partitioned into smaller blocks, see Freed, for example.

B.2 TWO LEVEL SYSTEM

The formal developements due to Freed, discussed in the previous section, will now be employed to determine the state amplitudes $b_j(t)$ for a simple two state system $\phi_1(r)$ and $\phi_2(r)$, with radiative widths $\gamma_1/2$ and $\gamma_2/2$ respectively, interacting with a single oscillating field. Equation 2.2.3 for the $b_j(t)$ will occur in the limit that the radiative widths are ignored.

The appropriate differential equations that need to be solved are given by

$$i\partial/\partial t\, b_1(t) = -\frac{\gamma_1}{2} b_1(t) + V_{12}\exp[-i\Delta\omega t]\, b_2(t)$$
$$i\partial/\partial t\, b_2(t) = -\frac{\gamma_2}{2} b_2(t) + V_{21}\exp[i\Delta\omega t]\, b_1(t) \qquad \text{B.2.1}$$

where

$$V_{12} = -\mu_{12}\mathcal{E}/2 = V_{21}\ ;\ \Delta\omega = \omega - \upsilon \equiv (E_2-E_1)-\upsilon \qquad \text{B.2.2}$$

Using the transformation given by equation B.1.2 yields the following set of coupled differential equations for the $C_j(t)$

$$i\partial/\partial t\, C_1(t) = (\alpha_1 - i\gamma_1/2)C_1(t) + V_{12}\exp[i(\alpha_2-\alpha_1-\Delta\omega)t]\, C_2(t)$$
$$i\partial/\partial t\, C_2(t) = (\alpha_2 - i\gamma_2/2)C_2(t) + V_{21}\exp[i(\alpha_1-\alpha_2+\Delta\omega)t]\, C_1(t) \qquad \text{B.2.3}$$

Choosing $\alpha_1 = -\Delta\omega$ and $\alpha_2 = 0$ removes* the time dependence from the coefficients of these differential equations and yields for the

constant matrix $\underline{\underline{H}}$, see equation B.1.3, the following result

$$\underline{\underline{H}} = \begin{pmatrix} -(i\gamma_1/2 + \Delta\omega) & V_{12} \\ V_{21} & -i\gamma_2/2 \end{pmatrix} \qquad \text{B.2.4}$$

The individual matrix elements of $\underline{\underline{D}}(\lambda)$ in equation B.1.6 are obtained from equation B.1.8 and are given explicitly by

$$D_{11}(\lambda) = -\left[i\frac{\gamma_2}{2} + \lambda\right] / (\lambda_1-\lambda_2)(\lambda-\lambda_2)$$

$$D_{12}(\lambda) = -V_{12} / (\lambda-\lambda_1)(\lambda-\lambda_2) \equiv D_{21}(\lambda)$$

$$D_{22}(\lambda) = -\left[\left(i\frac{\gamma_2}{2} + \Delta\omega\right) + \lambda\right] / (\lambda-\lambda_1)(\lambda-\lambda_2) \qquad \text{B.2.5}$$

where λ_1 and λ_2 are the two roots of the 2x2 determinant $\det \underline{\underline{H}}$ and are given explicitly by

$$\lambda_{1,2} = -\frac{1}{2}\left\{i\left(\frac{\gamma_1+\gamma_2}{2}\right) + \Delta\omega\right\} \pm \frac{1}{2}\sqrt{\Delta\omega^2 + 4|V_{12}|^2 - (\gamma_1-\gamma_2)\left[\left(\frac{\gamma_1-\gamma_2}{4}\right) - i\Delta\omega\right]} \qquad \text{B.2.6}$$

The functions $M_j(s)$, given by equation B.1.6, can now be written as follows,

$$\begin{pmatrix} M_1(s) \\ M_2(s) \end{pmatrix} = \frac{1}{(\lambda-\lambda_1)(\lambda-\lambda_2)} \begin{pmatrix} (-\frac{\gamma_2}{2} + i\lambda) & iV_{12} \\ iV_{21} & [(-\frac{\gamma_1}{2} + i\Delta\omega) + i\lambda] \end{pmatrix} \begin{pmatrix} g_1 \\ g_2 \end{pmatrix} \qquad \text{B.2.7}$$

Taking the inverse Laplace transform of $\underline{\underline{M}}(s)$, using the continued fraction expansion given by equation B.1.9, we obtain for $\underline{\underline{C}}(t)$

$$\begin{pmatrix} C_1(t) \\ C_2(t) \end{pmatrix} = \begin{pmatrix} (\frac{\gamma_2}{2}\Delta_0 + \Delta_1) & V_{12}\Delta_0 \\ V_{21}\Delta_0 & [(-\frac{\gamma_1}{2} + i\Delta\omega) + \lambda \end{pmatrix} \begin{pmatrix} C_1(0) \\ C_2(0) \end{pmatrix} \qquad \text{B.2.8}$$

where

$$\Delta_0 = \left[\exp[-i\lambda_1 t] - \exp[-i\lambda_2 t]\right] / (\lambda_1-\lambda_2)$$

$$\Delta_1 = \left[\lambda_1 \exp[-i\lambda_1 t] - \lambda_2 \exp[-i\lambda_2 t]\right] / (\lambda_1-\lambda_2) \qquad \text{B.2.9}$$

Finally, the state amplitudes $b_j(t)$ can be obtained by substituting

---

* There are several choices of phases α_j which accomplish this. We could just as easily have choosen $\alpha_1 = -\Delta\omega/2$, $\alpha_2 = \Delta\omega/2$ but the final result for the $b_j(t)$'s , would have been the same.

equation B.2.8 into equation B.1.2 with the definition of α_1 and α_2 given above. For simplicity we assume that $\gamma_1 = \gamma_2 = 0$ and that the initial conditions on the system are $C_1(0) = b_1(0) = 1$; $C_2(0) = b_2(0) = 0$ so that the final results for the state amplitudes $b_j(t)$ become

$$b_1(t) = \exp[-i\Delta\omega t/2]\left\{\sqrt{\Delta\omega^2+4|V_{12}|^2}\,\mathrm{Cos}\tfrac{1}{2}\sqrt{\Delta\omega^2+4|V_{12}|^2}\,t - i\Delta\omega\,\mathrm{Sin}\tfrac{1}{2}\sqrt{\Delta\omega^2+4|V_{12}|^2}\,t\right\}/\sqrt{\Delta\omega^2+4|V_{12}|^2}$$

$$b_2(t) = -2iV_{12}\exp[i\Delta\omega t/2]\,\mathrm{Sin}\tfrac{1}{2}\sqrt{\Delta\omega^2+4|V_{12}|^2}\,t\,/\sqrt{\Delta\omega^2+4|V_{12}|^2} \qquad \text{B.2.10}$$

Equation B.2.10 is identical to equation 2.4.3 with $\Delta\omega$ and V_{12} defined above.

B.3 TRANSITION RATES FOR A THREE LEVEL SYSTEM RESONANTLY COUPLED TO TWO OSCILLATING FIELDS

Roberts and Fortson [33] recently suggested the possibility of carrying out high resolution double quantum* spectroscopy in hydrogen by observing transitions between narrow s states with the much broader p states acting as intermediate states coupling the transition. The basic level configuration suggested for this experiment is shown in Figure B.1 with the infinitely narrow state $\phi_1(r)$ ($\gamma_1 = 0$) coupled to a broad intermediate state $\phi_2(r)$ of opposite parity, which in turn is coupled directly to a higher state $\phi_3(r)$ of much narrower width.**

---

* The term double quantum here can refer to two stepwise single photon transitions or a single two photon transition depending on whether both fields on resonance with the transition frequency ($E_3 - E_1$) are tuned precisely to the individual transitions, that is $\Delta\omega_1 = \Delta\omega_2 = 0$ or are mistuned from the intermediate level so that $\Delta\omega_1 = -\Delta\omega_2$ and $\Delta\omega_1 + \Delta\omega_2 = 0$; $\Delta\omega_1$ and $\Delta\omega_2$ are defined below.

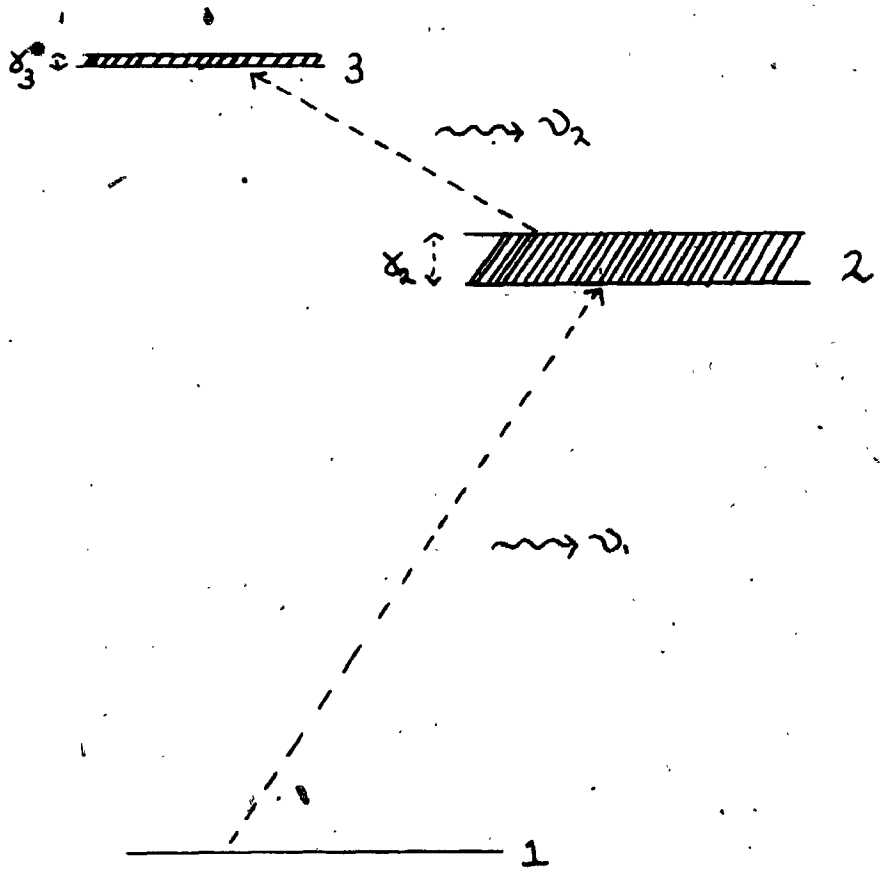

Figure B.1. The three level configuration employed by Roberts and Fortson [33] to investigate high precision double quantum spectroscopy in the H-atom. The very weak laser field at frequency ν_1 couples the transition $\phi_1(r) - \phi_2(r)$ while the arbitrarily strong radiofrequency field at frequency ν_2 couples the transition $\phi_2(r) \rightarrow \phi_3(r)$.

(that is $\gamma_2 \gg \gamma_3 \ggg \gamma_1$). The basic system of differential equations in the rotating field approximation describing the interaction of this system with two oscillating fields, one of frequency ν_1 near resonant with the transition $\omega_{21} = (E_2 - E_1)$ and the second of frequency ν_2 near resonant with the transition $\omega_{32} = (E_3 - E_2)$, are given by

$$i\frac{\partial}{\partial t} b_1(t) = -i\frac{\gamma_1}{2} b_1(t) + V_{12} b_2(t) \exp[-i\Delta\omega_1 t]$$

$$i\frac{\partial}{\partial t} b_2(t) = -i\frac{\gamma_2}{2} b_2(t) + V_{12} b_1(t) \exp[i\Delta\omega_1 t] + V_{23} b_3(t) \exp[-i\Delta\omega_2 t]$$

$$i\frac{\partial}{\partial t} b_3(t) = -i\frac{\gamma_3}{2} b_3(t) + V_{32} b_2(t) \exp[i\Delta\omega_2 t] \qquad \text{B.3.1}$$

where

$$V_{12} = -\mu_{12}\mathcal{E}_1/2 = V_{21} \quad , \quad V_{23} = -\mu_{23}\mathcal{E}_2/2 = V_{32}$$

$$\Delta\omega_1 = \omega_{21} - \nu_1 \quad , \quad \Delta\omega_2 = \omega_{32} - \nu_2 \, .$$

and the nonresonant terms have been dropped from these differntial equations. Roberts and Fortson [33] assume that the laser field $\mathcal{E}_1$ coupling the transition $\phi_1 \rightarrow \phi_2$ is very weak and acts as a probe, while no restriction is placed on the magnitude of the radiofrequency field* $\mathcal{E}_2$ whose frequency ν_2 is held fixed. These authors derive solutions for the state amplitudes $b_3(t)$ and $b_2(t)$ under the assumption that $b_1(t) \sim 1$ that are valid for times $t \gg \gamma_2^{-1}$ after which transient effects arising from the spontaneous decay terms have died out.

** Roberts and Fortson point out that only the very narrow widths of the initial and final states contribute to the width of the profile. They explicitly consider the transition $2S \rightarrow 3S$ (via $3p$) in hydrogen, with a weak laser field tuned to the $2S \rightarrow 3P$ transition, while a radiofrequency field is tuned to the $3S - 3P$ transition [33].

---

* Of course the fields must be sufficiently small for the rotating field approximation to remain valid [22,28].

In this section we will initially derive convenient closed form solutions for $b_2(t)$ and $b_2(t)$ within the restrictions $b_1(t) \sim 1$, but valid over all times. These solutions will allow us to study the temporal behaviour of the spectra presented by Roberts and Fortson in their Figure 2, for example. Finally, equations B.3.1 will be solved exactly and these final results for the transition rates will remain valid for arbitrary relative magnitudes of V_{12} and V_{32}.

(i) Solution for small V_{12}.

Equation B.3.1 can be approximated by

$$i\frac{\partial}{\partial t} b_2(t) = -i\frac{\gamma_2}{2} b_2(t) + V_{23} b_3(t) \exp[-i\Delta\omega_2 t] + V_{21} \exp[i\Delta\omega_1 t]$$

$$i\frac{\partial}{\partial t} b_3(t) = -i\frac{\gamma_3}{2} b_3(t) + V_{32} b_2(t) \exp[i\Delta\omega_2 t] \qquad \text{B.3.2}$$

since V_{12} small implies that $b_1(t) \sim 1$, see [33]. Equation B.3.2 can now be solved by following the formal methods of Section B.1. Using the transformation given by equation B.1.2 the system of differential equations satisfied by $C_j(t)$ are

$$i\frac{\partial}{\partial t} C_2(t) = (\alpha_2 - i\frac{\gamma_2}{2}) C_2(t) + V_{23} C_3(t) \exp[i(\alpha_3 - \alpha_2 - \Delta\omega_2)t] + V_{12} \exp[i(\Delta\omega_1 - \alpha_2)t]$$

$$i\frac{\partial}{\partial t} C_3(t) = (\alpha_3 - i\frac{\gamma_3}{2}) C_3(t) + V_{32} C_2(t) \exp[i(\alpha_2 - \alpha_3 + \Delta\omega_2)t] \qquad \text{B.3.3}$$

Choosing

$$\alpha_2 = \Delta\omega_1 \quad ; \quad \alpha_3 = \Delta\omega_1 + \Delta\omega_2 \qquad \text{B.3.4}$$

the set of differential equations satisfied by $C_j(t)$ becomes

$$i\frac{\partial}{\partial t} C_2(t) = [\Delta\omega_1 + i\frac{\gamma_2}{2}] C_2(t) + V_{23} C_3(t) + V_{12}$$

$$i\frac{\partial}{\partial t} C_3(t) = [\Delta\omega_1 + \Delta\omega_2 - i\frac{\gamma_3}{2}] C_3(t) + V_{32} C_2(t). \qquad \text{B.3.5}$$

Equation B.3.5 can easily be solved by the matrix inversion technique outlined in Section B.1, but the inhomogenous term V_{12} would need to be included in an additional constant matrix in equation B.1.3. It is just as easy however to take the Laplace transform of equation B.3.5 and solve the resulting set of two algebraic equations in two unknowns directly. These algebraic equations are

$$-ig_2 = [\Delta\omega_1 - i\tfrac{\gamma_2}{2} - iS]\,M_2(S) + V_{23}M_3(S) + V_{12}/S = 0$$

$$-ig_3 = [\Delta\omega_1 + \Delta\omega_2 - i\gamma_3/2 - iS]\,M_3(S) + V_{32}M_2(S) = 0 \qquad \text{B.3.6}$$

Solving directly for $M_2(S)$ and $M_3(S)$ we get

$$M_2(S) = -\frac{V_{12}}{S}\cdot\frac{[\Delta\omega_1+\Delta\omega_2 - i\frac{\gamma_3}{2} - iS]}{[\Delta\omega_1+\Delta\omega_2 - i\frac{\gamma_3}{2} - iS][\Delta\omega_1 - i\frac{\gamma_2}{2} - iS - |V_{23}|^2]}$$

$$= \frac{-iV_{12}[i(\Delta\omega_1+\Delta\omega_2)+\gamma_3/2]}{S[S^2+2\alpha S+K]} - \frac{iV_{12}}{[S^2+2\alpha S+K]}$$

$$M_3(S) = -\frac{V_{12}V_{32}}{S}\Big/\left[|V_{23}|^2 - (\Delta\omega_1+\Delta\omega_2 - i\gamma_3/2 - iS)(\Delta\omega_1 - i\gamma_2/2 - iS)\right]$$

$$= -\frac{V_{12}V_{23}}{S}\Big/[(S+\alpha)^2+b^2] \qquad \text{B.3.7}$$

where

$$\alpha = \tfrac{1}{4}(\gamma_2+\gamma_3) + i(\Delta\omega_1 + \Delta\omega_2/2)$$

$$b = \sqrt{|V_{23}|^2 - \frac{(\gamma_2-\gamma_3)^2}{4} + \frac{\Delta\omega_2}{4}(\Delta\omega_2 + i(\gamma_2-\gamma_3))}$$

$$K = \alpha^2 + b^2 \qquad \text{B.3.8}$$

Using the tabulated expressions for the inverse Laplace transform in [54] we obtain the final expressions for $C_2(t)$ and $C_3(t)$

$$C_2(t) = -iV_{12}\left\{\frac{i(\Delta\omega_1+\Delta\omega_2)+\gamma_3/2}{K}\left[1 - \exp[-\alpha t]\left[\cos bt + \frac{\alpha}{b}\sin bt\right] + \exp[-\alpha t]\sin bt/b\right]\right\}$$

$$C_3(t) = -\frac{V_{12}V_{32}}{K}\left[1 - \exp[-\alpha t]\left[\cos bt + \frac{\alpha}{b}\sin bt\right]\right] \qquad \text{B.3.9}$$

As both α and b are complex constants the solutions $C_2(t)$ and $C_3(t)$ contain damping terms. In both solutions the leading terms are constant while the remaining terms represent the transient decay terms which damp out approximately as $\exp[-(\gamma_2+\gamma_3)t/4] \sim \exp[-\frac{\gamma_2 t}{4}]$. Hence if $t \gg \gamma_2^{-1}$ we obtain for $b_2(t)$ and $b_3(t)$ using the values of α_2 and α_3 above in equation B.1.2

$$b_2(t) \doteq -i\frac{V_{12}}{K}[i(\Delta\omega_1+\Delta\omega_2)+\gamma_3/2]\exp[i\Delta\omega_1 t]$$

$$b_3(t) \approx -\frac{V_{12}V_{32}}{K}\cdot\exp[i(\Delta\omega_1+\Delta\omega_2)t] \qquad \text{B.3.10}$$

Equation B.3.10 agree precisely with Roberts and Fortsons equation (2) except for some misprints in their equations.

(ii) Exact Rotating Field Solutions

Next, we proceed to solve equation B.3.1 exactly using the matrix method of Section B.1. The transformed differential equations for $C_j(t)$ after the phase factoring transformation of equation B.1.2 are given by

$$\begin{aligned}
i\frac{\partial}{\partial t}C_1(t) &= (\alpha_1 - i\gamma_1/2)C_1(t) + V_{12}C_2(t)\exp[i(\alpha_2-\alpha_1-\Delta\omega_1)t] \\
i\frac{\partial}{\partial t}C_2(t) &= (\alpha_2 - i\gamma_2/2)C_2(t) + V_{21}C_1(t)\exp[i(\alpha_1-\alpha_2+\Delta\omega_1)t] \\
&\quad + V_{23}C_3(t)\exp[i(\alpha_3-\alpha_2-\Delta\omega_2)t] \\
i\frac{\partial}{\partial t}C_3(t) &= (\alpha_3 - i\gamma_3/2)C_3(t) + V_{32}C_2(t)\exp[i(\alpha_2-\alpha_3+\Delta\omega_2)t]
\end{aligned} \qquad \text{B.3.11}$$

where we retain γ_1 although it will be set to zero in the final results. Choosing

$$\alpha_1 = -\Delta\omega_1 \;,\; \alpha_2 = 0 \;,\; \alpha_3 = \Delta\omega_2 \qquad \text{B.3.12}$$

yields the following result for the constant matrix $\underline{\underline{H}}$ in equation B.1.3

$$\underline{\underline{H}} = \begin{pmatrix} -(\Delta\omega_1 + i\gamma_1/2) & V_{12} & 0 \\ V_{21} & -i\gamma_2/2 & V_{23} \\ 0 & V_{32} & (\Delta\omega_2 - i\gamma_3/2) \end{pmatrix} \qquad \text{B.3.13}$$

The elements of the matrix $\underline{\underline{D}}(\lambda)$ appearing in equation B.1.6 are given by

$$\begin{aligned}
D_{11}(\lambda) &= \left[(i\gamma_2/2+\lambda)(i\gamma_3/2-\Delta\omega_2+\lambda) - |V_{23}|^2\right] \Big/ \prod_{j=1}^{3}(\lambda-\lambda_j) \\
D_{12}(\lambda) &= V_{12}(i\gamma_3/2 - \Delta\omega_2 + \lambda) \Big/ \prod_{j=1}^{3}(\lambda-\lambda_j) = D_{21}(\lambda) \\
D_{13}(\lambda) &= V_{12}V_{23} \Big/ \prod_{j=1}^{3}(\lambda-\lambda_j) = D_{31}(\lambda) \\
D_{23}(\lambda) &= V_{23}(\Delta\omega_1 + i\gamma_1/2 + \lambda) \Big/ \prod_{j=1}^{3}(\lambda-\lambda_j) = D_{32}(\lambda) \\
D_{33}(\lambda) &= \left[(i\gamma_2/2+\lambda)(\Delta\omega_1 + i\gamma_1/2+\lambda) - |V_{12}|^2\right] \Big/ \prod_{j=1}^{3}(\lambda-\lambda_j) \\
D_{22}(\lambda) &= (\Delta\omega_1 + i\gamma_1/2 + \lambda)(i\gamma_3/2 - \Delta\omega_2 + \lambda) \Big/ \prod_{j=1}^{3}(\lambda-\lambda_j)
\end{aligned} \qquad \text{B.3.14}$$

where now λ_1, λ_2 and λ_3 represent the roots of the following cubic equation

$$\lambda^3 + b\lambda^2 + c\lambda + d = 0 \qquad \text{B.3.15}$$

where

$$b = \Delta\omega_1 + \Delta\omega_2 + \tfrac{i}{2}(\gamma_1+\gamma_2+\gamma_3)$$

$$c = -\left[|V_{12}|^2 + |V_{23}|^2 + \tfrac{1}{4}(\gamma_1\gamma_2 + \gamma_1\gamma_3 + \gamma_2\gamma_3) + \Delta\omega_1\Delta\omega_2\right]$$

$$- \tfrac{i}{2}\left(\Delta\omega_2(\gamma_1+\gamma_2) - \Delta\omega_1(\gamma_2+\gamma_3)\right)$$

$$d = -\left[\Delta\omega_2\left(|V_{12}|^2 + \gamma_1\gamma_2/4\right) - \Delta\omega_1\left(|V_{23}|^2 - \gamma_2\gamma_3/4\right)\right]$$

$$- \tfrac{i}{2}\left[\gamma_1|V_{23}|^2 + \gamma_3|V_{12}|^2 + \gamma_1\gamma_2\gamma_3/4\right] \qquad \text{B.3.16}$$

The cubic equation B.3.15 can be solved by standard techniques [88], but analytic closed form results can only be obtained in certain limiting cases [88], see below. The algebraic solutions to equation B.3.14 are well known and are given by [88]

$$\lambda_1 = \sqrt[3]{A} + \sqrt[3]{B} - b/3$$

$$\lambda_2 = \omega\sqrt[3]{A} + \omega^2\sqrt[3]{B} - b/3 \qquad \text{B.3.17}$$

$$\lambda_3 = \omega^2\sqrt[3]{A} + \omega\sqrt[3]{B} - b/3$$

where

$$A = -q/2 + \sqrt{R}\ , \quad B = -q/2 + \sqrt{R}\ , \quad R = p^3/27 + q^2/4$$

$$p = c - b^2/3\ , \quad q = d - bc/3 + \tfrac{2}{27}b^3 \qquad \text{B.3.18}$$

and $1, \omega^2$ and ω^3 represent the cube roots of unity [88]. The λ_j's will be very complicated complex numbers in general and will need to be numerically evaluated. Once these are evaluated the solution for $C_j(t)$, $j=1,3$ can be written down for any particular set of initial conditions q_j by inverting the Laplace transform given by equation B.1.6. Choosing $C_1(0) = 1$, $C_2(0) = C_3(0) = 0$ and using the values of α_j given by equation B.3.12 we finally obtain for the state amplitudes $b_j(t)$

$$b_1(t) = -\left[\Delta_2 - (\Delta\omega_2 - \tfrac{i}{2}(\gamma_2+\gamma_3))\Delta_1 - (\tfrac{\gamma_2\gamma_3}{4} + |V_{23}|^2 + i\tfrac{\gamma_2}{2}\Delta\omega_2)\Delta_0\right]$$
$$\times \exp[-i\Delta\omega_1 t]$$

$$b_2(t) = -V_{12}\left[\Delta_1 + (\Delta\omega_2 - i\gamma_3/2)\Delta_0\right]$$

$$b_3(t) = -V_{12}V_{23}\Delta_0 \exp[i\Delta\omega_2 t] \qquad \text{B.3.19}$$

where the partial fraction expansions Δ_n are given by equation

B.1.9.

(iii) Transition Rates

The transition rate R_j into state $\phi_j(r)$ is defined as

$$R_j = \frac{\partial}{\partial t} |b_j(t)|^2 = \frac{\partial}{\partial t} |C_j(t)|^2 \qquad \text{B.3.20}$$

where the state amplitudes $b_j(t)$ are given by equation B.3.19. Rewriting equation B.3.20 as follows

$$R_j = b_j(t) \frac{\partial}{\partial t} b_j^*(t) + b_j^*(t) \frac{\partial}{\partial t} b_j(t) \qquad \text{B.3.21}$$

and substituting for $\partial/\partial t\, b_j(t)$ and $\partial/\partial t\, b_j^*(t)$ from equations B.3.1, we obtain finally, after some algebra, the following expressions for the transition rates R_j

$$R_1 = -\gamma_1 |b_1(t)|^2 - V_{12}\left[\mathrm{Im}\,\delta_{12}^- \cos\Delta\omega_1 t + \mathrm{Re}\,\delta_{12}^+ \sin\Delta\omega_1 t\right]$$

$$R_2 = -\gamma_2 |b_2(t)|^2 - V_{21}\left[\mathrm{Im}\,\delta_{21}^- \cos\Delta\omega_1 t - \mathrm{Re}\,\delta_{21}^+ \sin\Delta\omega_1 t\right]$$
$$- V_{23}\left[\mathrm{Im}\,\delta_{23}^- \cos\Delta\omega_2 t + \mathrm{Re}\,\delta_{23}^+ \sin\Delta\omega_2 t\right]$$

$$R_3 = -\gamma_3 |b_3(t)|^2 - V_{32}\left[\mathrm{Im}\,\delta_{32}^- \cos\Delta\omega_2 t - \mathrm{Re}\,\delta_{32}^+ \sin\Delta\omega_2 t\right]$$

B.3.22

where

$$\delta_{ij}^{\pm} = b_i(t) b_j^*(t) \pm b_i^*(t) b_j(t) \qquad \text{B.3.23}$$

Using the fact that $\delta_{ij}^- = -\delta_{ji}^-$ and $\delta_{ij}^+ = \delta_{ji}^+$ in equation B.2.22 the sum of the transition rates R_j becomes

$$\sum_j R_j = -\sum_j \gamma_j |b_j(t)|^2 \qquad \text{B.3.24}$$

This result shows explicitly that the transition rate out of state $\phi_1(r)$ $(-R_1)$ can equal the sum of the transition rates into states $\phi_2(r)$ and $\phi_3(r)$ (R_2+R_3) only if the widths γ_j of all the states $\phi_j(r)$ are identically zero; that is, if the norm $\sum_j |b_j(t)|^2$ is conserved. These R_j's represent the instantaneous transition rates

and the transition rates discussed by Roberts and Fortson [33] correspond to their time average. The average transition rates $\bar{R}_j$ can be formally represented as follows

$$\bar{R}_j(\tau) = \frac{1}{\tau} \int_0^{\tau} \frac{\partial}{\partial t} |b_j(t)|^2 \, dt$$

$$= \gamma_j \left[|b_j(\tau)|^2 - |b_j(0)|^2 \right] \qquad \text{B.3.25}$$

where $\tau_j = \gamma_j^{-1}$ [2]. The time constant τ in equation B.3.25 can represent, for example, the time of measurement, or, a mean collision time for a gaseous system, see Section 3.7.

To compare with [33] we need to take $\tau \gg \gamma_2^{-1}$ but equation B.3.25 allows us to study in addition the temporal developement of the transition rate frequency spectra over the entire time domain. As the average transition rate is directly proportional to the induced transition probability $[|b_j(\tau)|^2 - |b_j(0)|^2]$ we study instead the temporal behaviour of its frequency spectrum, shown in Figure B.2, for $\tau = 10^6$, 10^9 and 10^{12} for the system in Figure B.1 initially in the ground state $\phi_1(r)$, that is, $b_1(0)=1$, $b_2(0) = b_3(0)=0$. The numerical values of the other parameters needed to generate this figure correspond to those used by Roberts and Fortson[33] and are given explicitly in Figure B.2. The value $\tau = 10^{12}$ satisfies the condition $\tau \gg \gamma_2^{-1}$ and hence reproduces the corresponding results of [33], see their Figure 2.

The exact transition rate expressions, given by equation B.3.22 have the obvious advantage that they can be used, in addition, to investigate situations for which the perturbation term V_{12} is no longer small and hence violates the condition $b_1(t) \sim 1$. Of particular interest recently for example is the situation where both fields are saturating[89].

In the expressions for the state amplitudes $b_j(t)$, given by equation B.3.19, the partial fraction expansions Δ_n depend solely on the eigenvalues λ_j of the (3x3) secular determinant. In general, these eigenvalues are complex and need to be computed numerically using the expressions given by equation B.3.17. In certain limiting cases however, closed form expressions can be given for the transition

Figure B.2. Average induced transition probabilities, $[1-|b_1(\tau)|^2]$, $|b_2(\tau)|^2$ and $|b_3(\tau)|^2$ as a function of frequency detuning $\Delta\omega_1(=\omega_{21}-\nu_1)$ for three values of the damping constant τ. (a) $\tau = 10^6$, (b) $\tau = 10^9$ and (c) $\tau = 10^{12}$. The frequency spectrum of $[1-|b_1(\tau)|^2]$ for $\tau = 10^6$ is not included as this quantity is zero to the accuracy of the computation. Numerical values of other parameters [33] used in this calculation are; $\Delta\omega_2 = 0$, $\gamma_1 = 0$, $\gamma_2 = 1.86 \times 10^{-8}$, $\gamma_3 = 6.3 \times 10^{-10}$, $V_{12} = 1 \times 10^{-12}$, $V_{23} = 1.526 \times 10^{-9}$.

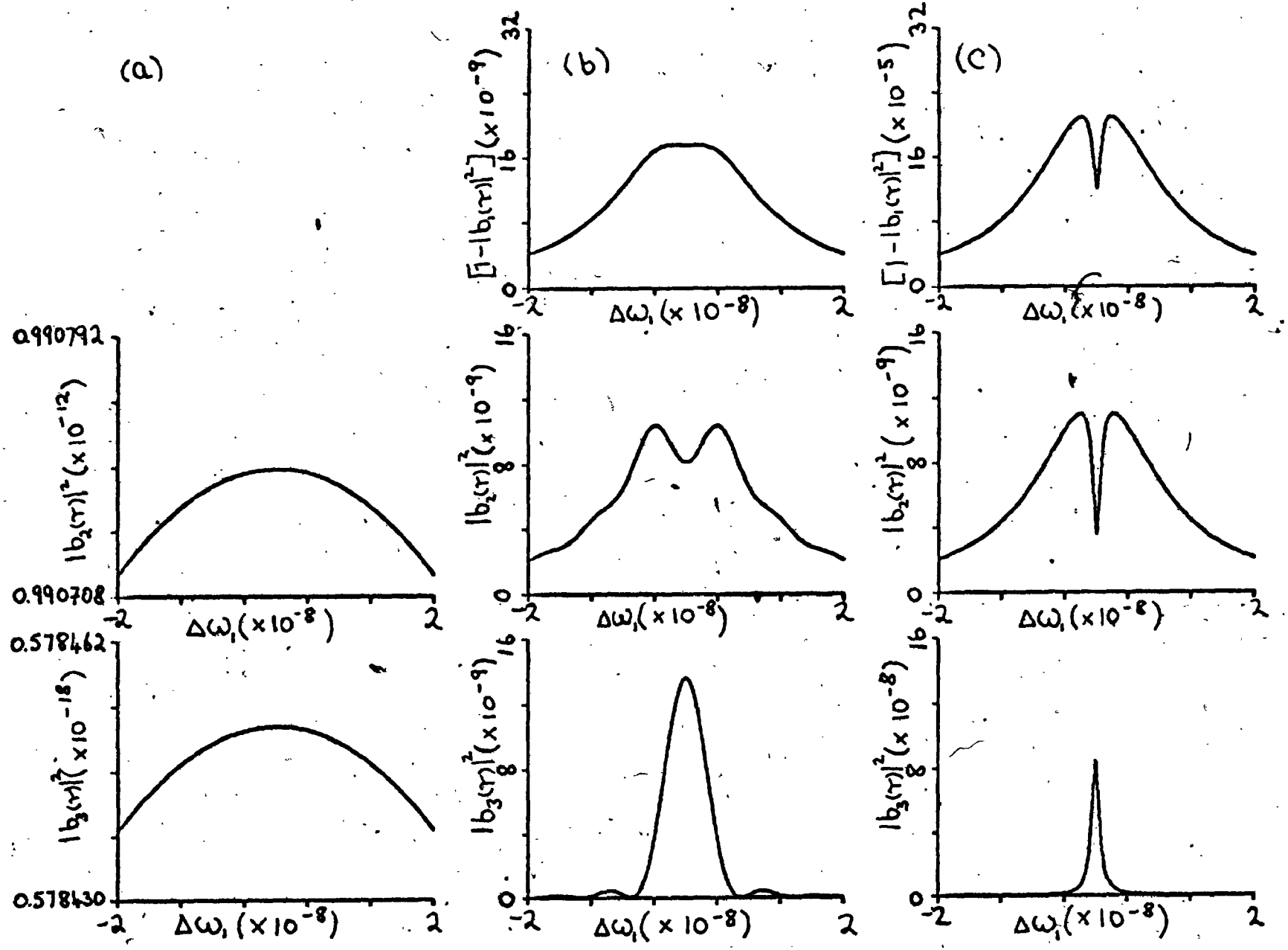
(a)
(b)
(c)
0.990792
0.990708
$|b_2(\tau)|^2(\times 10^{-12})$
$[1-|b_1(\tau)|^2](\times 10^{-9})$
$[1-|b_1(\tau)|^2](\times 10^{-5})$
$|b_2(\tau)|^2(\times 10^{-9})$
$|b_2(\tau)|^2(\times 10^{-8})$
0.578462
0.578430
$|b_3(\tau)|^2(\times 10^{-18})$
$|b_3(\tau)|^2(\times 10^{-9})$
$|b_3(\tau)|^2(\times 10^{-8})$
$\Delta\omega_1(\times 10^{-8})$
-2
2
0
16
32
8

rates R_j , given by equations B.3.22, and we now proceed to derive such expressions. For convenience we now write the expressions for λ_j in equivalent polar form [88]

$$\lambda_1 = 2\sqrt[3]{r}\,\cos\tfrac{1}{3}\theta - b/3$$

$$\lambda_2 = -\sqrt[3]{r}\,(\cos\tfrac{1}{3}\theta + \sqrt{3}\,\sin\tfrac{1}{3}\theta) - b/3$$

$$\lambda_3 = -\sqrt[3]{r}\,(\cos\tfrac{1}{3}\theta - \sqrt{3}\,\sin\tfrac{1}{3}\theta) - b/3 \qquad \text{B.3.26}$$

where

$$r = \sqrt{\frac{-p^3}{27}} \quad , \; p < 0$$

$$p = c - b^2/3 \quad , \; q = d - bc/3 + \tfrac{2}{27}b^3 \qquad \text{B.3.27}$$

and

$$\theta = \tan^{-1}\left[\frac{-2\sqrt{-p^3/27 - q^2/4}}{q}\right] \qquad \text{B.3.28}$$

As an explicit example we consider the situation in which all the widths γ_j are identically zero. In this case the eigenvalues λ_j are real as $\underline{\underline{H}}$ is a hermitian matrix and the constants in the preceding equations can now be written as

$$b = \Delta\omega_1 - \Delta\omega_2 \quad , \; c = -\left[|V_{12}|^2 + |V_{23}|^2 + \Delta\omega_1\Delta\omega_2\right]$$

$$d = \Delta\omega_1|V_{23}|^2 - \Delta\omega_2|V_{12}|^2$$

$$p = -\left[|V_{12}|^2 + |V_{23}|^2 + \tfrac{1}{3}(\Delta\omega_1^2 + \Delta\omega_1\Delta\omega_2 + \Delta\omega_2^2)\right]$$

$$q = \Delta\omega_1|V_{23}|^2 - \Delta\omega_2|V_{12}|^2 + \tfrac{1}{3}(\Delta\omega_1 - \Delta\omega_2)(|V_{12}|^2 + |V_{23}|^2 + \Delta\omega_1\Delta\omega_2) + \tfrac{2}{27}(\Delta\omega_1 - \Delta\omega_2)^3$$

$$\sqrt[3]{r} = \sqrt{\left[|V_{12}|^2 + |V_{23}|^2 + \tfrac{1}{3}(\Delta\omega_1^2 + \Delta\omega_1\Delta\omega_2 + \Delta\omega_2^2)\right]/3} \qquad \text{B.3.29}$$

When both fields are on resonance, $\Delta\omega_1 = \Delta\omega_2 = 0$

$$q = 0 \Rightarrow \theta = \tan^{-1}\infty = \pi/2 \qquad \text{B.3.30}$$

and

$$\lambda_1 - \lambda_2 = 2\sqrt{|V_{12}|^2 + |V_{23}|^2}$$

$$\lambda_1 - \lambda_3 = \sqrt{|V_{12}|^2 + |V_{23}|^2}$$

$$\lambda_2 - \lambda_3 = -\sqrt{|V_{12}|^2 + |V_{23}|^2} \qquad \text{B.3.31}$$

Finally, the transition rates corresponding to $\gamma_j = 0$, $j = 1, \ldots 3$ and $\Delta\omega_1 = \Delta\omega_2 = 0$ are given by

$$R_1 = \frac{|V_{12}|^2 |V_{23}|^2}{(|V_{12}|^2 + |V_{23}|^2)^{3/2}} \left\{ \frac{|V_{12}|^2}{|V_{23}|^2} \sin 2\sqrt{|V_{12}|^2 + |V_{23}|^2}\, t + 2 \sin \sqrt{|V_{12}|^2 + |V_{23}|^2}\, t \right\}$$

$$R_2 = \frac{|V_{12}|^2}{(|V_{12}|^2 + |V_{23}|^2)^{1/2}} \sin 2\sqrt{|V_{12}|^2 + |V_{23}|^2}\, t$$

$$R_3 = \frac{|V_{12}|^2 |V_{23}|^2}{(|V_{12}|^2 + |V_{23}|^2)^{3/2}} \left\{ 2 \sin \sqrt{|V_{12}|^2 + |V_{23}|^2}\, t - \sin 2\sqrt{|V_{12}|^2 + |V_{23}|^2}\, t \right\}$$

B.3.32

Although analytic closed form expressions can also be obtained for the situation in which all the widths are equal, that is $\gamma = \gamma_j$, $j = 1, \ldots, 3$, the final results, with the exception of those for R_3, are unweildy and serve no useful purpose in the context of Robert's and Fortson's work.

B.4 THE THREE LEVEL MASER

In this section we present expressions for the power emitted, P_e, and power absorbed, P_a, which are exact for the three level maser within the rotating field approximation. These quantities have been defined by Javan in his classic treatment of the problem [34] where he obtained closed form approximate expressions for them in the limit that one field is much weaker than the other. Javan employed these solutions to discuss the conditions under which Maser action should be observed when the amplifying field is weak. In the appendix of his article, see [34], a method for obtaining the exact solution within the rotating field approximation is indicated but not carried out explicitly. The purpose of this section is to use the formal methods of Section B.1 to obtain a convenient representation of the solution valid for all field strengths consistent with the validity of the rotating field approximation.

The basic three level configuration considered by Javan is shown in Figure B.3 where now the lowest state $\phi_1(r)$ is coupled directly to states $\phi_2(r)$ and $\phi_3(r)$. Javan assumes that the strong saturating field of frequency ν_1 induces transitions between the states $\phi_1(r)$ and $\phi_2(r)$, that is $\nu_1 \sim \omega_{31}$, while a weak radiofrequency field of frequency ν_2 is applied at $\nu_2 \sim \omega_{21}$. The basic set of differential equations describing the interaction of the two fields with this three level system are*

---

* Javan's set of equations, his equations (9), differ in that he uses $\mathcal{E}_1 \sin \nu_1 t$ and $\mathcal{E}_2 \sin \nu_2 t$ to represent the fields while we use $\mathcal{E}_1 \cos \nu_1 t$ and $\mathcal{E}_2 \cos \nu_2 t$. In the rotating field approximation the results are equivalent in both cases as the phase dependence of the fields cancels out in the final results. Spontaneous decay terms are not included in these differential equations but collision damping will be included later.

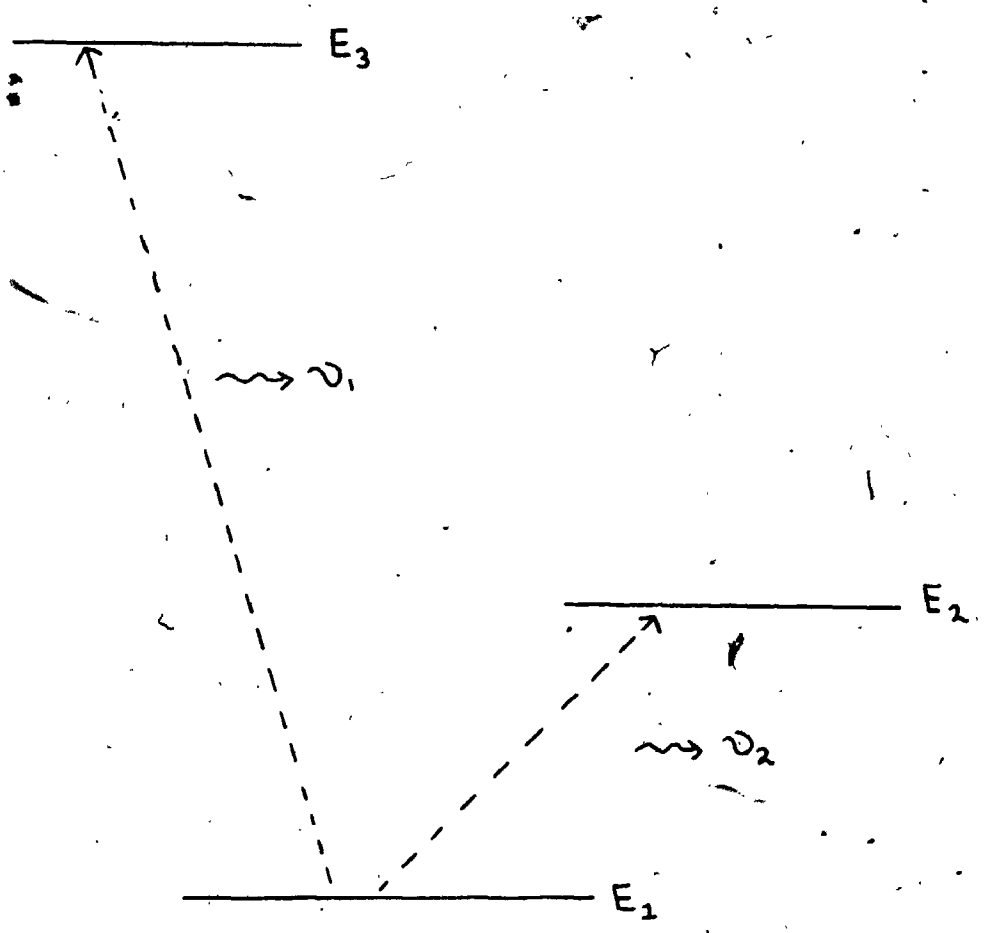

Figure B.3. The three level configuration employed by Javan [34] to investigate maser action. The field oscillating at frequency ν_1 and near resonant with the transition $\phi_1(r) \rightarrow \phi_3(r)$ represents the saturating field while that at frequency ν_2 and near resonant with the transition $\phi_1(r) \rightarrow \phi_2(r)$ represents a weak radiofrequency field.

$$i\frac{\partial}{\partial t}b_1(t) = V_{12}\,b_2(t)\exp[i\Delta\omega_1 t] + V_{13}\,b_3(t)\exp[i\Delta\omega_2 t]$$
$$i\frac{\partial}{\partial t}b_2(t) = V_{21}\,b_1(t)\exp[-i\Delta\omega_1 t]$$
$$i\frac{\partial}{\partial t}b_3(t) = V_{31}\,b_1(t)\exp[-i\Delta\omega_2 t] \qquad \text{B.4.1}$$

where $\Delta\omega_1 = \nu_2 - \omega_{21}$, $\Delta\omega_2 = \nu_1 - \omega_{31}$, are defined to be consistent with Javan's equations (9), and $V_{12} = -\mu_{12}\mathcal{E}_1/2$, $V_{13} = -\mu_{13}\mathcal{E}_2/2$. Applying the phase factoring transformation, given by equation B.1.2, and choosing $\alpha_1 = 0$, $\alpha_2 = \Delta\omega_1$ and $\alpha_3 = \Delta\omega_2$ we obtain the following result for the constant matrix $\underline{\underline{H}}$ in equation B.1.3

$$\underline{\underline{H}} = \begin{pmatrix} 0 & V_{12} & V_{13} \\ V_{21} & \Delta\omega_1 & 0 \\ V_{31} & 0 & \Delta\omega_2 \end{pmatrix} \qquad \text{B.4.2}$$

The elements of the matrix $\underline{\underline{D}}(\lambda)$ in equation B.1.6 are given by

$$D_{11}(\lambda) = \left[\lambda^2 - (\Delta\omega_1 + \Delta\omega_2)\lambda + \Delta\omega_1\Delta\omega_2\right] \Big/ \prod_{j=1}^{3}(\lambda - \lambda_j)$$
$$D_{12}(\lambda) = -V_{12}(\Delta\omega_2 - \lambda) \Big/ \prod_{j=1}^{3}(\lambda - \lambda_j) = D_{21}(\lambda)$$
$$D_{13}(\lambda) = V_{13}(\lambda - \Delta\omega_1) \Big/ \prod_{j=1}^{3}(\lambda - \lambda_j) = D_{31}(\lambda)$$
$$D_{22}(\lambda) = \left[\lambda^2 - \Delta\omega_2\lambda - |V_{13}|^2\right] \Big/ \prod_{j=1}^{3}(\lambda - \lambda_j)$$
$$D_{23}(\lambda) = V_{12}V_{13} \Big/ \prod_{j=1}^{3}(\lambda - \lambda_j) = D_{32}(\lambda)$$
$$D_{33}(\lambda) = \left[\lambda^2 - \Delta\omega_1\lambda - |V_{12}|^2\right] \Big/ \prod_{j=1}^{3}(\lambda - \lambda_j) \qquad \text{B.4.3}$$

Inverting the Laplace transform of $M_j(s)$ we obtain for $C_j(t)$

$$\begin{pmatrix} C_1(t) \\ C_2(t) \\ C_3(t) \end{pmatrix} = \begin{pmatrix} -\left[\Delta_2 - (\Delta\omega_1 + \Delta\omega_2)\Delta_1 + \Delta\omega_1\Delta\omega_2\Delta_0\right] & V_{12}(\Delta_1 - \Delta\omega_2\Delta_0) & V_{13}(\Delta_1 - \Delta\omega_1\Delta_0) \\ -V_{12}(\Delta_1 - \Delta\omega_2\Delta_0) & \left[\Delta_2 - \Delta\omega_2\Delta_1 - |V_{13}|^2\Delta_0\right] & V_{12}V_{13}\Delta_0 \\ -V_{13}(\Delta_1 - \Delta\omega_1\Delta_0) & V_{12}V_{13}\Delta_0 & \left[\Delta_2 - \Delta\omega_1\Delta_1 - |V_{12}|^2\Delta_0\right] \end{pmatrix}$$
$$\times \begin{pmatrix} C_1(0) \\ C_2(0) \\ C_3(0) \end{pmatrix} \qquad \text{B.4.4}$$

where the partial fractions Δ_n are given by equation B.1.9 and λ_j are the roots of the cubic equation

$$\lambda^3 + b\lambda^2 + c\lambda + d = 0 \qquad \text{B.4.5}$$

with

$$b = -(\Delta\omega_1 + \Delta\omega_2) \quad , \quad c = \Delta\omega_1\Delta\omega_2 - (|V_{12}|^2 + |V_{13}|^2)$$
$$d = \Delta\omega_2|V_{12}|^2 + \Delta\omega_1|V_{13}|^2 \qquad \text{B.4.6}$$

For convenience we write the formal solutions to this cubic equation in polar form [88], see equation B.3.26, where

$$r = \sqrt{\frac{-p^3}{27}} \quad , \quad p < 0$$
$$p = c - b^2/3 = \Delta\omega_1\Delta\omega_2 - (\Delta\omega_1+\Delta\omega_2)^2/3 - (|V_{12}|^2+|V_{13}|^2)$$
$$q = d - \frac{bc}{3} - \frac{2}{27}b^3 = -(\Delta\omega_1+\Delta\omega_2)\left[1 - (\Delta\omega_1\Delta\omega_2 - (|V_{12}|^2+|V_{13}|^2) + \frac{2}{27}(\Delta\omega_1+\Delta\omega_2)^2\right] \qquad \text{B.4.7}$$

and

$$\theta = \tan^{-1}\left[\frac{-2\sqrt{-p^3/27 - q^2/4}}{q}\right] \qquad \text{B.4.8}$$

The roots λ_j are real and distinct in this case, see [88]. Javan's expressions for the power absorbed, P_a and power emitted P_e are given in terms of the induced transition probabilities as follows

$$P_a = (n_1 - n_2)\frac{\nu}{T^2}\int_{-\infty}^{t} P_{12}(t-t_0)\exp\left[-(t-t_0)/T\right]dt_0$$
$$P_e = (n_2 - n_3)\frac{\nu}{T^2}\int_{-\infty}^{t} P_{32}(t-t_0)\exp\left[-(t-t_0)/T\right]dt_0 \qquad \text{B.4.9}$$

where $P_{12}(t-t_0) = |b_2(t-t_0)|^2$ subject to the initial conditions $b_1(0) = 1$, $b_2(0) = b_3(0) = 0$ and $P_{32}(t-t_0) = |b_2(t-t_0)|^2$ subject to the initial conditions $b_3(0) = 1$, $b_1(0) = b_2(0) = 0$. The integrals occurring in equation B.4.9 have been discussed previously in the collision damping calculations of Section 2.4 and n_j are the Boltzmann populations of the individual levels $\phi_j(r)$. Javan gives a detailed discussion of the derivation of these power expressions and our interest here is to derive exact expressions for these quantities within the rotating field approximation.

We can now write out the explicit expressions for the induced transition probabilities $P_{12}(t-t_0)$ and $P_{32}(t-t_0)$ from equation B.4.4, using equation B.1.3.

$$P_{12}(t-t_0) = |V_{12}|^2\left[|\Delta_1(t-t_0)|^2 - \Delta\omega_2\left(\Delta_0(t-t_0)\Delta_1^*(t-t_0) + \Delta_0^*(t-t_0)\Delta_1(t-t_0)\right) + \Delta\omega_2^2|\Delta_0(t-t_0)|^2\right]$$
$$P_{32}(t-t_0) = |V_{12}|^2|V_{13}|^2|\Delta_0(t-t_0)|^2 \qquad \text{B.4.10}$$

Substituting equation B.4.10 into the expression for P_e given by equation B.4.9 and after some algebra, we obtain

$$P_e = (n_2-n_3)\frac{\upsilon}{\tau^2}|V_{12}|^2|V_{13}|^2\int_{-\infty}^{t}|\Delta_0(t-t_0)|^2\exp[-(t-t_0)/\tau]\,dt_0$$

$$= 4(n_2-n_3)\frac{\upsilon}{\tau^2}|V_{12}|^2|V_{13}|^2\Big\{(\lambda_2+\lambda_3)(\lambda_1-\lambda_3)\int_{-\infty}^{t}\sin^2\tfrac{1}{2}[(\lambda_1-\lambda_2)(t-t_0)]\exp\Big[-\frac{(t-t_0)}{\tau}\Big]dt_0$$

$$-(\lambda_2-\lambda_3)(\lambda_1-\lambda_2)\int_{-\infty}^{t}\sin^2\tfrac{1}{2}[(\lambda_1-\lambda_3)(t-t_0)]\exp\Big[-\frac{(t-t_0)}{\tau}\Big]dt_0+(\lambda_1-\lambda_2)(\lambda_1-\lambda_3)\times$$

$$\int_{-\infty}^{t}\sin^2\tfrac{1}{2}[(\lambda_2-\lambda_3)(t-t_0)]\exp\Big[-\frac{(t-t_0)}{\tau}\Big]dt_0 \qquad \text{B.4.12}$$

$$=\frac{2(n_2-n_3)\,\upsilon\tau|V_{12}|^2|V_{13}|^2}{(\lambda_1-\lambda_2)(\lambda_2-\lambda_3)(\lambda_1-\lambda_3)}\Big\{\frac{(\lambda_1-\lambda_2)}{[1+(\lambda_1-\lambda_2)^2\tau^2]}-\frac{(\lambda_1-\lambda_3)}{[1+(\lambda_1-\lambda_3)^2\tau^2]}+\frac{(\lambda_2-\lambda_3)}{[1+(\lambda_2-\lambda_3)^2\tau^2]}\Big\}$$

The above integrals are tabulated in [66]. Next, substituting equation B.4.10 into the expression for the power absorbed P_a, given by equation B.4.9, , we obtain after similar manipulations an expression for P_a ;

$$P_a = (n_1-n_2)\frac{\upsilon}{\tau^2}|V_{12}|^2\int_{-\infty}^{t}\Big\{|\Delta_1(t-t_0)|^2-\Delta\omega_2(\Delta_0(t-t_0)\Delta_1^*(t-t_0)+\Delta_0^*(t-t_0)\Delta_1(t-t_0))$$
$$+\Delta\omega_2^2|\Delta_0(t-t_0)|^2\Big\}\exp\Big[-\frac{(t-t_0)}{\tau}\Big]\,dt_0$$

$$=4(n_1-n_2)\,\upsilon|V_{12}|^2\Big\{(\Delta\omega_2-\lambda_1)(\Delta\omega_2-\lambda_2)(\lambda_2-\lambda_3)(\lambda_1-\lambda_3)\int_{-\infty}^{t}\sin^2\tfrac{1}{2}[(\lambda_1-\lambda_2)(t-t_0)]\exp\Big[-\frac{(t-t_0)}{\tau}\Big]dt_0$$

$$-(\Delta\omega_2-\lambda_1)(\Delta\omega_2-\lambda_3)(\lambda_2-\lambda_3)(\lambda_1-\lambda_2)\int_{-\infty}^{t}\sin^2\tfrac{1}{2}[(\lambda_1-\lambda_3)(t-t_0)]\exp\Big[-\frac{(t-t_0)}{\tau}\Big]dt_0$$

$$+(\Delta\omega_2-\lambda_2)(\Delta\omega_2-\lambda_3)(\lambda_1-\lambda_2)(\lambda_1-\lambda_3)\int_{-\infty}^{t}\sin^2\tfrac{1}{2}[(\lambda_2-\lambda_3)(t-t_0)]\exp\Big[-\frac{(t-t_0)}{\tau}\Big]dt_0\Big\}$$

$$=\frac{2(n_1-n_2)\,\upsilon\tau|V_{12}|^2}{(\lambda_1-\lambda_2)(\lambda_2-\lambda_3)(\lambda_1-\lambda_3)}\Big\{\frac{(\Delta\omega_2-\lambda_1)(\Delta\omega_2-\lambda_2)(\lambda_1-\lambda_2)}{[1+(\lambda_1-\lambda_2)^2\tau^2]}-\frac{(\Delta\omega_2-\lambda_1)(\Delta\omega_2-\lambda_3)(\lambda_1-\lambda_3)}{[1+(\lambda_1-\lambda_3)^2\tau^2]}$$
$$+\frac{(\Delta\omega_2-\lambda_2)(\Delta\omega_2-\lambda_3)(\lambda_2-\lambda_3)}{[1+(\lambda_2-\lambda_3)^2\tau^2]}\Big\} \qquad \text{B.4.13}$$

Finally, using the expression for the total power $P=P_e-P_a$, we obtain

$$P=\frac{2(n_2-n_3)\,\upsilon\tau|V_{12}|^2}{}\Big\{\frac{[|V_{13}|^2-\eta(\Delta\omega_2-\lambda_1)(\Delta\omega_2-\lambda_2)](\lambda_1-\lambda_2)}{[1+(\lambda_1-\lambda_2)^2\tau^2]}$$
$$-\frac{[|V_{12}|^2-\eta(\Delta\omega_2-\lambda_1)(\Delta\omega_2-\lambda_3)](\lambda_1-\lambda_3)}{[1+(\lambda_1-\lambda_3)^2\tau^2]}+\frac{[|V_{12}|^2-\eta(\Delta\omega_2-\lambda_2)(\Delta\omega_2-\lambda_3)](\lambda_2-\lambda_3)}{[1+(\lambda_2-\lambda_3)^2\tau^2]}\Big\}$$

B.4.14

where $\eta=(n_1-n_2)/(n_2-n_3)$. The power expressions given by equations

B.4.12 and B.4.14 extend beyond the range of validity of Javan's expressions and can for example be used to study saturation effects at the amplifying frequency ν_2, see Javan [34].

Equation B.4.14 for the total power P reduces to a convenient closed form expression in the limit that $\Delta\omega_1 + \Delta\omega_2 = 0$. This condition can be satisfied if both fields are on resonance or are mistuned from resonance by the same magnitude; $\Delta\omega_1 = -\Delta\omega_2$. In this limit the constants appearing in equation B.4.8 reduce to

$$b = 0 \;,\; p = -[\Delta\omega_1^2 + |V_{12}|^2 + |V_{13}|^2] \;,\; q = 0 \;,\; \theta = \pi/2$$

$$\sqrt[3]{r} = \sqrt{(\Delta\omega_1^2 + |V_{12}|^2 + |V_{13}|^2)/3} \qquad \text{B.4.15}$$

and the eigenvalues λ_j become

$$\begin{aligned} \lambda_1 &= \sqrt{\Delta\omega_1^2 + |V_{12}|^2 + |V_{13}|^2} = \delta \\ \lambda_2 &= \sqrt{\Delta\omega_1^2 + |V_{12}|^2 + |V_{13}|^2} = -\delta \\ \lambda_3 &= 0 \end{aligned} \qquad \text{B.4.16}$$

Equation B.4.14 for the total power now becomes

$$P = \frac{2(n_2 - n_3)\, v\tau\, |V_{12}|^2}{\delta^2[1+4\delta^2\tau^2][1+\delta^2\tau^2]} \Big\{ 3|V_{13}|^2\delta^2\tau^2 - \eta\big[(1+\delta^2\tau^2)(|V_{12}|^2+|V_{13}|^2) + 2\Delta\omega_1^2(1+4\delta^2\tau^2)\big] \Big\} \qquad \text{B.4.17}$$

When both fields are exactly on resonance $\Delta\omega_1 = \Delta\omega_2 = 0$, equation B.4.17 simplifies further to

$$P = 2(n_2 - n_3)\, v\tau\, |V_{12}|^2 \left\{ \frac{3|V_{13}|^2\tau^2 - \eta\big[1 + (|V_{12}|^2 + |V_{13}|^2)\tau^2\big]}{\big[1 + 4(|V_{12}|^2 + |V_{13}|^2)\tau^2\big]\big[1 + (|V_{12}|^2 + |V_{13}|^2)\tau^2\big]} \right\} \qquad \text{B.4.18}$$

Equation B.4.18 agrees precisely with Javan's equation (21) for the total power in the limit that the field at the amplifying frequency ν_2 is much weaker than the saturating field at frequency ν_1, that is $|V_{13}|^2 \simeq |V_{13}|^2 + |V_{12}|^2$ [34]. While it would be extremely tedious to show that equations B.4.12 and B.4.13 for P_e and P_a, respectively, reduce to Javan's equations (16) and (19) in the limit $|V_{12}| \ll |V_{13}|$, the former equations can be used to reproduce his Figure 2 with the specified values of his parameters.

REFERENCES

[1] "Fundamentals of Applied Laser Physics", (1973), edited by M.S. Feld, A. Javan and N.A. Kurnit (Wiley-Interseience).

[2] Bennet, W.R., (1973),"Atomic Physics and Astrophysics", edited by M.C. Chretien and E. Lipworth (Gordon and Breach).

[3] "Laser Applications to Optics and Spectroscopy", (1975), edited by S.F. Jacobs, M.O. Scully, and M. Sargent III, (Addison-Wesley), 2.

[4] Ramsey, N.F., (1956)), "Molecular Beams" (Oxford University Press).

[5] Francis Bitter, "Selected Papers and Commentaries" ,(1969), edited by T. Erber and C.M. Fowler (M.I.T Press)

[6] Cohen-Tannoudji, C., (1968), "Cargese Lectures in Physics", edited by M. Levy (Gordon and Breach), 2, p.347-393.

[7] Agarbiceanu, I., and Popescu, M. (1975),"Optical Methods of Radiofrequency Spectroscopy" (Wiley).

[8] Shimoda, K., (1967), Japan. J. Appl. Phys., 6, 620.

[9] Shimoda, K., and Shimizu, T., (1972), "Nonlinear Spectroscopy of Molecules", (Pergamon Press).

[10] Steinfeld, J.I., (1974), "Molecules and Radiation", (Harper and Row), Chaps. 11-13.

[11] Brewer, R.G., (1972), Science, N.Y., 178, 247.

[12] Arimondo, E., and Corbalan, R., (1974), J.Phys.B., 7,2368 and references therein.

[13] Shirley, J.H., (1965), Phys. Rev., 138, B979.

[14] Autler, S.H., and Townes, C.H., (1955), Phys. Rev., 100,703.

[15] Gush, R., and Gush, P., (1972), Phys. Rev. A., 6, 129.

[16] Rahman, N.K, (1975), Physics Lett. A., 54, 8.

[17] Cohen-Tannoudji, C., Dupont-Roc, J., and Fabre, C., (1973), J. Phys. B., 6, L214.

[18] Pegg, D.T., (1973), J. Phys. B., 6,246.

[19] Hale, J.K., (1969), "Ordinary Differential Equations" (Wiley-Interscience), Chap. 3.

[20] Besset, C., Horowitz, J, Messiah, A., and Winter, J., (1954), J. Physique Rad., 15, 251.

[21] Ahmad, F., (1975), Phys. Rev. A., 12, 1539.

[22] Moloney, J. V., and Meath, W. J., (1976), Molec. Phys., 31, 1537.

[23] Stenholm, S., (1972), J. Phys. B., 5, 878.

[24] Fontana, P. R., and Thomann, P., (1976), Phys. Rev. A., 13, 1512.

[25] Dirac, P. A. M., (1927), Proc. Roy. Soc., A114, 243, 710.

[26] Schiff, L. I., (1955), "Quantum Mechanics" (Mc Graw-Hill), Chap 3.

[27] Moloney, J. V., Ali, M. K., and Meath, W. J., (1974), Physics Lett. A., 49, 207.

[28] Moloney, J. V., and Meath, W. J., (1975), Molec. Phys., 30, 171.

[29] Vasilenko, L. S., Chebotaev, V. P., and Shishaev, A. V., (1970), JETP Lett., 12, 113.

[30] Kopal, Z., (1961), "Numerical Analysis",(Chapman and Hall), Chap. 4.

[31] Wallace, R., (1970), Phys. Rev. A, 2, 1711.

[32] Freed, K., (1965), J. Chem. Phys., 43, 1113.

[33] Roberts, D. E., and Fortson, E. N., (1973), Phys. Rev. Lett., 31, 1539.

[34] Javan, A., (1957), Phys. Rev., 107, 1579.

[35] Bethe, H. A., and Salpeter, E. E., (1957), "Quantum Mechanics of One- and Two-Electron Atoms" (Academic Press).

[36] Bohm, D., (1951), "Quantum Theory" (Prentice-Hall), Chap. 19.

[37] Messiah, A., (1961), "Quantum Mechanics Vol. 2" (North Holland), Chap. 17.

[38] Pantell, R. H., and Puthoff, H. E., (1969), "Fundamentals Of Quantum Electronics" (Wiley), Chap. 5.

[39] Stenholm, S., (1971), "The Semiclassical Theory of the Gas Laser", (Pergamon Press), Chaps. 1 and 2.

[40] Weisskopf, V., and Wigner, E., (1930), Z. Physik, 63, 54 (an english translation of this article appears in reference [41]).

[41] Hindmarsh, W. R., (1967), "Atomic Spectra" (Pergamon Press), p304ff.

[42] Dalgarno, A., (1966), "Perturbation Theory and its Application in Quantum Mechanics" (Wiley), p145ff.

[43] Langoff, P. W., Epstein, S. T., and Karplus, M., (1972), Rev. Mod. Phys., 7, 602.

[44] Karplus, M., and Kolker, H. J., (1963), J. Chem. Phys., 39, 1493.

[45] Brooks, Jr., G. L., and Scarfone, L.M., (1969), Phys. Rev., 185, 82.

[46] Wong, J., Garrison, J. C., and Einwohner, T. H., (1976), Phys. Rev. A., 13, 674.

[47] Goeppart-Mayer, M., (1931), Ann. Phys., 9, 273.

[48] Gold, A., (1969), "Quantum Optics", edited by R.J. Glauber, (Academic Press), p397ff.

[49] Young, R. H., Deal, Jr., W.J., and Kestner, N.R., (1969), Molec. Phys., 17, 369.

[50] Sen Gupta, N.D., (1970), J. Phys. A., 3, 618.

[51] Rabi, I.I., (1937), Phys. Rev., 51, 652.

[52] Bloch, F., and Siegert, A., (1940), 57, 522.

[53] Cagnac, B., Grynberg, G., and Biraben, F., (1973), J. Physique Rad., 34, 845.

[54] Churchill, R.V., (1958), "Operational Mathematics" (McGraw-Hill) ,Chap. 1.

[55] Breene, Jr., R. G., (1961), "The Shift and Shape of Spectral Lines" (Pergamon Press), Chap. 1.

[56] Ahmad, F., and Bullough, R.K., (1974), J. Phys. B., 7, L275.

[57] Swain, S., (1974), J. Phys. B., 7, 2363.

[58] Shirley, J.H., (1963),thesis, California Institute of Technology, (unpublished).

[59] Shirley, J.H., (1963), J. Appl. Phys., 34, 783.

[60] Salwen, H., (1955), Phys. Rev., 99, 1274.

[61] Halany, N.P., (1966), "Differential Equations" (Academic Press), Chap. 1.

[62] Erugin, N.P., (1966), "Ordinary Differential Equations" (Wiley-Interscience), Chap 3..

[63] Margenau, H., and Murphy, G.M., (1956), "The Matematics of Physics and Chemistry" (Van Nostrand), Chap 3.

[64] Askar, A., (1974), Phys. Rev. A., 10, 2395.

[65] Salzman, W.R., (1971), Phys. Rev. Lett., 26, 220.

[66] Dwight, H.B., (1961), "Tables of Integrals and other Mathematical Data", (Macmillan).

[67] "International Mathematical and Statistical Libraries", (1974), Edition 4; Subroutine DCS1QE.

[68] "Eigenvalue Systems Package(EISPACK)", Version 1, subroutine COMLR2.

[69] Ralston, A., (1965), "A First Course in Numerical Analysis", (McGraw Hill), Chap. 10.

[70] Slichter, C.P., (1963), "Principles of Magnetic Resonance" (Harper and Row), Chap. 5.

[71] Stenholm, S., and Lamb, W.E., (1969), Phys. Rev., 181, 618.

[72] Yabusaki, T., Murakami, Y., and Ogawa, T., (1976), J. Phys. B., 9, 9.

[73] Cohen-Tannoudji, C., and Haroche, S., (1966), Compt. Rend., 262, 37B.

[74] Yabusaki, T., Nakayama, S., Murakami, Y., and Ogawa, T., (1974), Phys. Rev. A., 10, 1955.

[75] Bonch-Bruevich, A.M., and Khodovoi, V.A., (1967) ,Soviet Phys.-Usp., 10, 637.

[76] Kovarskii, V.A., and Perel'man, N.F., (1971), JETP, 33, 274.

[77] Pegg D.T., and Series, G.W., (1970), J. Phys. B.,3, L33.

[78] Chapman, G.D., (1970), J. Phys. B., 3, L36.

[79] McLean, W.A., and Swain, S., (1976), J. Phys. B., 9, 1673.

[80] Liao, P.F., and Bjorkholm, J.E., (1974), Phys. Rev. Lett., 34, 1.

[81] Pegg, D.T., (1973), Phys. Rev. A., 8, 2214.

[82] Hermann J., and Swain, S., (1976), Physics Lett., 55A, 446.

[83] Biraben, F., Cagnac, B., and Grynberg, G., (1974), Phys. Rev. Lett., 32, 643.

[83a] Wiese, W.L., Smith, M.W., and Glennon, B.M., "Atomic Transition Probabilities -Sodium through Calcium" ,1969, NSRDS-NBS 22, Vol. II.

[84] Pritchard, D., Apt, J., and Ducas, T.W., (1974), Phys. Rev. Lett., 32, 641.

[85] Levenson, M.D., and Bloembergen, N., (1974), Phys. Rev. Lett., 32, 645.

[86] Fano, G., (1971), "Mathematical Methods of Quantum Mechanics", (McGraw Hill), p40ff.

[87] Ahlberg, J.H., Nilson, E.N., and Walsh, J.L., (1967), "The Theory of Splines and Their Applications", (Academic Press), Chap. 2.

[88] Rosenbach, J.B., Whitman, E.A., Meserve, B.E., and Whitman, P.M., (1958), "College Algebra", (Ginn), p361ff.

[89] Sargent, M., and Horwitz, P., (1976), Phys. Rev. A., 13, 1962 and references theirin.

[90] Brandenberger, J.R., Lundeen S.R., and Pipkin F.M., (1976), Phys. Rev. A, 14,341.

[91] Pert, G.J., (1975), J. Phys. B., 8, L173.